University of Alberta

Finite Element Analysis of Fixed Sandwich Panels under Combined In-plane and Lateral Loads

by

Weijiang Luo 

A thesis submitted to the Faculty of Graduate Studies and Research
in partial fulfillment of the requirements for the degree of

Master of Science
in
Structural Engineering

Department of Civil and Environmental Engineering

Edmonton, Alberta
Fall, 2008

Your file Votre référence
ISBN: 978-0-494-47299-6
Our file Notre référence
ISBN: 978-0-494-47299-6

Abstract

SPS (sandwich plate system) panel has been developed as a replacement for the stiffened steel plate because of its higher bending stiffness and reduced fabrication effort. Although SPS panels have mostly been used in maritime structures such as for the rehabilitation of ship decks, new applications such as in bridge decks are emerging.

Three identical SPS panels 1200x1800 mm with fixed boundary conditions under combined in-plane and lateral loads were tested by Little (2007). An interaction diagram between the lateral and in-plane load capacity was obtained by testing the panels under three lateral load levels of 13%, 27% and 45% of the yield line load level. In this study, finite element models are validated based on these tests and a parametric study of the sandwich panel with varying aspect ratios, panel thickness, and lateral load levels is completed to expand the database of test results. A simple method to calculate deflections in sandwich panels by deriving shear flexibility factors will be derived in this study.

TABLE OF CONTENT

LIST OF Tables

LIST OF FIGURES

LIST OF SYMBOLS

L	=	Length of sandwich panel
w	=	Width of sandwich panel
E	=	modulus of elasticity
E_c	=	Elastomer modulus of elasticity
E_s	=	Steel modulus of elasticity
t	=	Thickness of a solid plate
t_{eq}	=	Equivalent thickness of sandwich panel
h_c	=	Elastomer thickness
t_s	=	Steel plate thickness
C	=	Concentrated load
C_i	=	Concentrated load at point i, i = 1, 2, 3,4
I	=	Moment of inertia
K	=	Spring constant
K_x	=	In-plane spring stiffness
K_z	=	Out-of-plane spring stiffness
P	=	In-plane compressive load
P_y	=	Yield in-plane compressive load
P_u	=	Axial compressive load capacity
q	=	Uniform lateral pressure
q_c	=	Yield line lateral load capacity
U_x	=	Deflection in x-direction
U_y	=	Deflection in y-direction
U_z	=	Deflection in z-direction
V	=	Potential energy from axial and lateral load
U	=	Strain energy from the core and exterior plates
α	=	Deflection factor
α_{ij}	=	Deflection factor at location j caused by concentrated load at i

k	=	Shear flexibility factor
k_{ij}	=	Shear flexibility factor at location j caused by concentrated load at i
Δ	=	Deflection of plate
Δ_i	=	Deflection at load point i, i = 1,2,3,4
$\Delta_{(SPS)}$	=	Deflection of sandwich panel
$\Delta_{(plate)}$	=	Deflection of solid plate
Δ_{max}	=	Maximum deflection
Δ_p	=	Deflection at point of concentrated load
σ_y	=	Yield strength of steel plate
σ_u	=	Tensile strength of steel plate
ε_y	=	axial strain in y-direction

Chapter 1

Introduction

1.1 General

Sandwich panels consist of two exterior plates bonded together by a continuous thick core of a much lighter material than the face plates (see Figure 1.1). Sandwich panels have been developed as an alternative to stiffened steel plates because of its higher bending stiffness, especially when compared to the portion of the plate between stiffeners, and reduced fabrication effort due to a much reduced welding requirement. The face plates, when separated by a continuous core, provide an increased stiffness to weight ratio compared to solid plates. Therefore, such construction has found applications in areas where lightweight is desirable such as in aircraft wings, wall and floor panels, ship hulls and decks, and several other applications. A recently developed patented system, called the Sandwich Plate System (SPS), consists of steel face plates bonded together by a high density elastomer core. It forms a high stiffness and high resistance structural system that has found several applications in the rehabilitation of ship structures and bridge decks. This system will be the main focus of the research presented in this report.

Local buckling (steel plate wrinkle) of sandwich panels is prevented because the face plates are bonded continuously to the core material, provided the core material has sufficient stiffness. The elastomer core material used in the patented SPS provides sufficient stiffness to prevent local buckling of the face plates. The design process therefore consists of checking the strength of the panels under combined in-plane and out-of-plane bending, which is based on global failure modes such as material failure and overall instability, or on serviceability considerations such as deflection. Although standard solutions exist for the calculation of deflections of solid panels subjected to out-of-plane loads, the solutions for sandwich panels are practically non-existent.

1.2 Objectives

The main objectives of this study are:

1. Developing and validating a finite element model for the analysis of sandwich panels under combined axial compressive and lateral loads.

2. Conducting a parametric study to investigate the effect on the sandwich panel behaviour the effect of panel aspect ratio, thickness of the elastomer core or steel plate, and the axial and lateral load levels.

3. Develop shear flexibility factor to calculate the out-of-plane deflection of sandwich panels when the effect of the soft elastomer core is considered.

1.3 Scope

This investigation is focused on sandwich panels consisting of steel face plates and elastomer core similar to the patented Sandwich Panel System developed by Intelligent Engineering Limited. A total of 39 finite element models with parameters including panel aspect ratio, thickness of the steel face plates and elastomer core and lateral load level are investigated.

Detailed finite element analysis is required to calculate the deflection of sandwich panels under lateral loads due to the significant flexibility effect from the elastomer core. The parametric study conducted as part of this investigation incorporates the effect of geometric and material non-linearity and is based on the assumption that a perfect bond between the face plates and the elastomer core exists. The effect of partial bond and imperfections such as voids in the elastomer core is beyond the scope of this investigation.

The shear flexibility factor is defined as the ratio of the deflection of the sandwich panel and a solid plate of equivalent thickness, which is used to calculate the deflection magnitude of sandwich panels from the solution obtained from a solid plate, for which standard solutions exist. Five sandwich panels with three aspect ratios, two boundary conditions and three load cases will be investigated

numerically. Five panels are 3-15-3, 3-50-3, 3-100-3, 6-50-6, and 10-50-6. The aspect ratios of 1.2, 1.7 and 2.5 are same as those used in parametric study. The boundary conditions are fixed along all four edges and fixed long edges only. Three load cases consist of uniform lateral pressure, concentrated loads and patch load. The analysis is conducted in the elastic range only since the deflection calculations are considered as a serviceability limit state.

1.4 Organization of the thesis

Chapter 2 of this thesis presents a review of the literature on sandwich panels, focused on sandwich panels made of steel face plates with a high density elastomer core. A finite element model for the analysis of these panels is developed and validated in Chapter 3. The validated model is used in Chapter 4 to conduct a parametric study to investigate the effect of various parameters on the strength and behaviour of sandwich panels under combined in-plane and out-of-plane loading. Chapter 5 presents the results of an elastic analysis investigation from which shear flexibility factors, used to take into account the effect of shear flexibility of the core on the deflection of panels, are derived. Finally, Chapter 6 presents a summary and the main conclusions from this research project.

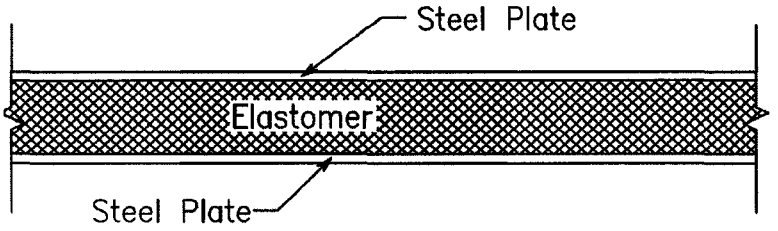

Figure 1.1 Sandwich Panel

Chapter 2

Literature Review

Sandwich panels have been developed and used for well over half a century, dating back to World War II. The Mosquito, a British World War II bomber, is said to be the first application of the sandwich construction in 1940 (Olsson and Reichard, 1989). At present time, sandwich construction finds applications in many different fields.

Structural sandwich panels are generally made of three layers; the face plates are most commonly steel plates and the core can be of different types such as honeycomb, solid foam, truss, concrete, or other, generally light, material. The steel plates are generally standard, but the behaviour of sandwich panels is usually a function of the unique properties of core material. The sandwich panel comprised of two exterior steel-plates and a high density polyurethane elastomer-core is the main subject of investigation in this study. The structural performance, the interface bond strength, and fatigue resistance are three key issues for sandwich panels. A review of the experimental work and finite element analysis on sandwich panels is presented in this chapter.

2.1 Properties of steel plate and elastomer core

The mechanical properties of the steel plate and elastomer core as well as the interface bond strength have been tested to assess the structural behaviour of the solid-core sandwich panel.

2.1.1 Steel plates

ASTM A588 Grade 50 steel was used for the steel plates of sandwich plate system (SPS) panels used for the investigation of the lateral load distribution in bridge decks made of sandwich panel system (SPS). The nominal yield and tensile strengths of ASTM A588 Grade 50 steel are 345 MPa and 485 MPa, respectively. It has been suggested that the design of SPS bridge decks is

governed by stiffness requirement, except for face plate thicknesses less than 3.2 mm where the fatigue limit state governs when the deck is designed using AASHTO's design provisions (Harris, 2007).

As part of a fatigue test program, Lui and Alexander (2007) tested two sets of steel tension coupons (four in each set) to characterize the mechanical properties of the steel plates used for the fabrication of SPS test specimens. The tensile strength, σ_u, was found to be 560 MPa and the elastic modulus, E_s, was 200 300 MPa obtained from one set of SPS specimens. The corresponding values for another set of SPS specimens were 530 MPa and 202 100 MPa, respectively. However the yield strength, σ_y, of 360 MPa from the first set of test specimens was much lower than 460 MPa from the other set.

Little *et al.* (2007) reported a yield strength of 352 MPa, a tensile strength of 575 MPa, and an elastic modulus of 199 300 MPa from ancillary tests conducted on the face plate of their test specimens. Engineering and true stress versus strain curves were also presented.

2.1.2 Elastomer

Ferro (1998) described the mechanical properties, temperature effects and energy absorption characteristics of a polyurethane elastomer used in the fabrication of the sandwich plate system, SPS, a patented system from Intelligent Engineering Ltd. The elastomer exhibits a significant increase in hardness, tensile strength, tear resistance and torsional stiffness at low temperature. A temperature range from -80°C to 80°C was suggested to keep the elastomer properties within proper range. Above 80°C, the structure of the polyurethane elastomer will undergo a non-reversible destructive chemical change. The material becomes brittle at the glass transition temperature in the range between -60°C to -80°C. The stress versus strain of the elastomer was reported and it showed that the elastomer has significantly different behaviour in tension and compression. The modulus of elasticity in tension is 300 MPa compared to

the modulus of elasticity in compression of150 MPa. Poisson's ratio of 0.5 was reported in his thesis.

Lui and Alexander (2007) conducted tension tests to quantify the elastomer properties of their test specimens. The elastomer was provided by Intelligent Engineering Ltd. The measured yield strength varied from 16.9 to 20.5 MPa, the elastic modulus varied from 493 to 510 MPa, and Poisson's ratio varied from 0.34 to 0.37, which is significantly different from the value of 0.5 reported by Ferro (1998).

Martin and Murray (2005) validated a finite element model based on field test results on the Shenley Bridge. Finite element analyses were performed using the software ANSYS (version 9.0). Material properties, including elastic modulus of 750 MPa, and Poisson's ratio of 0.36 were used in their finite element analysis. The elastomer core was modeled using HYPER 58 which was demonstrated to be effective for modeling elastomers (Ferro, 1998). HYPER 58 is a solid element defined by eight nodes having three degrees of freedom at each node and used to model solid hyperelastic structures. However, Wiessenborn (2007) concluded that an elastic-plastic material model is superior to a hyperelastic model for the elastomer core based on simple, planar and equibiaxial tension test results. The stress-strain curves showed an approximately bi-linear rather than the typical hyperelastic character. SOLID 45 is used to model the elastomer core in this study. SOLID 45 is a solid orthotropic material model. Detailed information about SOLID 45 element will be presented in Chapter 3

2.1.3 Bond strength at interface

Intelligent Engineering Ltd. (2007) summarized the test results of the bond strength at interface of the elastomer core and steel plate. It was found that the bond strength is influenced by several factors such as surface preparation, casting conditions, elastomer properties, ambient temperature, base metals, reduced bonded surface area (corrosion), altered elastomer material properties (fire, seawater exposure).

Bennett *et al.* (1998) conducted four shear-bond tests on two sets of steel-elastomer-steel composite plate sections. A sample of sandwich panel 6-50-6 was placed in the Shear-Bond Test Apparatus built specially to shear one of the steel faceplate from the elastomer core. The bond strength was obtained by the recorded pulling force divided by the measured contact shear area. The mean bond strength was found to be 4.2 MPa.

Lui and Alexander (2007) measured the bond strength of a sandwich panel 10-50-10 using a shear block and torsion test methods. Interface shear strength values from 5.0 to 10.2 MPa were obtained from shear block tests. Interface shear strengths from10.5 to12.7 MPa were obtained from torsion tests. They concluded that the torsion test is a better test method to get the bond strength because of its relatively small test specimens, exact failure locations, well-defined stress state, and consistent results.

Intelligent Engineering Ltd. (2007) suggest a minimum bond strength of 10 MPa between their patented elastomer core and steel plate once the sandwich panel has cured with steel plate grit blasted, clean, dry, and free of contaminants. Considering the range of bond strength values measured by Lui and Alexander (2007), this value lies at the upper end of the shear strength measured from a shear block test, but at the low end of the torsion test values.

2.2 Theories for the analysis of structural sandwich panels

Two theories applicable for the analysis of structural sandwich panels under the different load cases and boundary conditions are reviewed (Allen, 1975). The first one, a strain energy method, is based on the minimum potential energy principle expressed by equation (2-1). The strain energy, U, in the panel core and face plates, and the potential energy, V, from the axial and lateral loads can be derived in terms of the transverse deflection. The transverse deflection is assumed to satisfy the boundary condition. Shear deformation due to the soft core is taken into account in the strain energy calculation.

$$\frac{\partial}{\partial D_i}(U+V)=0 \tag{2-1}$$

where, D_i is the unknown displacements and i=1, 2, ..., n.

In the second method of analysis for sandwich panels, differential equations are set up in terms of bending, twisting and shearing stiffness in the x-and y-directions. The transverse deformation is regarded as the sum of two independent deformations, which are the bending deformation of the plate, U_{z1}, and the deformation associated with shear strain in the core, U_{z2}. The total curvatures and rate of twist of the plate from these two deformations are obtained by superimposing the two deformations as shown in equations (2-2a) to (2-2c). Three equilibrium equations about x-, y- and z- directions presented in equations (2-3a) to (2-3c) can be set up when the in-plane forces are constant throughout the plate. Substituting the bending and twisting moment from the differential equations into equilibrium equations (2-3a) and (2-3b) results in equations in terms of three unknowns, U_z, Q_x, and Q_y. Then, combined with equation (2-3c) to solve the unknown transverse deflection, shear forces.

$$\frac{\partial^2 U_z}{\partial x^2} = \frac{\partial^2 U_{z1}}{\partial x^2}+\frac{\partial^2 U_{z2}}{\partial x^2} = -\frac{M_x}{D_x}+\gamma_y\frac{M_y}{D_y}+\frac{1}{D_{Qx}}\frac{\partial Q_x}{\partial x} \tag{2-2a}$$

$$\frac{\partial^2 U_z}{\partial y^2} = \frac{\partial^2 U_{z1}}{\partial y^2}+\frac{\partial^2 U_{z2}}{\partial y^2} = -\frac{M_y}{D_y}+\gamma_x\frac{M_x}{D_x}+\frac{1}{D_{Qy}}\frac{\partial Q_y}{\partial y} \tag{2-2b}$$

$$\frac{\partial^2 U_z}{\partial x \partial y} = \frac{M_{xy}}{D_{xy}}+\frac{1}{2D_{Qx}}\frac{\partial Q_x}{\partial y}+\frac{1}{2D_{Qy}}\frac{\partial Q_y}{\partial x} \tag{2-2c}$$

$$\frac{\partial M_x}{\partial x} - \frac{\partial M_{xy}}{\partial y} - Q_x = 0 \tag{2-3a}$$

$$\frac{\partial M_y}{\partial y} - \frac{\partial M_{xy}}{\partial x} - Q_y = 0 \tag{2-3b}$$

$$\frac{\partial Q_x}{\partial x}+\frac{\partial Qy}{\partial y}+ q(x,y)+ P_x \frac{\partial^2 U_z}{\partial x^2}+ P_y \frac{\partial^2 U_z}{\partial y^2}+ P_{xy} \frac{\partial^2 U_z}{\partial x \partial y}= 0 \qquad (2\text{-}3c)$$

where, M_x, M_y, M_{xy} = Moments

P_x, P_y, P_{xy} = In-plane loads

q (x,y) = Lateral load

Q_x, Q_y = Shear forces

D_x, D_y, D_{xy} = Flexural rigidities of the sandwich panel

D_{Qx}, D_{Qy}, = Core shear stiffnesses

γ_x, γ_y, = Poisson's ratios

The strain and stress distributions of the sandwich panel can be derived from the displacements and the constitutive relationships. The axial buckling load and ultimate lateral load can be obtained based on the principle of minimum potential energy. The critical step in these two solutions is to assume a shape function that satisfies the boundary conditions. Both theories are all based on the small deflection assumption so that the classical bending theory can be applied to an isotropic plate.

Kim and Hughes (2004) have presented a closed-form analytical solution to solve sandwich panels with clamped edges under combined axial and lateral load. This method is based on the minimum potential strain energy principle. They used the displacement function expressed by equation (2-4) and the solution of clamped orthotropic rectangular plates presented by Mbakogu and Pavlovic. The small deflection and first order shear deformation deflection theory instead of large deflection theory are used.

$$U_z = \{x^2-\frac{w^2}{4}\}^2 \{y^2-\frac{L^2}{4}\}^2 \sum_{i=0}^{\infty}\sum_{j=0}^{\infty} a_{ij} x^i y^j \qquad (2\text{-}4)$$

This simple polynomial expression satisfies the clamped boundary conditions. By use of the principle of minimum potential energy, the stresses and strains at any point of the plate can be calculated. The ultimate strength of panel can also be obtained assuming that the ultimate limit state is reached at first yield. The material of core and steel plate is assumed isotropic and linear elastic in this analytical method.

The solutions presented here are based on small deflection. However, the small deflection theory will lose accuracy when the deflection is roughly equal to the thickness of the plate. Numerical procedures are required to develop a better behaviour understanding for the sandwich panel considering large deflections.

2.3 Behaviour of sandwich panels

2.3.1 Failure modes of the structural sandwich panels

Vinson (2005) discussed and analyzed failure modes of four types of sandwich panels under in-plane shear and compressive loads. Failure was defined as first yield in the steel plates. Two steel plates combined with a honeycomb, truss, web or solid foam core to form four conventional sandwich panels were included in the investigation. Different panel configurations showed different failure modes. Four failure modes were identified for the solid core sandwich panel, namely, yielding of the outer plates, overall buckling of the panel, core shear instability and face sheet wrinkling.

Sokolinsky and Frostig (1999) presented an investigation of face sheet wrinkling that can take place in sandwich panels with "soft" core under in-plane compression load. This mode of failure was found to take place when the modulus of elasticity and flexural rigidity of the core are about two or three orders of magnitude smaller than those of the face plate.

2.3.2 Global behaviour of sandwich panels

Martin and Murray (2005) performed a series tests to study the static and fatigue behaviour of sandwich plates. Sandwich panels 3000x9000 mm in size with the

configuration 6.4-38.1-6.4 (6.4 mm face plates with a 38.1 mm core) were tested under negative and positive bending. The test panel was supported with two beams, creating a simple span and two cantilevers. In the first test two wheel loads were applied, one on the cantilever portion and one between the two lines of support to create a negative moment in the panel. In the second test the panel was loaded with two wheel loads located in the simple span to create on positive moments. In the third test the wheels used for loading in the first two tests were replaced by bearing pads and two loads, applied in the same configuration as in the first elastic test, were increased up to 1156 kN, at which point linear elastic behaviour was still observed. The test results showed good correlation with finite element analysis results provided by Intelligent Engineering Limited. In addition to three static tests, fatigue tests were also conducted on sandwich panel welded connections. Based on the test results, the tested detail was found to follow the fatigue design curves for fatigue category E.

Little *et al.* (2007) tested three pairs of sandwich panels with fixed boundary under combined uniaxial compressive and uniform lateral load. Twin 5-32-5 panels were clamped together and water was pressurized between the two panels to apply a uniform lateral pressure. The twin panel assemblies were loaded in-plane in the direction of the long axis of the panels. Cyclic in-plane loading was applied in the elastic range to investigate the panel response under combined in-plane and out-of-plane loading. The in-plane load was then increased under constant lateral pressure until failure of the test specimens. Three lateral load levels, namely, 13%, 27% and 45% of the expected plastic collapse pressure were used for three tests on identical pairs of sandwich panels. The tests were conducted to derive an interaction diagram for sandwich panels. Tests were terminated either because of excessive loss of pressure due to water leakage or excessive in-plane deformation. No obvious failure mode such as delamination or local face buckling was observed during the tests.

Harris (2007) investigated the global behaviours of sandwich plate system (SPS) bridge deck by comparing the field test results on the Shenley Bridge and

numerical results. The Shenley Bridge, located in Saint-Martin, Quebec, was built in 2003. It is a single span bridge with a SPS deck supported by three parallel girders. The critical design parameters such as lateral load distribution factor, dynamic load allowance and bridge deck design procedures were studied to develop the design approach for SPS bridge decks. It was concluded that the lateral load distribution factors of SPS deck are larger than that of the equivalent steel-concrete deck. But that difference has no significant effect on the girder design except larger stresses with the girders for the same design. It was found that AASHTO LRFD provisions can be used to determine the lateral load distribution behaviour of the bridge with a sandwich plate deck. The lateral load distribution characteristics of SPS bridge decks were found to be similar to those of reinforced concrete decks. The simple lever rule was found to be conservative for all the cases investigated.

2.4 Applications of sandwich panels

The two-lane Shenley Bridge with simple span of 22 m and width of 7 m was constructed in Quebec in 2003. The bridge deck consists of ten sandwich panels supported by three longitudinal girders. The connection adopted between two sandwich panels is illustrated in figure 2.1 and the connection of the sandwich panel and girders is shown in figure 2.2. Static and dynamic field tests were conducted for the evaluation of SPS technology applied in bridge structures (Harris, 2007). The field test results showed good correlation with numerical analysis results. A total of 20 strain gauges were distributed at different locations of the girders and angles. A good agreement between the measured and predicted strains through the section of the girder was obtained.

Most applications of the sandwich plate system have been as overlays for strengthening of existing orthotropic decks (bridges and ships). An example of such applications is the overlay for rehabilitating the orthotropic fatigue-damaged bridge deck in Thyssen-Krupp Stahlbau, Germany (Kennedy *et al.*, 2006). The maximum stress range was reduced to 30% of original magnitude when the

sandwich panels applied on the existing all-steel orthotropic deck. The maximum transverse deck curvatures are reduced by 12 times.

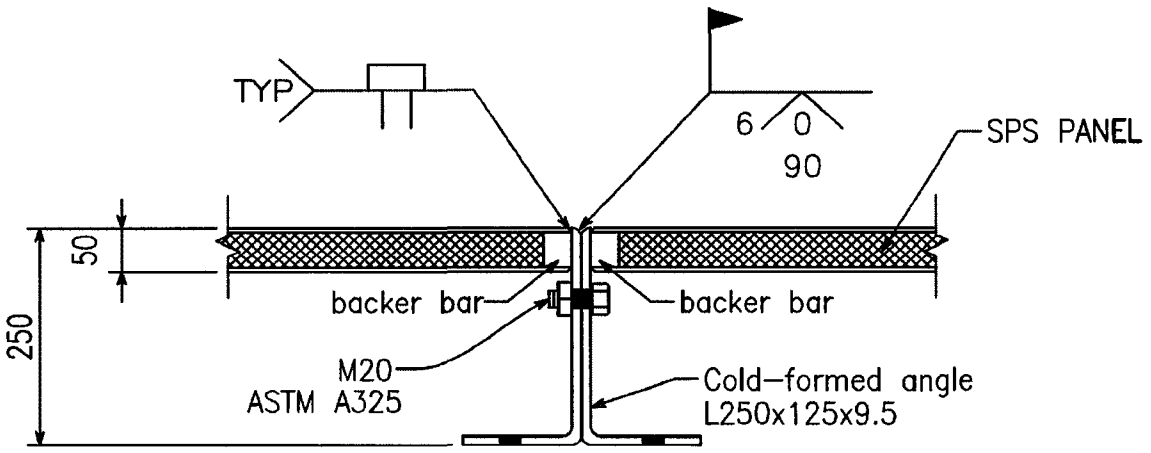

Figure 2.1 Connection of two sandwich plate system panels

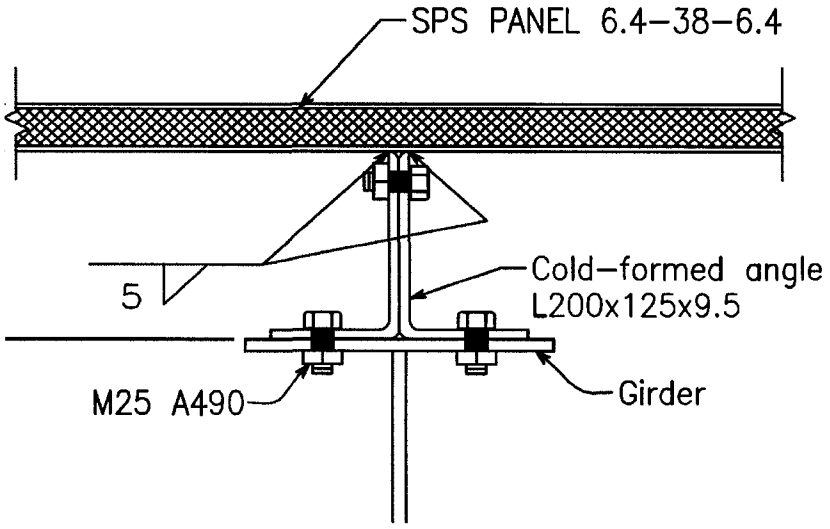

Figure 2.2 Connection of sandwich plate system panel to girder

Chapter 3

Model Validation

3.1 Introduction

Little *et al.* (2007) tested three sets of large scale sandwich panels under combine uniaxial compression and out-of-plane uniform pressure. The test specimens consisted of a pair of panels tested back-to-back, with a space between the two panels filled with pressurized water to generate the out-of-plane pressure. The panels were clamped together around their perimeter to prevent rotation. Figure 3.1 shows a section through an unloaded edge clamp (section A-A) of the test specimen. Rollers between the panels and boundary clamps were used to allow free shortening of the test panels during in-plane loading. Similar boundary conditions were used along the loaded edges, except that roller were not provided along these edges. Pretensioned high strength bolts were used to clamp the edged to prevent rotation around the boundaries.

Two different finite element models of the sandwich panel specimens were developed using the general-purpose finite element software ANSYS. One model used rotationally fixed boundary conditions around the perimeter of the panel and the other model used flexible unloaded edge restraints consisting of in-plane spring elements at the unloaded edges to provide lateral restraint while allowing free in-plane expansion at two unloaded edges in test.

Two other finite element models will be developed in this chapter. The out-of-plane spring elements at the unloaded edges are introduced to figure out the bending stiffness of the edge plates in the test specimens used for clamping two sandwich panels at unloaded edges. Total four FE models shown in figure 3.2 and 3.5 will be analyzed by ANSYS and compared with the test results presented by Little *et al.* (2007).

The panel dimensions, element types, material properties, loading cases, boundary conditions as well as results from finite element analysis will be demonstrated in this chapter.

3.2 Geometry

Finite element models FEA1 and FEA2, shown in figures 3.2 and 3.3 use a 1200x1800 mm panel made of 5 mm steel face plates and a 32 mm elastomer core as tested by Little *et al.* (2007). The in-plane dimensions correspond to the clear dimensions between the boundary restraints as reported by Little *et al.* (2007). For models FEA3 and FEA4 shown in figures 3.4 and 3.5 respectively, the panel width was increased to 1470 mm, which corresponds to the full width of the panels tested by Little *et al* (2007). The out-of-plane displacement (z-displacement) was prevented along the length of the panel at 135 mm from each unloaded edges. The partial rotational restraint was provided by springs in the z-direction attached to all the face nodes within 135 mm strips along the edges.

3.3 Element Type

SOLID 45 from ANSYS is used to model the steel face plates and the elastomer core. The face plates were modeled using one layer of solid elements through the thickness and the core was modeled with four layers of solid elements. The SOLID 45 element has plasticity, creep, swelling, stress stiffening, large deflection, and large strain capabilities. The solid element is defined by eight nodes with three orthogonal translational degrees of freedom at each node. Full rotational restraint along the panel edges can be obtained by constraining the lateral (x-) displacement at all edge nodes through the panel thickness. This is performed by using the command CP in ANSYS,

COMBIN14 has longitudinal or torsional capability in 1-D, 2-D, or 3-D applications. The longitudinal spring-damper option is a uniaxial tension-compression element with up to three degrees of freedom at each node: translations in the nodal x, y, and z directions. The element is defined by two

nodes, a spring constant K in force/length and damping coefficients (cv)1 and (cv)2. The damping capability is not used for static or undamped modal analyses.

Figure 3.2 to figure 3.5 display the number of nodes and elements for each finite element model from FEA1 to FEA 4.

3.4 Material properties

Figure 3.6 shows the real strain-stress curves of the steel and elastomer. Table 3.1 and table 3.2 list the points to define the curve of strain and stress of the steel and elastomer. Strains in the tables refer the total elastic and plastic strains. The properties of the steel plates including density, elastic modulus, Poisson's ratio, and tensile yield strength are obtained from tension coupon test done by Little *et al.* (2007). The properties of the elastomer core were obtained from test results provided by Intelligent Engineering Limited. Table 3.3 lists the mechanical properties of the steel and elastomer used in the finite element models. The elastomer yield strength of 18 MPa listed in table 3.3 is the compression strength at room temperature.

The spring stiffness is expressed by a spring constant K in units of force/length. K_x represents the stiffness of the lateral springs at the unloaded edges. It is estimated by the adhesive shear stiffness and glued contact area between the edge spacer bar and SPS panel, and 400 N/mm was used in Little's FE models corresponding to the mesh size of 24x24. The out-of-plane springs are labelled by K_z varied from 10^{-6} N/mm to 10^{6} N/mm corresponding to the free or clamped boundary conditions at unloaded edges.

3.5 Mesh convergence

Finite element model FEA1 shown in figure 3.2 is analyzed with two mesh sizes, namely, 20x20 and 24x24 to check for convergence of the finite element results. The number of nodes and elements for these two finite element models are listed in table 3.4. Two models are first loaded with a lateral uniform pressure of

415 kPa, followed by an in-plane deflection, U_y , from zero to 40 mm while keeping the lateral pressure of 415 kPa constant. Figures 3.7 shows the normalized axial compressive load, P/P_y , versus the in-plane deflection, U_y and the normalized axial load versus the out-of-plane deflection at panel centre, U_z , is displayed in figure 3.8. The axial compressive load P_y is the axial force to yield the sandwich panel fully (the axial load capacity from the elastomer core is neglected in this calculation). The same load versus deformation behaviour was for both mesh densities, indicating that the 20x20 mesh size has reached convergence. Table 3.4 lists the ultimate axial load P_u obtained from the finite element analysis, in-plane deflection U_y and out-of-plane deflection at panel centre U_z at the ultimate axial load.

3.6 Boundary conditions

The finite element model illustrated in Figure 3.2 consists of a panel with rotationally fixed boundaries around the perimeter of the panel. The finite element model shown in Figure 3.3 has rotationally fixed supports all around the perimeter, no lateral expansion at the loaded ends and restrained expansion along the two unloaded edges, which results from the friction between the unloaded edge clamps and the panels. The restraints are provided by lateral springs. A spring stiffness K_x of 333 N/mm for the model with a mesh size of 20x20 is equivalent to 400 N/mm used in the model with a mesh size of 24x24. The finite element model illustrated in Figure 3.4 has rotationally restrained unloaded edges with free lateral expansion. Finally, the finite element model illustrated in figure 3.5 has rotationally restrained unloaded edges with in-plane springs to restrain the lateral expansion of the plate. The partial rotational restraints along the unloaded edges were modeled by preventing out-of-plane displacement of the nodes on one face of the panel along lines 135 mm from the unloaded edges, thus forming hinge lines parallel to the unloaded edges. The rotational restraint about these hinge lines was provided by out-of-plane springs

placed at seven rows of nodes between the hinge lines and the unloaded edges. These springs were used to model the possible flexibility of the edge clamps used in the test program of Little *et al.* (2007). The fixed rotation at two unloaded edges can be achieved by increasing extremely the stiffness of out-of-plane springs K_z, and also the free boundary can be obtained by reducing the spring-stiffness K_z close to zero. The in-plane unloaded edge restraints were used to model possible edge restraints resulting from friction between the edge clamps and the tested panels.

3.7 Loading

Little *et al.* (2007) tested three identical sandwich panel sets under three combined in-plane and lateral load. The interaction diagram of the sandwich panel 1200x1800 with the configuration of 5-32-5 was obtained. For each panel, the uniform lateral pressure q was first applied, followed by the axial compressive load from zero until panel failure while maintaining the lateral load as constant. The specimens were tested under three lateral load levels of 13% q_c, 27% q_c, and 45% q_c. The plastic collapse load q_c is calculated based on the yield line theory. The collapse mechanism used for the rectangular panel is shown in figure 3.9 and the plastic collapse load q_c of 1550 kPa is obtained for the clamped sandwich panel 1200x1800 with the configuration of 5-32-5. The bending stiffness of the elastomer core is ignored because the elastic modulus of elastomer is much less than that of steel (Ec/Es =0.4%). The three loading cases investigated are as follows:

a) Lateral pressure corresponding to 13% of the plastic collapse pressure (207 kPa) is applied first and maintained constant while the in-plane load is applied until panel failure;

b) Lateral pressure corresponding to 27% of the plastic collapse pressure (415 kPa), followed by in-plane loading until panel failure;

c) Lateral pressure corresponding to 45% of the plastic collapse pressure

(690 kPa), followed by in-plane loading until panel failure;

3.8 FEA results

Numerical results of four FE models shown in figures 3.2 to 3.5 will be compared with the test results presented by Little *et al.* (2007).

3.8.1 Combined lateral pressure of 207 kPa and axial compressive load

An in-plane deflection of 40 mm was applied for models FEA1 and FEA2 compared to 50 mm for the test specimens. However, only 20 mm was applied to FEA3 and FEA4 because of convergence problems. The lateral spring stiffness K_x of 333 N/mm was used in FEA 2 and FEA 4. The out-of-plane spring stiffness K_z of 10^6 N/mm was used in FEA 3 and FEA 4.

Figure 3.10 displays the normalized axial compressive force versus in-plane deflections from four FE models and the test result. The load deformation curves obtained from all four FE models are very close together throughout the loading process. The test curve starts to deviate from a straight line at an in-plane deflection of 2.3 mm and a normalized axial load P/P_y of 0.75. The panel yield capacity P_y is 4224 kN for a 1200x1800 mm panel and 5174 kN for a 1470x1800 mm panel. Once again, the compression contribution from the elastomer core is neglected. In the absence of a distinct peak load in the figure, the 0.5% strain load (ASTM A370-07a) is used to define the axial load capacity of the panels. Therefore, the axial load capacity obtained from the finite element models is $1.05\,P_y$, compared to $1.1\,P_y$ for the test specimen. The axial load capacity of the test specimen is slightly higher than predicted by the finite element models partly because of friction developed between the rollers used between the sandwich panel and outer clamp bars in the test specimens.

Figure 3.11 shows the normalized axial loads, P/P_y, versus out-of-plane deflections at the centre of the panel. The out-of-plane deflections under the uniform lateral pressure of 207 kPa are slightly different for the various finite

element models. An out-of-plane deflection of 3.4 mm is obtained from FEA1 and FEA2 while a value of 4.4 mm is obtained from FEA3 and FEA4. The out-of-plane deflection of 3.6 mm from the test specimen is close to the first two FE models, which indicates that the test boundary condition was close to perfectly rigid. The out-of-plane deflections increased to 8.5 mm for FEA1 and FEA2 and to 16 mm for FEA3 and FEA4 by the time the finite element models reached the axial load capacity of $1.05P_y$. The out-of-plane deflection of the test specimen reached to 10 mm and started to deflect in the opposite direction. Figure 3.12 displays the out-of-plane deflection along the centreline of the panel at various load levels from the model FEA 1. The deformed shape of the panel changes from half wave to three and half wave after the axial load capacity of $1.05P_y$, which is similar behaviour to that observed from the test specimen.

3.8.2 Combined lateral pressure of 415 kPa and axial compressive load

3.8.2.1 Results from four finite element models and test

The four FE models were loaded with a uniform lateral pressure of 415 kPa combined with in-plane deflection of 40 mm. The overall behaviour of the panels evaluated by in-plane deflection and out-of-plane deflection at the centre of the panel are represented in figures 3.13 and 3.14, respectively. The test result for this loading condition is also displayed in the figures.

The load versus in-plane deflection curves shown in figure 3.13 show linear behaviour of the finite element models and test specimen up to a load of 0.6 P_y (in-plane deflection of 2.0 mm). The test curve shows a more rapid loss of stiffness than the finite element models. The model FEA4 displays the largest axial stiffness compared to the other models and the test specimen. No peak axial load was observed from the four models and test specimen for this load case. Once again the axial load capacity is defined as the load at 0.5% strain, which corresponds to 1.01 P_y for FEA1, FEA2 and FEA4 while 0.97 P_y for FEA3. The test specimen showed a capacity at 0.5% strain of 1.02 P_y, which

demonstrates that the finite element analysis results are in very good agreement with the test result.

Figure 3.14 displays the normalized axial compressive load, P/P_y, versus out-of-plane deflections at the centre of the panel. Under a lateral pressure of 415 kPa, FEA3 has the largest out-of-plane deflection of 9.1 mm compared to 7.9 mm for FEA4, 7.4 mm for the test specimen and 7.0 mm for both FEA1 and FEA2.

3.8.2.2 FEA 3 with various K_z

Figures 3.15 and 3.16 display the in-plane and out-of-plane deflections for finite element model FEA 3 with various spring stiffness K_z values from 10^{-6} to 10^6 N/mm. Figure 3.15 indicates that the initial panel behaviour is not affected by the out-of-plane spring stiffness. However, the plate capacity is found to increase as the spring stiffness increases, reaching a capacity very close to the test capacity as the stiffness approaches infinity (model FEA1). Once again, it is observed that the test boundary condition seems to be very close to fully rigid boundary condition.

The out-of-plane deflection curves shown in Figure 3.16 show a similar effect of spring stiffness values. The models with the smallest spring stiffness show larger out-of-plane deflections. The test specimen agrees closely with model FEA 1, which is fully rigid around the panel perimeter.

3.8.2.3 FEA 4 with various K_z

Figures 3.17 and 3.18 display the in-plane and out-of-plane deflections for FEA 4 for values of K_z varying from 1 to 10^6 N/mm and a value of K_x of 333 N/mm for each panel. Deflections from the finite element model with fixed boundary conditions, FEA1, and test results are also shown in the figures for comparison. The figures show that the out-of-plane spring stiffness, K_z, has no significant effect on in-plane and out-of-plane deflection curves when lateral springs K_x are

applied simultaneously at the unloaded edged of the sandwich panel. The axial load capacity reaches about 1.01 P_y for FEA 4 compared to 1.02 P_y for FEA 1 and the test specimen. The out-of-plane deflection at the lateral pressure of 415 kPa is very close for all the finite element models, namely, 7.1 mm from FEA1, 8.0 mm from FEA 4 and 7.4 mm from the test results. The out-of-plane deflection increased to around 20 mm at the lateral load capacity from FEA 4 and 23 mm from test results.

3.8.2.4 Summary of FE models under lateral load of 415 kPa

Figure 3.19 presents four curves of normalized axial load versus in-plane deflection, namely, one for FEA1 (rotationally fixed around the perimeter of the panel), one for FEA 4 with both $K_z = 10^6$ N/mm and K_x = 333 N/mm, FEA 3 with K_z = 1 N/mm, and the test result. It is found that the curves from FEA1, FEA4 and test result agree very well. However, the curve from FEA3 with K_z = 1 N/mm is quite different from the other three. FEA 3 has a capacity of 0.9 P_y compared to 1.0 P_y from the other three curves.

Figure 3.20 shows the out-of-plane deflections at the panel centre point. At the end of the lateral pressure step, FEA 3 has the largest out-of-plane deflection of 11 mm compared to 7~8 mm for other three curves. FEA3 also has the largest out-of-plane deflections under the same axial compressive load.

The finite element model FEA4 with both in-plane and out-of-plane springs along the unloaded edges is the model that provides the best prediction of the test results.

3.8.3 Combined lateral pressure of 690 kPa and axial compressive load

Figure 3.21 and figure 3.22 show the normalized axial load versus in-plane and out-of-plane deflections for four finite element models and test results for a lateral pressure of 690 kPa. The in-plane spring stiffness for models FEA2 and FEA4 is taken as 333 N/mm and the out-of-plane spring stiffness K_z of 10^6 N/mm is used

for the models FEA3 and FEA 4. All the predictions and the test results are similar. The models FEA 1 and FEA 2 reached their axial load capacity, load at 0.5% strain, of 0.88 P_y at an in-plane deflection of 6.4 mm. FEA3 and FEA 4 reached their capacity of 0.86 P_y at 6.0 mm. However, the axial load capacity of the test specimens is 0.89 P_y at an in-plane deflection of 9 mm. Under the lateral pressure of 690 kPa, the out-of-plane deflection reached 12.4 mm for FEA 1, 11.9 mm for FEA 2, 13.1 mm for FEA 3 and FEA 4 compared to 12.8 mm for the test specimen.

The excellent agreement between the test results and the finite element analysis results demonstrates that the finite element method can be used to predict the true behaviour of sandwich panels.

Table 3.1 Points defining the stress vs. strain curve for steel

Steel			
Strain (mm)	Stress (MPa)	Strain (mm)	Stress (MPa)
0.00176	352	0.15	575
0.015	358	0.16	582
0.02	378	0.17	590
0.03	419	0.18	597
0.04	440	0.19	601
0.05	460	0.20	609
0.06	480	0.30	655
0.07	498	0.40	702
0.08	510	0.50	750
0.09	522	0.60	798
0.10	532	0.70	848
0.11	542	0.80	898
0.12	550	0.90	945
0.13	559	0.98	982
0.14	567		

Table 3.2 Points defining the stress vs. strain curve for Elastomer

Elastomer			
Strain (mm)	Stress (MPa)	Strain (mm)	Stress (MPa)
0.021	18	0.13	36
0.03	20	0.20	40
0.04	23	0.30	44
0.05	29	0.40	49
0.06	29	0.50	51
0.07	31	0.60	57
0.08	31	0.70	60
0.09	31	0.80	64
0.10	31	0.90	69
0.11	31	0.98	71
0.12	31		

Table 3.3 Material Properties

Properties	Steel	Elastomer
Modulus elasticity (MPa)	199000	860
Yield Strength (MPa)	352	18
Density (kg/m^3)	7850	1150
Poisson's ratio	0.3	0.36

Table 3.4 FE models with two mesh density

	FE Model with 20x20	FE Model with 24x24
Node	19747	13832
Element	16200	11250
q (kPa)	415	415
P_u (kN)	4310	4316
U_y (mm)	26	27
U_z (mm)	68	72

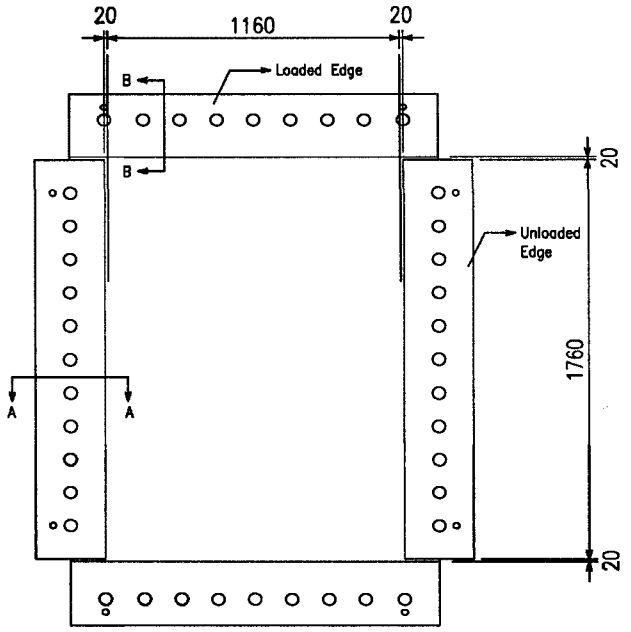

(a) Overall View of Test Specimen

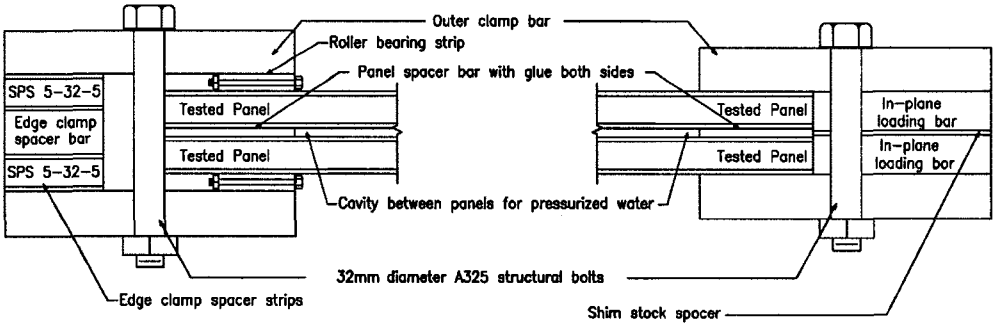

(b) Sections Through Panel Edges

Figure 3.1 Edge Clamp of Test Specimen

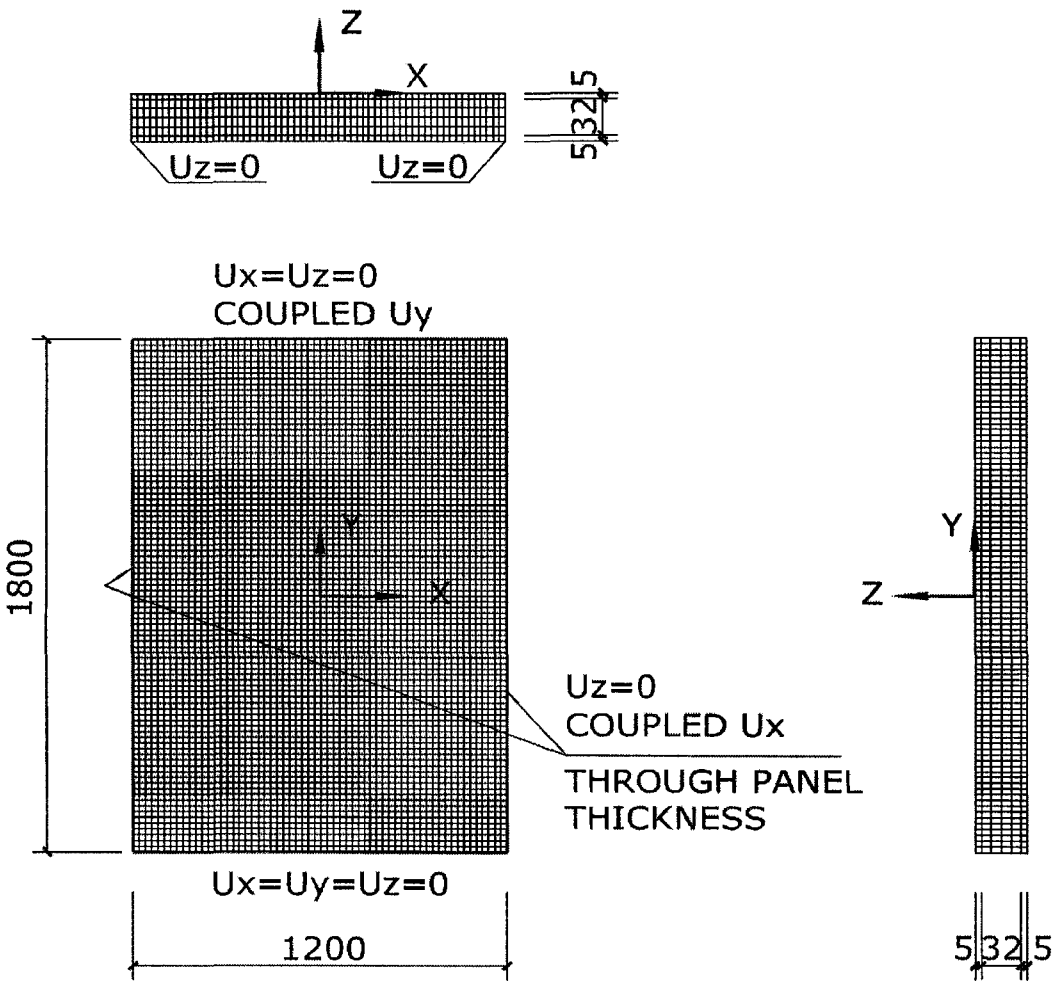

Number of nodes: 19747
Number of elements: 16200
Element type: Steel: SOLID 45
Elastomer: SOLID 45

Figure 3.2 FEA1 — Finite element model with rotationally fixed boundary conditions

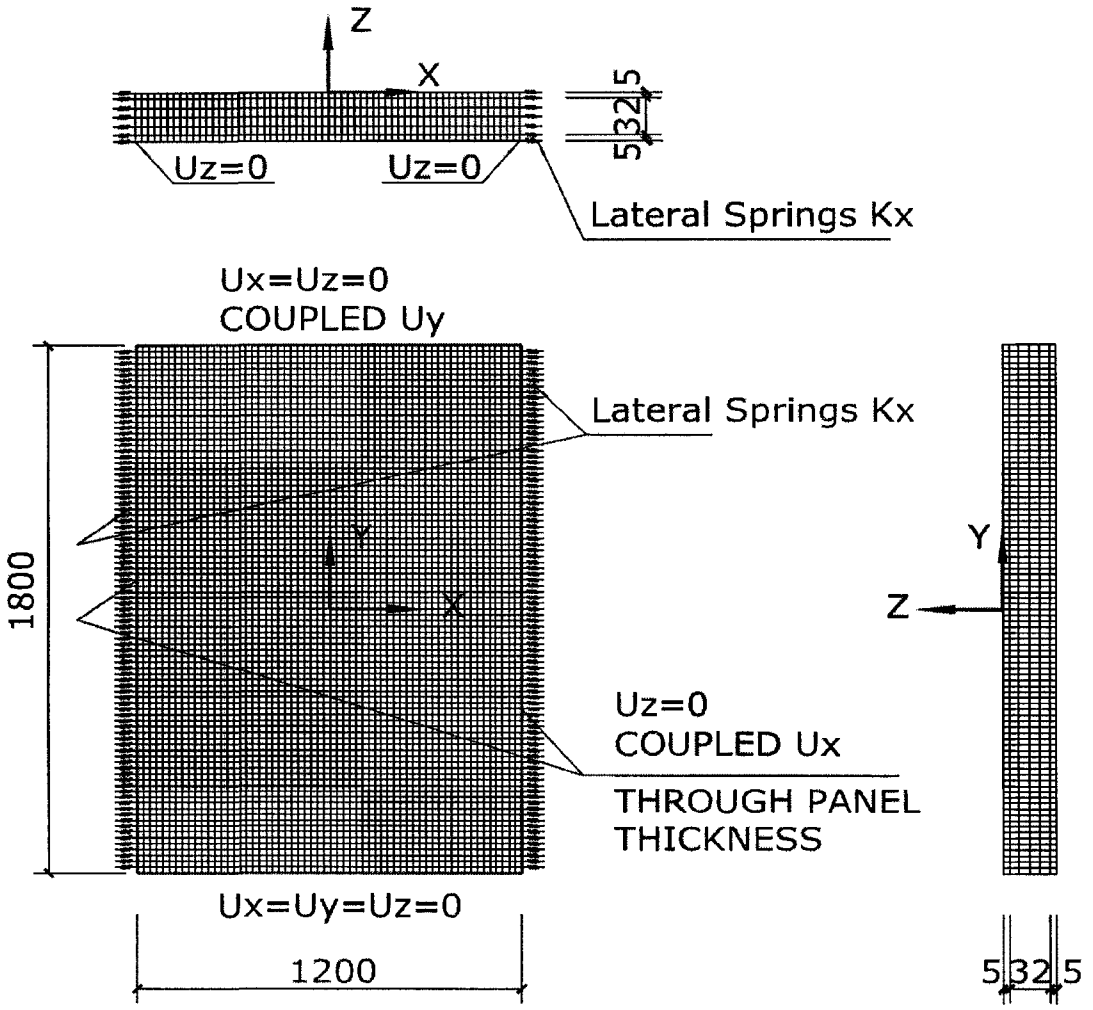

Number of nodes: 20384
Number of elements: 16837
Element type: Steel: SOLID 45
Elastomer: SOLID 45
Lateral Spring: COMBIN 14

Figure 3.3 FEA2 — Finite element model with flexible in-plane restraints along the unloaded edges

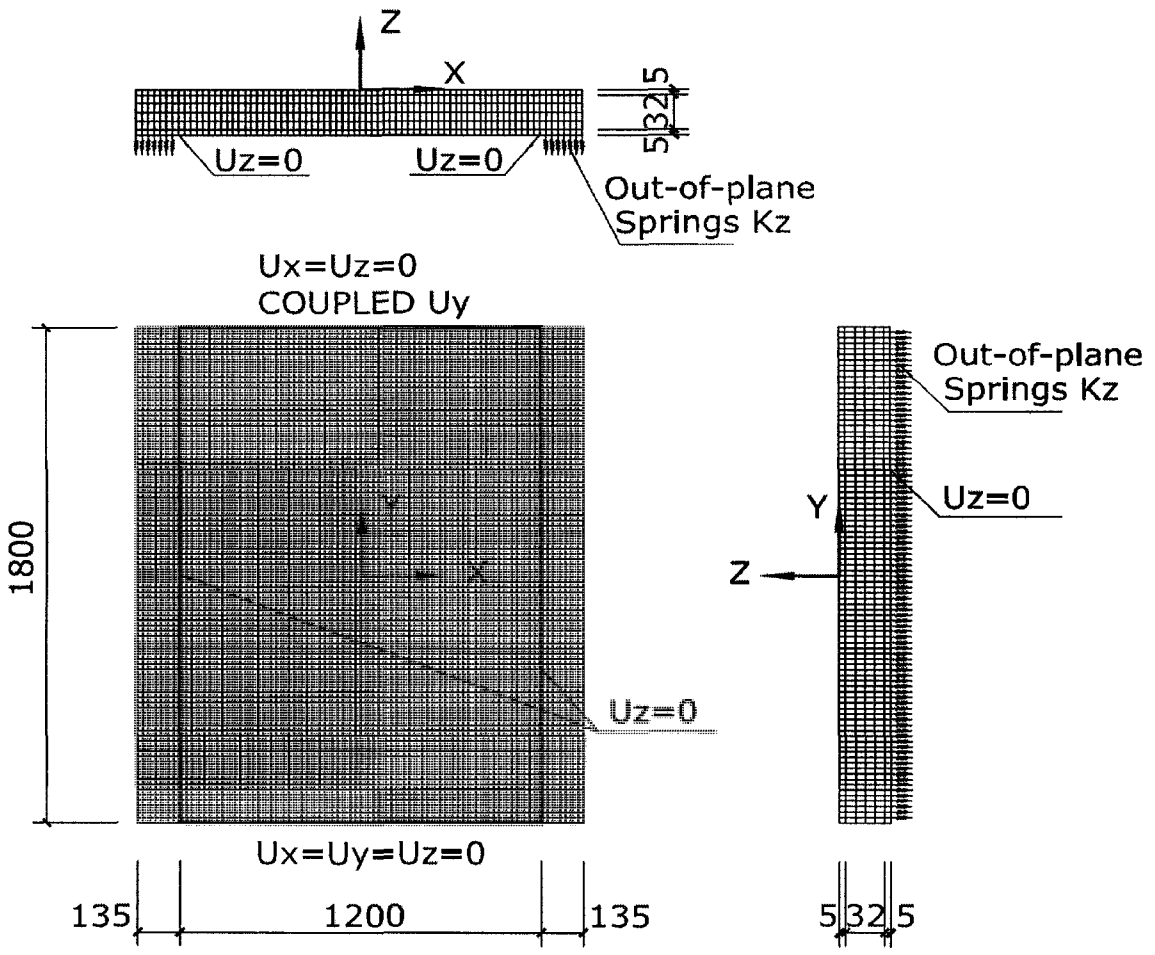

Number of nodes: 24934
Number of elements: 20603
Element type: Steel: SOLID 45
Elastomer: SOLID 45
Out-of-plane Spring: COMBIN 14

Figure 3.4 FEA3 — Finite element model with out-of-plane springs at the unloaded edges

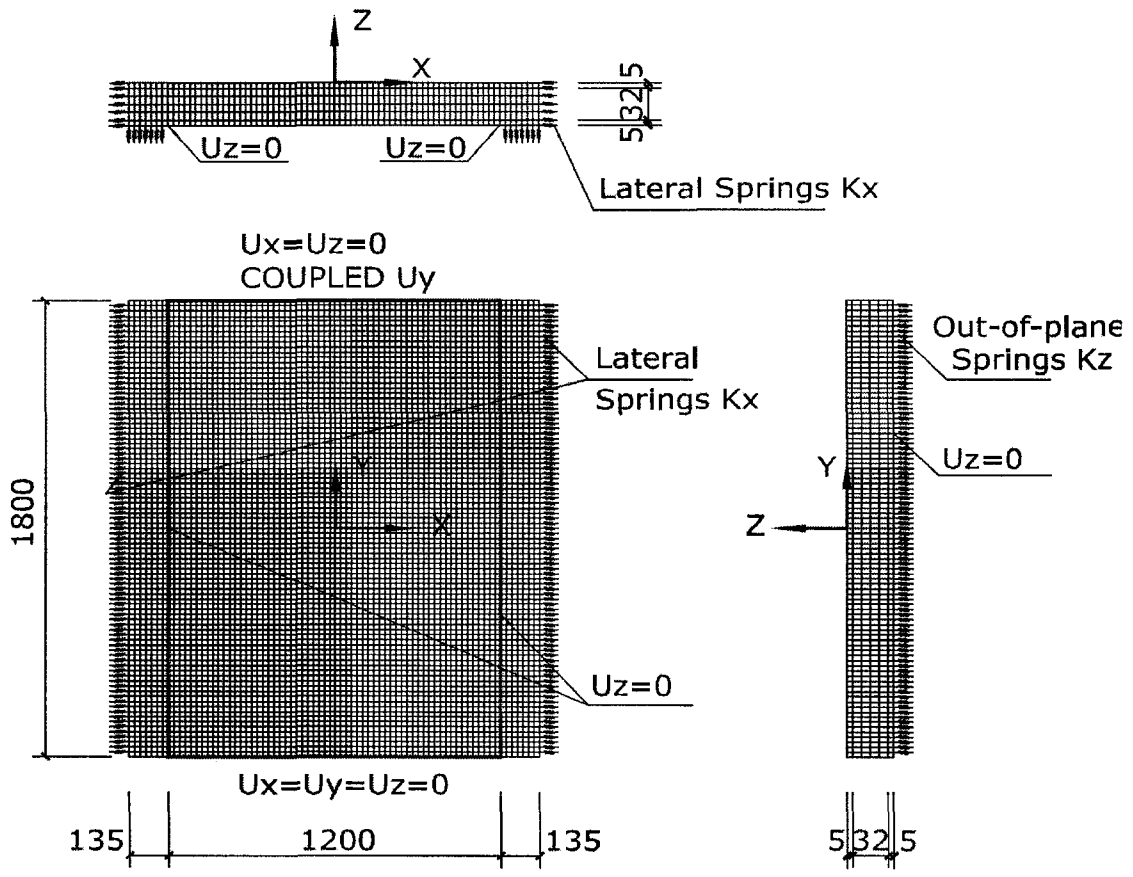

Number of nodes: 25646
Number of elements: 21226
Element type: Steel: SOLID 45
Elastomer: SOLID 45
Lateral Spring: COMBIN 14
Out-of-plane Spring: COMBIN 14

Figure 3.5 FEA 4 — Finite element model with both lateral and out-of-plane springs at unloaded edges

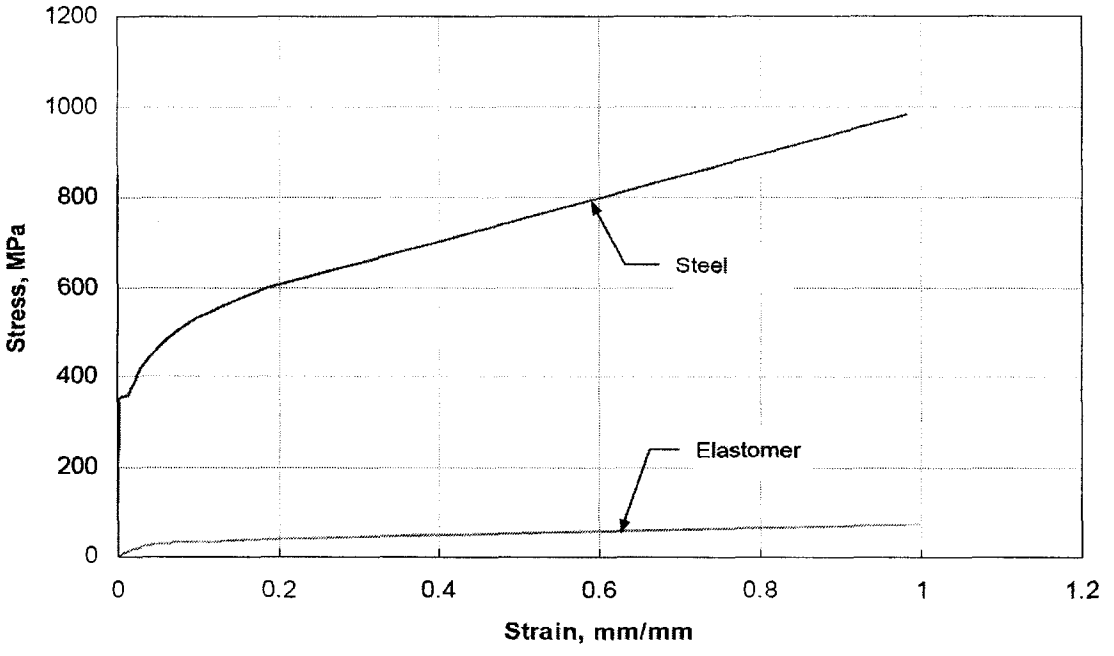

Figure 3.6 Steel and Elastomer Stress vs. Strain curves used in the Analysis

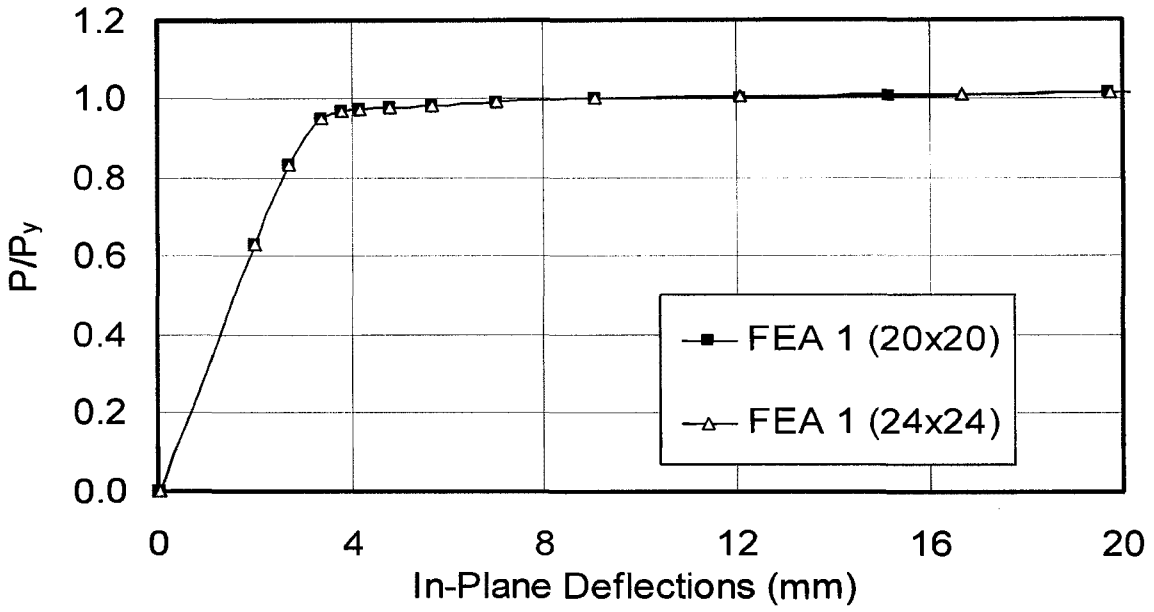

Figure 3.7 In-plane deflections from FEA1 with two mesh sizes

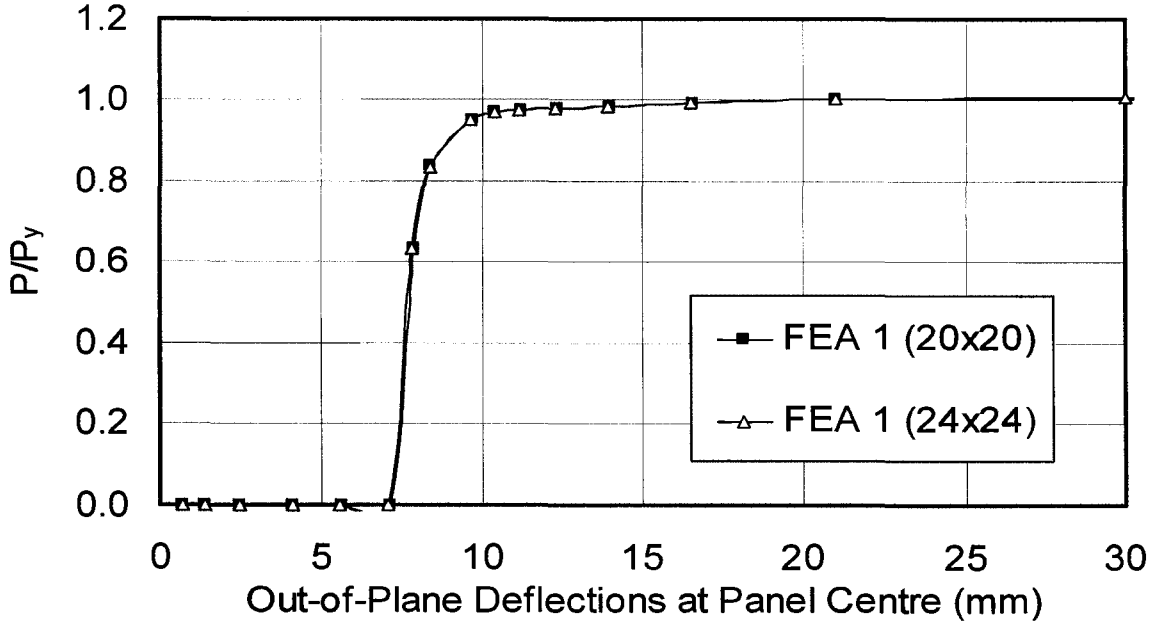

Figure 3.8 Out-of-plane deflections from FEA1 with two mesh sizes

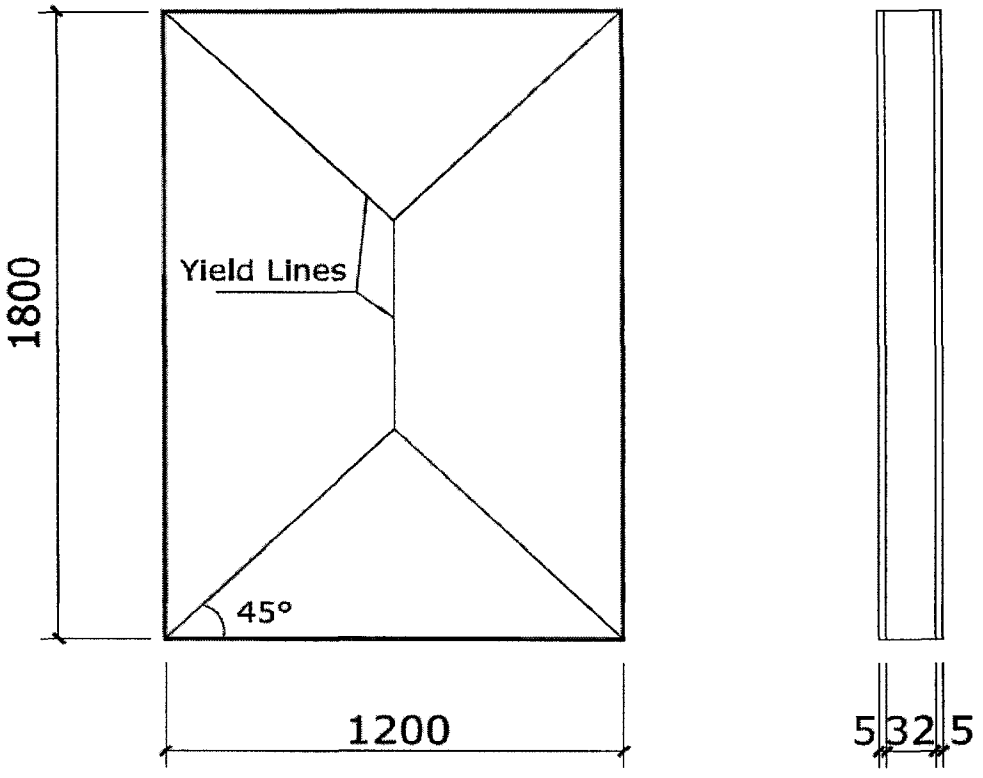

Figure 3.9 Yield line pattern for sandwich panel

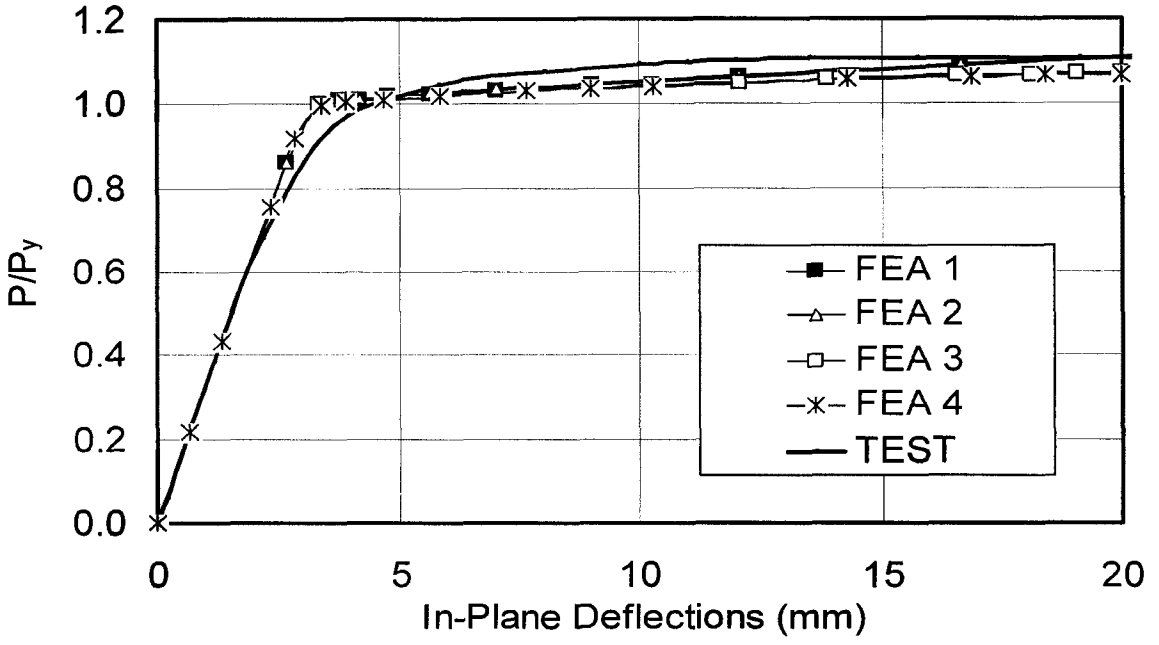

Figure 3.10 In-plane deflections from four FE models and test results for $q/q_c = 0.13$

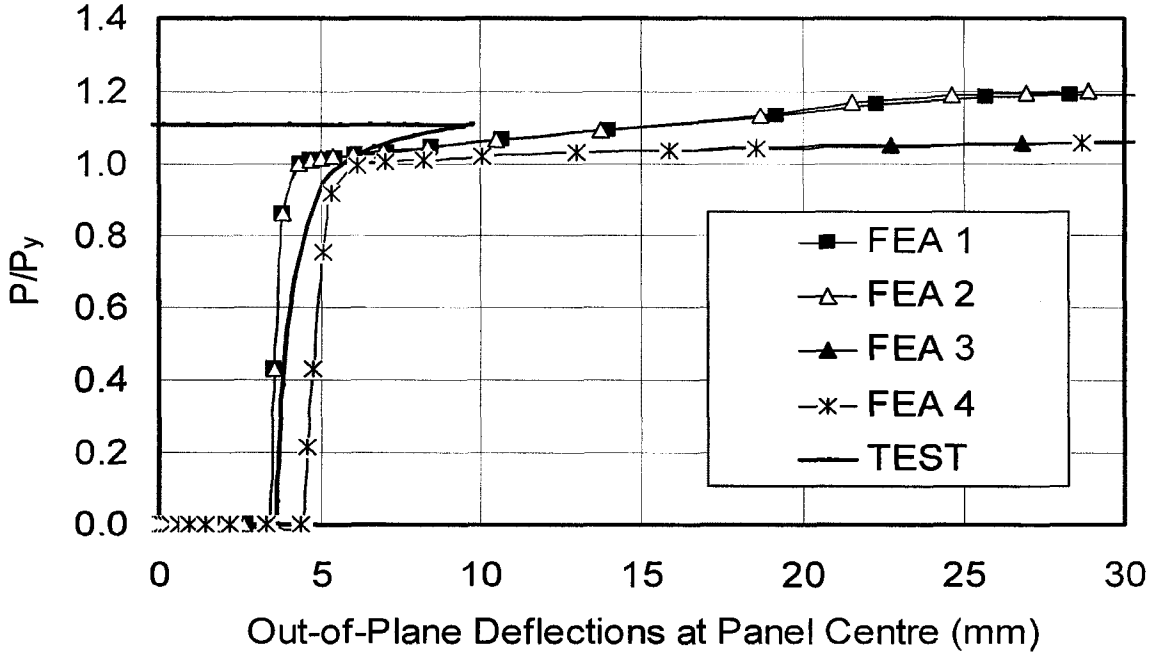

Figure 3.11 Out-of-plane deflections from four FE models and test results for $q/q_c = 0.13$

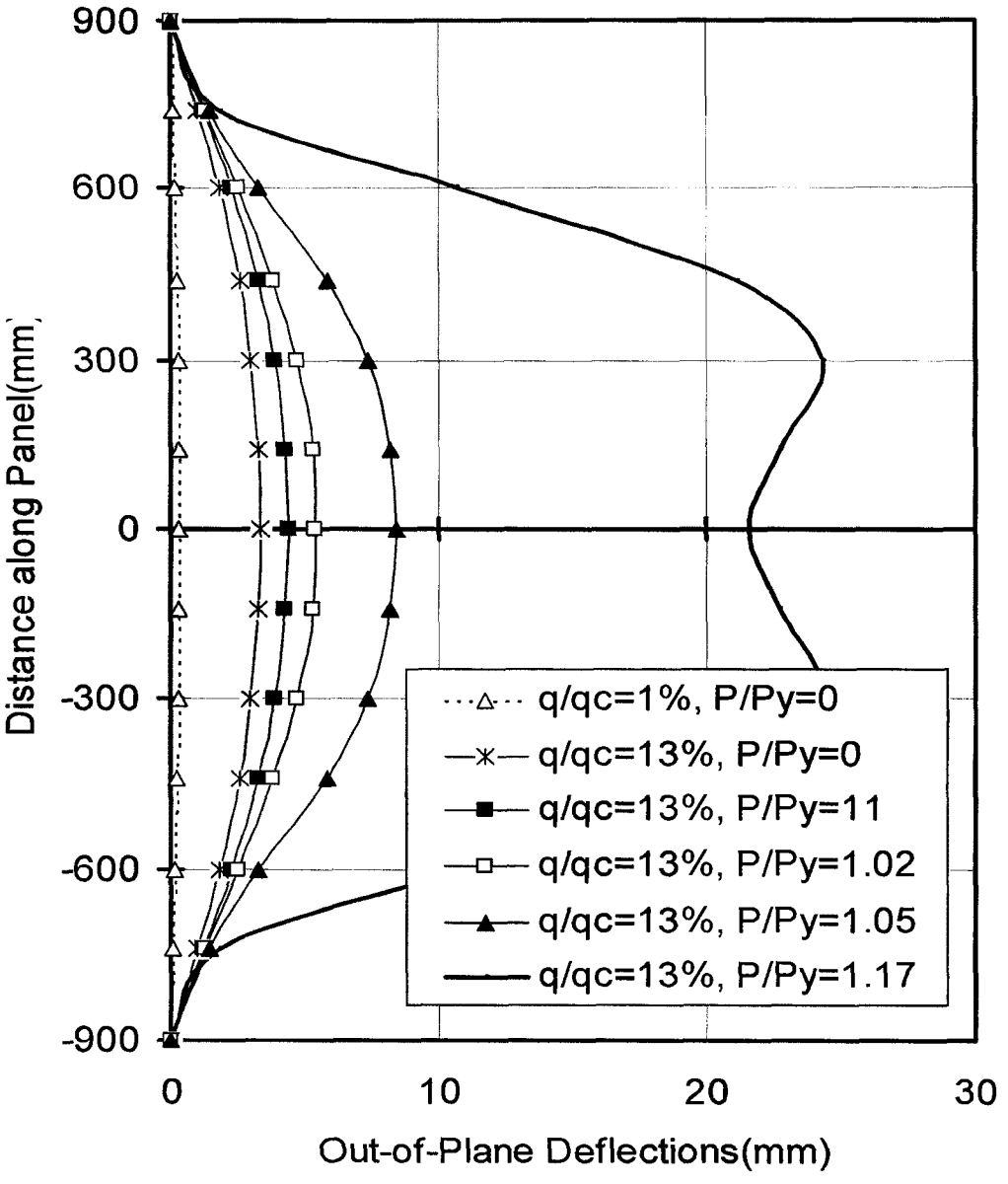

Figure 3.12 Out-of-plane deflections along the panel centreline as predicted by the finite element model FEA1 for $q/q_c = 0.13$

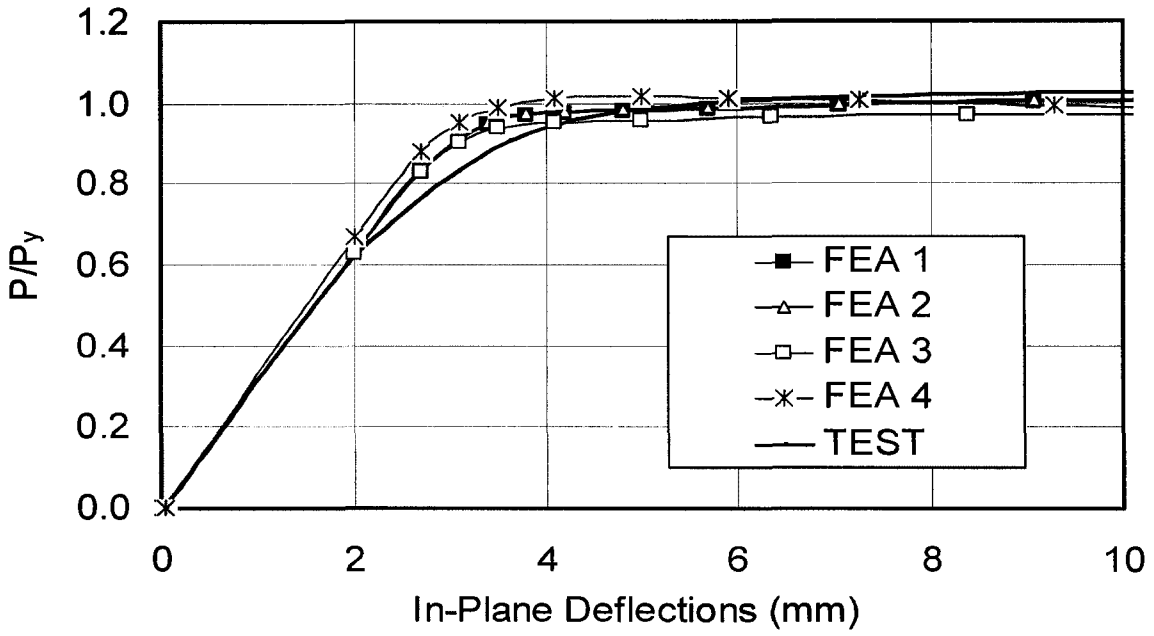

Figure 3.13 In-plane deflections from four FE models and test results for $q/q_c = 0.27$

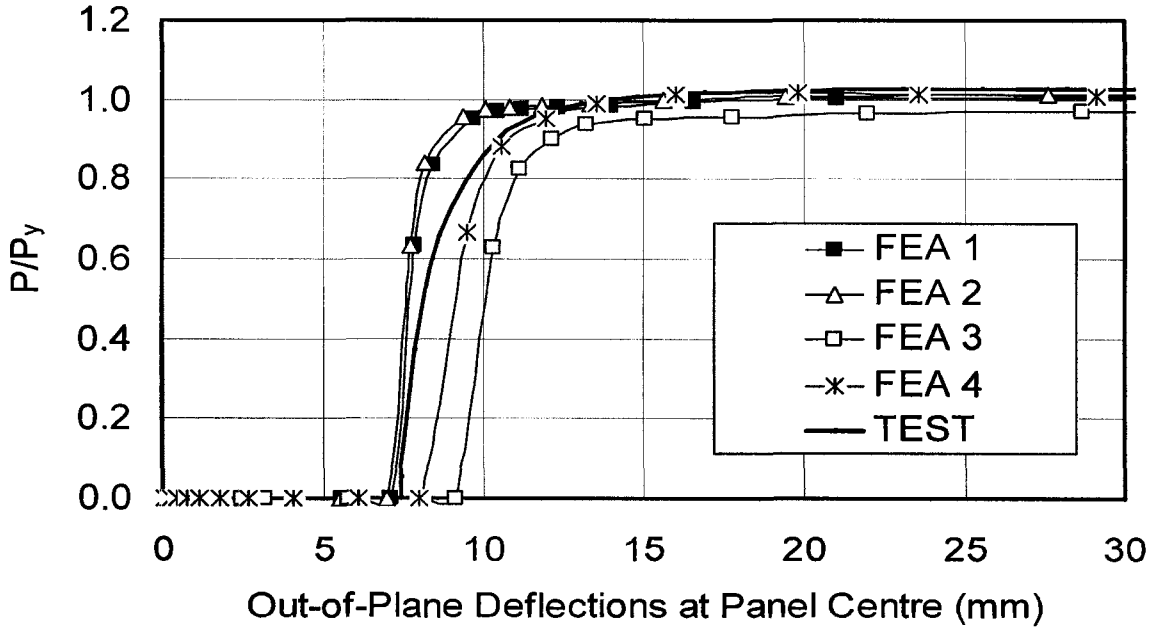

Figure 3.14 Out-of-plane deflections from four FE models and test results for $q/q_c = 0.27$

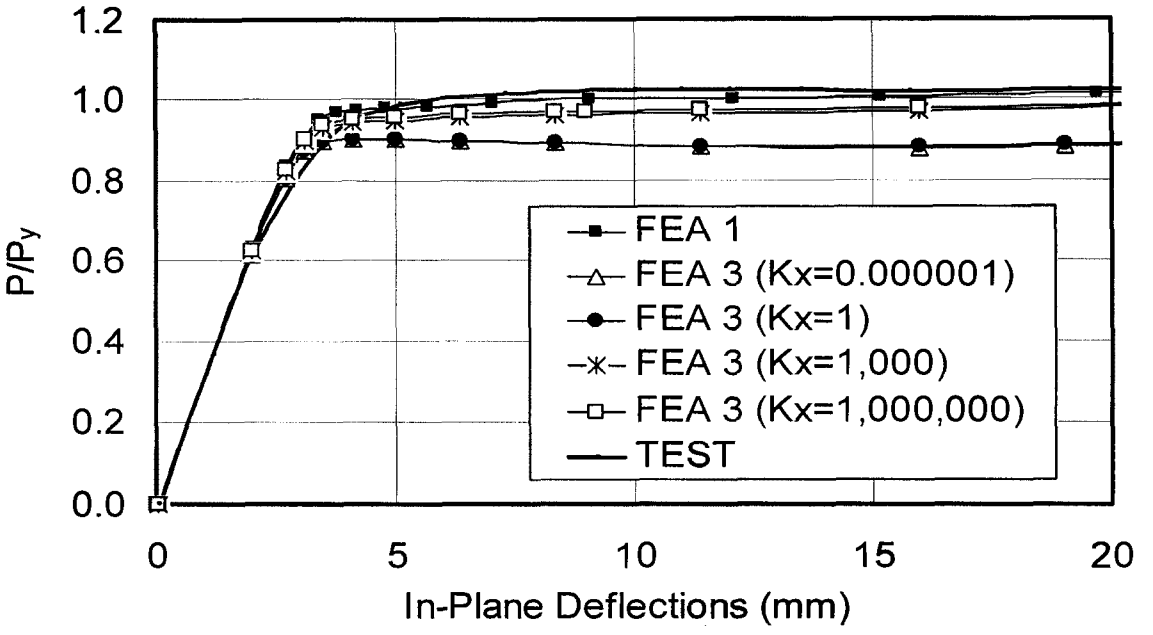

Figure 3.15 In-plane deflections from FEA 3 with various in-plane spring stiffness

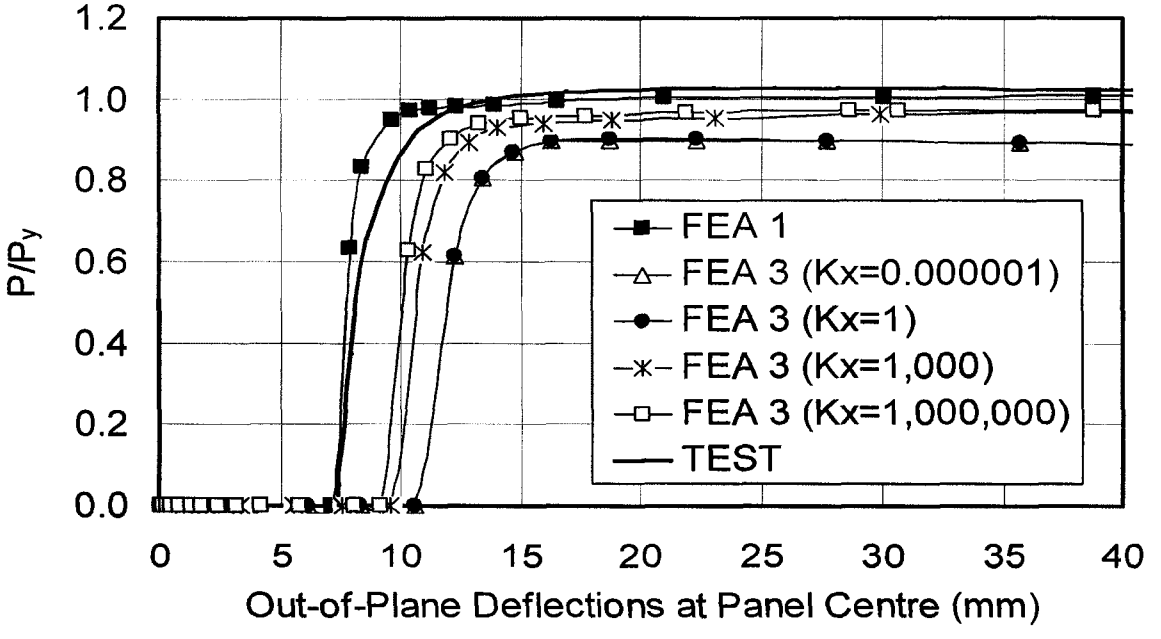

Figure 3.16 Out-of-plane deflections of FEA 3 under various out-of-plane spring stiffness

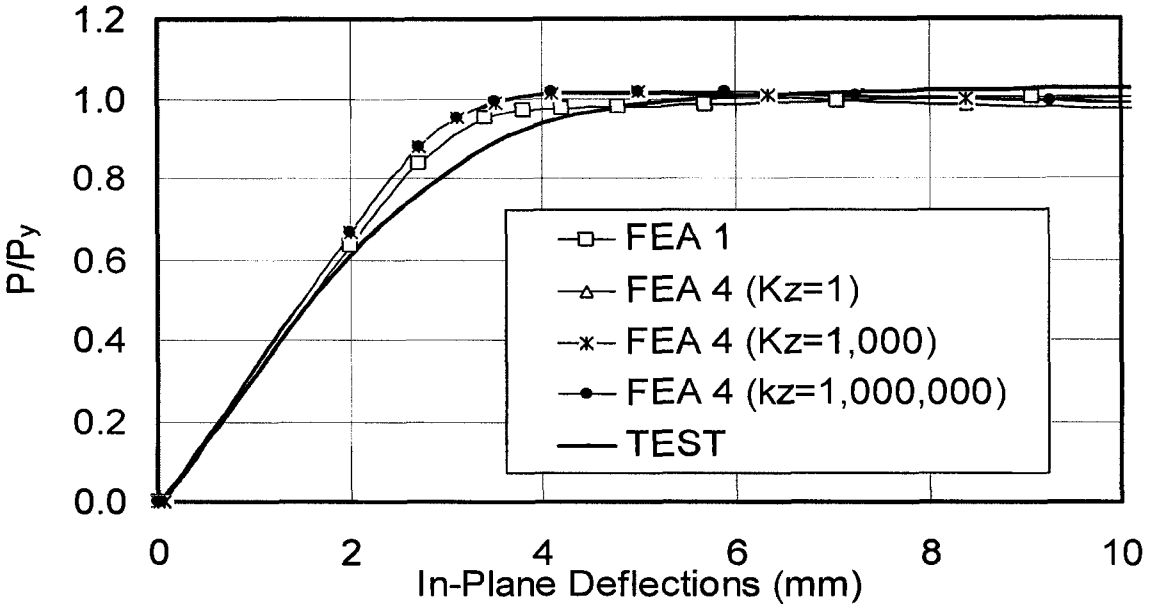

Figure 3.17 In-plane deflections of FEA 4 under various out-of-plane spring stiffness

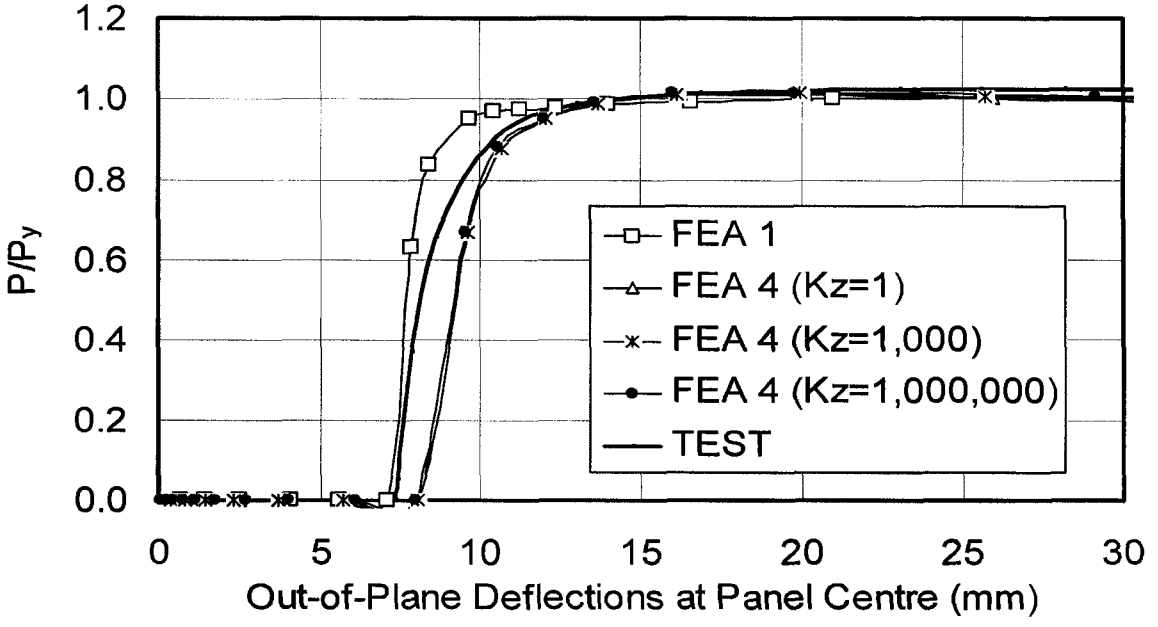

Figure 3.18 Out-of-plane deflections of FEA 4 under various out-of-plane spring stiffness

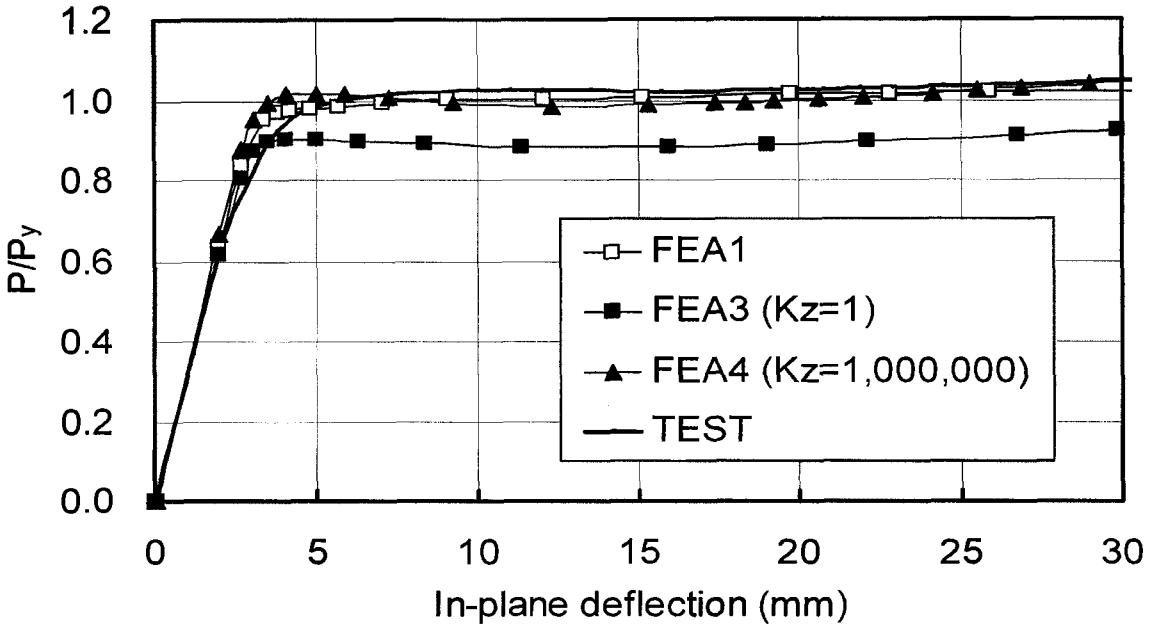

Figure 3.19 In-plane deflections from FE models with two boundary conditions

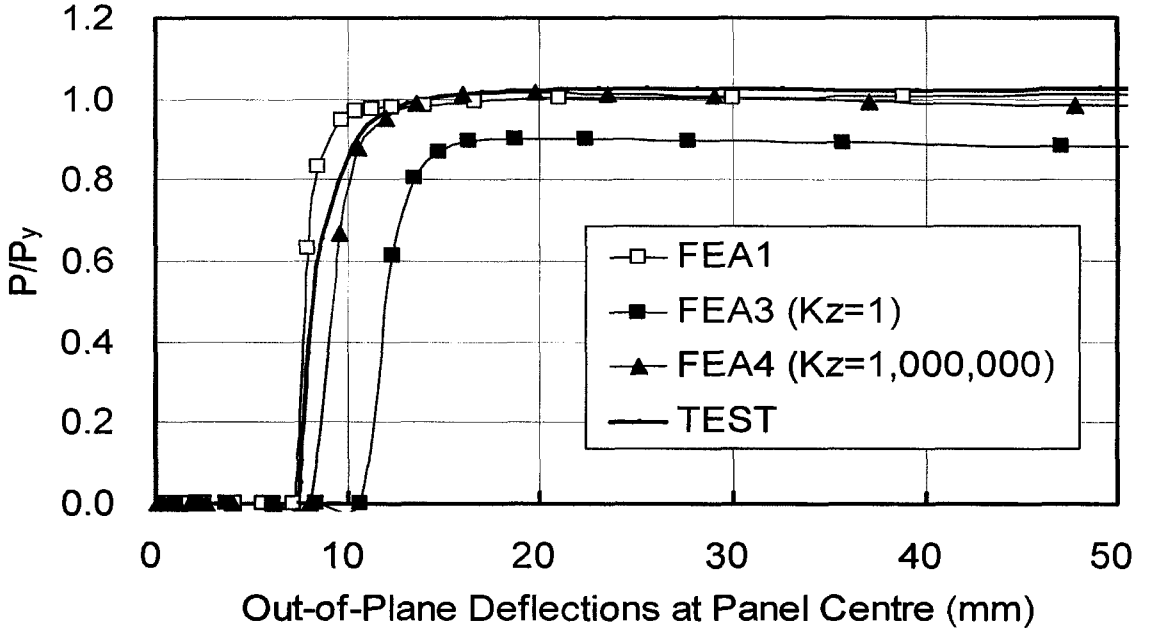

Figure 3.20 Out-of-plane deflections from FE models with two boundary conditions

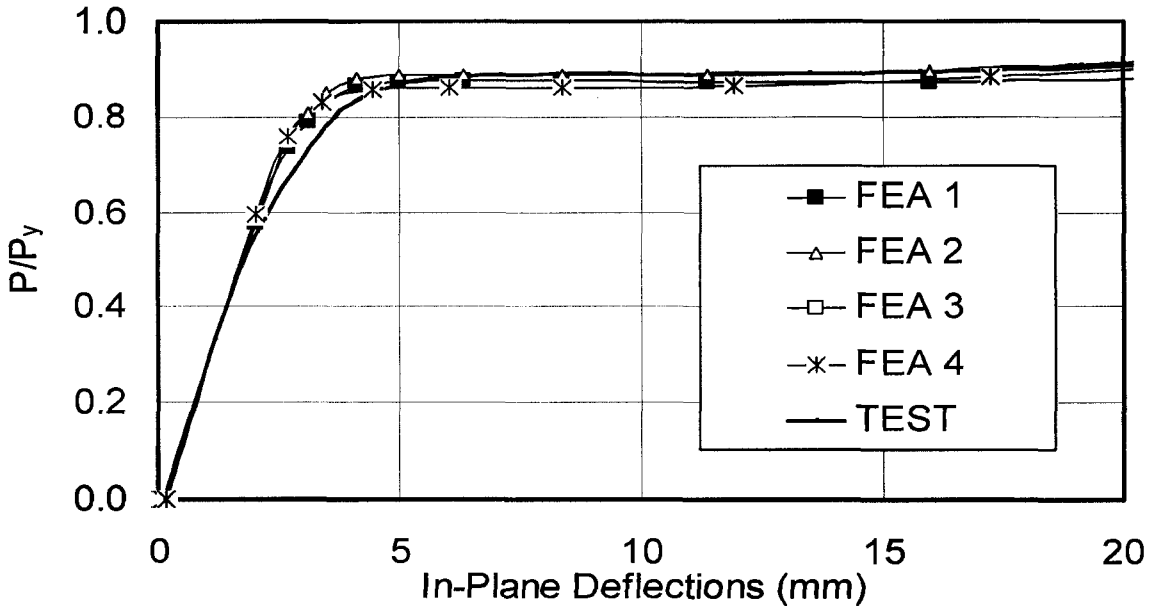

Figure 3.21 In-plane deflections from four FE models and test results for q/q_c=45%

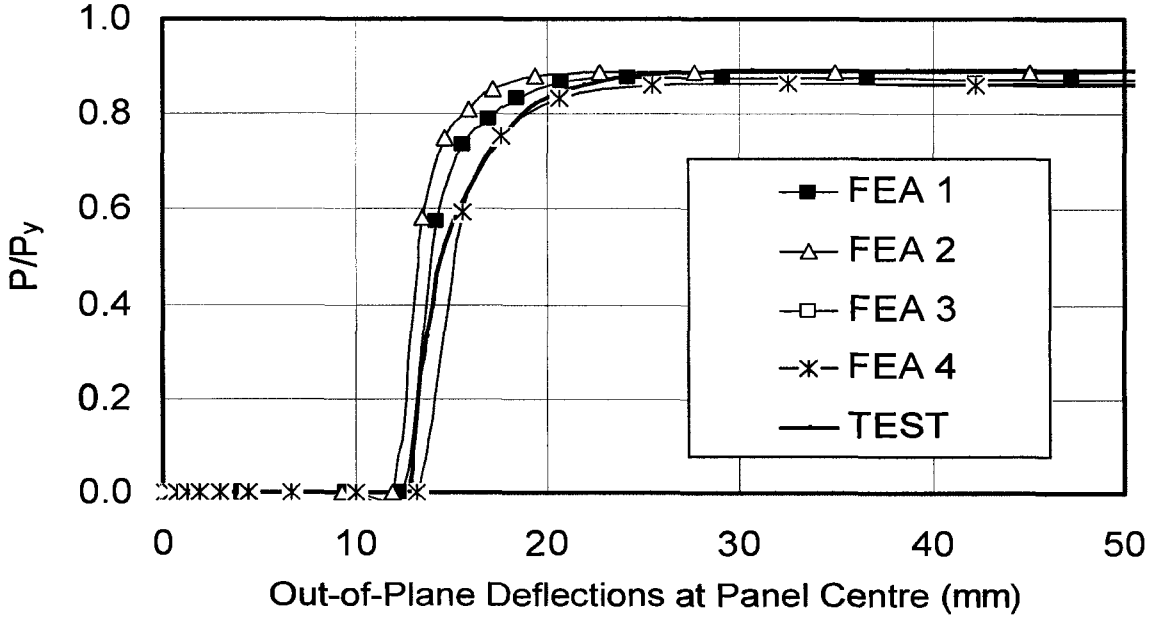

Figure 3.22 Out-of-plane deflections from four FE models and test results for q/q_c=45%

Chapter 4

Parametric study

4.1 Finite element model

A finite element model of a SPS panel was developed using the finite element software ANSYS. It was validated in Chapter 3 by comparing analysis results with test results presented by Little *et al.* (2007). The model with rotationally fixed boundary condition shown in figure 3.1 will be used to conduct a parametric study. The material properties and real stress versus real strain curves for the steel and the elastomer core material shown in table 3.1 and figure 3.5 are used for the finite element analysis presented in this chapter. The proposed parameters for this investigation are:

1. Panel aspect ratio;
2. Thickness of the steel plates and elastomer core;
3. Loading condition.

4.1.1 Aspect ratio

Based on the Lloyd's Register Provisional Rules (2006), the panels' aspect ratio should be between 1.2 and 1.7 for SPS used in ship structures. The behaviour of a sandwich panel with aspect ratio of 1.5 was tested and analyzed by Little *et al.* (2007).

Aspect ratios of 1.2, 1.7, and 2.5 are selected for the parametric study. The first two values correspond to the limits recommended by the Lloyd's Register and the last value extends the limit in the Provisional Rules, which should lead to one-way action for the out-of-plane load.

4.1.2 Thickness of face plates and elastomer core

Lloyd's Register Provisional Rules recommend a minimum steel plate thickness of 3 mm and minimum elastomer core of 15 mm. The behaviour of sandwich

panels with configuration of 3-15-3 will therefore be used as the start to be parametric study.

Kennedy, Dorton, and Alexander (2002) presented a box girder built-up from 6-45-6 stiffened SPS panels as deck and 4-32-4 panels as soffit to replace an orthotropic deck box girder. A similar panel size was selected for this investigation, namely, a 6-50-6 panel is selected as a reference "average" panel for the parametric study. Other configurations ranging from 3-15-3 to 10-200-10 are considered for this investigation as summarized in Table 4.1. To reduce the number of sandwich panels to consider in the parametric study, a fractional factorial design was adopted for these two parameters. The effect of core thickness will be investigated for panels with plate thickness of 3 mm and 10 mm. Three different core thicknesses will be investigated at each of the two plate thicknesses to determine whether the trend is linear or non-linear. The effect of plate thickness will be investigated for a core thickness of 50 mm. Three different thicknesses will be investigated to determine whether the plate thickness has a linear or non-linear effect on the sandwich panel behaviour. The thickness of face plate and elastomer core, the length and width of the sandwich panels are summarised in table 4.2.

4.1.3 Loading conditions

The loading procedure for the analysis consists of applying the out-of-plane load first. The in-plane load is then applied to failure of the panel while the out-of-plane load remains constant. Load interaction curves are derived for six lateral load level magnitudes, namely,

a) 1% of the plastic collapse load (based on a yield line analysis),
b) 13% of the plastic collapse load,
c) 27% of the plastic collapse load,
d) 45% of the plastic collapse load, and
e) 50% of the plastic collapse load, and
f) 90% of the plastic collapse load.

Lateral pressures corresponding to 13%, 27% and 45% of the plastic collapse load were investigated experimentally by Little *et al.* (2007). The minimum value of lateral pressure was introduced to create out-of-plane deformations in the panel to allow buckling of the panels when subjected to in-plane loading. The maximum value was selected at 90% of the theoretical plastic collapse load rather than 100% because initial analyses indicated that the plastic collapse load determined from the finite element analysis could be slightly lower than the value determined from a simple manual calculation determined based on a simple yield line pattern.

In summary, the panel aspect ratio, thickness of face plates and elastomer core, and loading conditions are the parameters investigated in the parametric study. If a full factorial design for the proposed parameter values outlined above were implemented, 105 analysis runs would be required. In order to reduce the number of analysis runs to a more manageable number, a total of 39 models, shown in table 4.3, are included in this study. Column (1) of Table 4.3 lists the sandwich panel designation and column (2) shows the aspect ratio. The aspect ratio is varied by varying the plate length (dimension in the y-direction) while the plate width (dimension in the x-direction) is kept constant (width = 1200 mm). Columns (3) and (4) present the axial load capacity, P_y, and the lateral load capacity, q_c, of the panels. The axial load capacity is taken as the yield strength of the panel, ignoring the contribution from the elastomer core. The lateral load capacity, q_c, is obtained based on yield line analysis (figure 3.8). Columns (5) to (9) list the lateral pressures corresponding to each lateral pressure level, varying from 1% to 90% of the plastic collapse load (the lateral load capacity).

4.2 Criteria for termination of analysis

The sandwich panels applied under combined axial and lateral load are mainly studied in this research, and the axial load capacity is defined by the following three ways:

1) The peak axial load when the sandwich panel starts to lose its load bearing capacity. Sandwich panel 3-15-3 with lateral loads of 1% q_c and 27% q_c displayed a distinct peak load.

2) The 0.5% strain load (ASTM A370-05) when there is no distinct peak axial load. The axial load capacity of most panels is defined by this method.

3) The maximum axial load at which convergence was reached during the analysis. This was the case for only one sandwich panel model, namely, panel 10-50-10 loaded under combined out-of-plane pressure of 50% q_c and axial load.

4.3 Finite element analysis results

In the following sections, the results of finite element analyses are demonstrated through in-plane and out-of-plane deflections at panel centre, the load carrying capacity in the y-direction (in-plane loading direction), and strains in the y-direction. The out-of-plane direction corresponds to the z-direction as shown in figures 3.1 to 3.4. The effect of panel aspect ratio, plate and core thickness, and lateral pressure on the behaviour of sandwich panels will be discussed.

4.3.1 Effects of aspect ratio on sandwich panels

A total of 39 finite element models described in table 4.3 were analyzed using the finite element software ANSYS to investigate the effect of aspect ratio on the strength and behaviour of sandwich panels.

4.3.1.1 3-15-3 panels with lateral pressure of 1% of the yield line pressure ($q/q_c = 1\%$)

Figure 4.1 presents normalized axial compressive load, P/P_y, versus the in-plane deflection, U_y for the finite element models with an aspect ratio of 1.2, 1.7, and 2.5 under a lateral pressure of q/q_c=1%. The axial compressive force P was obtained from the finite element analysis for an imposed in-plane

deflection, U_y, up to 12 mm, measured at the displaced end of each panel. The axial compressive force is normalized by dividing the axial load by the yield force, P_y, defined earlier. Figure 4.1 shows a reduction of the load carrying capacity after the axial load reaches $1.01\,P_y$ for all three plates. A plot normalized axial load, P/P_y, versus average axial strain, U_y/L, is shown in Figure 4.2. The plot shows that all three plates have the same initial slope, the same peak capacity, and the same post-buckling capacity, which is about $0.75P_y$.

Figure 4.3 shows the out-of-plane deflection, U_z, at the centre of the panel as a function of P/P_y. For the panel with an aspect ratio of 1.2, the out-of-plane deflection increases as the in-plane load increases and it reaches a value of 2.8 mm at the ultimate in-plane load of $1.01P_y$. However, the out-of-plane deflection in the models with aspect ratio of 1.7 and 2.5 reverses as the axial load reaches $0.66P_y$ and $0.70P_y$, respectively. A better visualization of the panels' out-of-plane deflection is presented in figures 4.4 to 4.6 for the panels with aspect ratios of 1.2 to 2.5, respectively. The deflected shape of the panels along their centreline is plotted for various load levels in the pre- and post-buckling ranges. All three panels show the same general deflected shape. However, the centre portion of the panel with the smallest aspect ratio deflects in the direction of the applied lateral pressure. It is also observed that the panels deform in three half waves, symmetrically about mid-height. Since the loaded ends are rotationally restrained, the centre half wave deforms significantly more than end ones. Points of inflection are observed at about the quarter points from the ends.

4.3.1.2 3-15-3 panels with lateral pressure of 27% of the yield line pressure ($q/q_c = 27\%$)

In this group of panels the lateral pressure is increased to 27% of the plastic collapse load ($q/q_c = 27\%$). The analysis of the three sample panels is

conducted under displacement control up to an in-plane deflection of 6 mm. The normalized axial load versus in-plane deflection curves are shown in figure 4.7. Of the three panels investigated, the panel with an aspect ratio of 1.2 reached the lowest ultimate axial load of $0.85P_y$ at an in-plane deflection of 2.8 mm. The panel with an aspect ratio of 1.7 reached its peak capacity of $0.93P_y$ at 3.8 mm and the panel with an aspect ratio of 2.5 reached its peak of $0.95P_y$ at 5.6 mm.

The normalized axial load versus axial strain curves for the same three panels are shown in figure 4.8. As was observed for the panels loaded at $q/q_c = 1\%$, the three panels display the same initial slope and reach their peak capacity at the same strain, although they reach their peak capacity at a lower strain than for the panels loaded with a lower lateral pressure in a range of 1800 to 1900 με compared to a range of 1900 to 2100 με for the panels subjected to $q/q_c = 1\%$.

Curves of normalized axial load versus out-of-plane deflection at the centre of the panel for the three 3-15-3 panels with $q/q_c = 27\%$ are plotted in figure 4.9. Although all panels show approximately the same out-of-plane deflection under the action of the lateral pressure alone, the panel with an aspect ratio of 1.7 has a slightly larger out-of-plane deflection under the lateral pressure of 27% of the yield line capacity, namely, 7.8 mm compared to 7.5 mm for the panel with an aspect ratio of 1.2 and 7 mm for the panel with an aspect ratio of 2.5. For the panels with an aspect ratio of 1.7 and 2.5, the out-of-plane deflection at the centre of the panel reverses when the axial load reaches $0.91P_y$ and $0.81P_y$, respectively. The out-of-plane deflection in the model with an aspect ratio of 1.2 keeps increasing as the axial load increases (the load carrying capacity of $0.85P_y$ is reached at a deflection of 18.3 mm).

The overall deformed shape along the panel centreline for various levels of lateral pressure and axial load is presented in figures 4.10 to 4.12 for panels with

aspect ratios varying from 1.2 to 2.5, respectively. The panel with an aspect ratio of 1.2 shows a single half wave throughout the loading process (figure 4.10). The panels with aspect ratios of 1.7 and 2.5 show a change in configuration from one half wave to three half waves as the panel reaches it buckling capacity and deform in the post-buckling range. As the buckling load is approached, the point of maximum deflection shifts from mid span to a point roughly at a quarter to one third of the plate length from the end supports.

4.3.1.3 3-15-3 panels with lateral pressure of 90% of the yield line pressure ($q/q_c = 90\%$)

The lateral pressure of 90% of the yield line pressure is expected to develop nearly the full capacity of the panels in bending before an axial load is applied to the panel. Loading for these panels was increased until the axial (in-plane) deflection reached a value in excess of 13 mm without reaching a distinct peak in the loading curves (see figure 4.13). In the absence of a distinct peak load, the 0.5% strain load (ASTM A370-05) is used to define the axial load capacity of the panels. These results in axial load capacities are $0.38P_y$, $0.46P_y$ and $0.57P_y$ for the panels with an aspect ratio of 1.2, 1.7 and 2.5, respectively (see figure 4.14).

The curves of normalized axial load versus the out-of-plane deflection at the centre of the three panels are presented in Figure 4.15. As for the in-plane displacement curves, a non-linear response is observed from the start of loading. The out-of-plane pressure creates out-of-plane deflections varying from 32 mm to 39 mm as the aspect ratio of the panel increases from 1.2 to 2.5.

The deformed shapes of the panels along their centreline are presented in figures 4.16 to 4.18 for aspect ratios of 1.2 to 2.5, respectively. For the three aspect ratios the deformed shape consists of a single half wave.

4.3.1.4 3-50-3 panels with lateral pressure of 1% of the yield line pressure ($q/q_c = 1\%$)

Three panels with aspect ratios of 1.2, 1.7 and 2.5 were analysed for a 3-50-3 sandwich panel configuration and a lateral pressure of 1% of the yield line pressure. An in-plane deflection of 24 mm was applied to each panel of this group. Plots of normalized axial load versus in-plane deflections are presented in figure 4.19 and normalized axial load versus axial strain are shown in figure 4.20. None of the panels reached their full axial load capacity within the 24 mm imposed axial deformation. Panels of similar configuration tested by Little *et al.* (2007) showed similar behaviour. As proposed by Little *et al.* the load at 0.5% strain is taken as axial strength for this group of panels. Since all three panels show the same axial load versus axial strain curve, the ultimate axial compressive load is the same ($1.13P_y$) for all three panels. This exceeds the yield capacity of the panels by 13% because the panels strain hardened before failure and at 50 mm the elastomer core is starting to contribute to the cross-section capacity of the panels. A comparison of the initial slope of the normalized load versus axial strain indicates an increase in slope of average 2.9% compared to the 3-15-3 sandwich panels examined earlier. The difference in slope reflects the contribution from the elastomer core, which is neglected in the calculation of the yield load, P_y.

The out-of-plane deflection at the centre of the panel is displayed in Figure 4.21 for panels of three aspect ratios. As expected, only very small out-of-plane deflections take place under the 1% lateral pressure. As the axial load is applied, all three panels show little lateral deflection response up to approximately $1.13P_y$ where the lateral deflection starts to increase rapidly.

The deformed shapes of the panel centreline at various load stages are shown in figures A.1 to A.3 of Appendix A. The panel with an aspect ratio of 1.2 showed a single half wave throughout the loading process whereas the panels with aspect ratios of 1.7 and 2.5 displayed three half waves.

4.3.1.5 3-50-3 panels with lateral pressure of 27% of the yield line pressure ($q/q_c = 27\%$)

An in-plane deflection of 20 mm was applied for each panel of this group. Figure 4.22 shows normalized axial load versus axial strain. Because a peak load was not reached within the imposed in-plane deformation of 20 mm, the load at 0.5% strain was used as the ultimate axial compressive load for the panels of this group. The axial load capacities of the panels are 1.09 P_y for three panels.

The out-of-plane deflection at the panel centre is shown in figure 4.23. The panel deformation along the centerline of the panels is presented in figures A.4 to A.6 of Appendix A. A single half wave deformed shape was observed for the panels with aspect ratio of 1.2 and 1.7, and three half waves is observed on the panel with aspect ratio of 2.5.

4.3.1.6 3-50-3 panels with lateral pressure of 90% of the yield line pressure ($q/q_c = 90\%$)

The normalized axial compressive load versus axial strain curves are shown in figure 4.24. An in-plane deflection of 12 mm was applied on the panels with aspect ratio of 1.2 and 1.7 and 20 mm is applied on the panel with aspect ratio of 2.5. No peak point of the axial compressive loads was observed in figure 4.24. The axial load capacity of $0.56P_y$, $0.68P_y$ and $0.83P_y$ was taken as the 0.5% strain load for the panels with aspect ratio of 1.2, 1.7 and 2.5, respectively. It is found the axial load capacity increases with an increase of aspect ratio, which did not take place at the lower lateral pressures $q/q_c = 1\%$ and $q/q_c = 27\%$.

Figure 4.25 displays normalized axial load versus out-of-plane deflections at the panel centre. Nonlinear load versus deformation behaviour was observed from the beginning of the in-plane load. The panel deformation along the centerline of the panel length for three models at different axial compressive load levels can be found in figures A.7 to A.9 (Appendix A). A single half wave deformed shape is observed for each panel.

4.3.1.7 3-100-3 panels with lateral pressure of 13% of the yield line pressure ($q/q_c = 13\%$)

An in-plane deflection of 20 mm was imposed on each panel of this group. The normalized axial compressive load versus axial strain curves are shown in figure 4.26. Since the peak load was not reached within the 20 mm deformation the ultimate axial load was taken as the load at 0.5% strain. The axial load capacity for the three panels is $1.23P_y$. The contribution of 18% from steel strain hardening and 5% from the elastomer core, which are both neglected in the calculation of P_y, causes 23% higher than yield line load capacity P_y. Figure 4.27 displays the normalized axial compressive load as a function of the out-of-plane deflection at the centre of the panel. The lateral deflection starts to increase rapidly at a load of $1.05P_y$. The panel centreline deformation for the three panel aspect ratios are presented in figures A.10 to A.12 (Appendix A). The panel with aspect ratios of 1.2 and 1.7 deformed in a single half wave while the panel with an aspect ratio of 2.5 deformed in three half waves.

4.3.1.8 3-100-3 panels with lateral pressure of 27% of the yield line pressure ($q/q_c = 27\%$)

An in-plane deflection of 20 mm was imposed on each panel of this group. Figure 4.28 displays normalized axial load versus axial strain curves for each plate aspect ratio. The axial load capacity, determined using the load at the 0.5% strain, for the three panels of this series is $1.21P_y$. The axial load capacity is only 21% higher than the yield line load capacity. A comparison of the initial slope of the normalized load versus axial strain indicates an increase in slope of 3.2% compared to the sandwich panels 3-50-3 and 6.1% to 3-15-3. The difference in slope reflects the contribution from the elastomer core, which is neglected in the calculation of the yield load, P_y.

The out-of-plane deflections at the panel centre are shown in figure 4.29. The out-of-plane deflections along the panel centerline are presented in figures A.13

to A.15 (Appendix A). The panels with an aspect ratio of 1.2 and 1.7 show only a half wave over their length whereas the plate with an aspect ratio of 2.5 shows three half waves.

4.3.1.9 3-100-3 panels with lateral pressure of 45% of the yield line pressure ($q/q_c = 45\%$)

Figure 4.30 shows the normalized axial load versus axial strain for the three panels from this series. Once again, since a peak load was not reached, the axial strength is taken as the axial force at 0.5% strain. The capacities of the panels with aspect ratios of 1.2, 1.7, and 2.5 are $1.14\,P_y$, $1.17\,P_y$, and $1.18\,P_y$, respectively. The axial load capacity decreases by 6.1% and 7.9% compared to the same panel subjected to a lateral load of $27\%\,q_c$ and $13\%\,q_c$, respectively.

Figure 4.31 presents the normalized lateral load versus out-of-plane deflection at the centre of the panel. The out-of-plane deflections along the panel width at various load levels are shown in figures A.16 to A.18 (Appendix A). The panels with an aspect ratio of 1.2 and 1.7 showed one half wave at failure whereas the panel with an aspect ratio of 2.5 showed three half waves. The configuration of the panel with an aspect ratio of 2.5 starts changing from a single half wave to three half waves at an axial load of about $1.13\,P_y$.

4.3.1.10 6-50-6 panels with lateral pressure of 27% of the yield line pressure ($q/q_c = 27\%$)

An in-plane deflection of 20 mm is imposed on each panel of this group. Figure 4.32 shows the normalized axial load versus axial strain curves of sandwich panel 6-50-6 with three aspect ratios applied by $q/q_c = 27\%$. No peak axial compressive load was found and the axial compressive load capacity is defined as the 0.5% strain load. $1.01\,P_y$, $1.03\,P_y$, and $1.04\,P_y$ are therefore obtained for the panels with aspect ratio of 1.2, 1.7 and 2.5, respectively.

Figure 4.33 plots the normalized axial load versus out-of-plane deflection at panel centre of the panels. The out-of-plane deflections along the panel width are shown in figure A.19 to A.21 (Appendix A). The panel with an aspect ratio of 1.2 shows a single half wave throughout the loading procedure. The panel with aspect ratio of 1.7 deformed in one half wave till the axial load capacity of $1.03P_y$, then the configuration changes to three half wave. Three-half wave deformation is observed on the panel with an aspect ratio of 2.5 at its axial load capacity of $1.04P_y$.

4.3.1.11 10-50-10 panels with lateral pressure of 1% of the yield line pressure ($q/q_c = 1\%$)

Figure 4.34 displays the normalized axial load versus axial strain of three panels. Bilinear behaviour is seen on three panels. The panels keep in linear elastic till to $1.0P_y$, and then the axial load keep increasing slowly as the in-plane deflection increase largely. The axial load capacity of 1.04 P_y for three panels was taken as the 0.5% strain load.

Normalized axial compressive load versus out-of-plane deflections at panel centre is plotted in figure 4.35. Almost zero out-of-plane deflection at panel center due to 1% of lateral load is observed. The lateral deflection increases little when the axial compressive loads applied from zero to $1.0P_y$, and then the deflection increases largely. The out-of-plane deflections along the panel width at various load stages are plotted in figure A.22 to A.24 (Appendix A) corresponding the panels with aspect ratio of 1.2, 1.7 and 2.5, respectively. The configuration of a single half wave is took place on the panel with an aspect ratio of 1.2 whereas three half waves are observed on the panel with other two aspect ratios.

4.3.1.12 10-50-10 panels with lateral pressure of 27% of the yield line pressure ($q/q_c = 27\%$)

In-plane deflection of 20mm is imposed on three panels of this group. Curves of the normalized axial load versus axial strain are plotted in figure 4.36. The axial

load capacities of $0.96P_y$, $1.0P_y$ and $1.02P_y$ are for the panel with aspect ratio of 1.2, 1.7, and 2.5, respectively. The 0.5 % strain load was taken as the axial load capacity due to no peak load was found throughout the load process.

Figure 4.37 displays the out-of-plane deflection, U_z, at the centre of the panel as a function of normalized axial load P/P_y. The panel with an aspect ratio of 1.2 has the largest lateral deflection under the same axial load. The deformed shapes along the panel centerline of three panels are shown in figure A.25 to A.27 (Appendix A). The panel with aspect ratios of 1.2 and 1.7 deformed in a single half wave (A25 and A26) while the panel with an aspect ratio of 2.5 deformed in three half waves (A.27).

4.3.1.13 10-50-10 panels with lateral pressure of 50% of the yield line pressure ($q/q_c = 50\%$)

The lateral load of $0.9q_c$ could not run through on the sandwich panel 10-50-10 because no convergence solution could be completed. Reduced the lateral load to $0.5q_c$ which is the highest lateral load level can obtained the converged solution on each panel. The in-plane deflections of 3 mm, 2.6 mm and 4 mm were imposed on the panels with aspect ratio of 1.2, 1.7, and 2.5, respectively. The different applied in-plane deflections were governed by if the solution converged.

Figure 4.38 plots curves of the normalized axial compressive load versus axial strain. The axial load capacities of three panels were taken as the stopped load of the converged solution. Therefore, $0.56P_y$, $0.52P_y$ and $0.66P_y$ are the axial load capacity of the panels with aspect ratio of 1.2, 1.7 and 2.5, respectively.

The normalized lateral loads versus out-of-plane deflections at panel centre curves are shown in figure 4.39. Aspect ratio has no significant effect on the lateral deflection of the sandwich panel applied by lateral load alone. The deformed shapes along the panel centerline of three panels at various load levels

are displayed in figure A.28 to A.30 (Appendix A). Three panels deformed in one half wave throughout the load process.

4.3.1.14 Summary of aspect ratio

Figure 4.40 plots the curves of the normalized axial load capacity versus normalized lateral load capacity of three panels 3-15-3, 3-50-3, and 3-100-3 with three aspect ratios. For the panel 3-15-3, aspect ratio has zero effect on the axial load capacity at the lateral load of 1% of the yield line load capacity, but the effect is getting large with the increasing of the lateral load level. The axial load capacity of the panel with an aspect ratio of 2.5 is 12% higher than that of the panel with an aspect ratio of 1.2 at the lateral load of $27\%q_c$ and 50% higher at lateral load of $90\%q_c$. Similarly, it is 2% higher than the panel with an aspect ratio of 1.7 at the lateral load of $27\%q_c$ and 24% higher at $90\%q_c$. For the panel 3-50-3, aspect ratio has no significant effect on the axial load capacity at the lateral load of $1\%q_c$ to $27\%q_c$. However, the effect is getting large as the lateral load level is getting higher. The axial load capacity of the panel with an aspect ratio of 2.5 is 48% and 22% higher the panel with aspect ratio of 1.2 and 1.7, respectively. For the panel 3-100-3, aspect ratio has no large influence on the axial load capacity at three load levels of $13\%q_c$, $27\%q_c$ and $45\%q_c$. Compared the effect of aspect ratio of three panels, it is found the effect of aspect ratio on the axial load capacity is getting smaller as the thickness of the elastomer core is getting thicker. Table 4.4 shows the axial load capacity, axial strain and deformed curves of total 39 panels.

4.3.2 Effects from the thickness of the steel plate and elastomer core

4.3.2.1 Five panels with an aspect ratio of 1.2

Figure 4.41 plots the normalized axial load versus axial strain of five sandwich panels at lateral load of 27% of the yield line load capacity. The curves of five panels keep a close slope till to the axial load of $0.8P_y$. Then the curves start to discrete as the normalized axial load increased. The axial load capacity was

defined as the 0.5% strain load for the panels without peak load examined earlier. The sequence of the axial load capacity from high to low is the panel 3-100-3, 3-50-3, 6-50-6, 10-50-10, and 3-15-3, respectively. The interaction diagrams between the normalized axial load, P_u / P_y, versus normalized lateral load, q/q_c, of the panels with an aspect ratio of 1.2 are plotted in figure 4.42. The thickness ratio, t_c / t_s, of 5, 16.7, and 33.3 from four panels of 3-15-3, 3-50-3,3-100-3 and 10-50-10 are presented in the figure to compare, where t_c refers the thickness of the elastomer core and t_s is the thickness of the steel plate. The axial load capacity of the panel 10-50-10 at q/q_c=0.5 was taken as the maximum load reached in the analysis before convergence problems occurred. It is found that the thickness ratio, t_c / t_s, is a function of the axial load capacity. The axial load capacity, P_u / P_y, increases with the increasing of the thickness ratio. For the panel with same thickness ratio, like the panel 3-15-3 and 10-50-10, the thicker panel (10-50-10) has higher axial load capacity, P_u / P_y.

4.3.2.2 Five panels with an aspect ratio of 1.7

Normalized axial compressive loads versus axial strain curves of five panels with an aspect ratio of 1.7 are shown in figure 4.43. The linear elastic behaviours took place on five panels before the axial compressive loads reach to $0.9P_y$. Then, the panel 3-15-3 quickly reaches its ultimate load of $0.93P_y$ and the other four panels have no distinct peak load as discovered earlier. The sequence of the axial load capacity from high to low is still followed by the panel from 3-100-3, 3-50-3, 6-50-6, 10-50-10, and 3-15-3. Figure 4.44 plots the normalized axial load versus normalized lateral load curves of the panels with an aspect ratio of 1.7. Same as the panels with an aspect ratio of 1.2, the panel with high thickness ratio of the elastomer core and steel plate has the highest axial load capacity, For the panel with same thickness ratio, the higher axial load capacity occurs on the thicker panel.

4.3.2.3 Five panels with an aspect ratio of 2.5

Figure 4.45 displays the normalized axial compressive load versus axial strain curves of the panels with aspect ratio of 2.5 at the lateral load of $27\%q_c$. It is observed that load deformations of five panels are very close before the axial load reaches to $0.95P_y$. The axial load capacity from high to low still follows a series of panel of 3-100-3, 3-50-3, 6-50-6, 10-50-10, 3-15-3. The same result can be found in figure 4.46 shown the normalized axial load versus normalized lateral load. The axial load capacity increases with the increasing of the thickness ratio.

4.3.2.4 Summary of the thickness of elastomer core and steel plate

The axial load capacity of five panels of 3-15-3, 3-50-3, 3-100-3, 6-50-6, and 10-50-10 were compared and discussed. Two conclusions can be obtained. First one, the normalized axial load capacity increases with the increasing of the thickness ratio of the elastomer core and steel plate. Second one, the panels with same thickness ratio of elastomer core and steel plate, the thicker panel has higher axial load capacity.

4.3.3 Effects of load levels on sandwich panel

The panels of 3-15-3 and 3-50-3 with three aspect ratios at three lateral load levels of $1\%q_c$, $27\%q_c$ and $90\%q_c$ were conducted earlier. The effect of the lateral load level on the structural behaviour of the sandwich panel is discussed in the following sections.

4.3.3.1 Panel 3-15-3 with an aspect ratio of 1.2

The curves of the normalized axial load versus axial strain of panel 3-15-3 with an aspect ratio of 1.2 at three load levels are plotted in figure 4.48. The panels at the lateral load levels of $1\%q_c$ and $27\%q_c$ have a close initial slope till to the normalized axial load of $0.66P_y$. Nonlinear load deformation occurred on the panel at lateral load of $90\%q_c$ from beginning of the axial load. The axial load

capacity reduced 16% when the lateral load level increased from 1% to 27%, and decreased 62% when load level increased from 1% to 90%.

4.3.3.2 Panel 3-50-3 with an aspect ratio of 1.2

Figure 4.48 plots the normalized axial compressive load versus axial strain of the panels 3-50-3 with an aspect ratio of 1.2 at three lateral load levels. Same initial slope between two first lower load levels was keep till to the normalized axial load of $0.84\,P_y$. The panel at higher lateral load level deformed nonlinear response from the axial load beginning. The axial load capacity went down 4% only when the lateral load level increased from 1% to 27% and lower 50% when the load level increased from 1% to 90% of q_c.

4.3.3.3 Panel 3-15-3 with an aspect ratio of 1.7

Figure 4.49 presents normalized axial load versus axial strain for the panels 3-15-3 with an aspect ratio of 1.7 under three lateral pressures. The initial slopes of the panels at two lower load levels are very close till to the normalized axial load of $0.8P_y$. The panel under the lateral load of $90\%q_c$ has 54% lower axial load capacity than the panel under the lateral load of $1\%q_c$ and 8% lower than the panel under $27\%q_c$.

4.3.3.4 Panel 3-50-3 with an aspect ratio of 1.7

The normalized axial load versus axial strain curves of the panel 3-50-3 are shown in figure 4.50. The curves of the panels at the lateral load of 1% and 27% of the yield line load capacity are very close throughout load process. The difference of the axial load capacity between two load levels is only 2%. And 40% of the axial load capacity reduced when the lateral load increased from $1\%q_c$ to $90\%q_c$.

4.3.3.5 Panel 3-15-3 with an aspect ratio of 2.5

Curves of normalized axial load versus axial strain of the panel 3-15-3 with an aspect ratio of 2.5 at three load levels are plotted in figure 4.51. Linear curves keep till the normalized axial load of $0.94P_y$. The difference of the axial load capacity at two lower load levels reduced to 6% compared to 16% and 8% on the panel with aspect ratio of 1.2 and 1.7, respectively. When the lateral load level increased from 1% to $90\%q_c$, the axial load capacity decreased 44% compared with 62% and 54% occurred on the panel with aspect ratio of 1.2 and 1.7, respectively

4.3.3.6 Panel 3-50-3 with an aspect ratio of 2.5

Plots of normalized axial load versus axial strain of the panel 3-50-3 are presented in figure 4.52. Again, the curves of the panels at two lower load levels are very close during whole load process. The curve of $q/q_c = 90\%$ shows nonlinear behaviour from the starting of the axial load. Compared to 50% and 40% of the axial load capacity reduced in the panels with aspect ratios of 1.2 and 1.7 respectively when the lateral load increased from $1\%q_c$ to $90\%q_c$, 26% decreased on the panel with an aspect ratio of 2.5.

4.3.3.7 Summary of the lateral pressure level

Two panels with same thickness of the steel plate and varied thickness of the elastomer core at same lateral load levels of 1%, 27% and 90% of q_c were discussed. It is found that the effect of the lateral load level on the axial load capacity is getting smaller as the panel is getting thicker. And this effect reduces with the increasing of the aspect ratio.

Table 4.1 Sandwich Panels Considered in the Parametric Study

Plate Thickness (mm)	Core Thickness (mm)			
	15	50	100	200
3	3-15-3	3-50-3	3-100-3	
6		6-50-6		
10		10-50-10	10-100-10	10-200-10

Table 4.2 Thickness and Dimensions of Sandwich Panels

Panel Configuration	Plate Thickness (mm)	Core Thickness (mm)	Aspect Ratio	Panel length (mm)	Panel width (mm)
3-15-3	3	15	1.2	1200	1440
			1.7	1200	2040
			2.5	1200	3000
3-50-3	3	50	1.2	1200	1440
			1.7	1200	2040
			2.5	1200	3000
3-100-3	3	100	1.2	1200	1440
			1.7	1200	2040
			2.5	1200	3000
6-50-6	6	50	1.2	1200	1440
			1.7	1200	2040
			2.5	1200	3000
10-50-10	10	50	1.2	1200	1440
			1.7	1200	2040
			2.5	1200	3000

Table 4.3 Total 39 Finite Element Models Performed in Parametric Study

Sandwich panel	Aspect ratio	Axial load P_y (kN)	Lateral load q_c (kPa)	Lateral load level (kPa)					
				1%	13%	27%	45%	50%	90%
(1)	(2)	(3)	(4)	(5)	(6)	(7)	(8)	(9)	(10)
3-15-3	1.2	2534	536	5	—*	145	—	—	483
	1.7	2534	417	4	—	113	—	—	376
	2.5	2534	341	3	—	92	—	—	307
3-50-3	1.2	2534	1579	16	—	426	—	—	1421
	1.7	2534	1229	12	—	332	—	—	1106
	2.5	2534	1005	10	—	271	—	—	904
3-100-3	1.2	2534	3068	—	399	828	1381	—	—
	1.7	2534	2388	—	311	645	1074	—	—
	2.5	2534	1952	—	254	527	879	—	—
6-50-6	1.2	5069	3336	—	—	901	—	—	—
	1.7	5069	2596	—	—	701	—	—	—
	2.5	5069	2123	—	—	573	—	—	—
10-50-10	1.2	8448	5957	60	—	1608	—	2978	—
	1.7	8448	4636	46	—	1252	—	2318	—
	2.5	8448	3791	38	—	1024	—	1895	—

* No entry indicates the corresponding panel was not analyzed

Table 4.4 Numerical results of total 39 models

Panel	Lateral pressure q/q_c	Aspect ratio	P/P_y	Strain at peak load (%)	Observation
3-15-3	1%	1.2	1.01	0.21	Single half wave
		1.7	1.01	0.19	Single half wave
		2.5	1.01	0.19	Single half wave
	27%	1.2	0.85	0.19	Single half wave
		1.7	0.93	0.18	Three half waves
		2.5	0.95	0.18	Three half waves
	90%	1.2	0.38	0.50	Single half wave
		1.7	0.46	0.50	Single half wave
		2.5	0.57	0.50	Single half wave
3-50-3	1%	1.2	1.13	0.50	Single half wave
		1.7	1.13	0.50	Three half waves
		2.5	1.13	0.50	Three half waves
	27%	1.2	1.08	0.50	Single half wave
		1.7	1.09	0.50	Single half wave
		2.5	1.10	0.50	Three half waves
	90%	1.2	0.56	0.50	Single half wave
		1.7	0.68	0.50	Single half wave
		2.5	0.83	0.50	Single half wave
3-100-3	13%	1.2	1.23	0.50	Single half wave
		1.7	1.23	0.50	Single half wave
		2.5	1.23	0.50	Three half waves
	27%	1.2	1.21	0.50	Single half wave
		1.7	1.21	0.50	Single half wave
		2.5	1.21	0.50	Three half waves
	45%	1.2	1.14	0.50	Single half wave
		1.7	1.17	0.50	Single half wave
		2.5	1.18	0.50	Three half waves
6-50-6	27%	1.2	1.01	0.50	Single half wave
		1.7	1.03	0.50	Three half waves
		2.5	1.04	0.50	Three half waves
10-50-10	1%	1.2	1.05	0.50	Single half wave
		1.7	1.05	0.50	Three half waves
		2.5	1.04	0.50	Three half waves
	27%	1.2	0.96	0.50	Single half wave
		1.7	1.00	0.50	Single half wave
		2.5	1.02	0.50	Three half waves
	50%	1.2	0.56	0.21	Single half wave
		1.7	0.52	0.13	Single half wave
		2.5	0.66	0.13	Single half wave

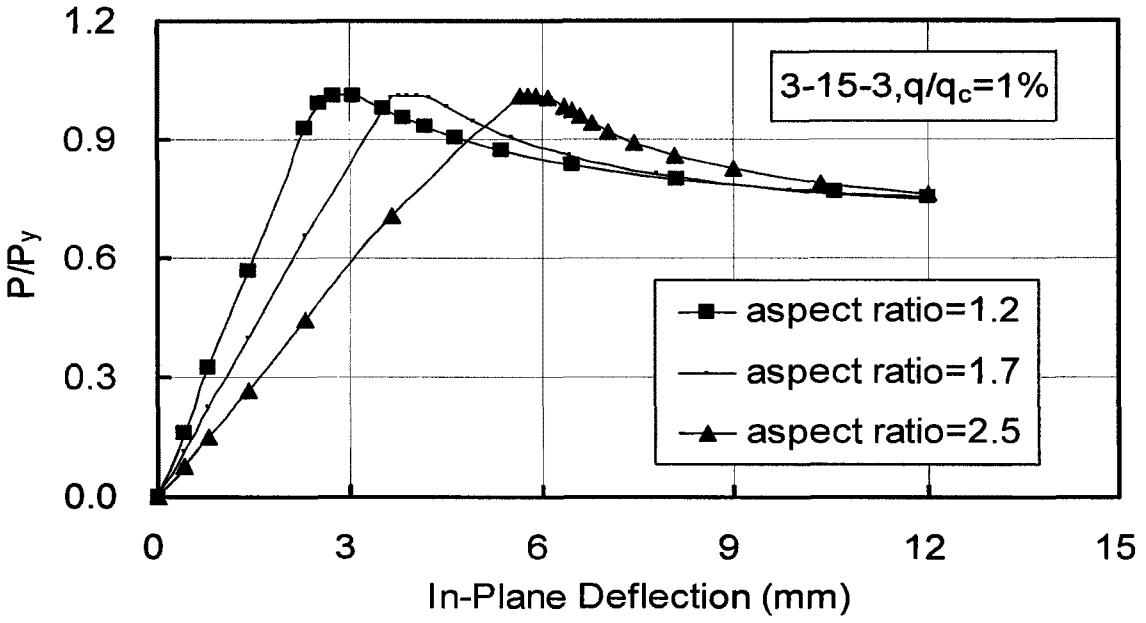

Figure 4.1 Normalized axial load versus in-plane deflections (3-15-3, q/q_c = 1%)

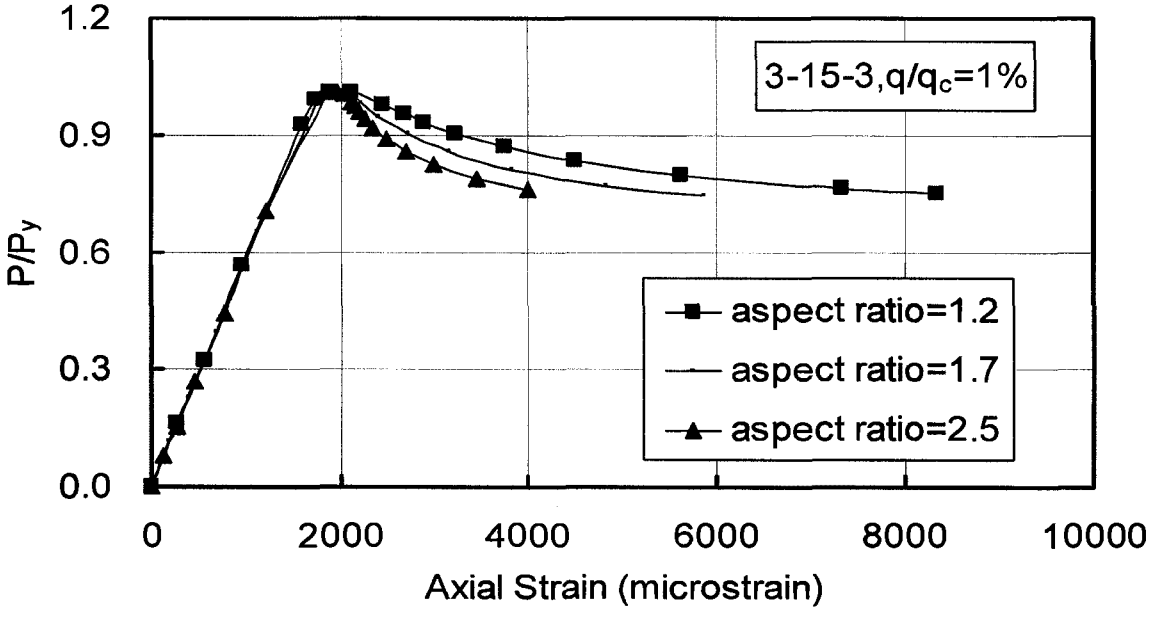

Figure 4.2 Normalized axial load versus axial strain (3-15-3, q/q_c = 1%)

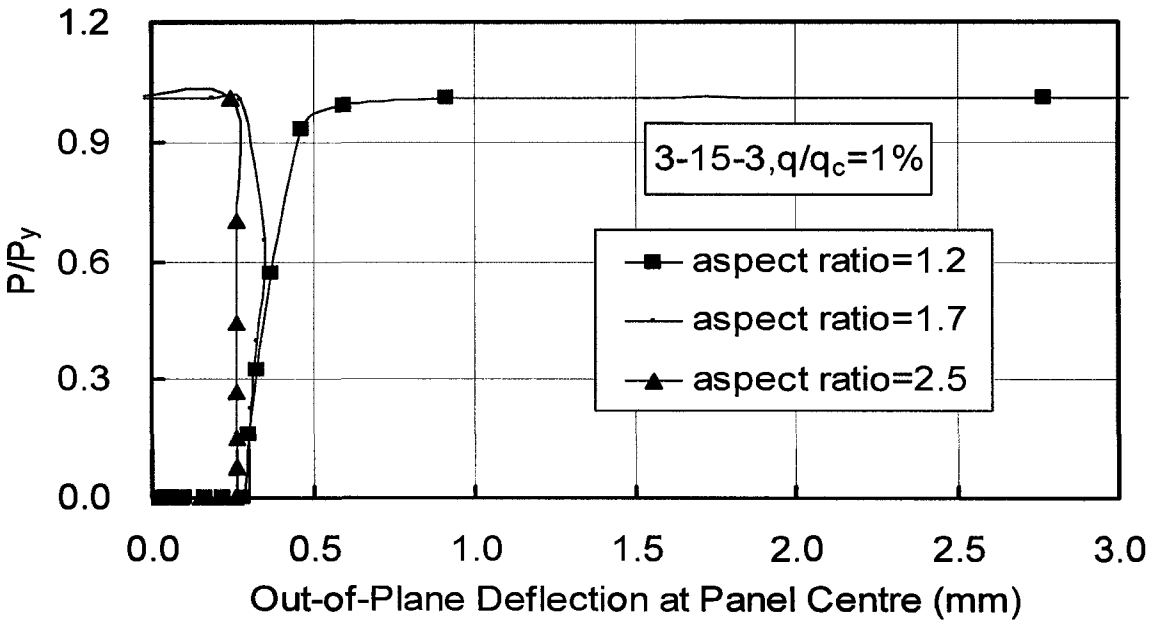

Figure 4.3 Normalized axial load versus out-of-plane deflections at panel centre (3-15-3, q/q_c = 1%)

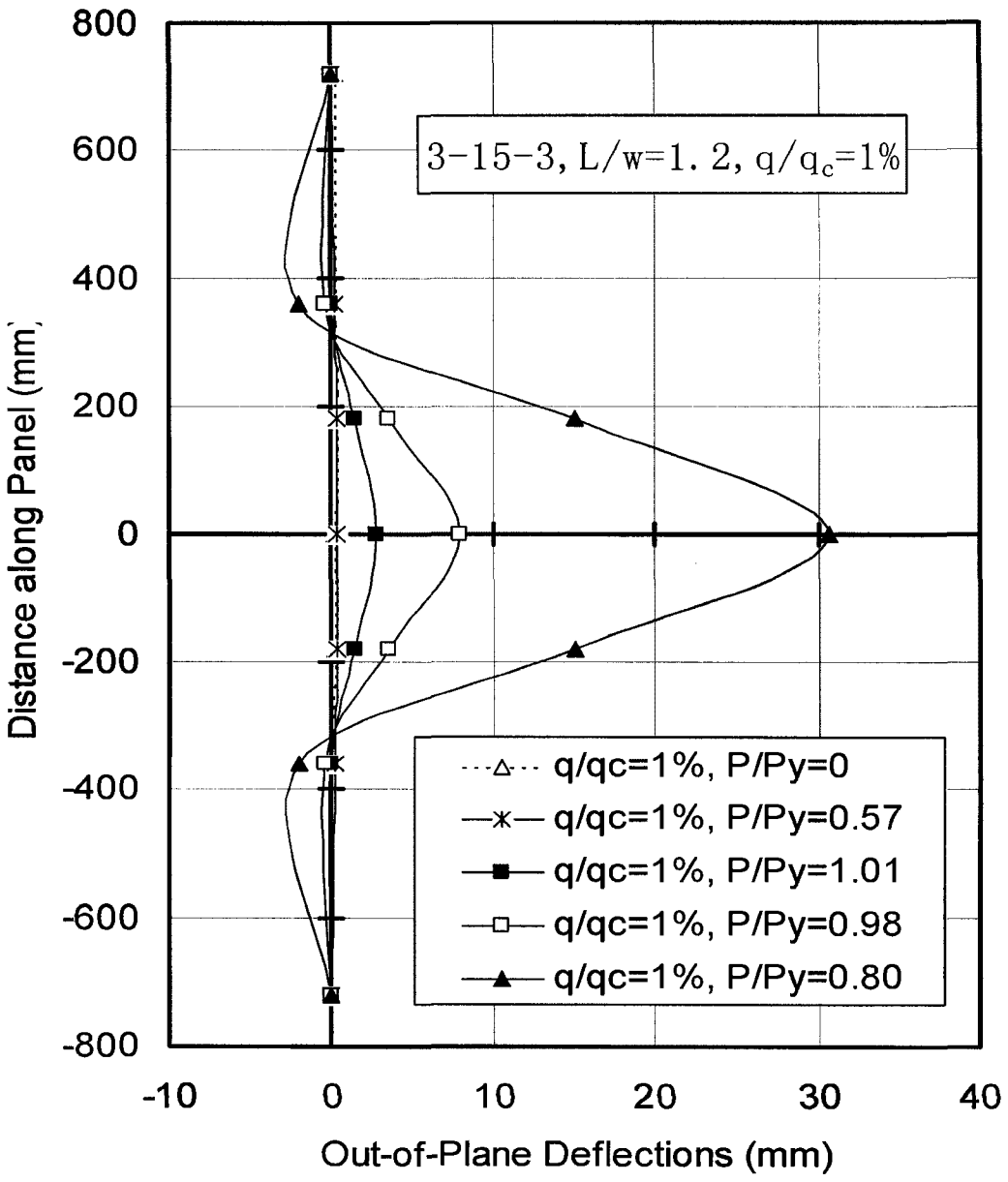

Figure 4.4 Out-of-plane deflections along panel length
(3-15-3, L/w = 1.2, q/q_c = 1%)

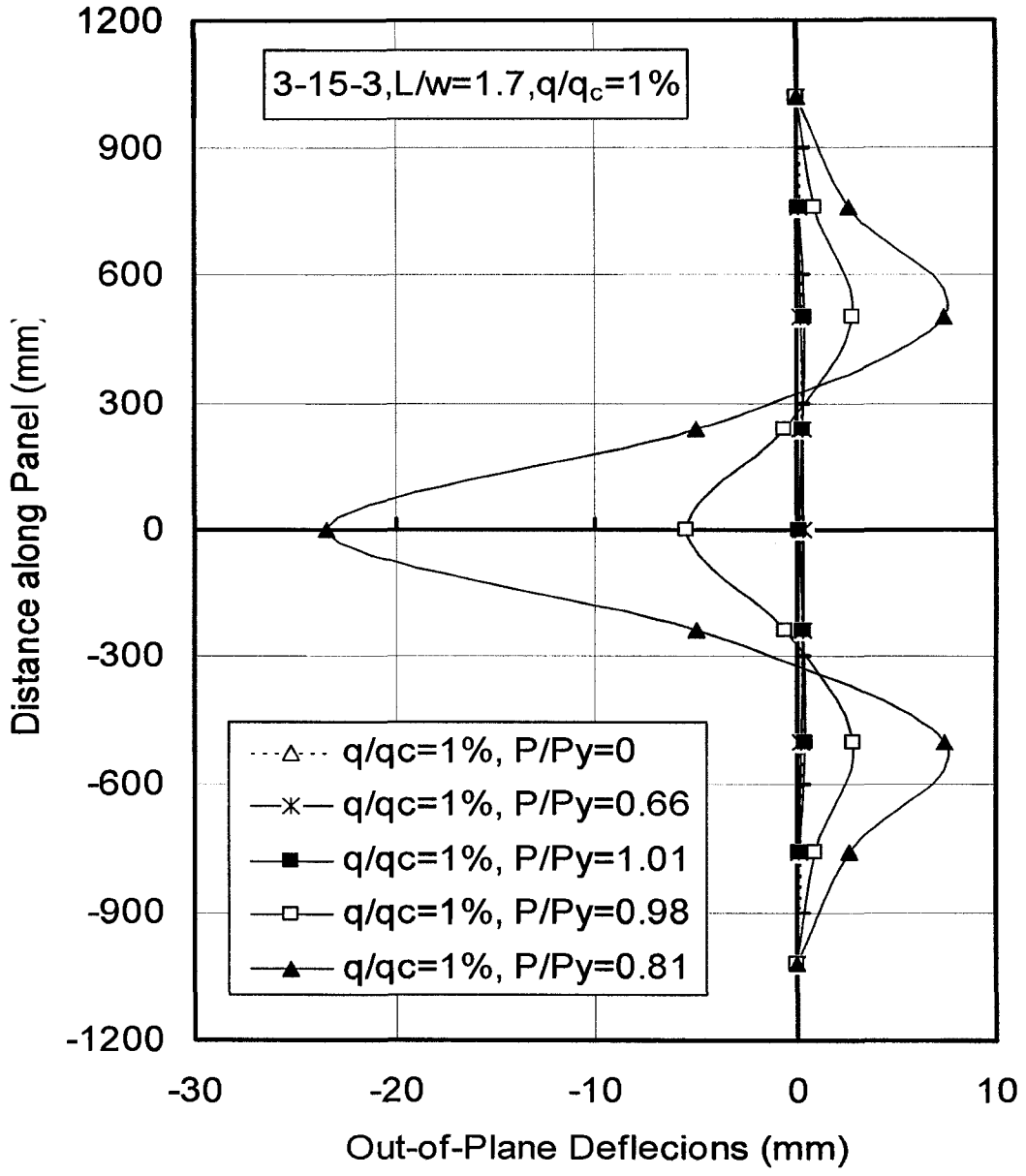

Figure 4.5 Out-of-plane deflections along panel length
(3-15-3, L/w = 1.7, q/q_c = 1%)

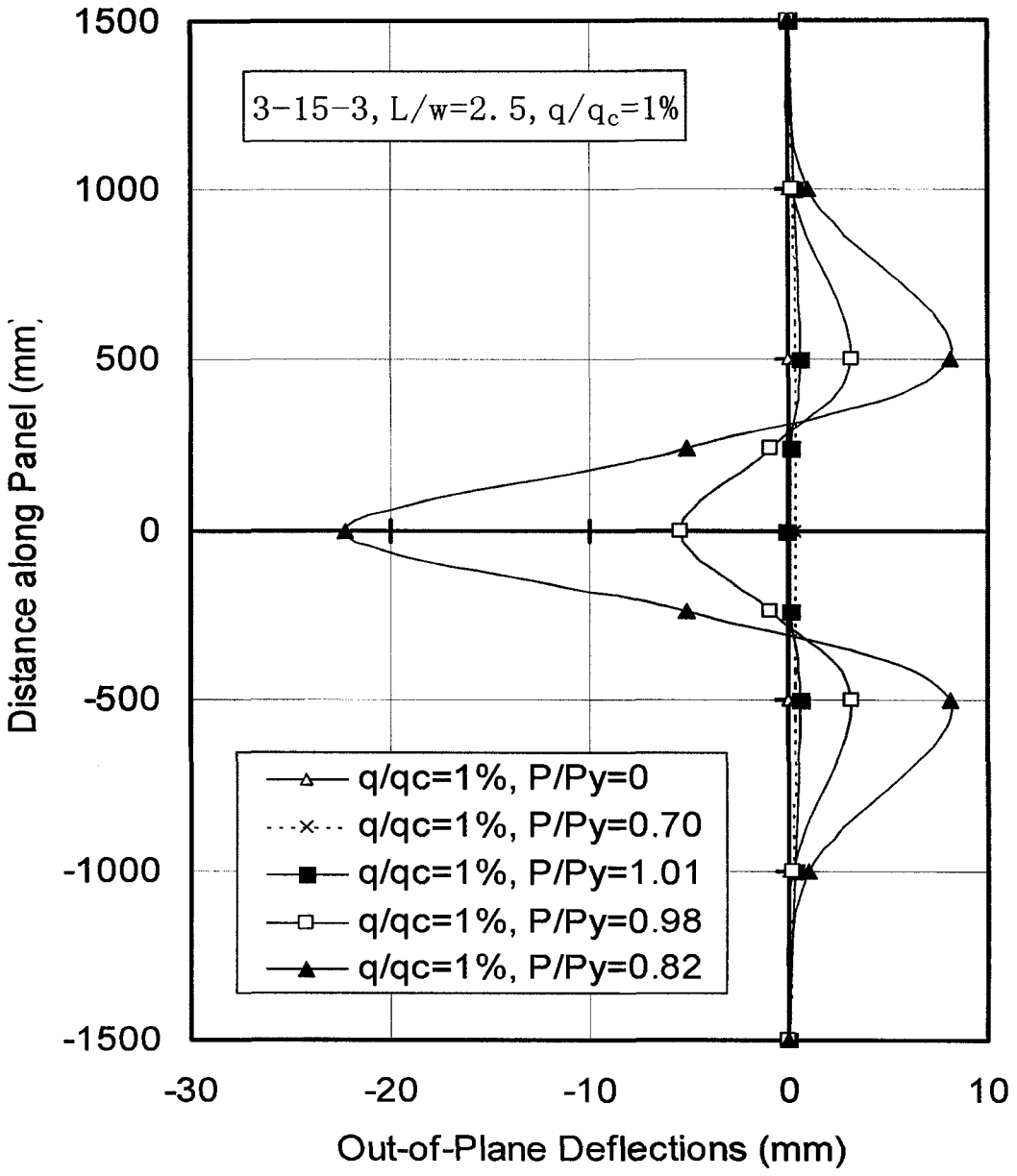

Figure 4.6 Out-of-plane deflections along panel length
(3-15-3, L/w = 2.5, q/q_c = 1%)

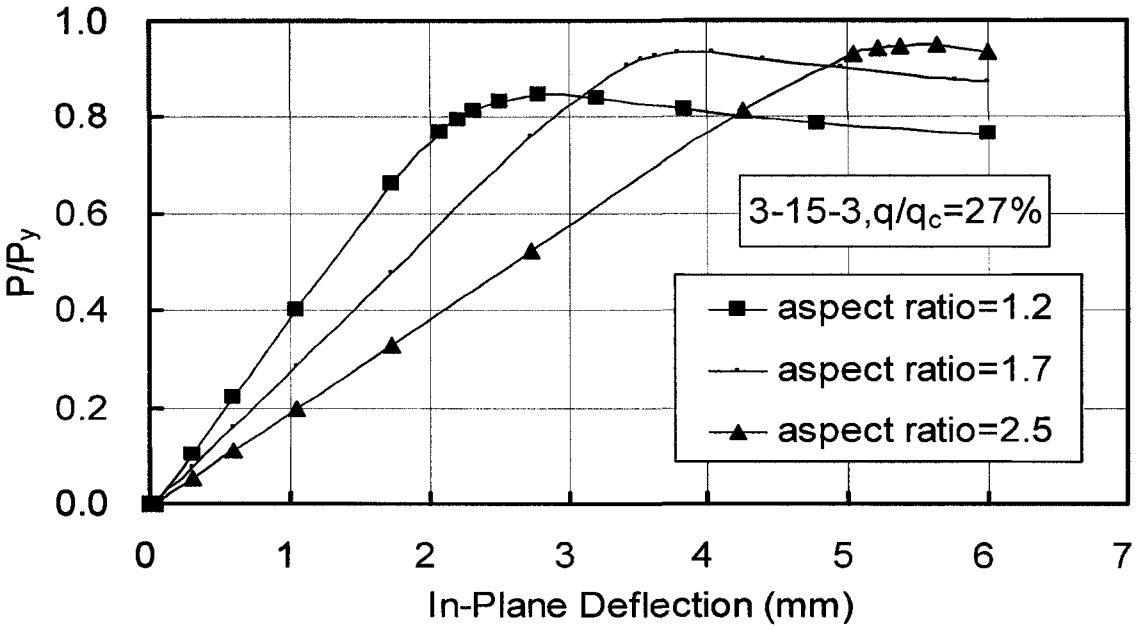

Figure 4.7 Normalized axial load versus in-plane deflection (3-15-3, q/q_c = 27%)

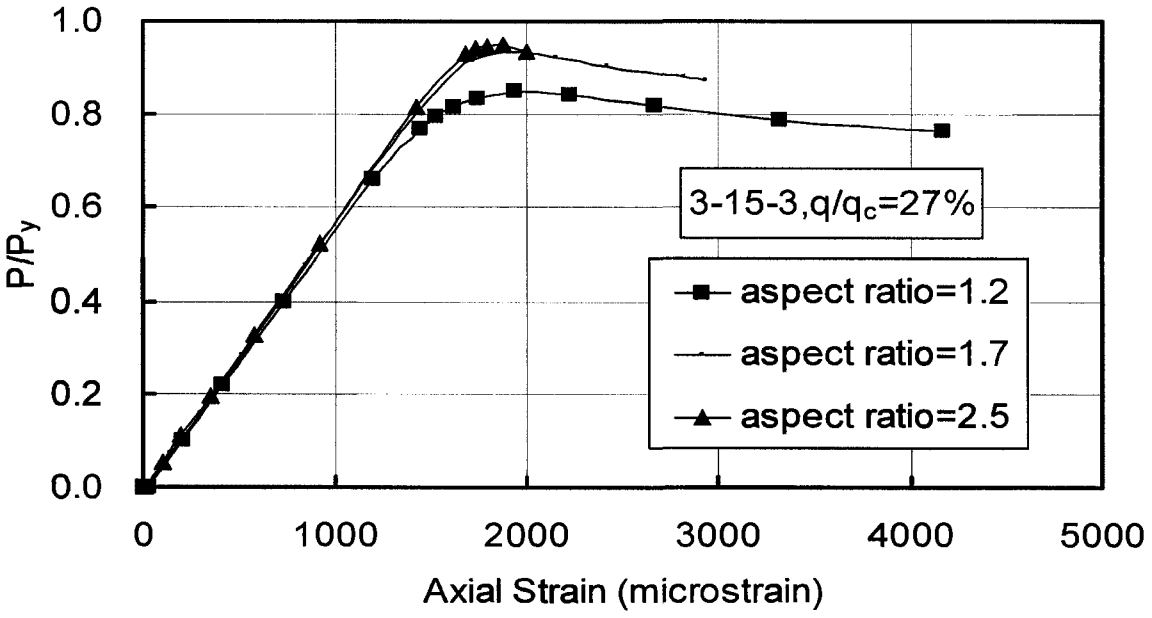

Figure 4.8 Normalized axial load versus axial strain (3-15-3, q/q_c = 27%)

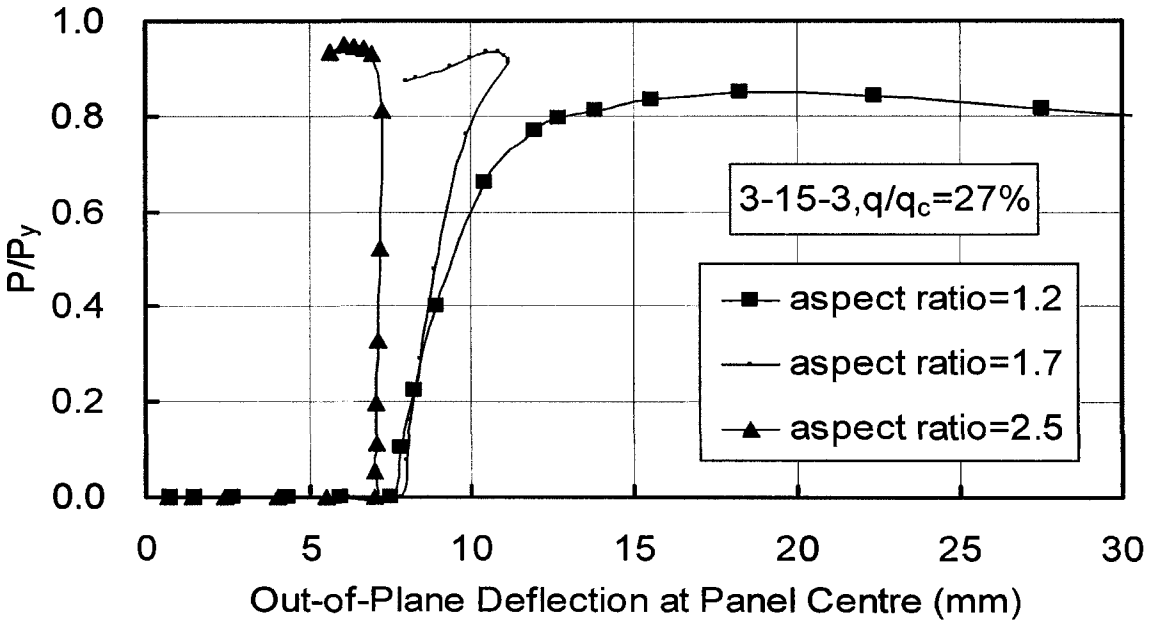

Figure 4.9 Normalized axial load versus out-of-plane deflection at panel centre (3-15-3, q/q_c = 27%)

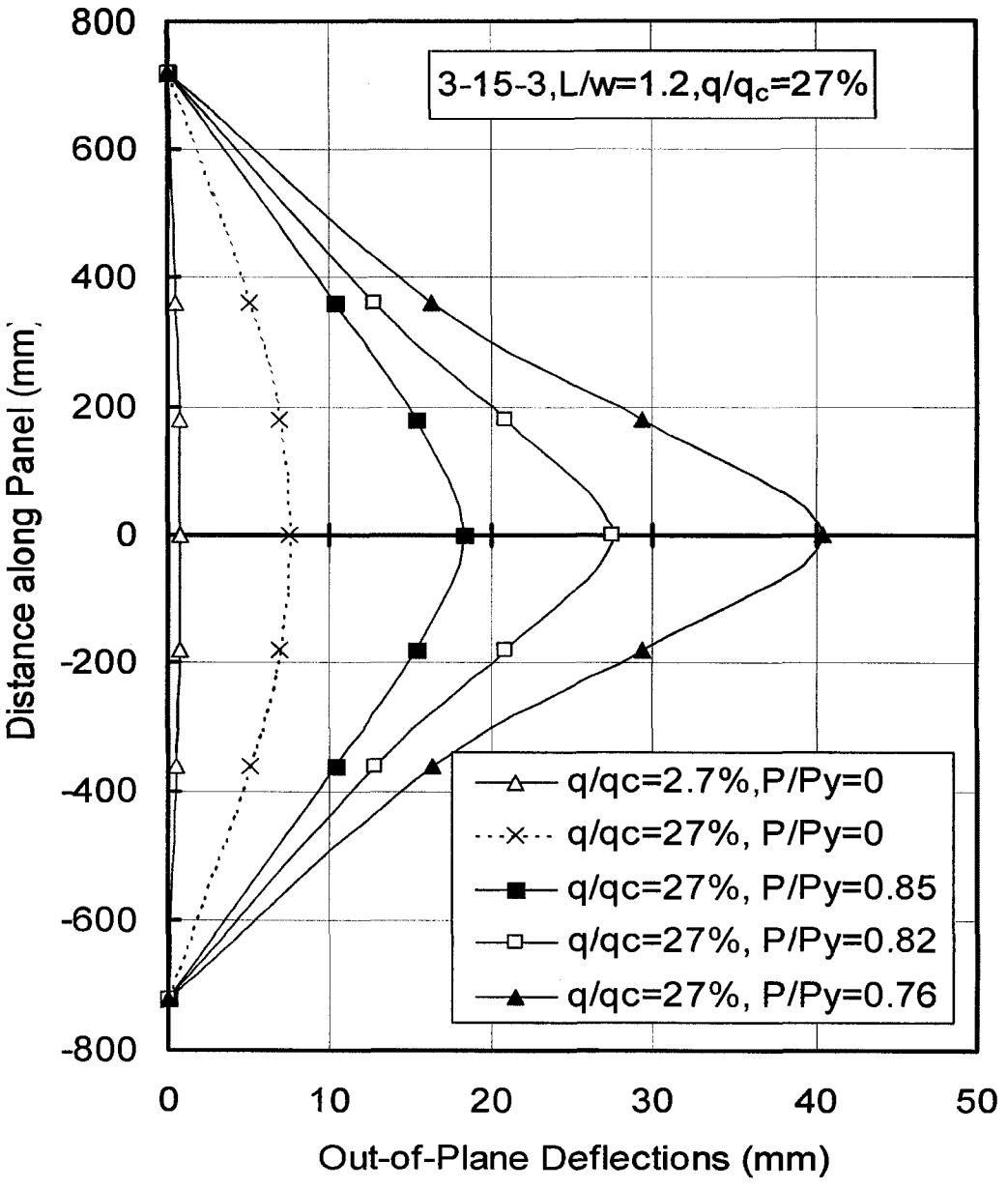

Figure 4.10 Out-of-plane deflections along panel length
(3-15-3, L/w = 1.2, q/q_c = 27%)

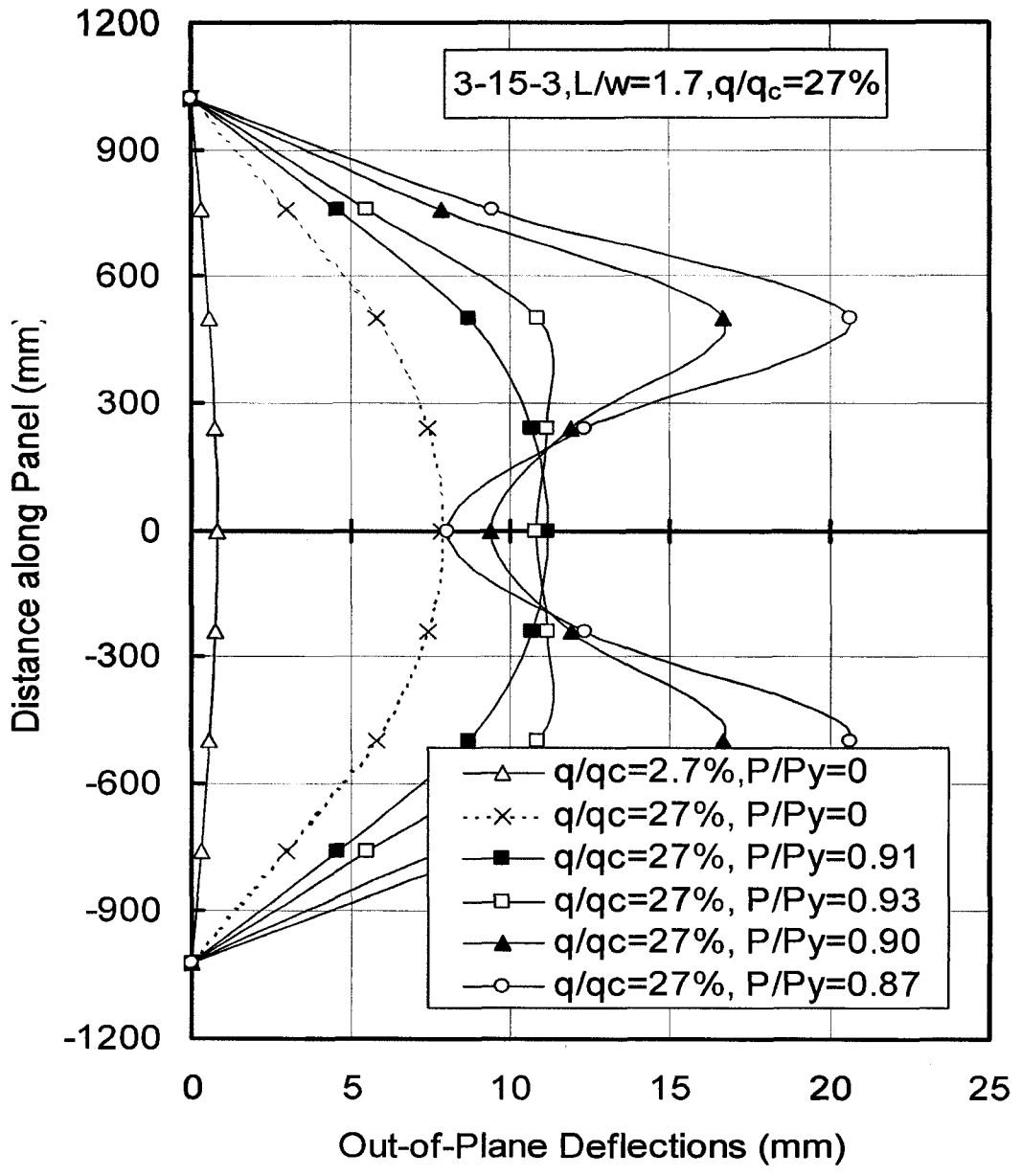

Figure 4.11 Out-of-plane deflections along panel length
(3-15-3, L/w = 1.7, q/q_c = 27%)

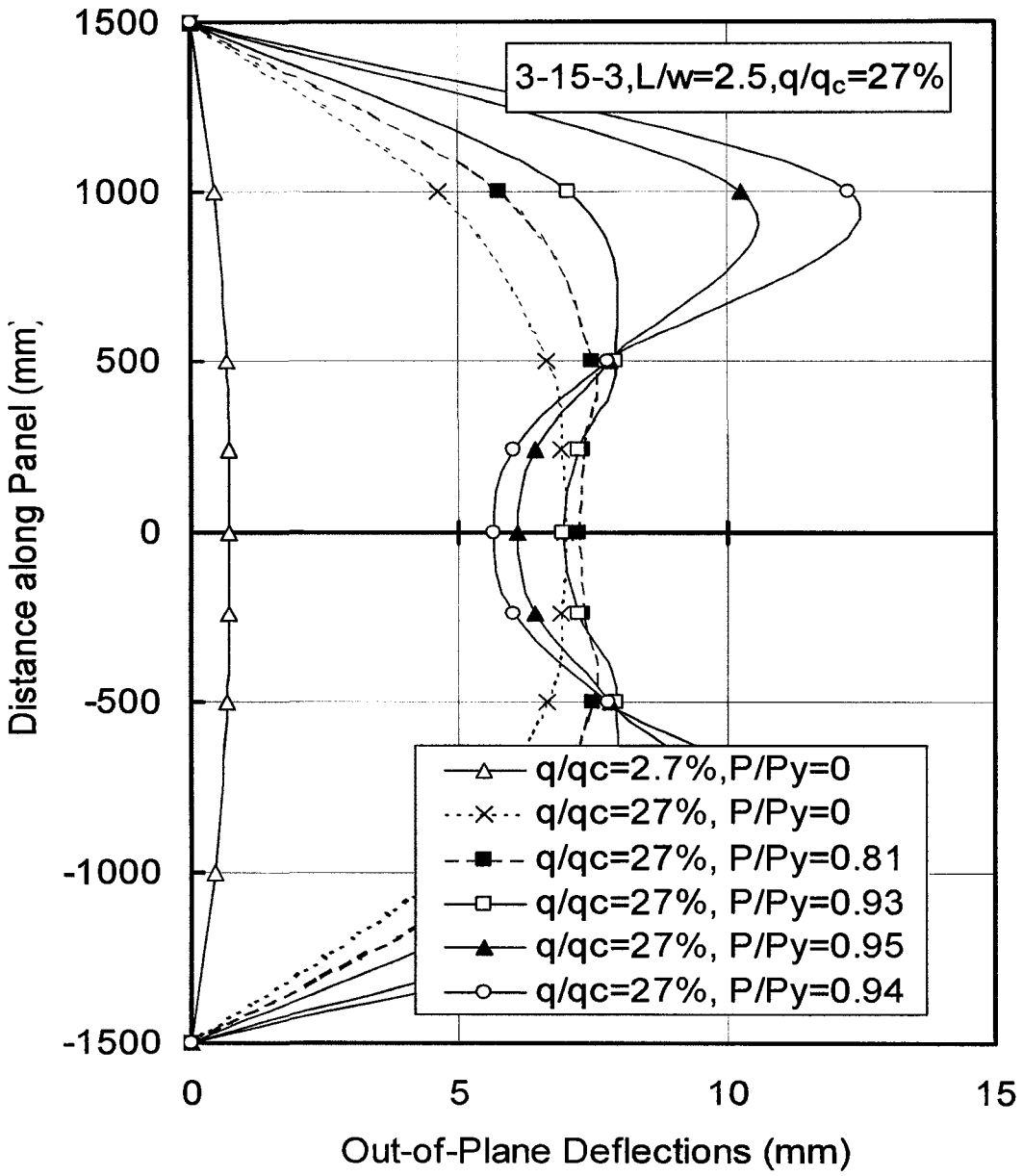

Figure 4.12 Out-of-plane deflections along panel length
(3-15-3, L/w = 2.5, q/q_c = 27%)

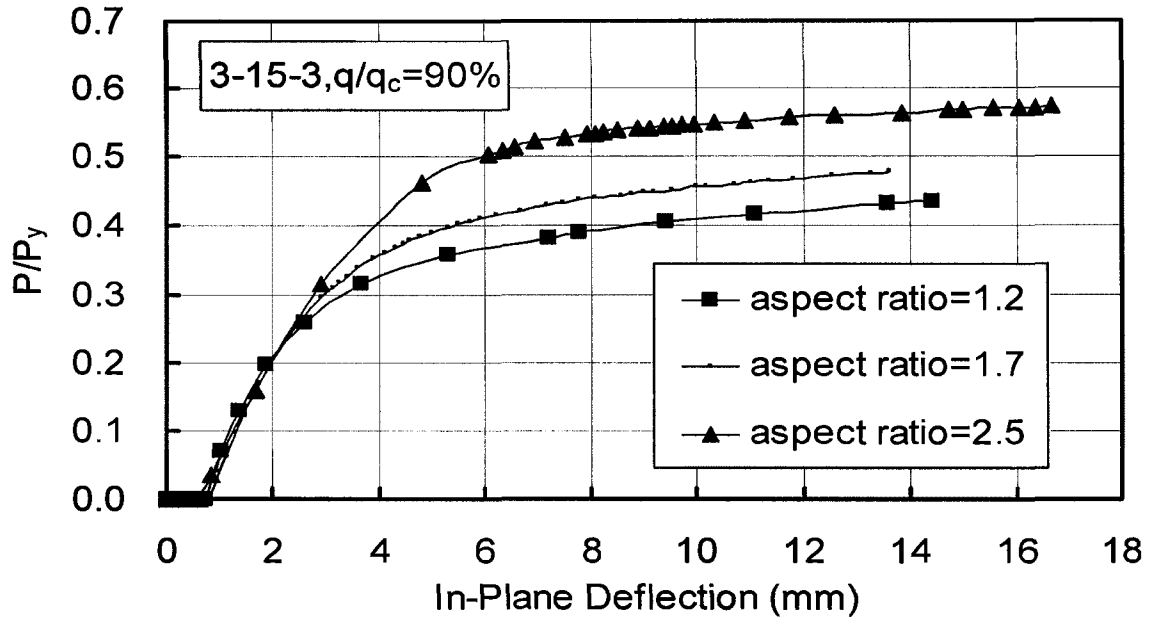

Figure 4.13 Normalized axial load versus in-plane deflections (3-15-3, q/q_c = 90%)

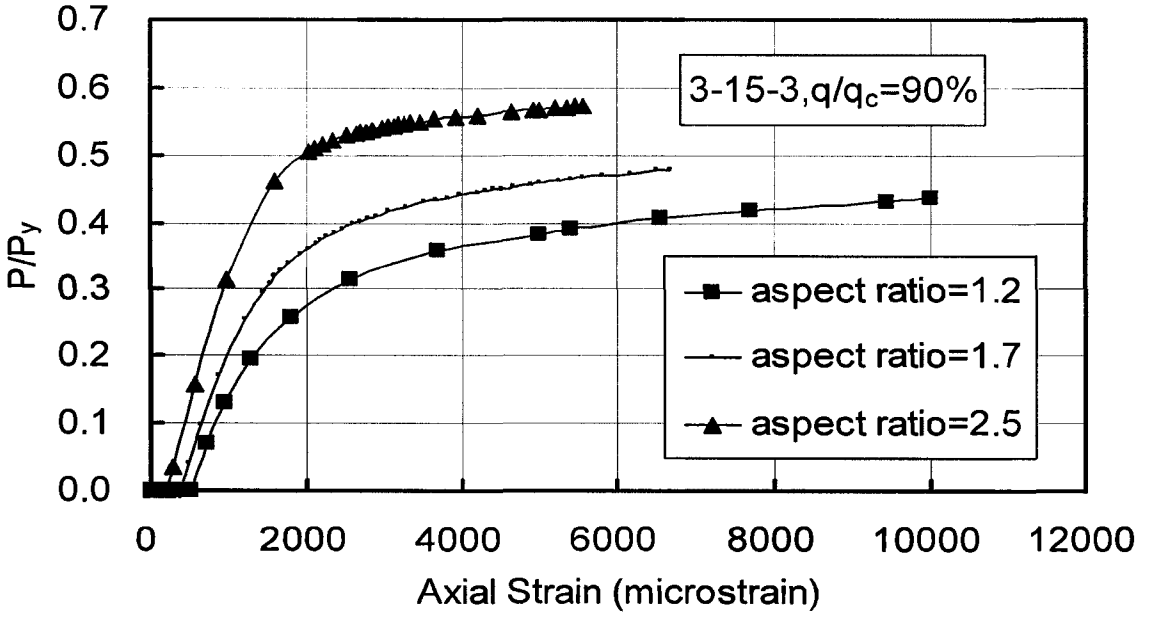

Figure 4.14 Normalized axial load versus axial strain (3-15-3, q/q_c = 90%)

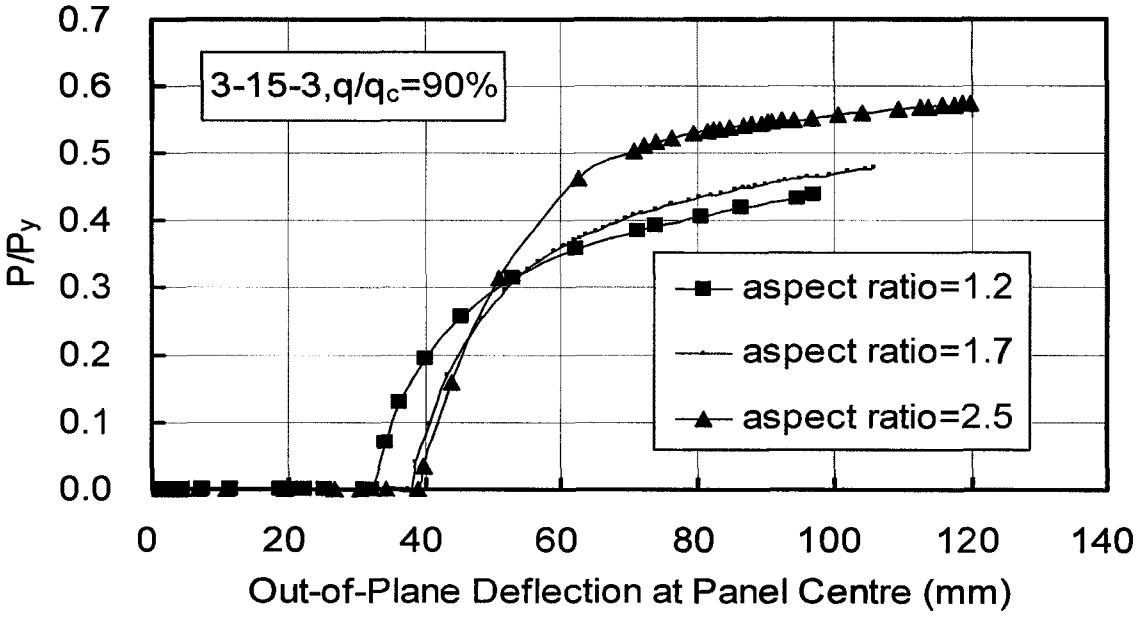

Figure 4.15 Normalized axial load versus out-of-plane deflection at panel centre (3-15-3, q/q_c = 90%)

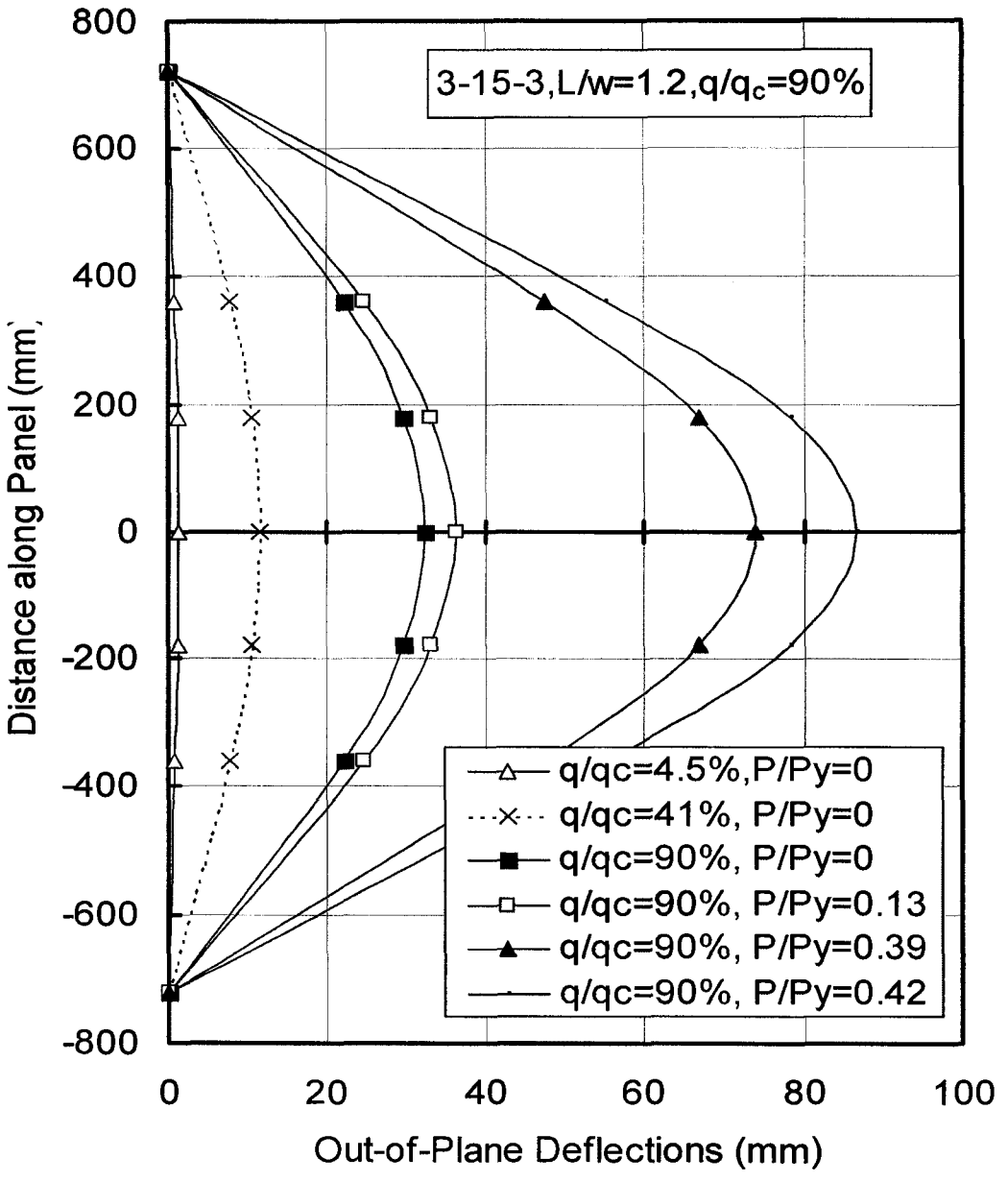

Figure 4.16 Out-of-plane deflections along panel length (3-15-3, L/w = 1.2, q/q_c = 90%)

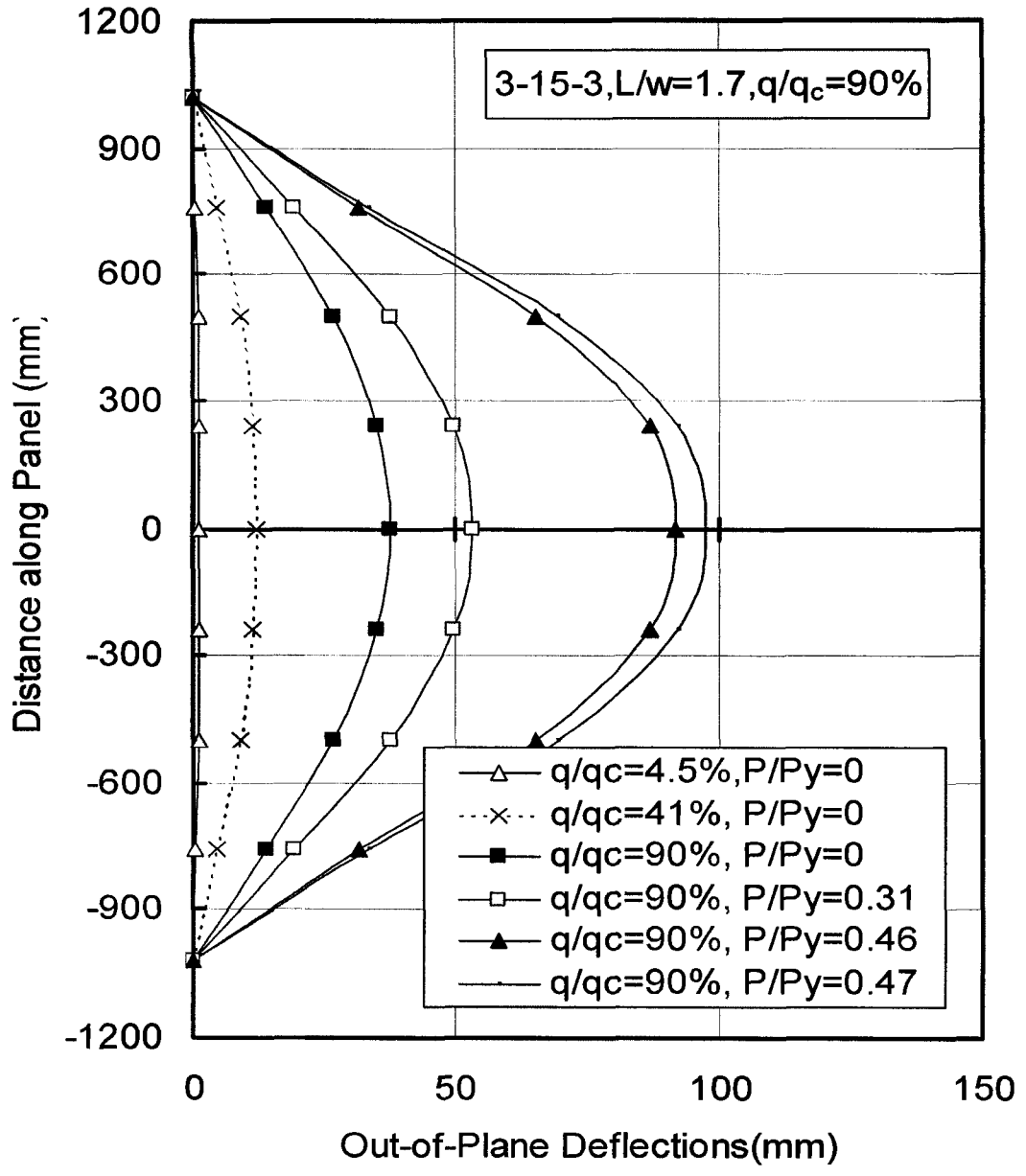

Figure 4.17 Out-of-plane deflections along panel length
(3-15-3, L/w = 1.7, q/q_c = 90%)

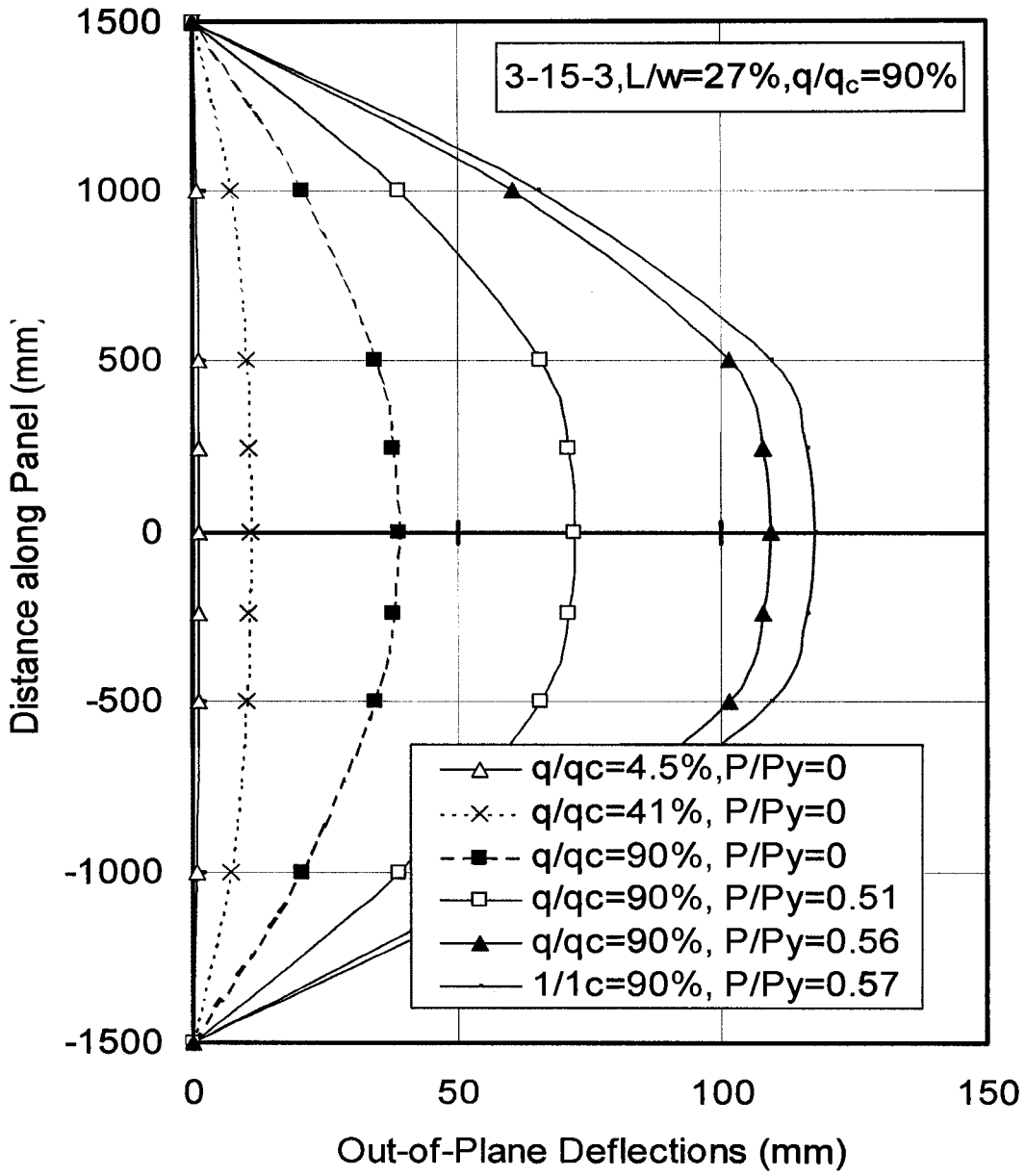

Figure 4.18 Out-of-plane deflections along panel length
(3-15-3, L/w = 2.5, q/q_c = 90%)

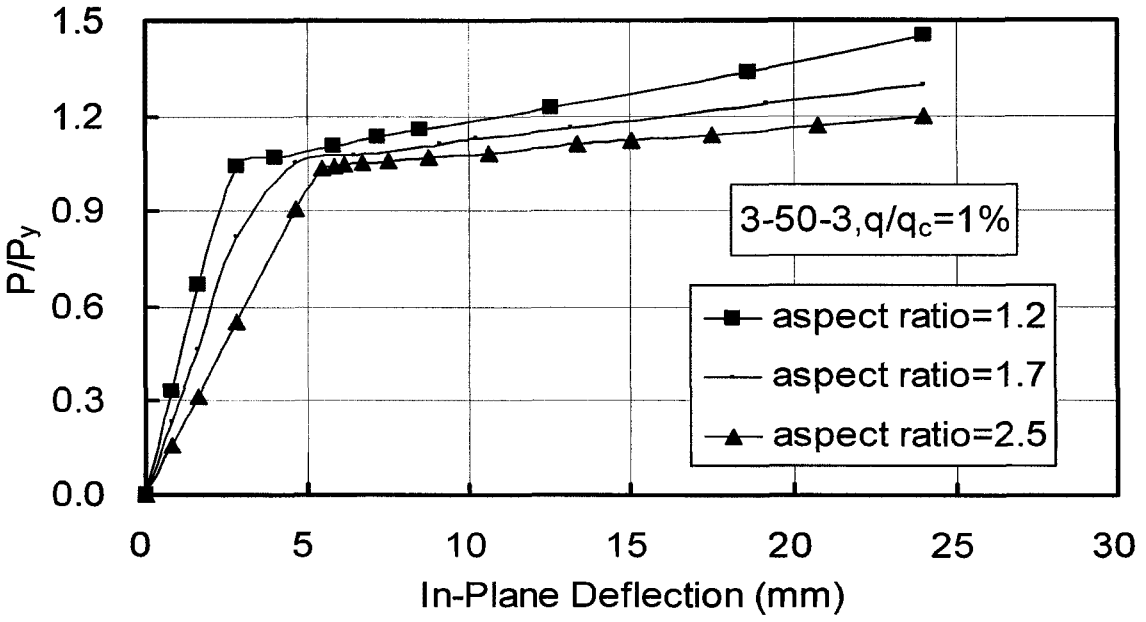

Figure 4.19 Normalized axial load versus in-plane deflections (3-50-3, q/q_c = 1%)

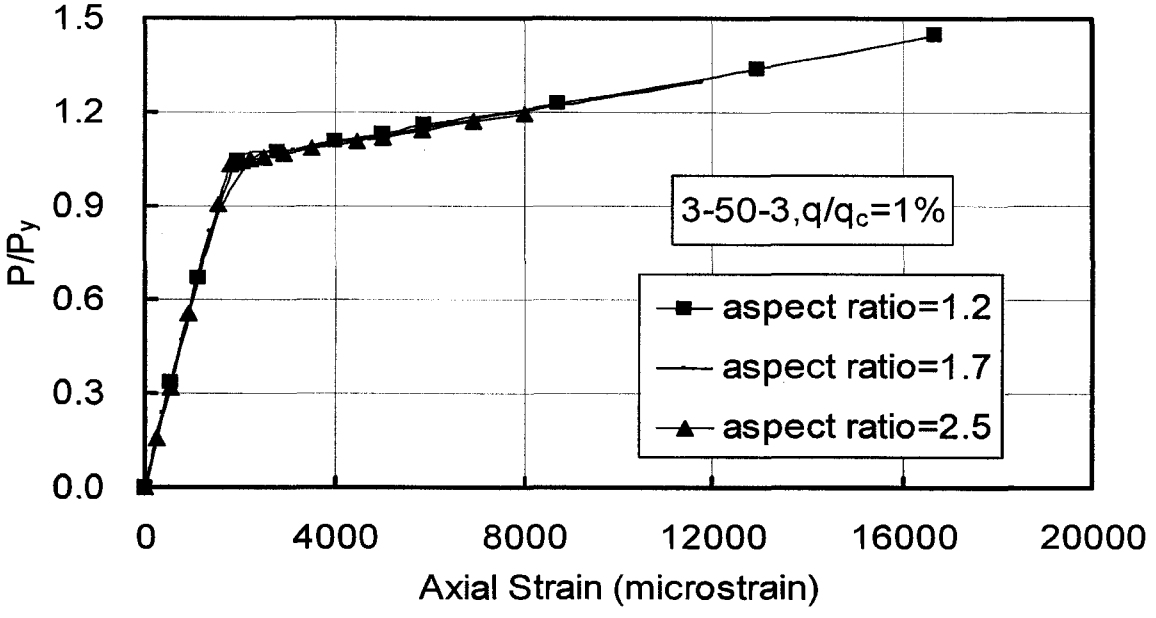

Figure 4.20 Normalized axial load versus axial strain (3-50-3, q/q_c = 1%)

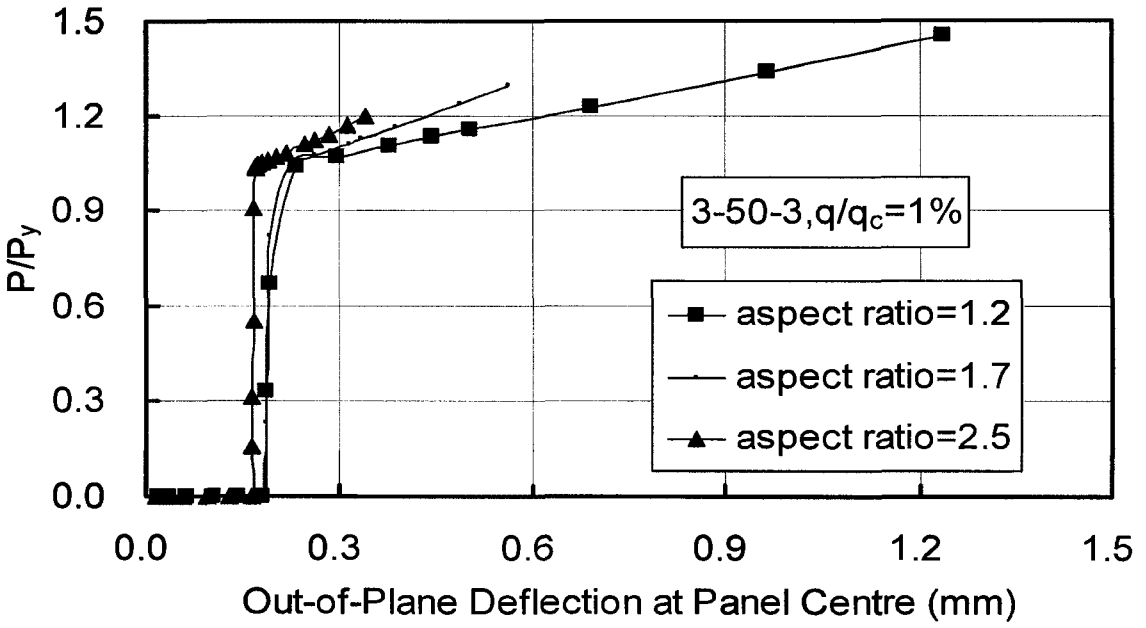

Figure 4.21 Normalized axial load versus out-of-plane deflection at panel centre (3-50-3, q/q_c = 1%)

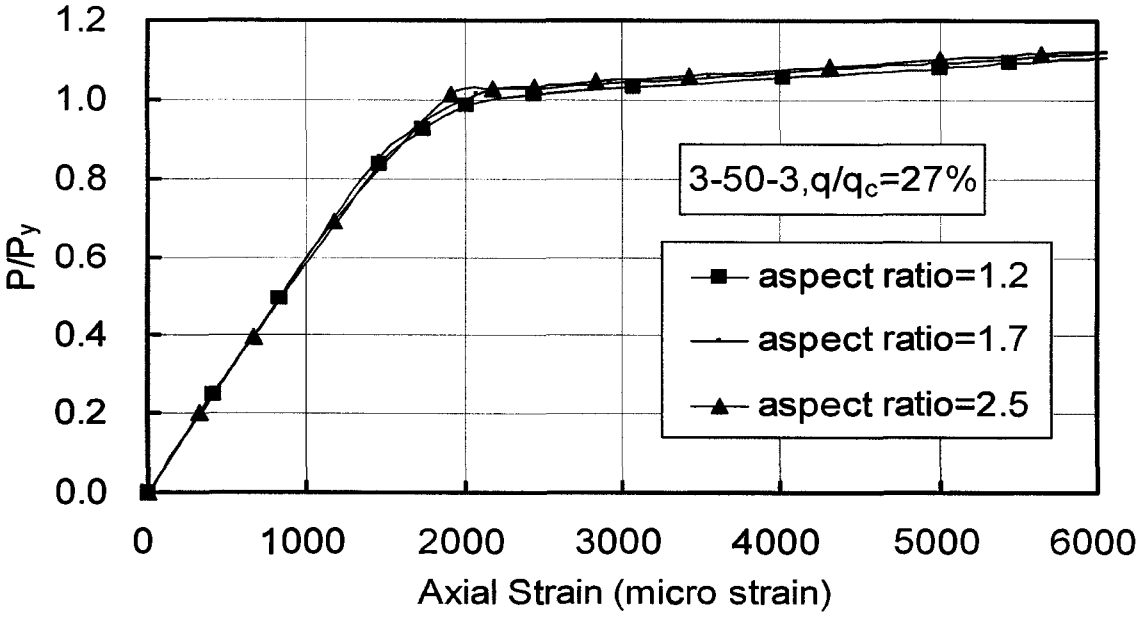

Figure 4.22 Normalized axial load versus axial strain (3-50-3, q/q_c = 27%)

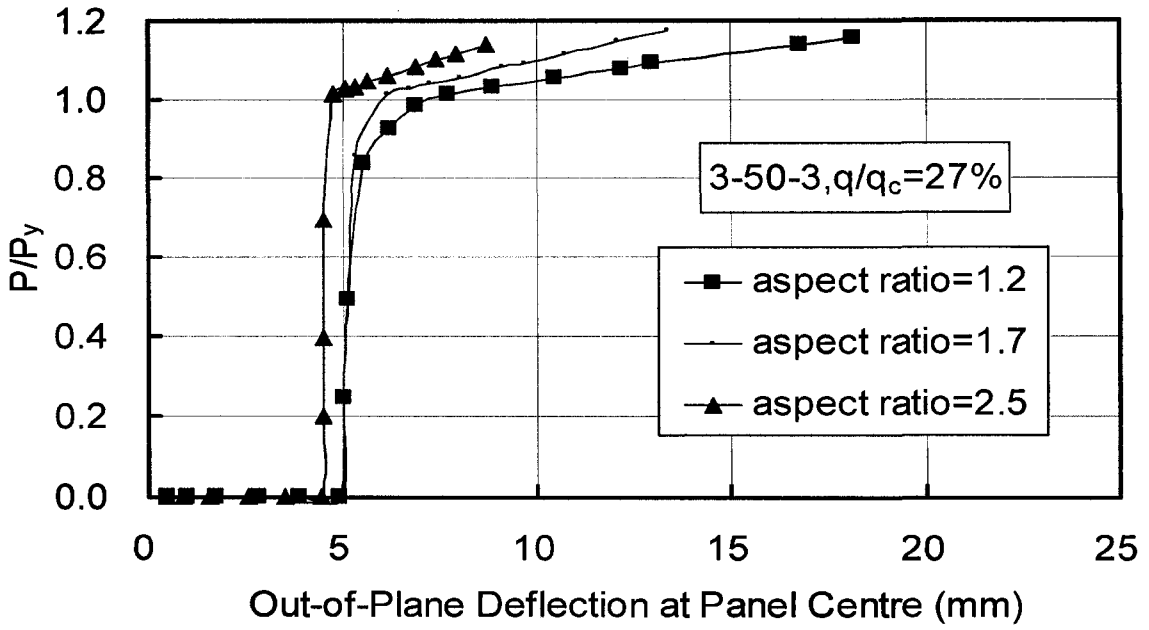

Figure 4.23 Normalized axial load versus out-of-plane deflection at panel centre (3-50-3, q/q_c = 27%)

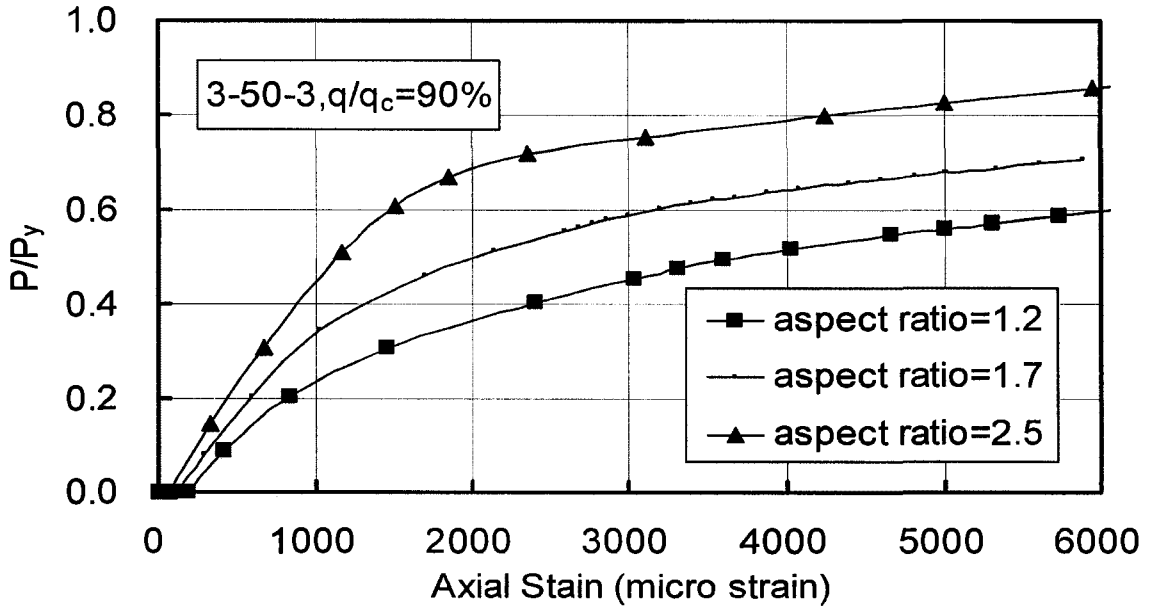

Figure 4.24 Normalized axial load versus axial strain (3-50-3, q/q_c = 90%)

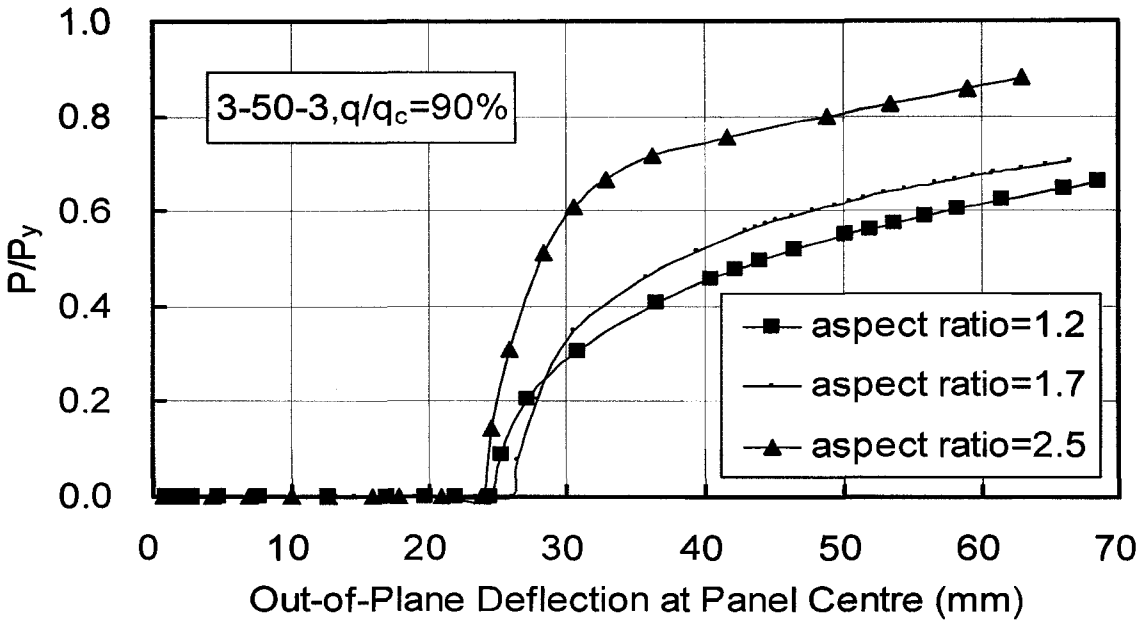

Figure 4.25 Normalized axial load versus out-of-plane deflection at panel centre (3-50-3, q/q_c = 90%)

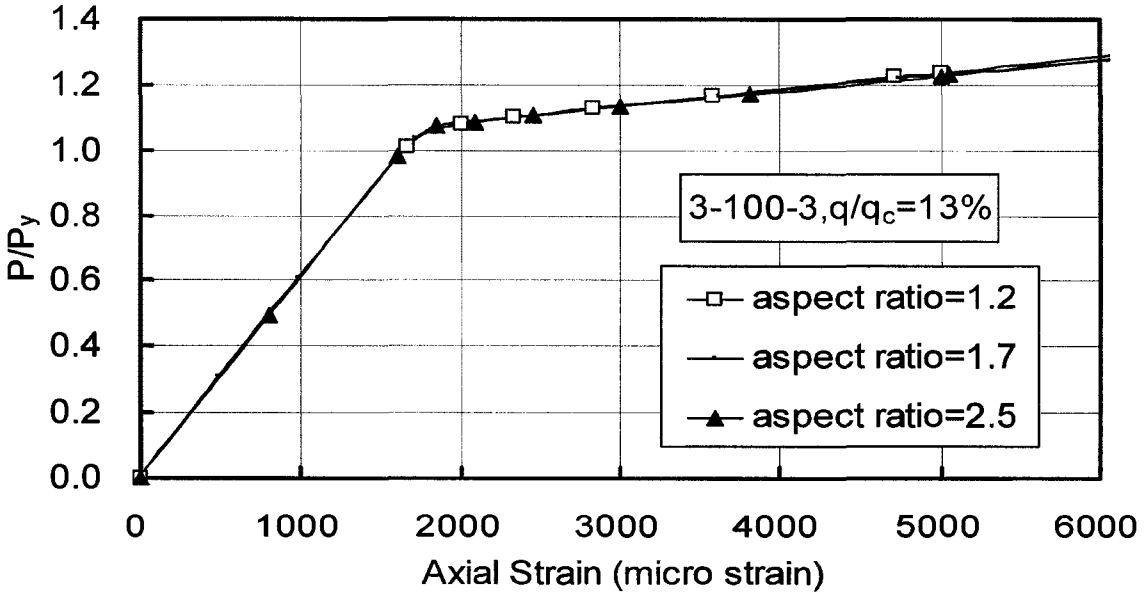

Figure 4.26 Normalized axial load versus axial strain (3-100-3, q/q_c = 13%)

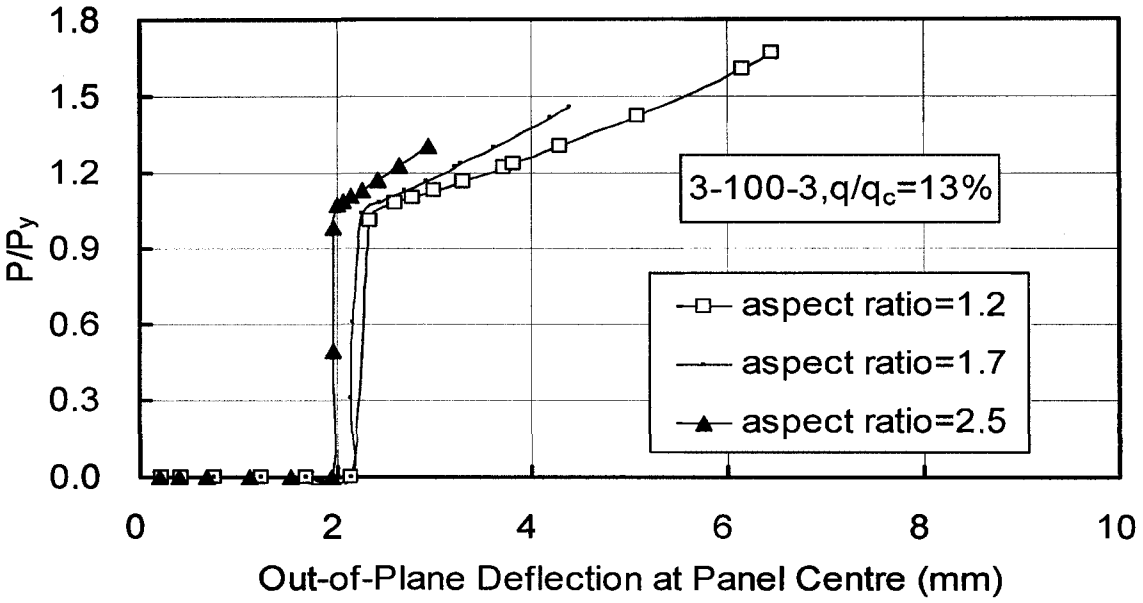

Figure 4.27 Normalized axial load versus out-of-plane deflection at panel centre (3-100-3, q/q_c = 13%)

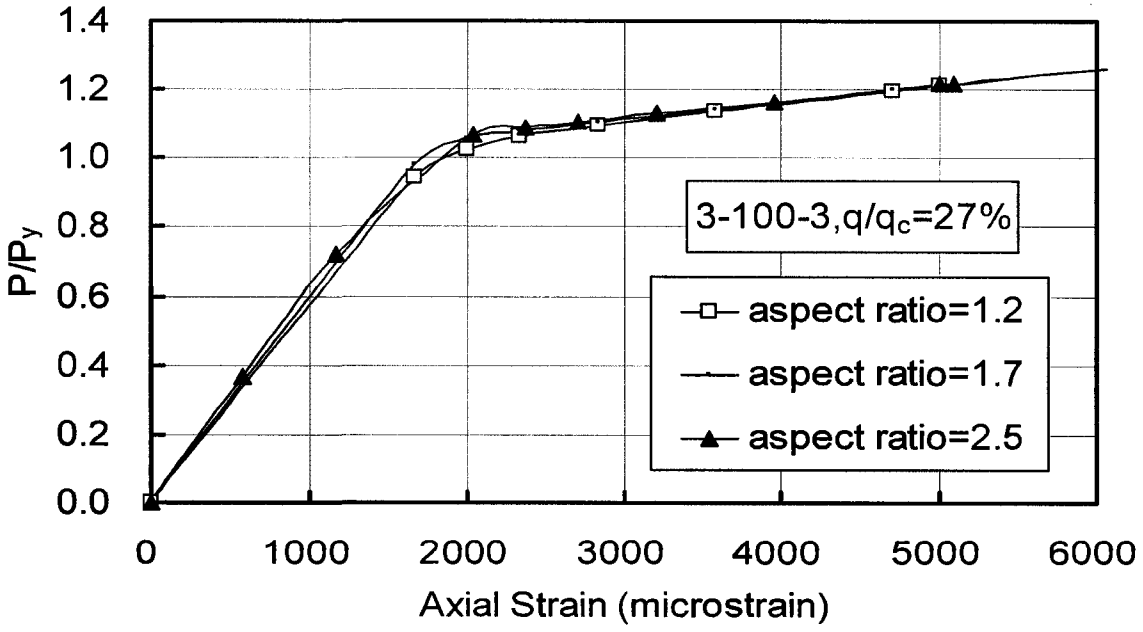

Figure 4.28 Normalized axial load versus axial strain (3-100-3, q/q_c = 27%)

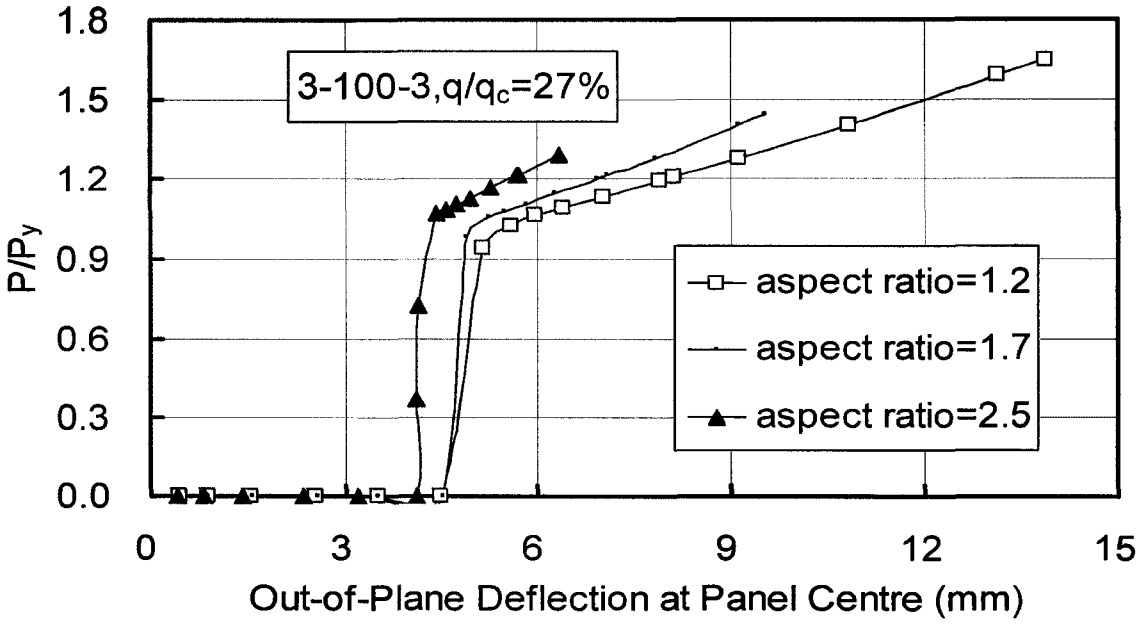

Figure 4.29 Normalized axial load versus out-of-plane deflection at panel centre (3-100-3, q/q_c = 27%)

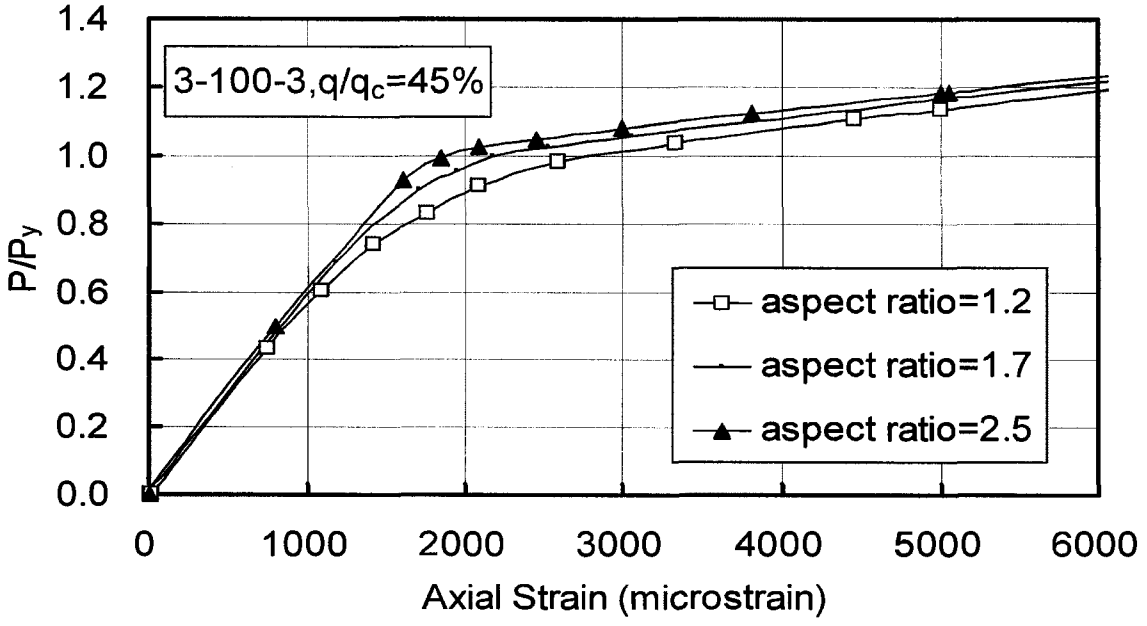

Figure 4.30 Normalized axial load versus axial strain (3-100-3, q/q_c = 45%)

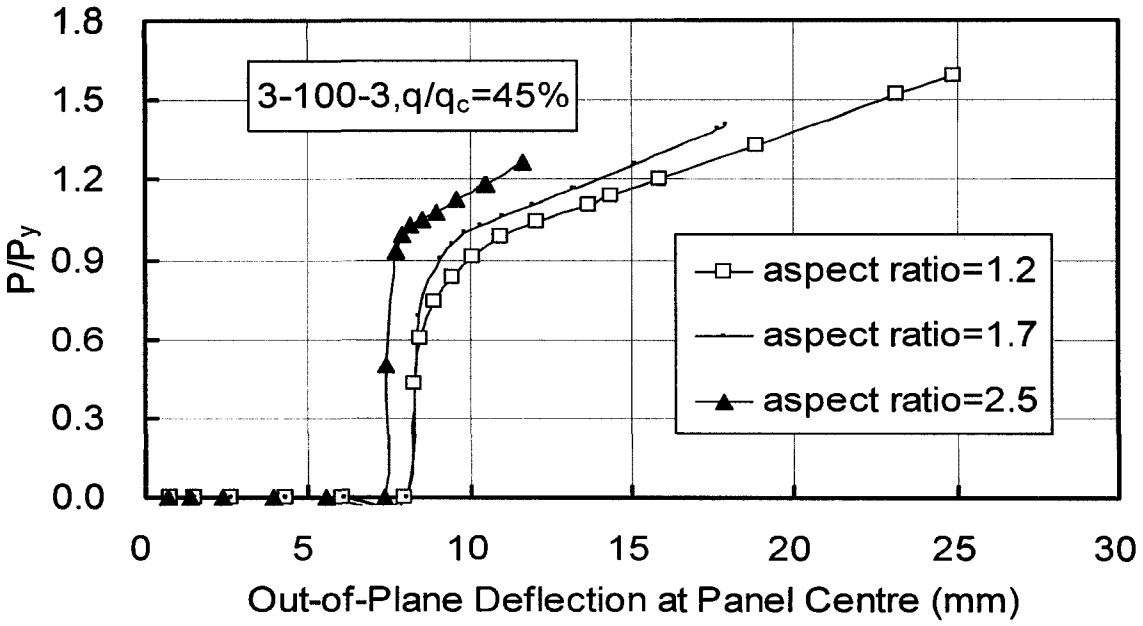

Figure 4.31 Normalized axial load versus out-of-plane deflection at panel centre (3-100-3, q/q_c = 45%)

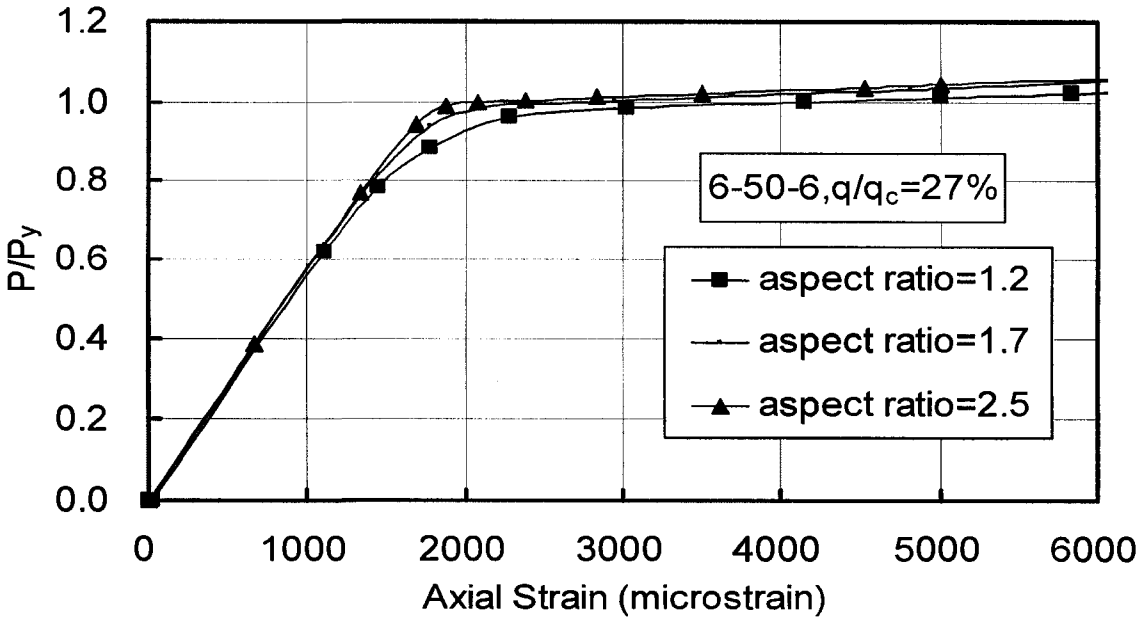

Figure 4.32 Normalized axial load versus axial strain (6-50-6, q/q_c = 27%)

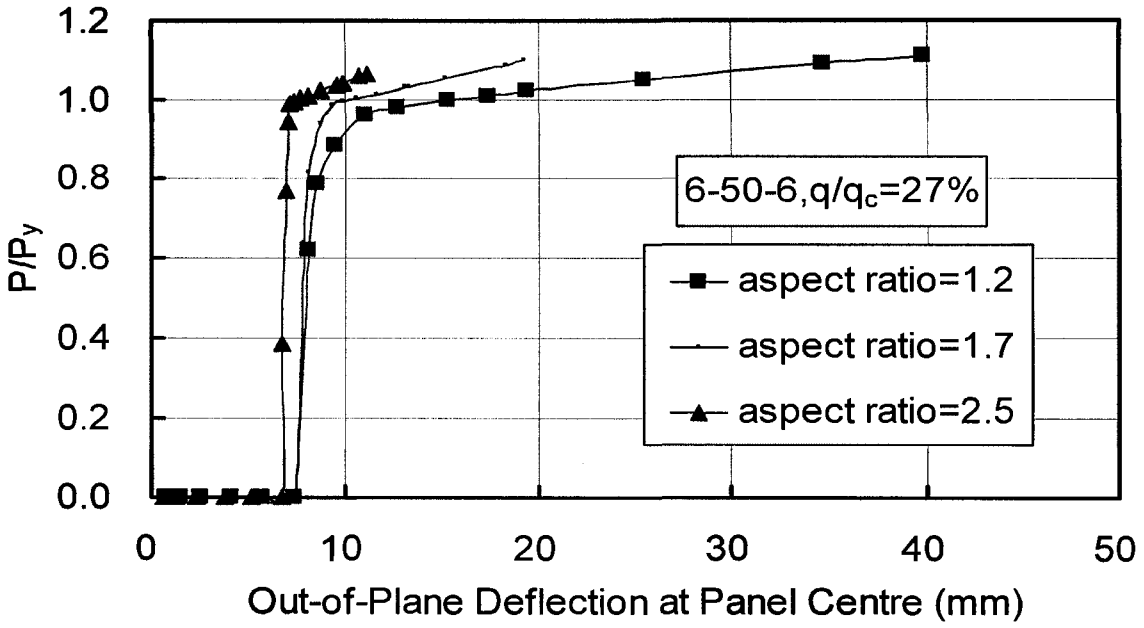

Figure 4.33 Normalized axial load versus out-of-plane deflection at panel centre (6-50-6, q/q_c = 27%)

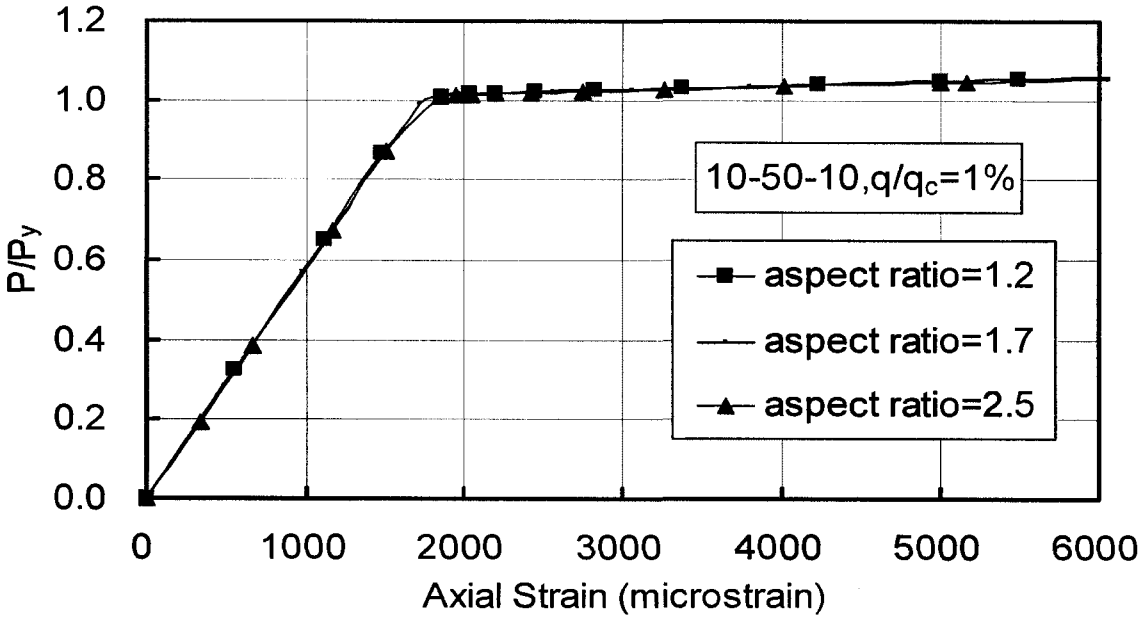

Figure 4.34 Normalized axial load versus axial strain (10-50-10, q/q_c = 1%)

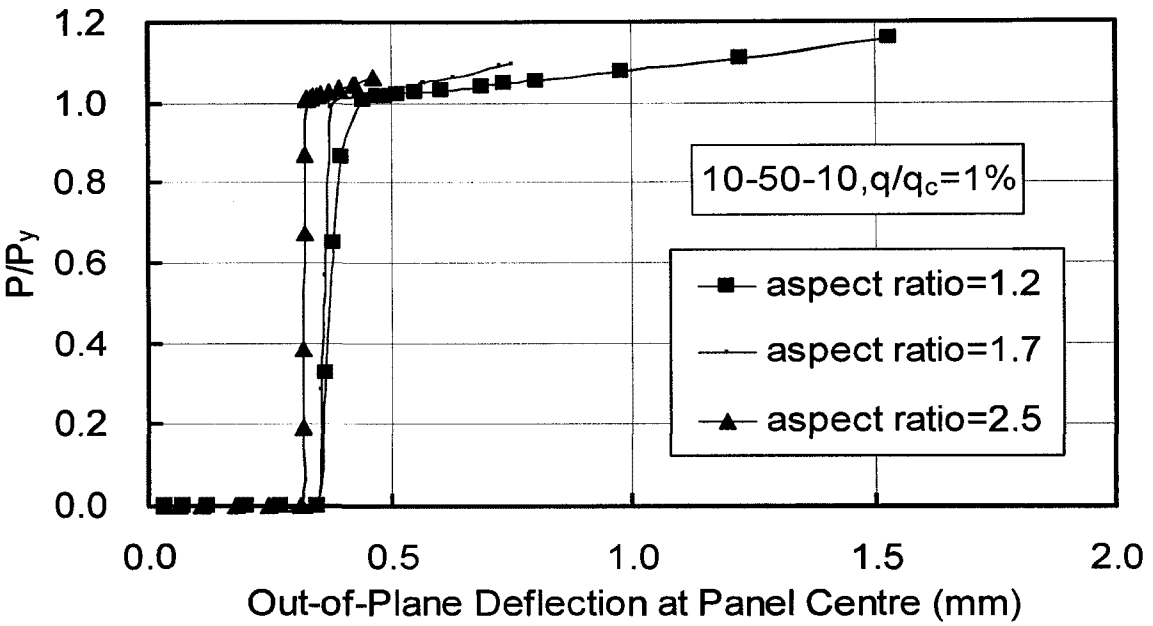

Figure 4.35 Normalized axial load versus out-of-plane deflection at panel centre (10-50-10, q/q_c = 1%)

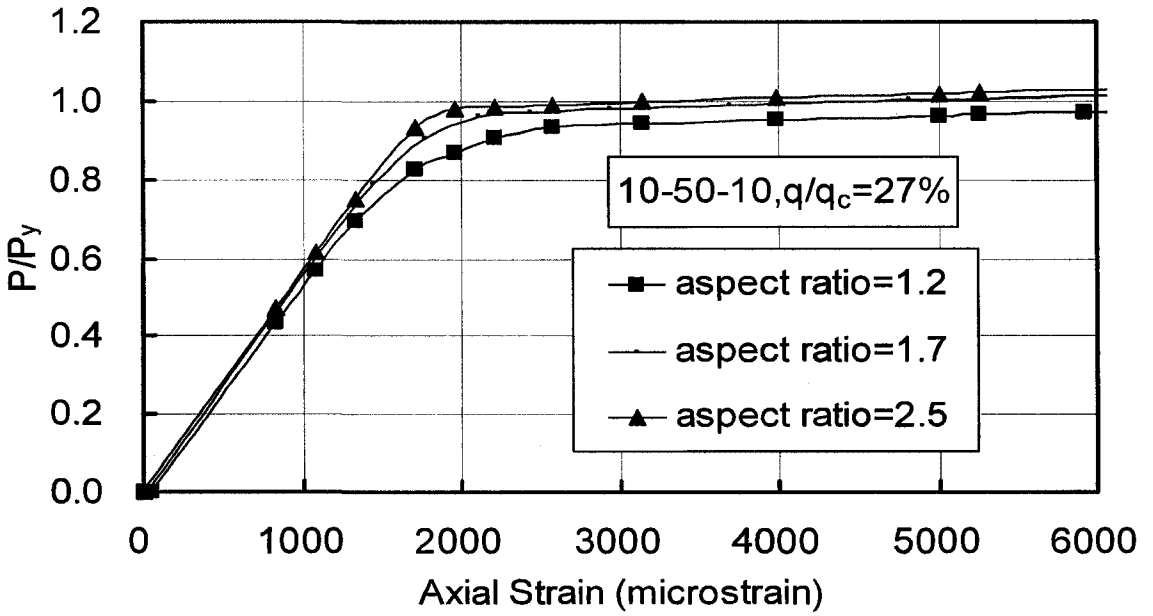

Figure 4.36 Normalized axial load versus axial strain (10-50-10, q/q_c = 27%)

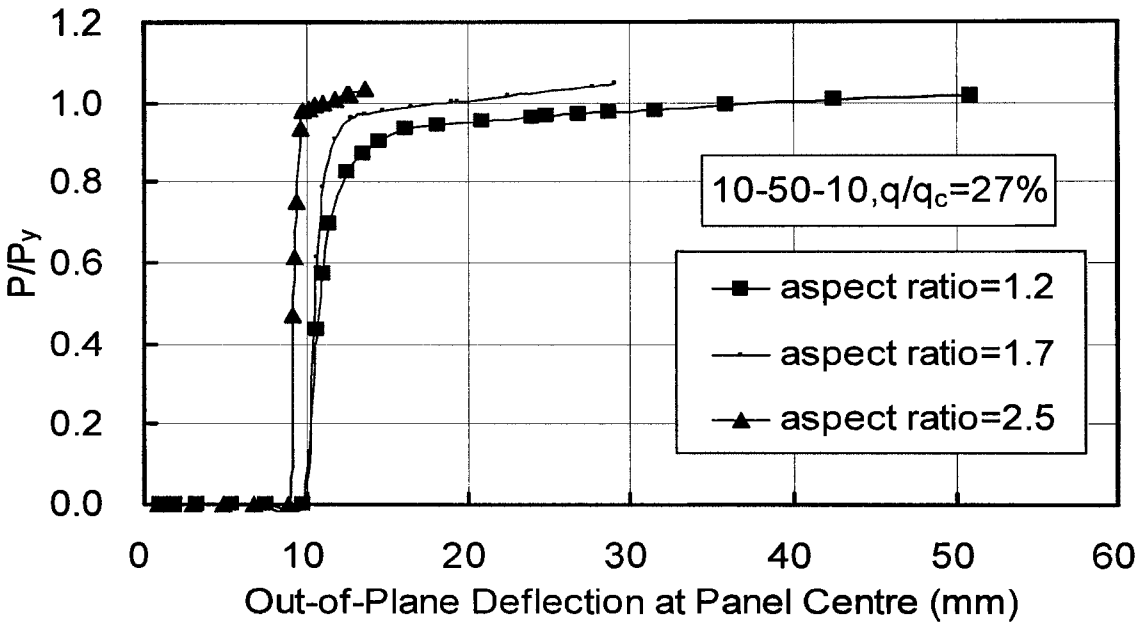

Figure 4.37 Normalized axial load versus out-of-plane deflection at panel centre (10-50-10, q/q_c = 27%)

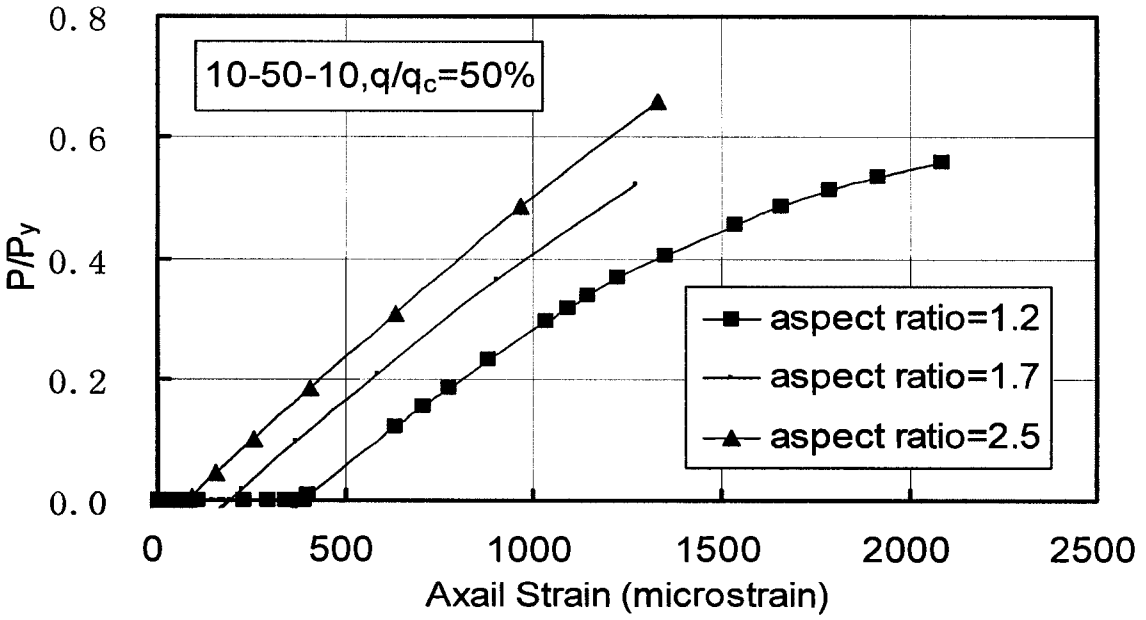

Figure 4.38 Normalized axial load versus axial strain (10-50-10, q/q_c = 50%)

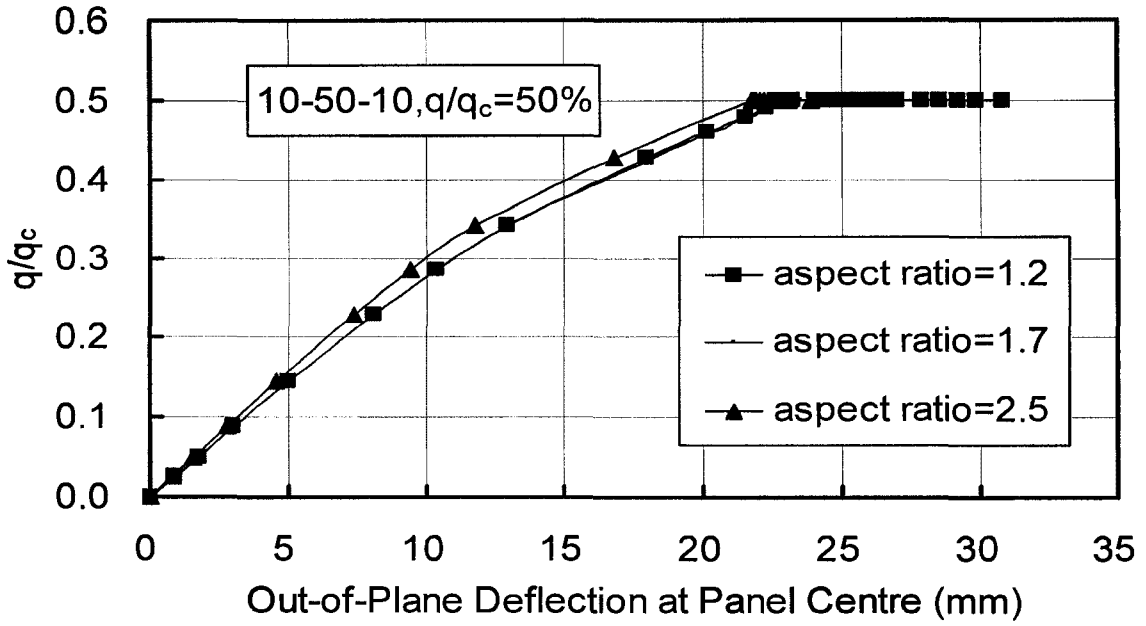

Figure 4.39 Normalized axial load versus out-of-plane deflection at panel centre (10-50-10, q/q_c = 50%)

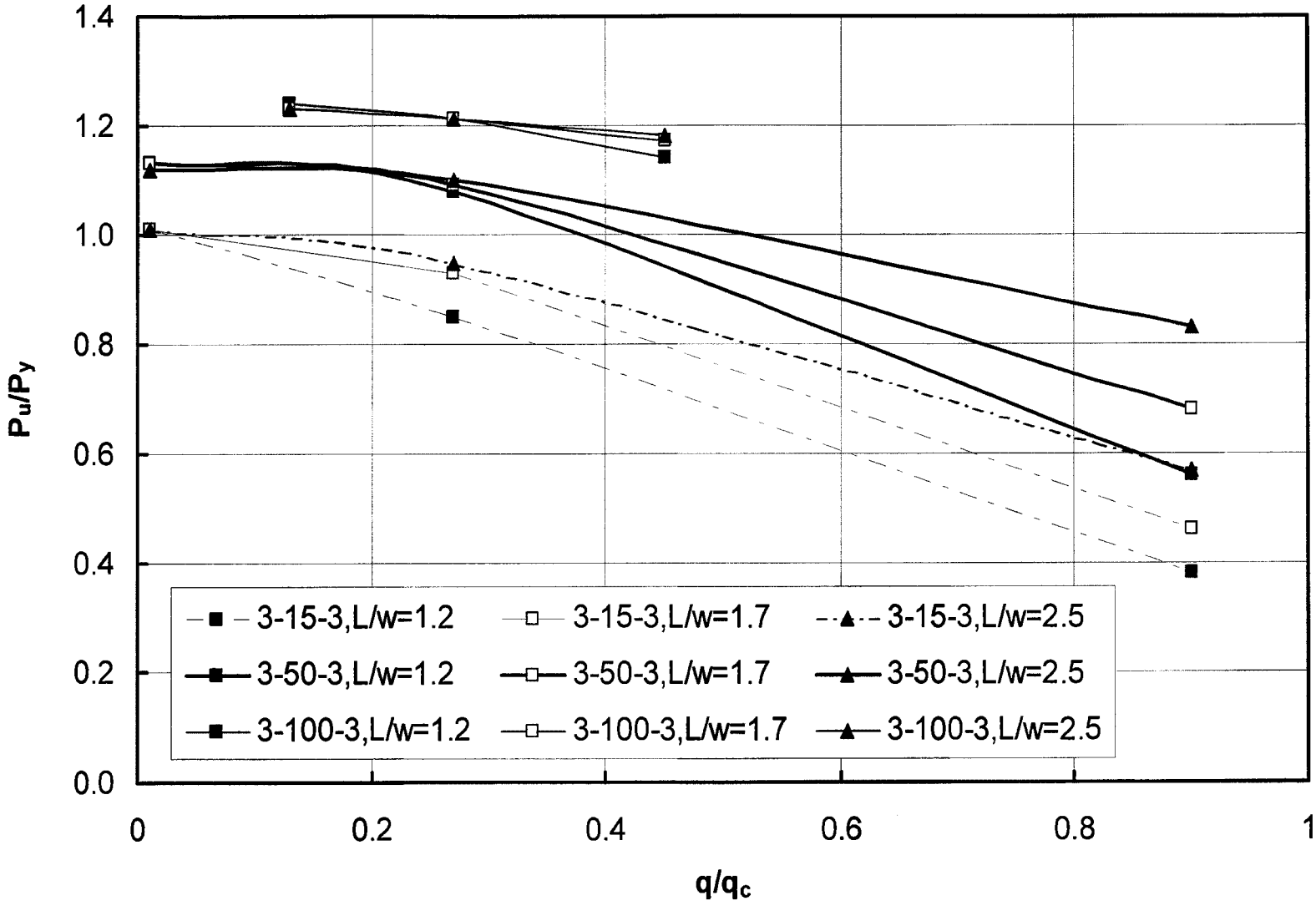

Figure 4.40 Normalized axial load capacity versus normalized lateral pressure capacity

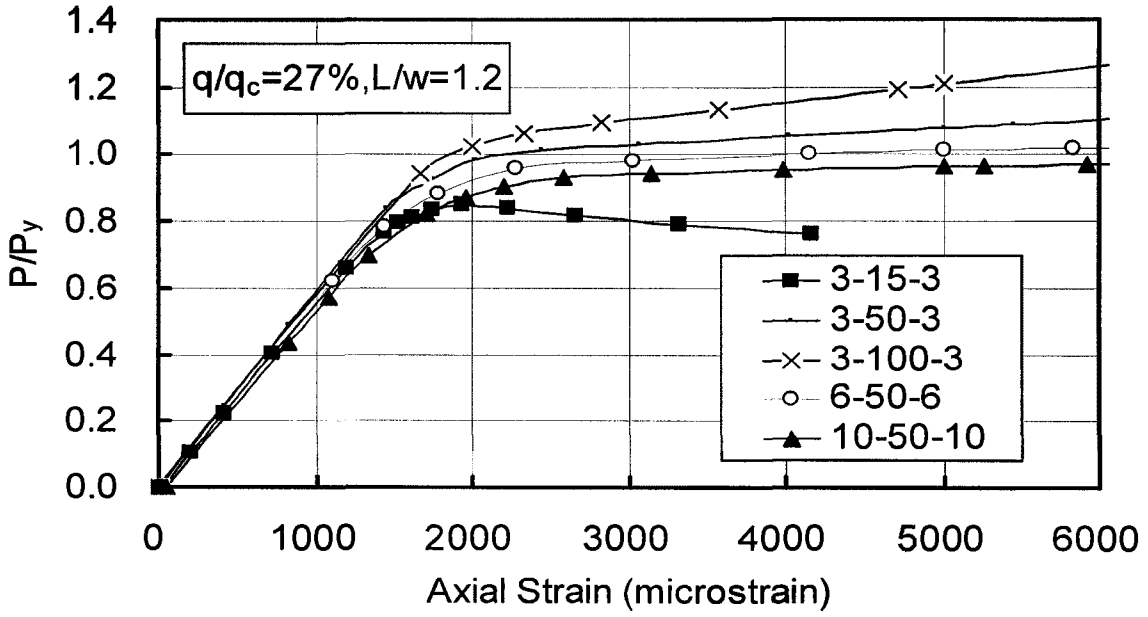

Figure 4.41 Normalized axial load versus axial strain (L/w = 1.2, q/q_c = 27%)

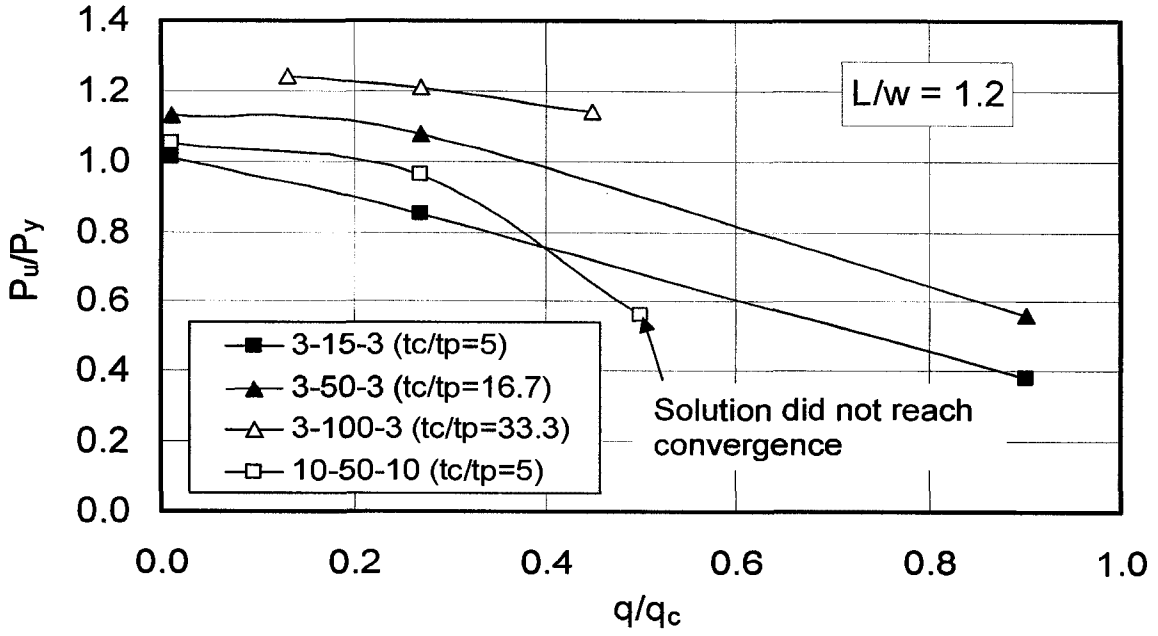

Figure 4.42 Normalized axial load versus normalized lateral pressure capacity (L/w = 1.2)

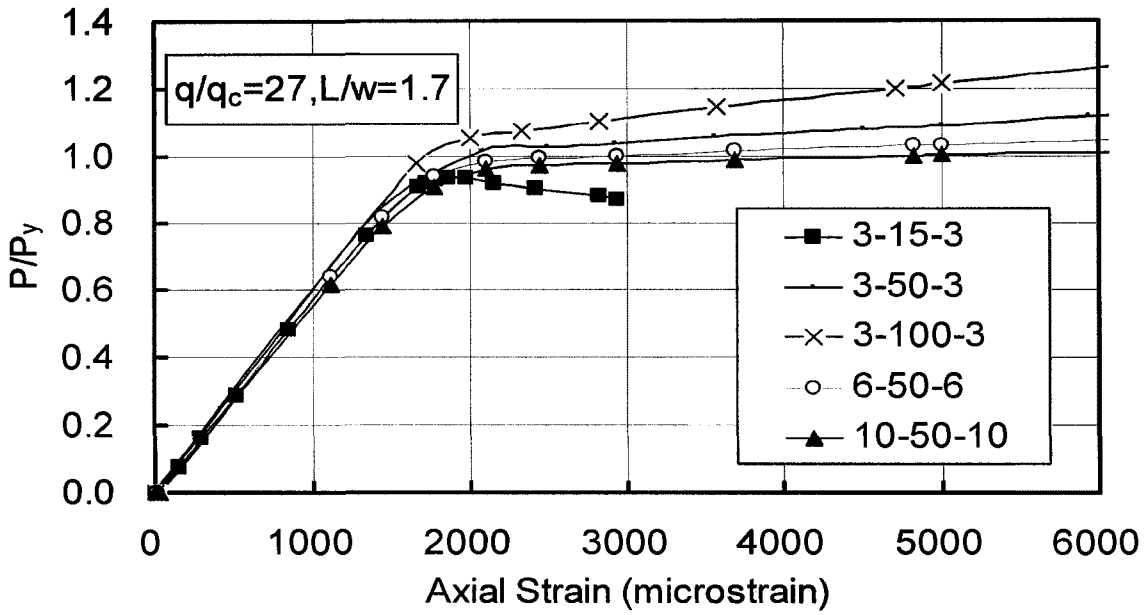

Figure 4.43 Normalized axial load versus axial strain (L/w = 1.7, q/q_c = 27%)

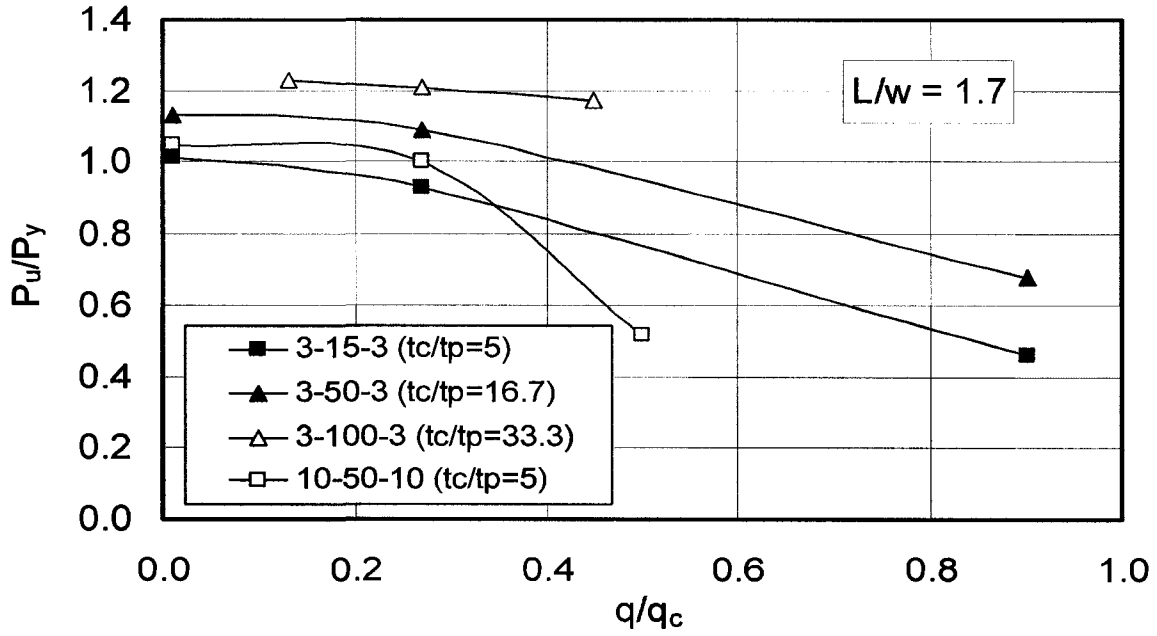

Figure 4.44 Normalized axial load versus normalized lateral pressure capacity (L/w = 1.7)

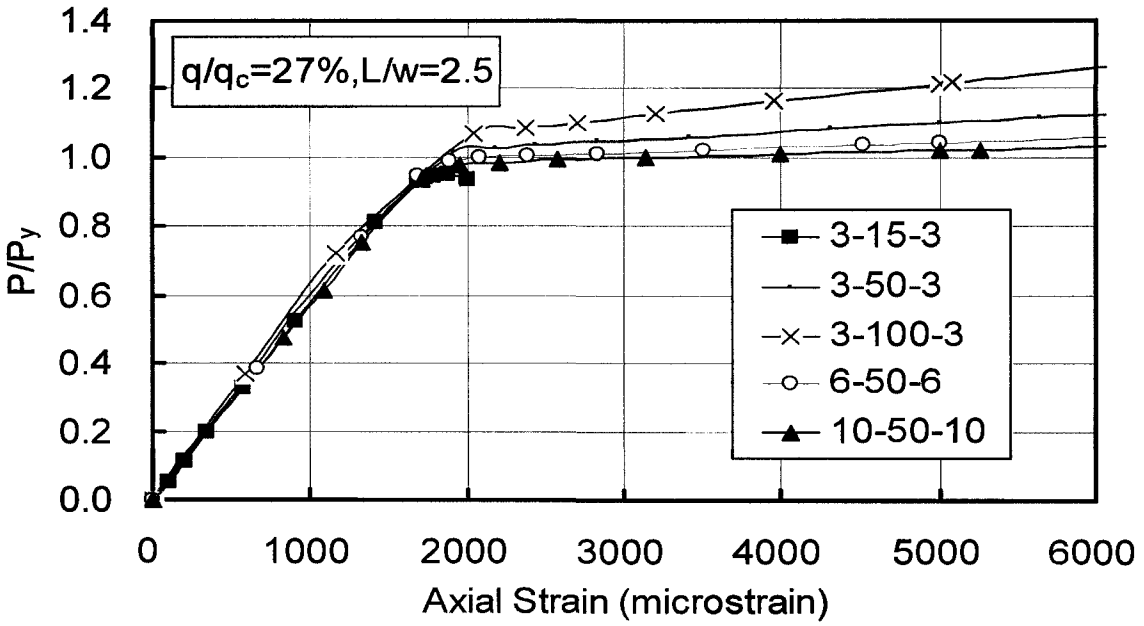

Figure 4.45 Normalized axial load versus axial strain (L/w = 2.5, q/q_c = 27%)

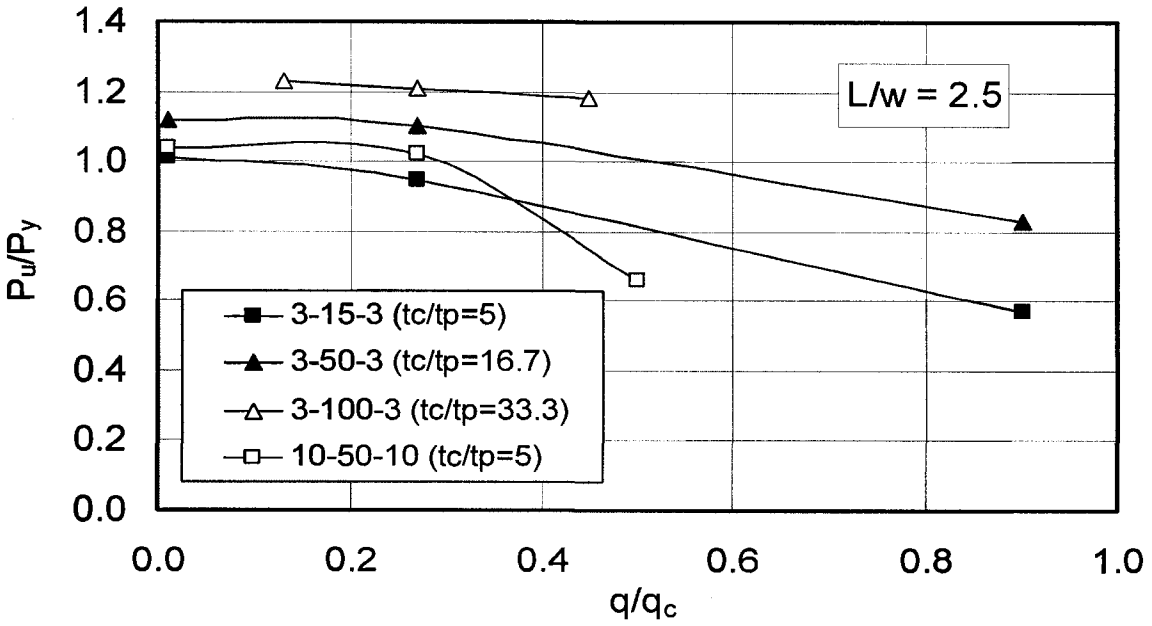

Figure 4.46 Normalized axial load versus normalized lateral pressure capacity (L/w = 2.5)

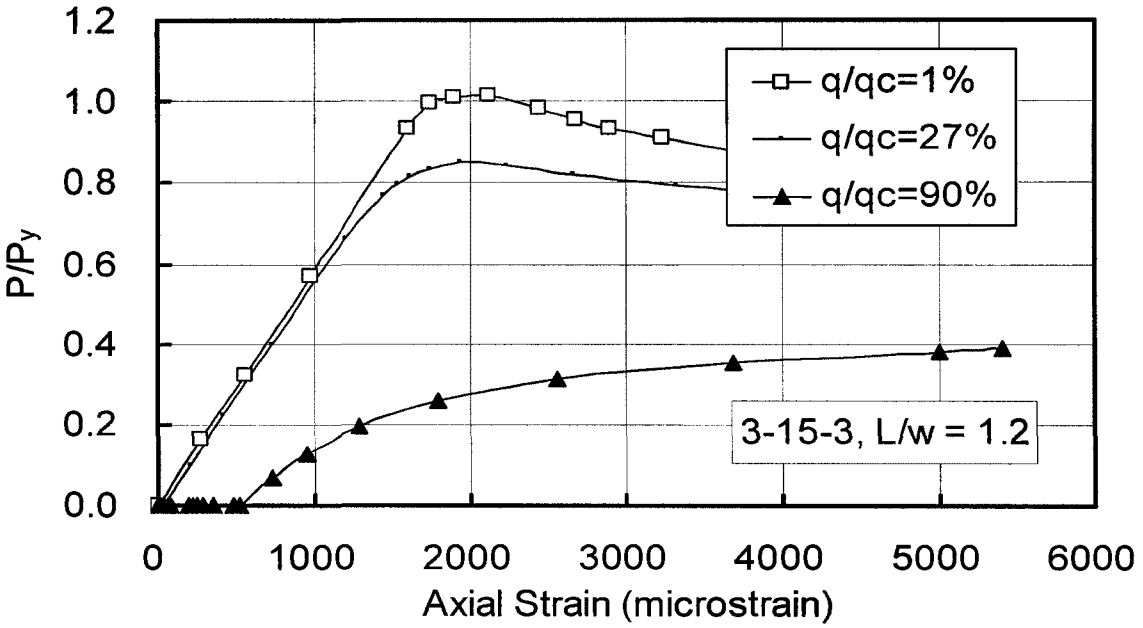

Figure 4.47 Normalized axial load versus axial strain (3-15-3, L/w = 1.2)

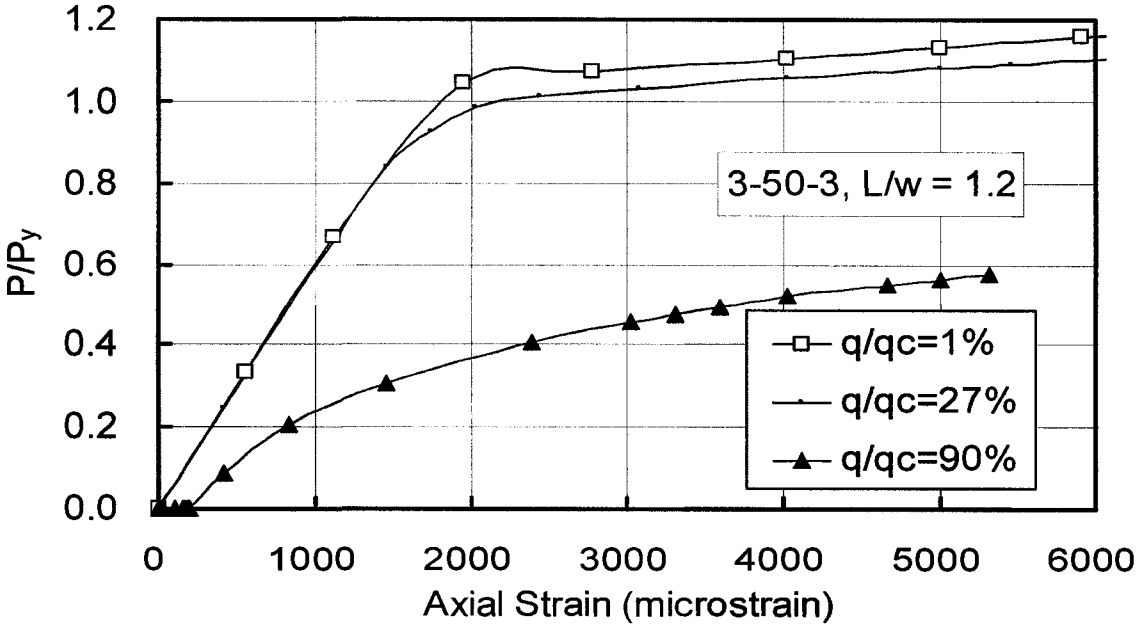

Figure 4.48 Normalized axial load versus axial strain (3-50-3, L/w = 1.2)

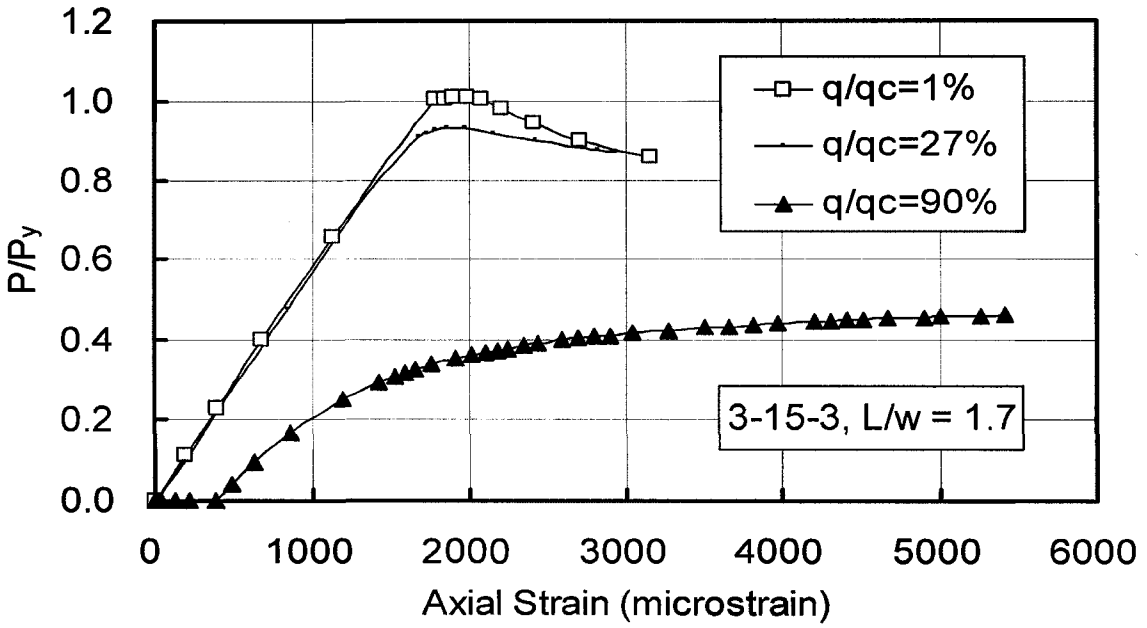

Figure 4.49 Normalized axial load versus axial strain (3-15-3, L/w = 1.7)

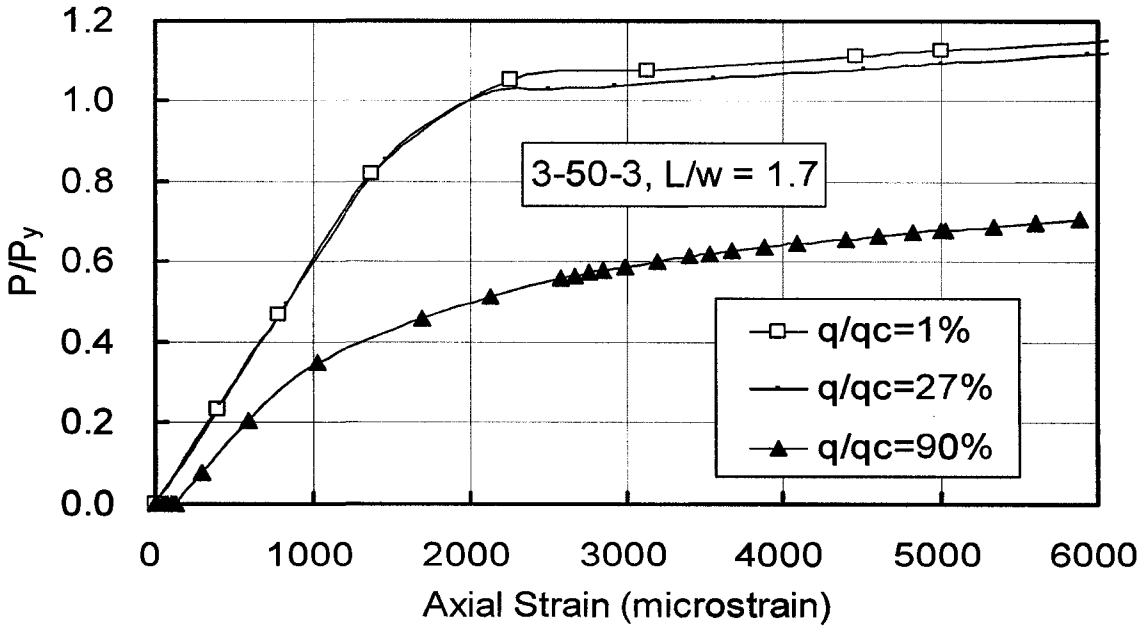

Figure 4.50 Normalized axial load versus axial strain (3-50-3, L/w = 1.7)

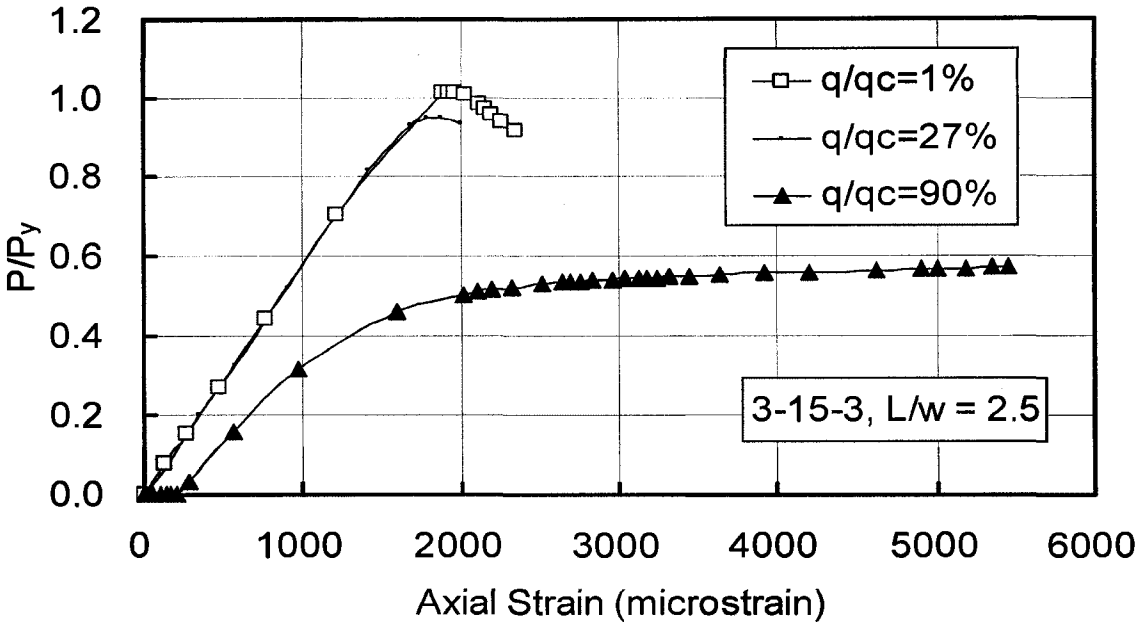

Figure 4.51 Normalized axial load versus axial strain (3-15-3, L/w = 2.5)

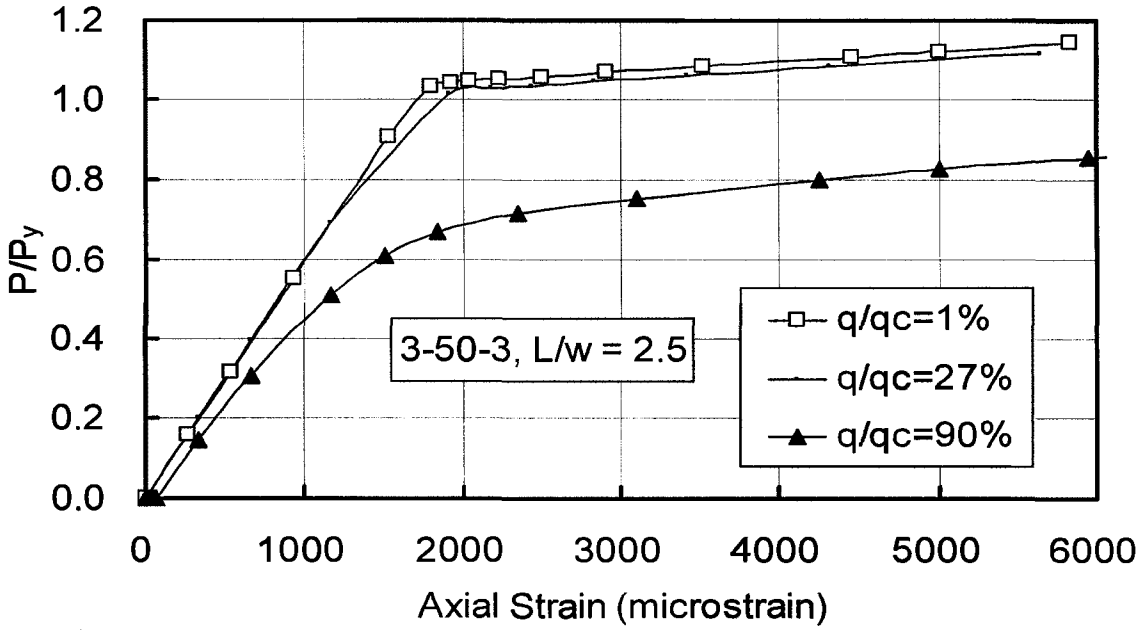

Figure 4.52 Normalized axial load versus axial strain (3-50-3, L/w = 2.5)

Chapter 5

Shear flexibility factor

The main objectives of this chapter are: 1) to provide deflection factors for calculating the deflections of a monolayer plate loaded with one to four concentrated loads; 2) to provide shear flexibility factors to transform deflections of monolayer plate to deflections for sandwich panels. The shear flexibility factor is defined as the ratio of the deflection of the sandwich panel to that of a solid plate of equivalent thickness calculated based on the same moment of inertia.

5.1 Deflection factor α

The maximum deflection of a rectangular plate fixed against rotation around its perimeter and loaded with a concentrated load at its centre is obtained from (Davison and Owens, 2003):

$$\Delta_{max} = \alpha \frac{C w^2}{E t^3} \tag{5-1}$$

where the constant α is function of the plate aspect ratio and is given as:

L/w	1.0	1.2	1.4	1.6	1.8	2.0	∞
α	0.0611	0.0706	0.0754	0.0777	0.0786	0.0788	0.0791

where, α = deflection factor

C = concentrated load at center of plate in N

t = plate thickness in mm

w = plate width in mm

L = plate length in mm (L> w)

E = modulus of elasticity in MPa

Figure 5.1 shows four load locations, identified as 1 to 4, where 4 is at the panel centre, on a plate with fixed boundary condition. These four points will serve as

reference points for loading and deflection calculations. The maximum deflection of the plate will be obtained using the finite element software ANSYS and a model similar to the model validated in Chapter 3. The same material properties as those used in chapter 3 are used for this investigation. The deflection factors for each load case are calculated based on equation (5-1). Therefore, deflection factor tables will be derived for each load case. The table shown above for a point load at the centre of the plate will be used to verify the analysis results from ANSYS.

The calculations were performed for a plate 1200 mm wide, 18 mm thick and varying lengths, with fixed boundary condition around the perimeter. Based on the moment of inertia, a 18 mm steel plate is equivalent to a sandwich panel with 3 mm face plate and a 15 mm core (3-15-3). The deflection factors listed in tables 5.1a to 5.1d are for a plate with an aspect ratio from 1.0 to 3.0. It is found that the deflection factor is increasing with increasing aspect ratio for each load case and the deflection factors increase very slowly once the plate aspect ratio exceeds 2.0. Therefore, deflection factors for a plate with an aspect ratio of 3.0 can be applied to calculate the maximum deflection in plates with aspect ratio over 3.0.

Table 5.2 shows a comparison between deflection factors from two resources, namely, from the finite element analysis (α from ANSYS) and from Davison and Owen (2003) (α from manual). The maximum difference between the two approaches is 1.16% and it occurs in the plate with an aspect ratio of 1.0. The difference between the two approaches is less than 1% for all the other cases. It is therefore concluded that the deflection factors listed in tables 5.1a to 5.1d obtained from the finite element analysis, are accurate. The maximum deflection of the plate under the concentrated load at other locations can therefore be obtained from the finite element analysis.

The deflection factors listed in tables 5.1a to 5.1d are obtained using equation (5 -1) and the maximum deflection in the plate using the finite element

analysis results. However, the maximum deflections are not always at the location where the point load is applied. Table 5.3 compares the maximum deflection, Δ_{max} and the deflections at the load point, on the panel face opposite to the loaded face, Δ_p. A maximum difference of 8% is found between the maximum plate deflection and the deflection at the point of loading. Therefore, the deflection at the point of load was taken as the maximum deflection of the fixed plate loaded with a concentrated load.

The deflection factors presented in table 5.4 are used for calculating the deflections of a solid plate when more than one concentrated load are applied on the plate. The deflection factor α_{ij} represents the deflection factor at location j caused by a concentrated load applied at i location. For example, α_{12} is the deflection factor at location 2 caused by a concentrated load at location 1. The principle of superposition can be used for calculating the deflection when two or more concentrated loads are applied on the plate. The deflection at location 1 when four concentrated loads are applied on the plate simultaneously at points 1 to 4, identified in Figure 5.1, can be obtained from equation (5-2a). Similarly, the deflections at the other three locations caused by the combination of four loads can be obtained from equations (5-2b) to (5-2d).

$$\Delta_1 = \alpha_{11}\frac{C_1 w^2}{Et^3} + \alpha_{21}\frac{C_2 w^2}{Et^3} + \alpha_{31}\frac{C_3 w^2}{Et^3} + \alpha_{41}\frac{C_4 w^2}{Et^3} \quad (5\text{-}2a)$$

$$\Delta_2 = \alpha_{12}\frac{C_1 w^2}{Et^3} + \alpha_{22}\frac{C_2 w^2}{Et^3} + \alpha_{32}\frac{C_3 w^2}{Et^3} + \alpha_{42}\frac{C_4 w^2}{Et^3} \quad (5\text{-}2b)$$

$$\Delta_3 = \alpha_{13}\frac{C_1 w^2}{Et^3} + \alpha_{23}\frac{C_2 w^2}{Et^3} + \alpha_{33}\frac{C_3 w^2}{Et^3} + \alpha_{43}\frac{C_4 w^2}{Et^3} \quad (5\text{-}2c)$$

$$\Delta_4 = \alpha_{14}\frac{C_1 w^2}{Et^3} + \alpha_{24}\frac{C_2 w^2}{Et^3} + \alpha_{34}\frac{C_3 w^2}{Et^3} + \alpha_{44}\frac{C_4 w^2}{Et^3} \quad (5\text{-}2d)$$

5.2 Shear flexibility factor k

In above section, deflection factors were obtained for solid plates subjected to four different point loads in one quadrant of a rectangular plate. In order to apply these findings to the sandwich panels, the effect of the shear flexibility of the elastomer core on the panel deflection must be accounted for. This section presents the results of a finite element study conducted to determine *shear flexibility factors,* which are used to calculate the deflection magnitude of sandwich panels from the solution obtained from a solid plate. Five configurations of sandwich panels with three aspect ratios, two boundary conditions and three load cases will be investigated numerically. The aspect ratios are 1.2, 1.7 and 2.5. The two boundary conditions investigated are fixed along all four edges (figure 5.1) and fixed along the long edges of the plate (figure 5.2). Three load cases consist of uniform lateral pressure, concentrated loads located at the four points identified in figure 5.1 and patch loads centered on the same four points. The analysis is conducted in the elastic range only since the deflection calculations are considered as a serviceability limit state. The material properties for the steel and the elastomer are the same as used in chapter 3.

5.2.1 Plate with four fixed edges under uniform lateral pressure

Three sandwich panel sizes were considered, namely, 1200x1440 (aspect ratio of 1.2), 1200x2040 (aspect ratio of 1.7), and 1200x3000 (aspect ratio of 2.5). These panel sizes were considered with five different configurations, namely, 3-15-3, 3-50-3, 3-100-3, 6-50-6, and 10-50-10. The various combinations of plate size and sandwich panel configurations were analyzed with a uniform lateral pressure to determine the maximum deflection. Table 5.5 displays the selected sandwich panels and their maximum deflections obtained from finite element analysis.

The maximum deflection $\Delta(plate)$ of a solid plate rigidly supported around its perimeter can be calculated using equation (5-3) presented by Salvadori and Levy (1981).

$$\Delta(plate) = \alpha \frac{q\, w^4}{E\, t^3} \tag{5-3}$$

where the constant α is a function of the plate aspect ratio and is given as:

L/w	1.0	1.1	1.2	1.3	1.4	1.5	2.0	∞
α	0.0138	0.0165	0.0189	0.0210	0.0228	0.0242	0.0279	0.0286

where, α, t, w, L and E are as defined above, and q is the uniform lateral pressure in MPa

The panel thickness used in equation (5-3) is an equivalent thickness t_{eq}, of a solid plate that has the same moment of inertia as a sandwich panel.

$$t_{eq} = \left(24\, t_s \left(\frac{h_c + t_s}{2} \right)^2 \right)^{1/3} \tag{5-4}$$

where, t_s = face plate thickness

h_c = polymer core thickness

Table 5.5 displays the equivalent thicknesses t_{eq} for five different sandwich panels.

The shear flexibility factor is determined as the ratio of the deflection of the sandwich panel, obtained from the finite element analysis, to the deflection of a solid plate with an equivalent thickness, calculated using Equation (5-3) where t is taken as the equivalent thickness. The shear flexibility factors k for the five sandwich panel configurations and three aspect ratios are presented in Table 5.5.

Figure 5.3 displays curves of shear flexibility factors as a function of plate thickness for sandwich panels with three aspect ratios. The figure shows that the shear flexibility factor increases with increasing equivalent thickness, t_{eq} . Figure 5.3 also shows that plate aspect ratio has no significant effect on the shear flexibility factor for the panels with four edges fixed and loaded under uniform pressure.

5.2.2 Plate with two fixed edges under uniform lateral pressure

Figure 5.2 shows the boundary conditions for a sandwich panel with rotationally fixed long edges and free short edges. The maximum deflection of the sandwich panel with these boundary conditions was obtained from a finite element analysis. The panel configurations, dimensions, material properties, and load conditions are the same as those used for the panels with four fixed edges investigated in the previous section.

The maximum deflections of a solid steel plate of thickness t_{eq} and the same boundary conditions as described above for the sandwich panel, can be obtained from the following equation:

$$\Delta(t_{eq}) = \frac{q w^4}{384\, E I} \tag{5-5}$$

Table 5.6 presents the calculated shear flexibility factors for the sandwich panels with two long edges rotationally fixed and two short edges free and subjected to a uniform lateral pressure. The data presented in Table 5.6 indicate that the shear flexibility factor increases with the increasing of the equivalent plate thickness and the aspect ratio has no effect on the shear flexibility factor for panels with two fixed edges and two free edges.

Figure 5.4 presents a plot of shear flexibility factor versus plate thickness for sandwich panels with the boundary conditions illustrated in figures 5.1 and 5.2. For clarity, only the results for a panel with an aspect ratio of 1.2 are presented in the figure. It is observed that the panels with four rotationally fixed edges have

higher shear flexibility factors than the panels with only two fixed edges. For the range of equivalent thickness illustrated in Figure 5.4, the difference in shear flexibility factor varies from 15% for an equivalent thickness of 18 mm to 22% for an equivalent thickness of 60 mm.

5.2.3 Plate with four fixed edges and a concentrated load at the panel centre

Table 5.7 presents the shear flexibility factors for sandwich panels with four rotationally fixed edges and loaded with a concentrated load at the centre point. The same panel aspect ratios and configuration as those used in the previous sections were used for the analysis results presented in table 5.7. As for the other cases presented above, the maximum deflection in the sandwich panels was obtained from the finite element analysis and the deflection of the solid plate of equivalent thickness was calculated using equation (5-1). As for the previous cases investigated, the data presented in Table 5.7 shows that the shear flexibility factor increases with increasing plate thickness, and the plate aspect ratio only has a minor effect on the magnitude of the shear flexibility factor.

Figure 5.5 displays the shear flexibility factor versus the equivalent panel thickness for the rotational fixed edges and two load cases: uniform pressure and a single point load at the centre of the panel. The sandwich panel under the central concentrated load shows a higher shear flexibility factors than the panel under uniform lateral load. It is 59 % higher for an equivalent plate thickness of 18 mm (3-15-3) and 78% higher for an equivalent plate thickness of 60 mm (10-50-10).

5.2.4 Plate with four edges fixed and loaded with a concentrated load

This section presents the results of an analysis on sandwich panels with all four edges fixed and loaded with a concentrated load at three different locations identified as points 1 to 3 in Figure 5-1. Since no closed form solutions for the deflection of a solid plate under a concentrated load at locations 1, 2 and 3 was found in the literature, and the deflections for the solid plates are determined using finite element analysis. Table 5.8 provides a summary of the shear

flexibility factors for sandwich panels loaded with a point load at four different locations. Contrary to earlier findings for a panel loaded with a uniform pressure or a point load at the centre of the panel, the flexibility factor is found to vary with plate aspect ratio. For each point load location the maximum shear flexibility factor is obtained for an aspect ratio of 1.0. Also, for a given aspect ratio, the shear flexibility factor reaches its maximum value for the point load located at point 3.

Based on the above results, the maximum deflection of a sandwich panel resulting from a point load at one of the four locations identified in Figurer 5-1 can be obtained from:

$$\Delta\,(\mathrm{SP}) = k\alpha \frac{P w^2}{E t^3} \tag{5-6}$$

where, α = the deflection factor presented in table 5.1

k = the shear flexibility factor tabulated in table 5.8

The shear flexibility factors k_{ij} presented in table 5.9 are used to calculate the deflection at location j due to a point load at location i. The deflection at any point 1 to 4 can be calculated using the principle of superposition.

$$\Delta_1 = \alpha_{11}k_{11}\frac{C_1 w^2}{Et^3} + \alpha_{21}k_{21}\frac{C_2 w^2}{Et^3} + \alpha_{31}k_{31}\frac{C_3 w^2}{Et^3} + \alpha_{41}k_{41}\frac{C_4 w^2}{Et^3} \tag{5-7a}$$

$$\Delta_2 = \alpha_{12}k_{12}\frac{C_1 w^2}{Et^3} + \alpha_{22}k_{22}\frac{C_2 w^2}{Et^3} + \alpha_{32}k_{32}\frac{C_3 w^2}{Et^3} + \alpha_{42}k_{42}\frac{C_4 w^2}{Et^3} \tag{5-7b}$$

$$\Delta_3 = \alpha_{13}k_{13}\frac{C_1 w^2}{Et^3} + \alpha_{23}k_{23}\frac{C_2 w^2}{Et^3} + \alpha_{33}k_{33}\frac{C_3 w^2}{Et^3} + \alpha_{43}k_{43}\frac{C_4 w^2}{Et^3} \tag{5-7c}$$

$$\Delta_4 = \alpha_{14}k_{14}\frac{C_1 w^2}{Et^3} + \alpha_{24}k_{24}\frac{C_2 w^2}{Et^3} + \alpha_{34}k_{34}\frac{C_3 w^2}{Et^3} + \alpha_{44}k_{44}\frac{C_4 w^2}{Et^3} \tag{5-7d}$$

where, α_{ij} = the deflection factor presented in table 5.4

k_{ij} = the shear flexibility factor tabulated in table 5.9

5.2.5 Plate with four fixed edges and loaded with a patch load at four locations

An investigation of panel deflection under a loaded area equivalent to the footprint area of a CL-625 truck wheel (CSA, 2006) was carried out to compare the effect of distributing the load over an area rather than at a point. An area of 0.25 m by 0.6 m, as specified in CSA-S16-06 for a wheel load, corresponds to the footprint of a truck wheel. A patch area of 0.24x0.6m was actually used since the mesh size for this study uses elements that are 20 mm x 20 mm. The magnitude of the point load was arbitrarily selected as 50 kN for a 18 mm plate and 100 kN for a 60 mm plate. This corresponds to contact pressure of 0.347 MPa for the 18 mm plate and 0.694 MPa for the 60 mm plate.

Table 5.10 lists the maximum deflections calculated for a 1200 x 1440 mm panel of two equivalent thicknesses, namely, 18 mm and 60 mm under a single point load or a patch load. The four loading locations, designated as 1* to 4*, shown in figures 5.7a and 5.7b. The center of each patch load corresponds respectively to the location of the point load identified as 1 to 4 in figure 5.1. The deflection caused by the concentrated load is 2.1 to 2.8 times the deflection caused by the patch load.

Table 5.11 lists the shear flexibility factors for the panels under a patch load. Some of the results from Table 5.11 are also presented in Figure 5.6. It is observed that the shear flexibility factor is greater for a panel under a point load than under a load patch (the difference between the two is expected to decrease as the size of the panel increases). The difference of the shear flexibility factor between the concentrated and patch load cases increases with an increasing in equivalent thickness.

In order to investigate the effect of size of the loaded patch relative to the size of the plate, flexibility factors for 3-15-3 sandwich panels 3000x3600 mm were calculated and the results are presented in table 5.12. A patch load of 0.1 MPa was applied at four locations 1** to 4** shown in figure 5.8, both for a solid plate and a sandwich panel, to determine the deflection of both panels, from which the

flexibility factors are obtained. A comparison of the data from Table 5.12 with the data from Table 5.11 indicates that the shear flexibility factors for the 3000x3600 mm sandwich panels loaded with a patch load are all smaller than those calculated for the smaller panels. Therefore, for the patch load case the shear flexibility factor is a function of the panel size.

Table 5.1

Deflection factors for calculating maximum deflections of a solid plate with a concentrated load

(a) P = 50kN at (X = -Width/4, Y = 0, Z = 0)

aspect ratio	Width mm	Length mm	E_s MPa	t_{eq} mm	P kN	Δ (t_{eq}) mm	α
1.0	1200	1200	199000	18	50	2.34	0.0382
1.2	1200	1440	199000	18	50	2.57	0.0419
1.4	1200	1680	199000	18	50	2.69	0.0439
1.6	1200	1920	199000	18	50	2.75	0.0448
1.8	1200	2160	199000	18	50	2.77	0.0452
2.0	1200	2400	199000	18	50	2.77	0.0452
3.0	1200	3600	199000	18	50	2.77	0.0452

(b) P = 50kN at (X = 0, Y = Length/4, Z = 0)

aspect ratio	Width mm	Length mm	E_s MPa	t_{eq} mm	P kN	Δ (t_{eq}) mm	α
1.0	1200	1200	199000	18	50	2.34	0.0382
1.2	1200	1440	199000	18	50	2.91	0.0475
1.4	1200	1680	199000	18	50	3.38	0.0551
1.6	1200	1920	199000	18	50	3.76	0.0613
1.8	1200	2160	199000	18	50	4.07	0.0664
2.0	1200	2400	199000	18	50	4.31	0.0703
3.0	1200	3600	199000	18	50	4.80	0.0783

Table 5.1 (cont'd)

(c) P = 50kN at (X = -Width/4, Y = Length/4, Z = 0)

aspect ratio	Width mm	Length mm	E_s MPa	t_{eq} mm	P kN	Δ (t_{eq}) mm	α
1.0	1200	1200	199000	18	50	1.62	0.0264
1.2	1200	1440	199000	18	50	1.90	0.0310
1.4	1200	1680	199000	18	50	2.13	0.0347
1.6	1200	1920	199000	18	50	2.31	0.0377
1.8	1200	2160	199000	18	50	2.44	0.0398
2.0	1200	2400	199000	18	50	2.55	0.0416
3.0	1200	3600	199000	18	50	2.75	0.0448

(d) P = 50kN at (X = 0, Y = 0, Z = 0)

aspect ratio	Width mm	Length mm	E_s MPa	t_{eq} mm	P kN	Δ (t_{eq}) mm	α
1	1200	1200	199000	18	50	3.79	0.0618
1.2	1200	1440	199000	18	50	4.37	0.0713
1.4	1200	1680	199000	18	50	4.66	0.0760
1.6	1200	1920	199000	18	50	4.80	0.0783
1.8	1200	2160	199000	18	50	4.85	0.0791
2.0	1200	2400	199000	18	50	4.87	0.0794
3.0	1200	3600	199000	18	50	4.87	0.0794

Table 5.2

Comparison of the deflection factor for 18 mm thick plate from two sources

aspect ratio	α from ANSYS	α from Manual*	difference (%)
1.0	0.0618	0.0611	1.16
1.2	0.0713	0.0706	0.95
1.4	0.0760	0.0754	0.79
1.6	0.0783	0.0777	0.75
1.8	0.0791	0.0786	0.63
2.0	0.0794	0.0788	0.79
3.0	0.0794	0.0791	0.41

* Deflection coefficient obtained from Davison and Owens (2003)

Table 5.3

Comparison of maximum deflection and deflection at load point

	P = 50kN at 1*		P = 50kN at 2		P = 50kN at 3		P = 50kN at 4	
aspect ratio	Δ_{max} mm	Δ_p mm	Δ_{max} mm	Δ_p mm	Δ_{max} mm	Δ_p mm	Δ_{max} mm	Δ_p mm
1.0	2.34	2.23	2.34	2.23	1.62	1.56	3.79	3.78
1.2	2.57	2.42	2.91	2.83	1.90	1.83	4.37	4.35
1.4	2.69	2.51	3.38	3.33	2.13	2.04	4.66	4.65
1.6	2.75	2.54	3.76	3.74	2.31	2.2	4.80	4.78
1.8	2.77	2.56	4.07	4.06	2.44	2.31	4.85	4.84
2.0	2.77	2.56	4.31	4.30	2.55	2.39	4.87	4.86
3.0	2.77	2.56	4.80	4.79	2.75	2.54	4.87	4.86

*See Figure 5.1 for a description of the point load locations.
Note: All deflections were obtained on the panel face opposite to the loaded face.

Table 5.4

Deflection factor for plate loaded with multiple concentrated loads

(a) P = 50kN at location 1

aspect ratio	α_{11}	α_{12}	α_{13}	α_{14}
1.0	0.0359	0.0135	0.0132	0.0269
1.2	0.0392	0.0152	0.0126	0.0319
1.4	0.0405	0.0150	0.0111	0.0345
1.6	0.0409	0.0137	0.0095	0.0356
1.8	0.0413	0.0119	0.0077	0.0361
2.0	0.0413	0.0100	0.0063	0.0363
3.0	0.0413	0.0029	0.0156	0.0363

(b) P = 50kN at location 2

aspect ratio	α_{21}	α_{22}	α_{23}	α_{24}
1.0	0.0135	0.0359	0.0132	0.0269
1.2	0.0152	0.0456	0.0182	0.0292
1.4	0.0148	0.0537	0.0226	0.0284
1.6	0.0137	0.0603	0.0263	0.0258
1.8	0.0119	0.0654	0.0290	0.0226
2.0	0.0100	0.0693	0.0313	0.0190
3.0	0.0029	0.0772	0.0355	0.0060

Table 5.4 (cont'd)

(c) P = 50kN at location 3

aspect ratio	α_{31}	α_{32}	α_{33}	α_{34}
1.0	0.0132	0.0132	0.0251	0.0134
1.2	0.0126	0.0184	0.0295	0.0150
1.4	0.0111	0.0227	0.0329	0.0148
1.6	0.0095	0.0264	0.0355	0.0135
1.8	0.0077	0.0292	0.0372	0.0118
2.0	0.0063	0.0314	0.0385	0.0155
3.0	0.0156	0.0358	0.0409	0.0029

(d) P = 50kN at location 4

aspect ratio	α_{41}	α_{42}	α_{43}	α_{44}
1.0	0.0268	0.0268	0.0134	0.0609
1.2	0.0318	0.0290	0.0148	0.0701
1.4	0.0343	0.0282	0.0147	0.0750
1.6	0.0355	0.0258	0.0135	0.0770
1.8	0.0359	0.0226	0.0118	0.0780
2.0	0.0361	0.0190	0.0100	0.0783
3.0	0.0361	0.0060	0.0029	0.0783

Table 5.5

Shear Flexibility Factors for a panel rotationally fixed along four edges and under uniform lateral pressure

(a) Aspect ratio=1.2

Steel thickness mm	Core thickness mm	Width mm	Length mm	t_{eq} mm	q MPa	Δ (t_{eq}) mm	Δ (SP) mm	k $\Delta(SP)/\Delta(t_{eq})$
3	15	1200	1440	18	0.1458	4.87	7.51	1.54
3	50	1200	1440	37	0.4266	1.64	4.89	2.98
6	50	1200	1440	48	0.9018	1.56	7.30	4.68
3	100	1200	1440	58	0.8289	0.84	4.50	5.36
10	50	1200	1440	60	1.6092	1.45	9.72	6.70

(b) Aspect ratio=1.7

Steel thickness mm	Core thickness mm	Width mm	Length mm	t_{eq} mm	q MPa	Δ (t_{eq}) mm	Δ (SP) mm	k $\Delta(SP)/\Delta(t_{eq})$
3	15	1200	2040	18	0.1134	5.14	7.82	1.52
3	50	1200	2040	37	0.3321	1.74	4.96	2.85
6	50	1200	2040	48	0.7020	1.65	7.35	4.45
3	100	1200	2040	58	0.6453	0.88	4.50	5.11
10	50	1200	2040	60	1.2528	1.53	9.73	6.36

(c) Aspect ratio=2.5

Steel thickness mm	Core thickness mm	Width mm	Length mm	t_{eq} mm	q MPa	Δ (t_{eq}) mm	Δ (SP) mm	k $\Delta(SP)/\Delta(t_{eq})$
3	15	1200	3000	18	0.0920	4.65	7.00	1.51
3	50	1200	3000	37	0.2700	1.57	4.45	2.83
6	50	1200	3000	48	0.5724	1.50	6.66	4.44
3	100	1200	3000	58	0.5265	0.80	4.11	5.14
10	50	1200	3000	60	1.0230	1.40	8.85	6.32

Table 5.6

Shear flexibility factor for a panel with two long edges fixed and under uniform lateral pressure

(a) Aspect ratio=1.2

Steel thickness mm	Core thickness mm	Width mm	Length mm	t_{eq} mm	q MPa	$\Delta\ (t_{eq})$ mm	$\Delta\ (SP)$ mm	k $\Delta(SP)/\Delta(t_{eq})$
3	15	1200	1440	18	0.1	5.58	7.40	1.33
3	50	1200	1440	37	0.2	1.29	3.22	2.50
6	50	1200	1440	48	0.4	1.15	4.51	3.91
10	50	1200	1440	60	0.5	0.75	4.12	5.47

(b) Aspect ratio=1.7

Steel thickness mm	Core thickness mm	Width mm	Length mm	t_{eq} mm	q MPa	$\Delta\ (t_{eq})$ mm	$\Delta\ (SP)$ mm	k $\Delta(SP)/\Delta(t_{eq})$
3	15	1200	2040	18	0.05	2.79	3.72	1.33
10	50	1200	2040	60	0.40	0.60	3.29	5.46

(c) Aspect ratio=2.5

Steel thickness mm	Core thickness mm	Width mm	Length mm	t_{eq} mm	q MPa	$\Delta\ (t_{eq})$ mm	$\Delta\ (SP)$ mm	k $\Delta(SP)/\Delta(t_{eq})$
3	15	1200	3000	18	0.02	1.12	1.50	1.34
10	50	1200	3000	60	0.20	0.30	1.65	5.47

Table 5.7

Shear flexibility factors for panel fixed along four edges with a concentrated load at the centre

(a) Aspect ratio=1.2

Steel thickness mm	Core thickness mm	Width mm	Length mm	t_{eq} mm	P kN	$\Delta\ (t_{eq})$ mm	$\Delta\ (SP)$ mm	k $\Delta(SP)/\Delta(t_{eq})$
3	15	1200	1440	18	50	4.37	10.43	2.39
10	50	1200	1440	60	100	0.24	2.65	11.20

(b) Aspect ratio=1.7

Steel thickness mm	Core thickness mm	Width mm	Length mm	t_{eq} mm	P kN	$\Delta\ (t_{eq})$ mm	$\Delta\ (SP)$ mm	k $\Delta(SP)/\Delta(t_{eq})$
3	15	1200	2040	18	50	4.83	11.04	2.29
10	50	1200	2040	60	100	0.26	2.74	10.51

(c) Aspect ratio=2.5

Steel thickness mm	Core thickness mm	Width mm	Length mm	t_{eq} mm	P kN	$\Delta\ (t_{eq})$ mm	$\Delta\ (SP)$ mm	k $\Delta(SP)/\Delta(t_{eq})$
3	15	1200	3000	18	50	4.87	9.54	1.96
10	50	1200	3000	60	100	0.26	2.46	9.36

Table 5.8

Shear flexibility factor for panel fixed along four edges

under the concentrated load at four locations

(a) P = 50kN at Point 1 (X= - Width/4, Y = 0, Z = 0)

aspect ratio	Width mm	Length mm	E_s MPa	t_{eq} mm	P kN	$\Delta\ (t_{eq})$ mm	$\Delta\ (SP)$ mm	k $\Delta(SP)/\Delta(t_{eq})$
1.0	1200	1200	199000	18	50	2.34	7.89	3.37
1.2	1200	1440	199000	18	50	2.57	8.17	3.18
1.4	1200	1680	199000	18	50	2.69	8.30	3.09
1.6	1200	1920	199000	18	50	2.75	8.37	3.04
1.8	1200	2160	199000	18	50	2.77	8.39	3.03
2.0	1200	2400	199000	18	50	2.77	8.40	3.03
3.0	1200	3600	199000	18	50	2.77	6.87	2.48

(b) P = 50kN at Point 2 (X = 0, Y = Length/4, Z = 0)

aspect ratio	Width mm	Length mm	E_s MPa	t_{eq} mm	P kN	$\Delta\ (t_{eq})$ mm	$\Delta\ (SP)$ mm	k $\Delta(SP)/\Delta(t_{eq})$
1.0	1200	1200	199000	18	50	2.34	7.84	3.35
1.2	1200	1440	199000	18	50	2.91	8.59	2.95
1.4	1200	1680	199000	18	50	3.38	9.21	2.72
1.6	1200	1920	199000	18	50	3.76	9.70	2.58
1.8	1200	2160	199000	18	50	4.07	10.00	2.46
2.0	1200	2400	199000	18	50	4.31	10.38	2.41
3.0	1200	3600	199000	18	50	4.80	9.44	1.97

Table 5.8 (cont'd)

(c) P = 50kN at Point 3 (X = -Width/4, Y = Length/4, Z = 0)

aspect ratio	Width mm	Length mm	E_S MPa	t_{eq} mm	P kN	$\Delta\ (t_{eq})$ mm	$\Delta\ (SP)$ mm	k $\Delta(SP)/\Delta(t_{eq})$
1.0	1200	1200	199000	18	50	1.62	6.92	4.27
1.2	1200	1440	199000	18	50	1.90	7.32	3.85
1.4	1200	1680	199000	18	50	2.13	7.62	3.58
1.6	1200	1920	199000	18	50	2.31	7.85	3.40
1.8	1200	2160	199000	18	50	2.44	8.01	3.28
2.0	1200	2400	199000	18	50	2.55	8.14	3.19
3.0	1200	3600	199000	18	50	2.75	6.84	2.49

(d) P = 50kN at Point 4 (X = 0, Y = 0, Z = 0)

aspect ratio	Width mm	Length mm	E_S MPa	t_{eq} mm	P kN	$\Delta\ (t_{eq})$ mm	$\Delta\ (SP)$ mm	k $\Delta(SP)/\Delta(t_{eq})$
1.0	1200	1200	199000	18	50	3.79	9.72	2.56
1.2	1200	1440	199000	18	50	4.37	10.43	2.39
1.4	1200	1680	199000	18	50	4.66	10.81	2.32
1.6	1200	1920	199000	18	50	4.80	11.00	2.29
1.8	1200	2160	199000	18	50	4.85	11.08	2.28
2.0	1200	2400	199000	18	50	4.87	11.11	2.28
3.0	1200	3600	199000	18	50	4.87	9.54	1.96

Table 5.9

Shear flexibility factors at four locations for panel under a concentrated load

(a) P = 50kN at Point 1 (X = -Width/4, Y = 0, Z = 0)

aspect ratio	k_{11}	k_{12}	k_{13}	k_{14}
1.0	3.02	1.63	1.88	1.57
1.2	2.88	1.55	1.78	1.53
1.4	2.85	1.52	1.74	1.52
1.6	2.84	1.49	1.69	1.52
1.8	2.83	1.49	1.67	1.52
2.0	2.83	1.48	1.62	1.52
3.0	2.54	1.44	1.44	1.52

(b) P = 50kN at Point 2 (X = 0, Y = Length/4, Z = 0)

aspect ratio	k_{21}	k_{22}	k_{23}	k_{24}
1.0	1.63	3.00	1.87	1.56
1.2	1.55	2.63	1.73	1.46
1.4	1.53	2.42	1.65	1.43
1.6	1.51	2.28	1.59	1.41
1.8	1.49	2.20	1.57	1.39
2.0	1.48	2.14	1.54	1.39
3.0	1.44	1.89	1.52	1.32

Table 5.9 (cont'd)

(c) P = 50 kN at Point 3 (X = -Width/4, Y = Length/4, Z = 0)

aspect ratio	k_{31}	k_{32}	k_{33}	k_{34}
1.0	1.88	1.87	3.70	1.63
1.2	1.78	1.72	3.37	1.55
1.4	1.74	1.64	3.17	1.51
1.6	1.69	1.59	3.04	1.50
1.8	1.67	1.56	2.97	1.49
2.0	1.62	1.54	2.92	1.47
3.0	1.44	1.51	2.54	1.44

(d) P = 50kN at Point 4 (X = 0, Y = 0, Z = 0)

aspect ratio	k_{41}	k_{42}	k_{43}	k_{44}
1.0	1.57	1.57	1.63	2.26
1.2	1.53	1.47	1.57	2.13
1.4	1.52	1.43	1.53	2.07
1.6	1.52	1.41	1.50	2.06
1.8	1.52	1.39	1.49	2.05
2.0	1.52	1.39	1.48	2.05
3.0	1.52	1.35	1.44	1.88

Table 5.10

Maximum deflection comparison for a panel under a point load or a patch load

(a) Concentrated or patch load centered at Point 1* (X = -Width/4, Y = 0, Z = 0)

aspect ratio	Width mm	Length mm	t_{eq} mm	P kN	Δ (Point Load) mm	q MPa	Δ (Patch Load) mm
1.2	1200	1440	18	50	8.17	0.347	3.68
1.2	1200	1440	60	100	2.32	0.694	0.93

(b) Concentrated or patch load centered at Point 2* (X = 0, Y = Length/4, Z = 0)

aspect ratio	Width mm	Length mm	t_{eq} mm	P kN	Δ (Point Load) mm	q MPa	Δ (Patch Load) mm
1.2	1200	1440	18	50	8.59	0.347	3.71
1.2	1200	1440	60	100	2.40	0.694	0.97

(c) Concentrated or patch load centered at Point 3* (X = -Width/4, Y = Length/4, Z = 0)

aspect ratio	Width mm	Length mm	t_{eq} mm	P kN	Δ (Point Load) mm	q MPa	Δ (Patch Load) mm
1.2	1200	1440	18	50	7.32	0.347	2.79
1.2	1200	1440	60	100	2.18	0.694	0.79

(d) Concentrated or patch load centered at Point 4* (X = 0, Y = 0, Z = 0)

aspect ratio	Width mm	Length mm	t_{eq} mm	P kN	Δ (Point Load) mm	q MPa	Δ (Patch Load) mm
1.2	1200	1440	18	50	10.43	0.347	5.08
1.2	1200	1440	60	100	2.65	0.694	1.18

Table 5.11

Shear flexibility factor for a panel under a patch load (panel 1200 x1440 mm)

(a) Centre of patch load at (X = -Width/4, Y = 0, Z = 0)

aspect ratio	E_s MPa	t_{eq} mm	q MPa	$\Delta\ (t_{eq})$ mm	$\Delta\ (SP)$ mm	k $\Delta(SP)/\Delta(t_{eq})$
1.2	199000	18	0.347	2.16	3.68	1.70
1.2	199000	60	0.694	0.12	0.93	7.75

(b) Centre of patch load at (X = 0, Y = Length/4, Z = 0)

aspect ratio	E_s MPa	t_{eq} mm	q MPa	$\Delta\ (t_{eq})$ mm	$\Delta\ (SP)$ mm	k $\Delta(SP)/\Delta(t_{eq})$
1.2	199000	18	0.347	2.15	3.71	1.73
1.2	199000	60	0.694	0.12	0.97	8.08

(c) Centre of patch load at (X = -Width/4, Y = Length/4, Z = 0)

aspect ratio	E_s MPa	t_{eq} mm	q MPa	$\Delta\ (t_{eq})$ mm	$\Delta\ (SP)$ mm	k $\Delta(SP)/\Delta(t_{eq})$
1.2	199000	18	0.347	1.47	2.79	1.90
1.2	199000	60	0.694	0.084	0.79	9.40

(d) Centre of patch load at (X = 0, Y = 0, Z = 0)

aspect ratio	E_s MPa	t_{eq} mm	q MPa	$\Delta\ (t_{eq})$ mm	$\Delta\ (SP)$ mm	k $\Delta(SP)/\Delta(t_{eq})$
1.2	199000	18	0.347	3.25	5.08	1.56
1.2	199000	60	0.694	0.18	1.18	6.56

Table 5.12

Shear flexibility factor for a panel under a patch load (panel 3000x3600 mm)

(a) Centre of patch load at Point 1** (X = -Width/4, Y = 0, Z = 0)

aspect ratio	E_s MPa	t_{eq} mm	q MPa	$\Delta(t_{eq})$ mm	$\Delta(SP)$ mm	k $\Delta(SP)/\Delta(t_{eq})$
1.2	199000	18	0.1	4.41	5.09	1.15

(b) Centre of patch load at Point 2** (X = 0, Y = Length/4, Z = 0)

aspect ratio	E_s MPa	t_{eq} mm	q MPa	$\Delta(t_{eq})$ mm	$\Delta(SP)$ mm	k $\Delta(SP)/\Delta(t_{eq})$
1.2	199000	18	0.1	4.83	5.53	1.14

(c) Centre of patch load at Point 3** (X = -Width/4, Y = Length/4, Z = 0)

aspect ratio	E_s MPa	t_{eq} mm	q MPa	$\Delta(t_{eq})$ mm	$\Delta(SP)$ mm	k $\Delta(SP)/\Delta(t_{eq})$
1.2	199000	18	0.1	3.17	3.80	1.20

(d) Centre of patch load at Point 4** (X = 0, Y = 0, Z = 0)

aspect ratio	E_s MPa	t_{eq} mm	q MPa	$\Delta(t_{eq})$ mm	$\Delta(SP)$ mm	k $\Delta(SP)/\Delta(t_{eq})$
1.2	199000	18	0.1	7.16	8.05	1.12

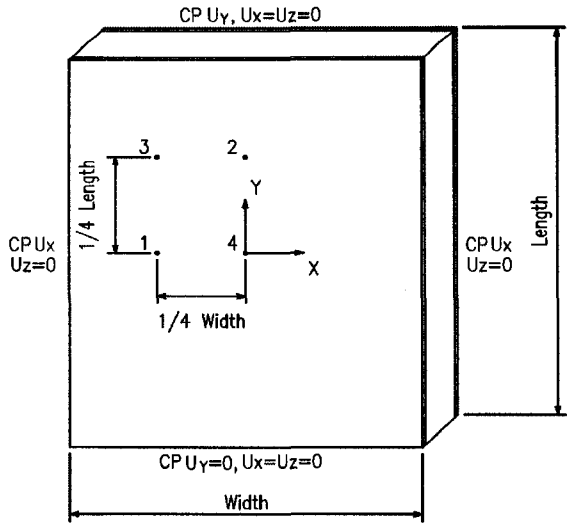

Figure 5.1 Panel with four fixed edges
(E_s = 199000 MPa, E_c = 860 MPa)

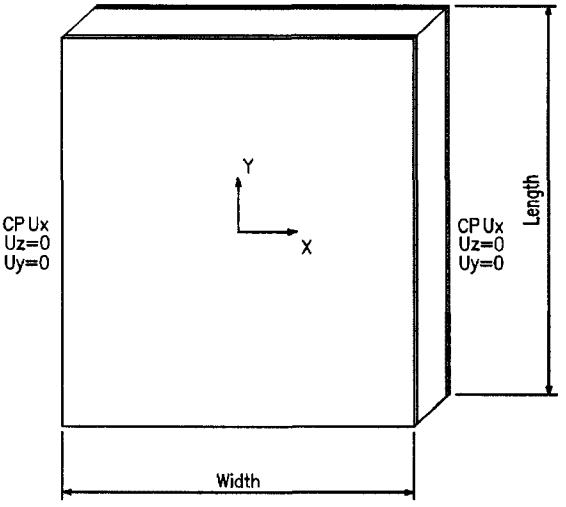

Figure 5.2 Panel with two fixed edges
(E_s = 199000 MPa, E_c = 860 MPa)

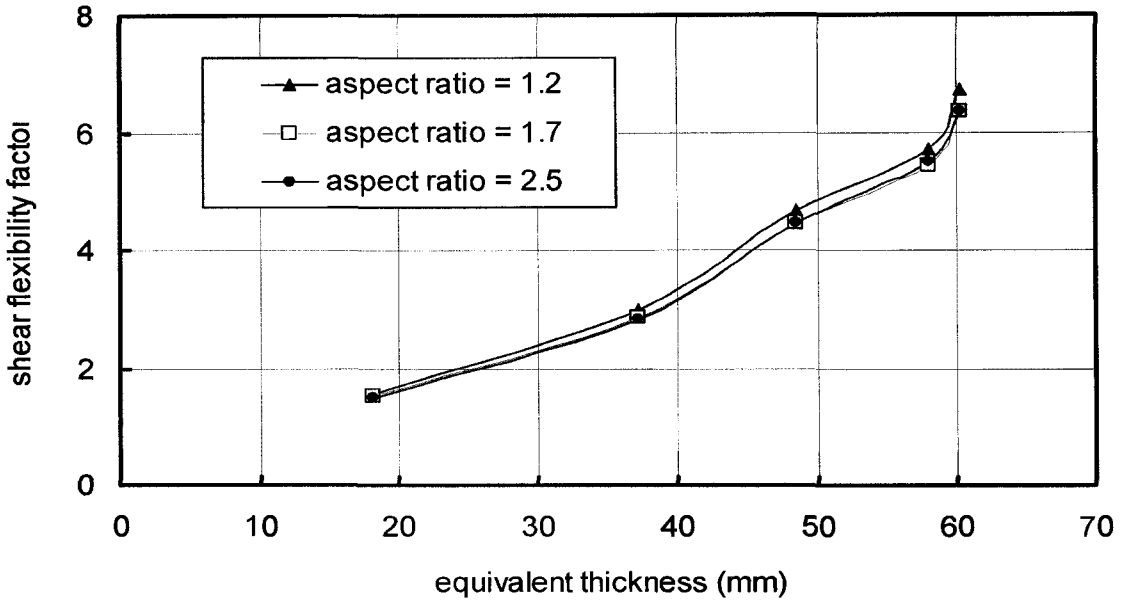

Figure 5.3 Shear flexibility factors for sandwich panels of different aspect ratios

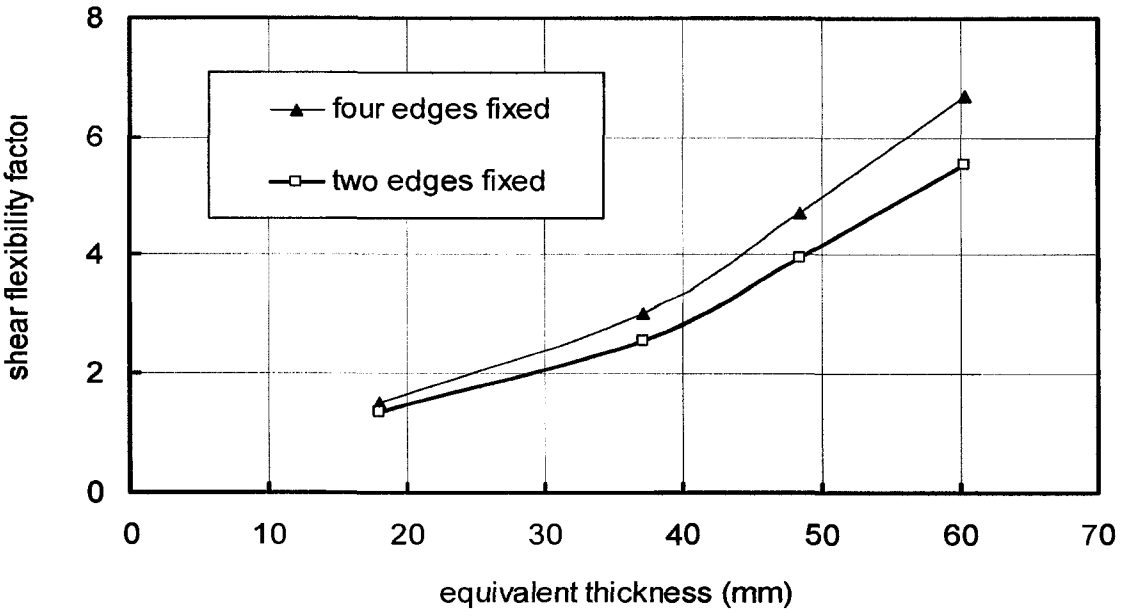

Figure 5.4 Shear flexibility factors for sandwich panels with different boundary conditions

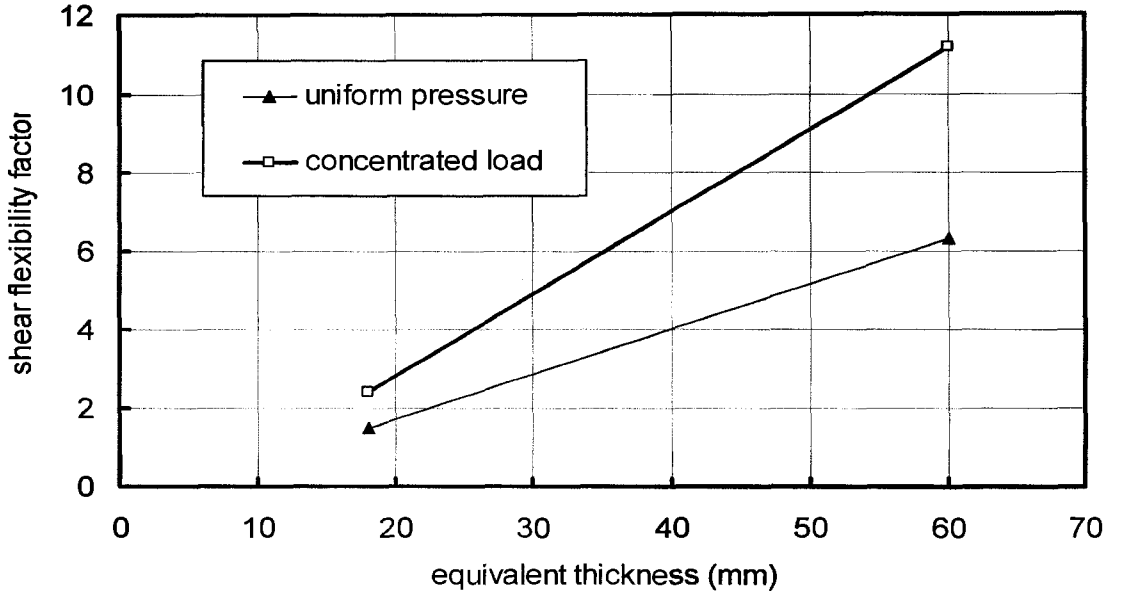

Figure 5.5 Shear flexibility factors for sandwich panels under two load cases

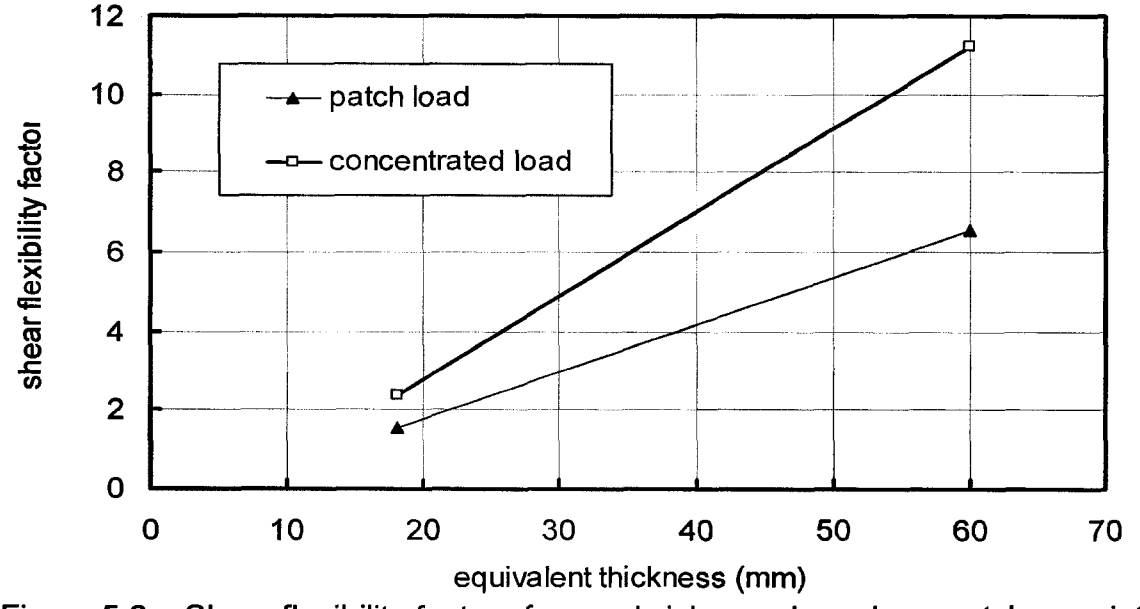

Figure 5.6 Shear flexibility factors for sandwich panels under a patch or point load

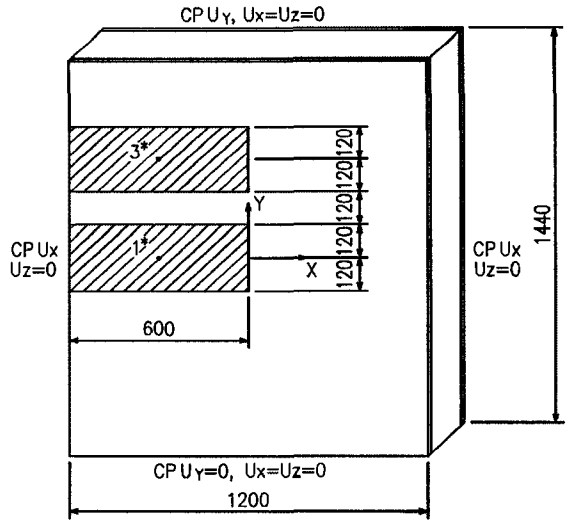

Figure 5.7a Locations of patch load on 1200x1440 sandwich panel
(E_s = 199000 MPa, E_c = 860 MPa)

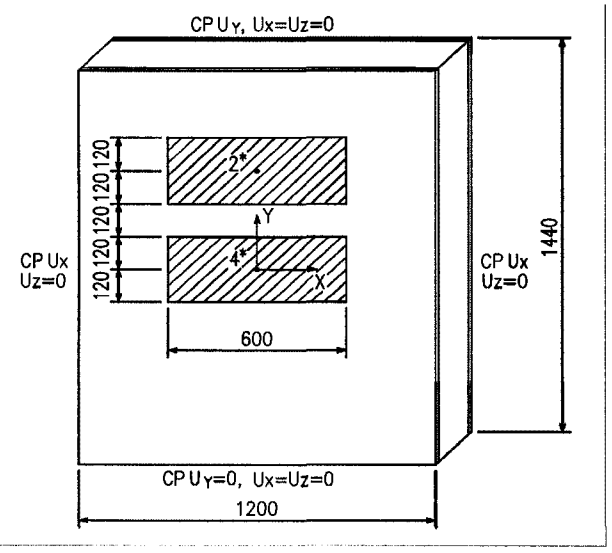

Figure 5.7b Locations of patch load on 1200x1440 sandwich panel
(E_s = 199000 MPa, E_c = 860 MPa)

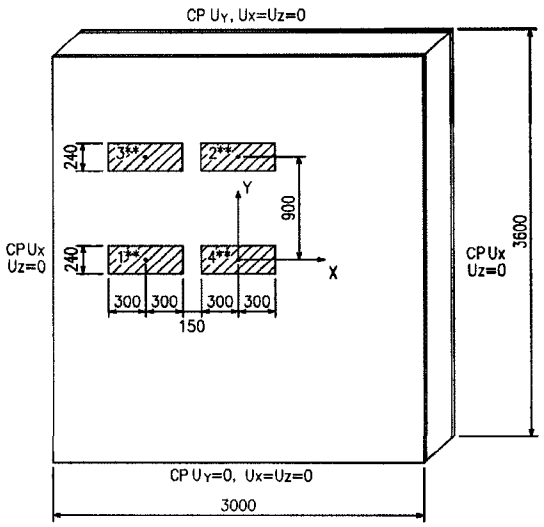

Figure 5.8 locations of patch load on 3000x3600 sandwich panel
(E_s = 199000 MPa, E_c = 860 MPa)

Chapter 6

Summary and Conclusions

6.1 Summary

A finite element model of a steel face plate and elastomer core sandwich panel was developed and validated using the results of an experimental program by Little *et al.* (2007). The validated model was used to conduct a parametric study where 39 finite element models were used to investigate the effect on the strength and behaviour of panel aspect ratio, thickness of the steel plate and elastomer core, and the magnitude of the lateral pressure. The effects of material and geometric non-linearity were incorporated into the analysis. Shear flexibility factors, used for considering the effect of the flexible elastomer core on panel deflection, were derived using linear elastic finite element analysis. Sandwich panels with three aspect ratios, five panel configurations, two boundary conditions and three load cases were investigated numerically.

6.2 Conclusions

6.2.1 Model Validation

The global behaviour of sandwich panels as characterized by in-plane and out-of-plane deflections, axial compressive strength from four finite element models were compared with test results presented by Little *et al.* (2007). The following conclusions were drawn from this comparison:

1) Predicted axial strength is within 5% of the test results.

2) The initial axial stiffness of sandwich panels subjected to lateral pressures from 207 kPa to 690 kPa was within 3% of the measured stiffness.

3) Out-of-plane deflections resulting from the lateral pressure were underestimated by finite element models FEA 1 and FEA 2. On the other hand, finite element models FEA 3 and FEA 4 overestimated the out-of-

plane deflection. The difference between numerical and test results decrease from 5.9% to 3.2% for FEA 1, 22% to 2.3% for FEA 3 and FEA 4 as the lateral pressure increased from 207 to 690 kN. The difference in model FEA 2 increased from 5.9% ~ 7.6% with the same increase in lateral pressure.

6.2.2 Parametric Study

Five sandwich panels with configurations 3-15-3, 3-50-3, 3-100-3, 6-50-6, and 10-50-10, with three aspect ratios (1.2, 1.7 and 2.5) and under five load cases were analyzed to investigate the effect of panel aspect ratio, panel thickness and lateral load levels on the global behaviour of sandwich panels. The following conclusions can be drawn from this investigation:

1) Panel aspect ratio has no significant effect on axial load capacity at low lateral pressure (q/qc<27%). However, the axial load capacity increases with increasing aspect ratio at high lateral pressure level. For example, the axial load capacity of the panel 3-15-3 with an aspect ratio of 2.5 is 50% higher than for a panel with an aspect ratio of 1.2 when the panel is loaded with a lateral pressure of $0.9q_c$.

2) Thickness ratio of elastomer core to steel plate is the function of the normalized axial capacity, P_u / P_y. The normalized axial load capacity increases with an increase of the elastomer core thickness to steel plate thickness ratio. For a given aspect ratio, the capacity of a sandwich panel, P_u / P_y, increases as the panel thickness increases.

3) The effect of the lateral pressure q / q_c on the axial load capacity decreases as the thickness of the elastomer core increases. The axial load capacity of a 3-15-3 panel with aspect ratio of 1.2 decreased by 38% when the lateral pressure increased from $0.9q_c$ to $0.1q_c$, but the capacity of a 3-50-3 panel decreased by 50% under the same condition.

6.2.3 Shear Flexibility Factor

Shear flexibility factors for sandwich panels were obtained for various loading conditions and panel configurations, aspect ratio, boundary conditions and panel sizes. The main conclusions from this investigation are:

1) Higher shear flexibility factors are obtained for sandwich panels of larger equivalent thickness (larger core thickness).

2) The panel aspect ratio has no significant effect on the shear flexibility factor for sandwich panels under uniform load. However, the shear flexibility factor decreases with increasing panel aspect ratio for concentrated loads.

3) The boundary conditions have an effect on the shear flexibility factor, and this effect increases with increasing equivalent thickness. For a panel with an equivalent thickness of 18 mm, the shear flexibility factor decreases by 15% as the boundary conditions change from four fixed edges to only two fixed edges and two free short edges. Similarly, the decrease of shear flexibility factor for a panel with an equivalent thickness of 60 mm is 22% and the boundary conditions change from four to two edges fixed.

4) Concentrated loads result in a higher shear flexibility factor than uniformly distributed loads and the difference increases with increasing equivalent thickness.

5) The shear flexibility factor for sandwich panels under concentrated loads are two to three times that of sandwich panels under an equal patch load. This is affect by the ratio of the patch load area and panel dimensions.

6.3 Future work

The parametric study presented in this research focused on clamped sandwich panels of various aspect ratios, panel thicknesses and lateral load levels. Future

study is recommended to investigate the effect from boundary condition and the material properties of the elastomer core.

The parametric study conducted in this project assumed that the bond between the elastomer core and the face plates was perfect over the entire surface. The effect of bond strength and the impact of localized debonding on the overall behaviour of sandwich panels need to be investigated both experimentally and numerically.

Two panel sizes, namely, 1200x1440 mm and 3000x3600 mm, were used to investigate the effect of patch load on the s*hear flexibility factors*. More panel dimensions with the same patch load size should be analyzed to investigate the effect of loaded area to panel area ratio.

References

Allen, Howard G. (1975), "Analysis and Design of Structural Sandwich Panels", PERGAMON PRESS, Toronto. 283p.

American Society for Testing and Materials (ASTM), ASTM A370-07a (2007), "Standard Test Methods and Definitions for the Mechanical Testing of Steel Products", West Conshohocken, Pennsylvania

Bennett, Michael. (1998), "Development and Behaviour of Unidirectional Double Hull Sandwich Plate System: Experimental Investigation", Master's Thesis submitted to the Department of Civil and Environmental Engineering, Carleton University. Ottawa, Canada.

Canadian Highway Bridge Design Code (CSA), CAN/CSA-S6-06 (2006), "Canadian Highway Bridge Design Code", Toronto, Ontario.

Davison, Buick and Owens, Graham W. (2003), "Steel Designer's Manual", Oxford, UK; Malden, MA, USA: Blackwell Science. pp. 906-910.

Ferro, Angelo. (1998), "Development and Behaviour of Unidirectional Double Hull Sandwich Plate System: Analytical Investigation", Master's Thesis submitted to the Department of Civil and Environmental Engineering, Carleton University. Ottawa, Canada.

Harris, D. K. (2007), "Lateral Load Distributions and Deck Design Recommendations for the Sandwich Plate System (SPS) in Bridge Applications", Ph.D. Thesis submitted to the Department of Civil and Environment Engineering, Virginia Polytechnic Institute and State University, Blacksburg, VA.

Canadian Institute of Steel Construction, (2006), "Handbook of Steel Construction", Willowdale, Ont.

Harris, D., Cousins, T., Murray, T., and Ferro, A. (2006), "Live Load Test of a SPS Deck Bridge", Virginia Polytechnic Institute and State University, Blacksburg, VA. & Intelligent Engineering, Ottawa, ON.

Intelligent Engineering (Canada) Limited (2007), "Sandwich Plate System "SPS": An Innovative Construction Technology for Engineered Structures" Stahlbau, January, Germany, 22p.

Kennedy, D. J. L., Dorton, R. A., and Alexander, S. D. B. (2002), "the Sandwich Plate System for Bridge Deck", Intelligent Engineering (Canada) Limited. Ottawa, Canada.

Kennedy S. J. and Murray T. M. (2004), "Ultimate Strength of an SPS Bridge-The Shenley Bridge, Quebec, Canada", paper presented at 2004 Annual Conference of Transportation Association of Canada. September, Quebec city, Canada.

Kennedy, S. J., Kennedy, D. J. L., Dorton, R. A., Wright, D. G., and Vincent, R. B. (2006), " A True Innovation: Steel Plate with a Structural Elastomer Core", ASCE Composite Construction in Steel and Concrete, V. Reston, VA.

Kim B. J. and Hughes O. F. (2004), "Analytical Solution for the Ultimate Strength of Metal-faced Elastomer-cored Sandwich Panels under In-plane Edge Compression and Lateral Pressure", Department of Aerospace and Ocean Engineering, Virginia Polytechnic Institute and State University, Blacksburg, VA

Little, J, G.Y. Grondin and S.D.B.Alexander (2007), "Sandwich Plate System Panels under In-plane load and Uniform Lateral Pressure", Structural Engineering Report No.266. University of Alberta.

Lui, G. and Alexander, S. D. B. (2003), "Fatigue of Steel Plate – Elastomer Composite Beams", Structural Engineering Report No.274. University of Alberta.

Martin, J. D. and Murray, T. M. (2005), "Sandwich Plate System Bridge Deck Tests", Research Report CEE/VPI-ST04/07, Department of Civil and Environmental Engineering, Virginia Polytechnic Institute and State University. Blacksburg, VA.

Marzahn, G. A. and Hamme, M. (2008), "Strengthening of Orthotropic Bridge Deck by SPS Technology", ASCE Structures 2008: Crossing Borders. Strassen. NRW, Gelsenkirchen, Germany.

Olsson, Karl-Axel and Reichard, Ronnal P. (1989), "Sandwich Constructions 1", Warley, England: Engineering Materials Advisory Services Ltd., 605p.

Lloyd's Register Group (2006), "Provisional Rules for the Application of Sandwich Panel Construction to Ship Structure", London, UK.

Salvadori, Mario and Levy, Matthys (1981), "Structural Design in Architecture", Englewood Cliffs, N.J.: Prentice-Hall.

Sokolinsky, V. and Frostig, Y. (1999), "Boundary Condition Effects in Buckling of Soft Core Sandwich Panels", Journal of Engineering Mechanics, August, pp.885-874.

Vincent, R. B. and Ferro, Angelo (2005), "A New Orthotropic Bridge Deck: Design, Fabrication and Construction of the Shenley Bridge Incorporating an SPS Orthotropic Bridge Deck", Paper presented at the 2005 Annual Conference of the Transportation Association of Canada, Calgary, AB.

Vinson, Jack R. (2005), "Plate and Panel Structures of Isotropic, Composite and Piezoelectric Materials, Including Sandwich Construction", Springer, Netherlands, 418p.

Wiessenborn, Christian (2007), "Material and Failure Models for SPS Sandwich Plate Subject to Extreme Loads", PhD Thesis submitted to the Technischen Universitat Hamburg-Harburg, Aachen, Germany.

Appendix A

Out-of-Plane Deflections along the Panel Centerline of Panels 3-50-3, 3-100-3, 6-50-6, and 10-50-10

Appendix A

The out-of-plane deflections along the panel centerline of 3-15-3 sandwich panels with aspect ratios of 1.2, 1.7 and 2.5 at three load levels of $1\%q_c$, $27\%q_c$ and $90\%q_c$, were presented in chapter 4. The following figures display the out-of-plane deflections along the panel centerline for the other four sandwich panels investigated, namely, 3-50-3, 3-100-3, 6-50-6, and 10-50-10 with three aspect ratios at different lateral load levels. The panel configuration is described as steel-elastomer-steel, aspect ratio, L/w and lateral load level, q/q_c, are shown in each figure.

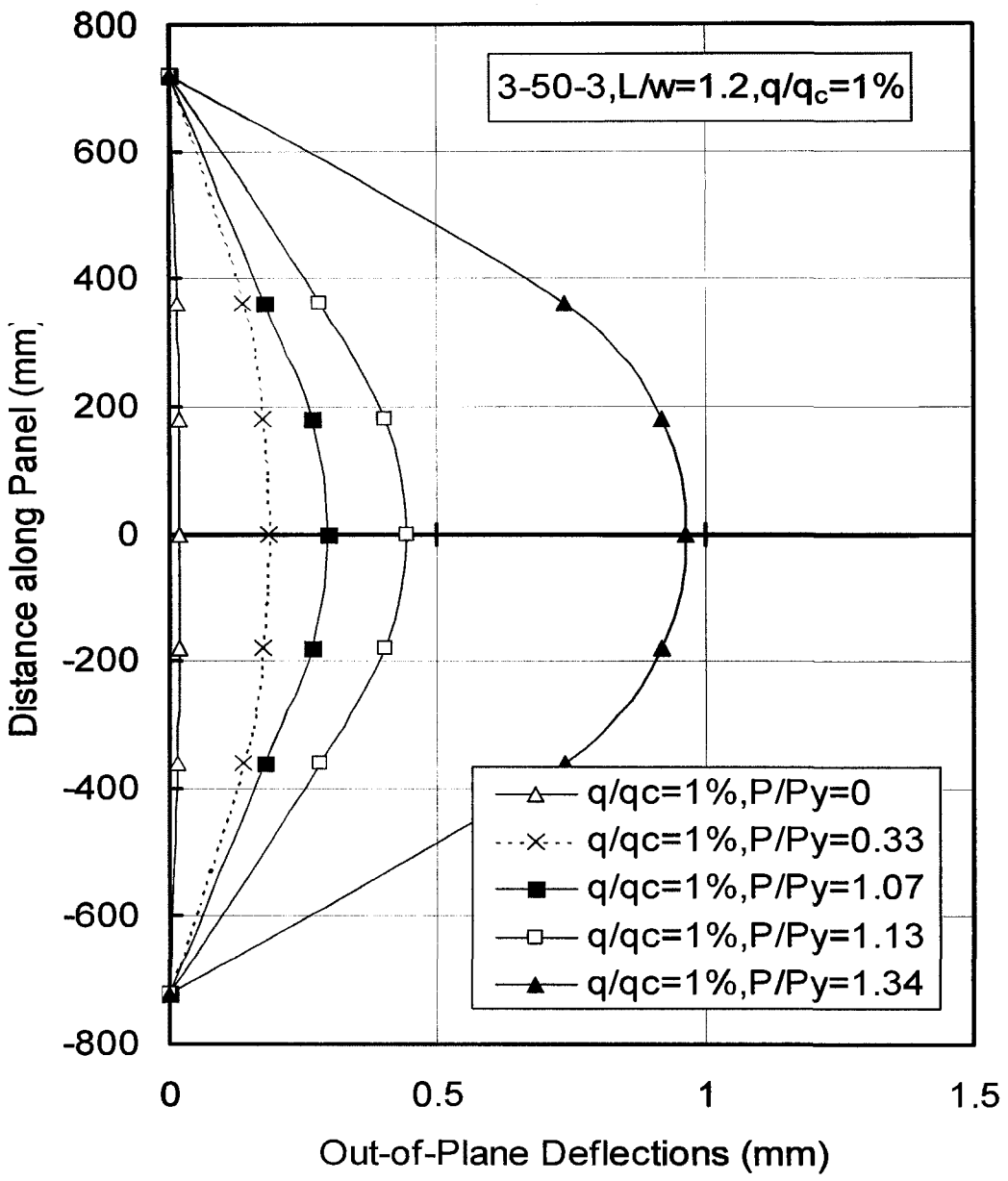

Figure A.1 Out-of-plane deflections along panel length for finite element mode (3-50-3, L/w=1.2, q/q_c =1%)

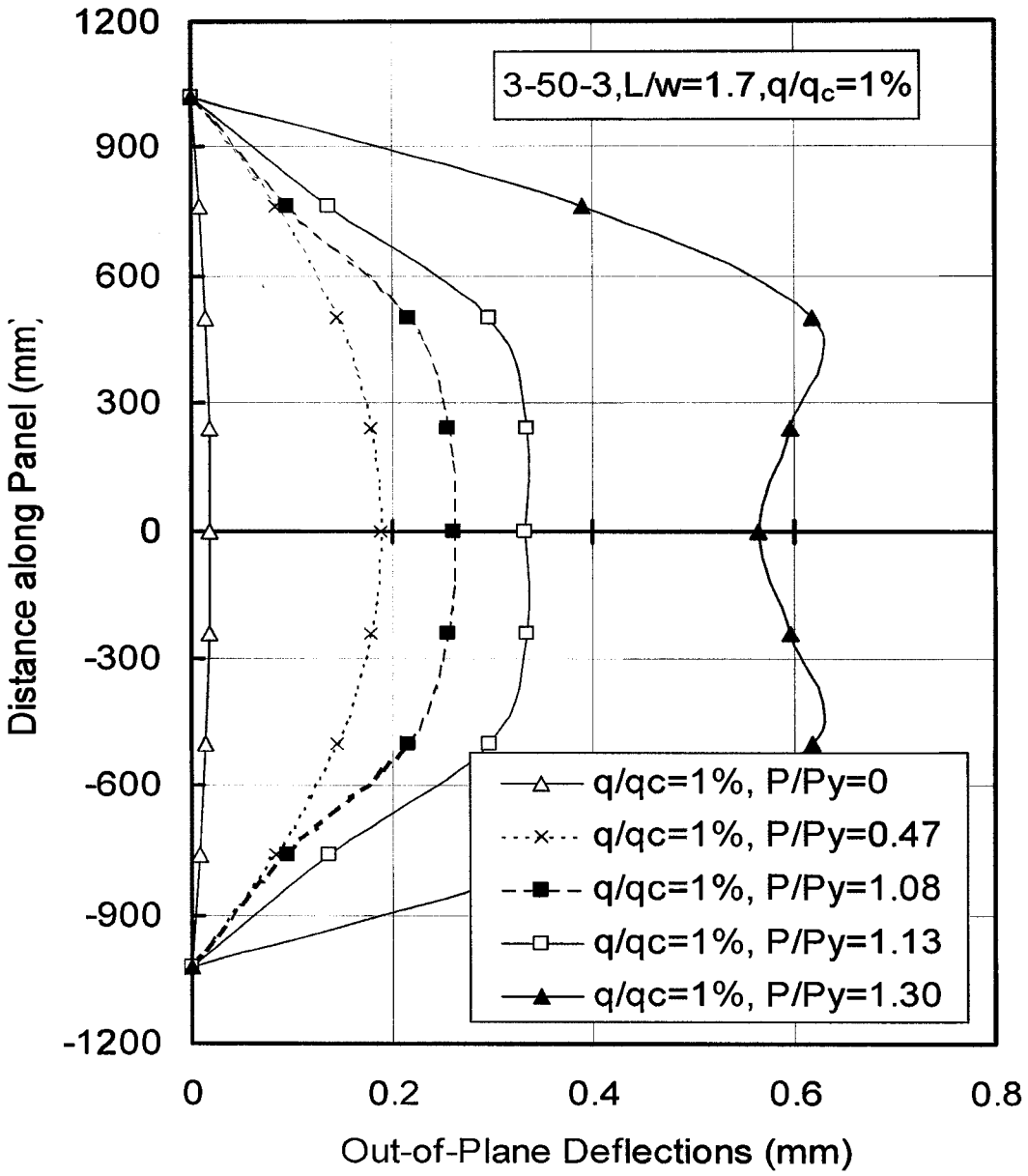

Figure A.2 Out-of-plane deflections along panel length for finite element mode (3-50-3, L/w=1.7, q/q_c =1%)

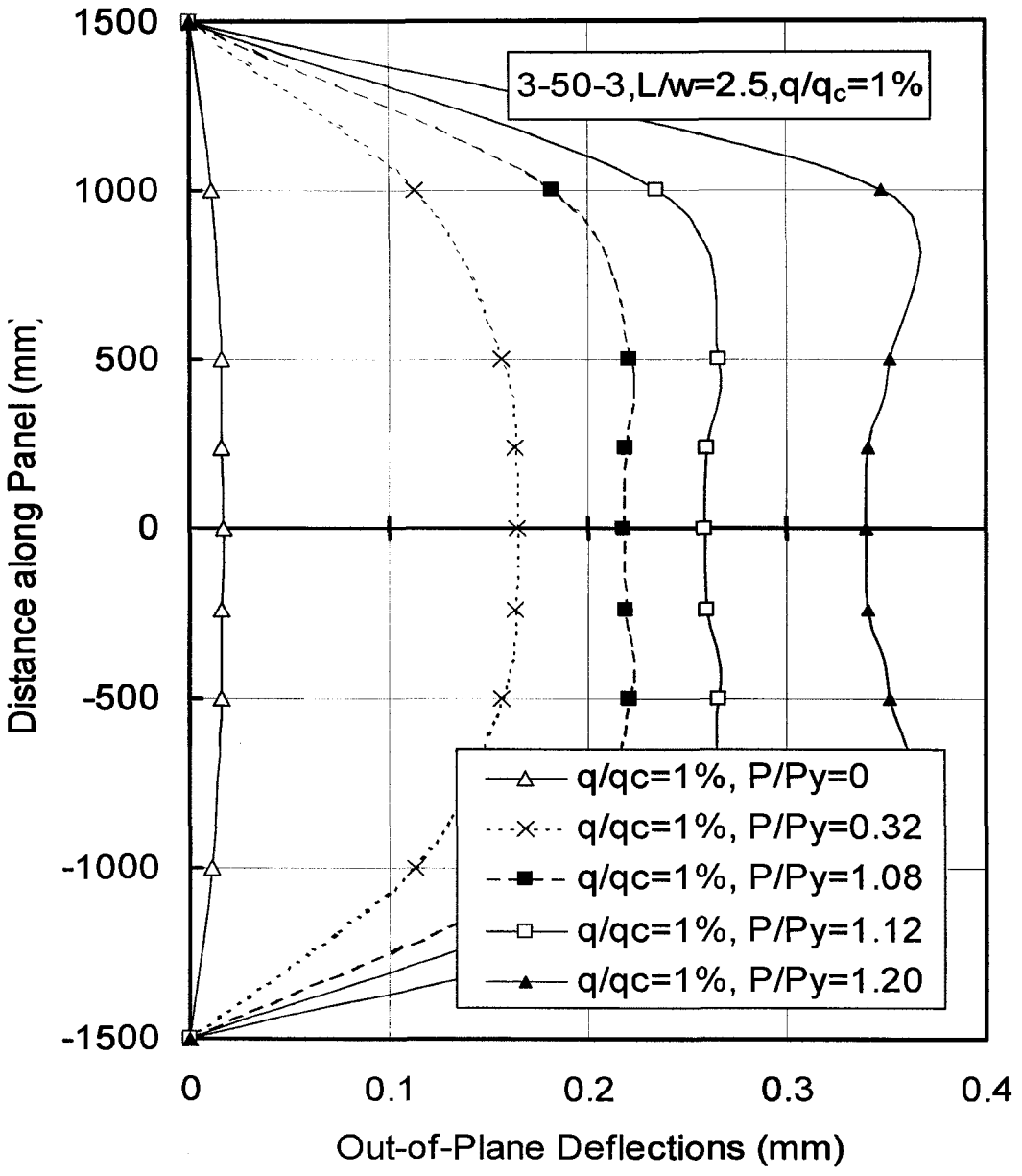

Figure A.3 Out-of-plane deflections along panel length for finite element mode (3-50-3, L/w=2.5, q/q_c =1%)

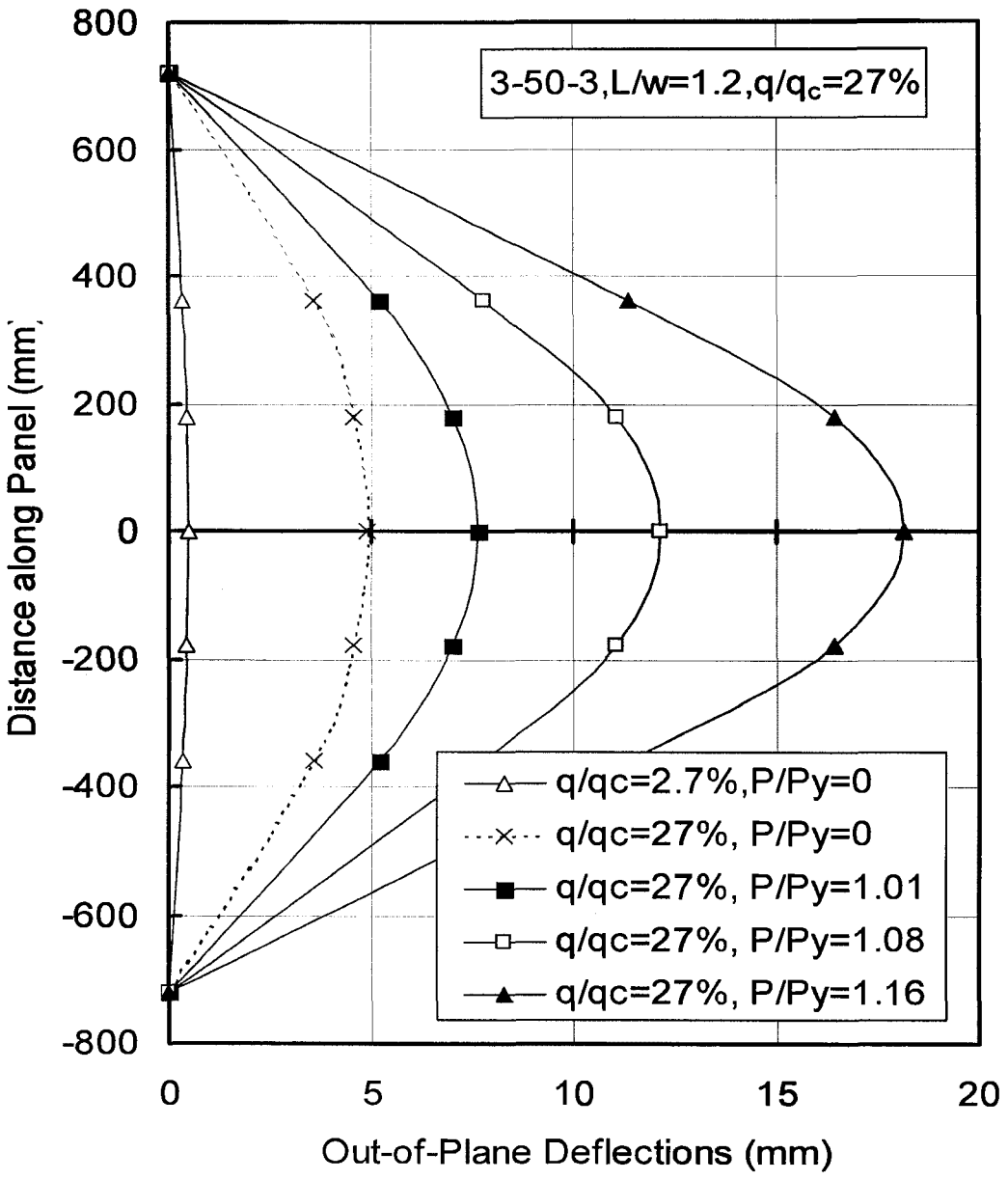

Figure A.4 Out-of-plane deflections along panel length for finite element mode (3-50-3, L/w=1.2, q/q_c =27%)

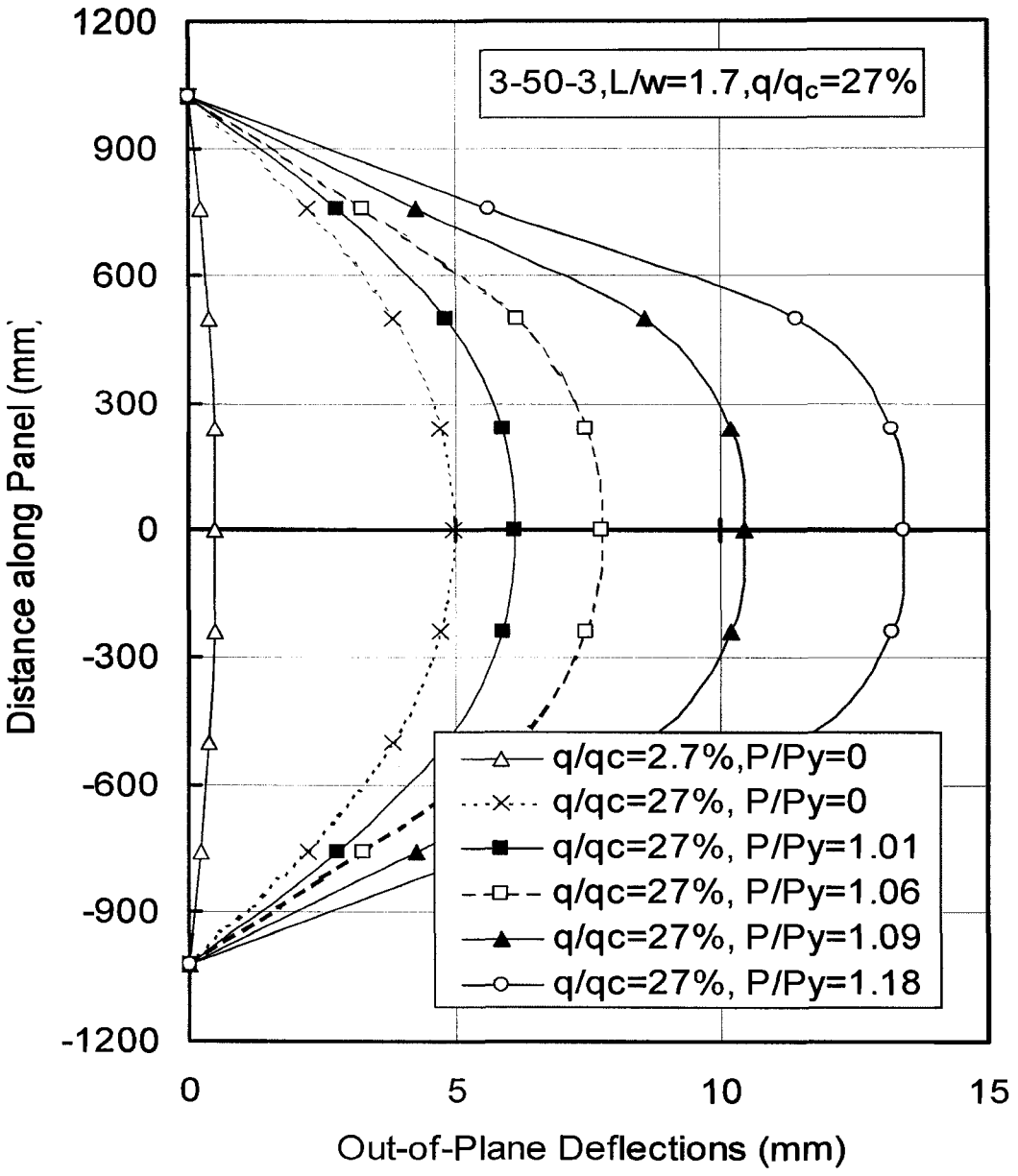

Figure A.5 Out-of-plane deflections along panel length for finite element mode (3-50-3, L/w=1.7, q/q_c =27%)

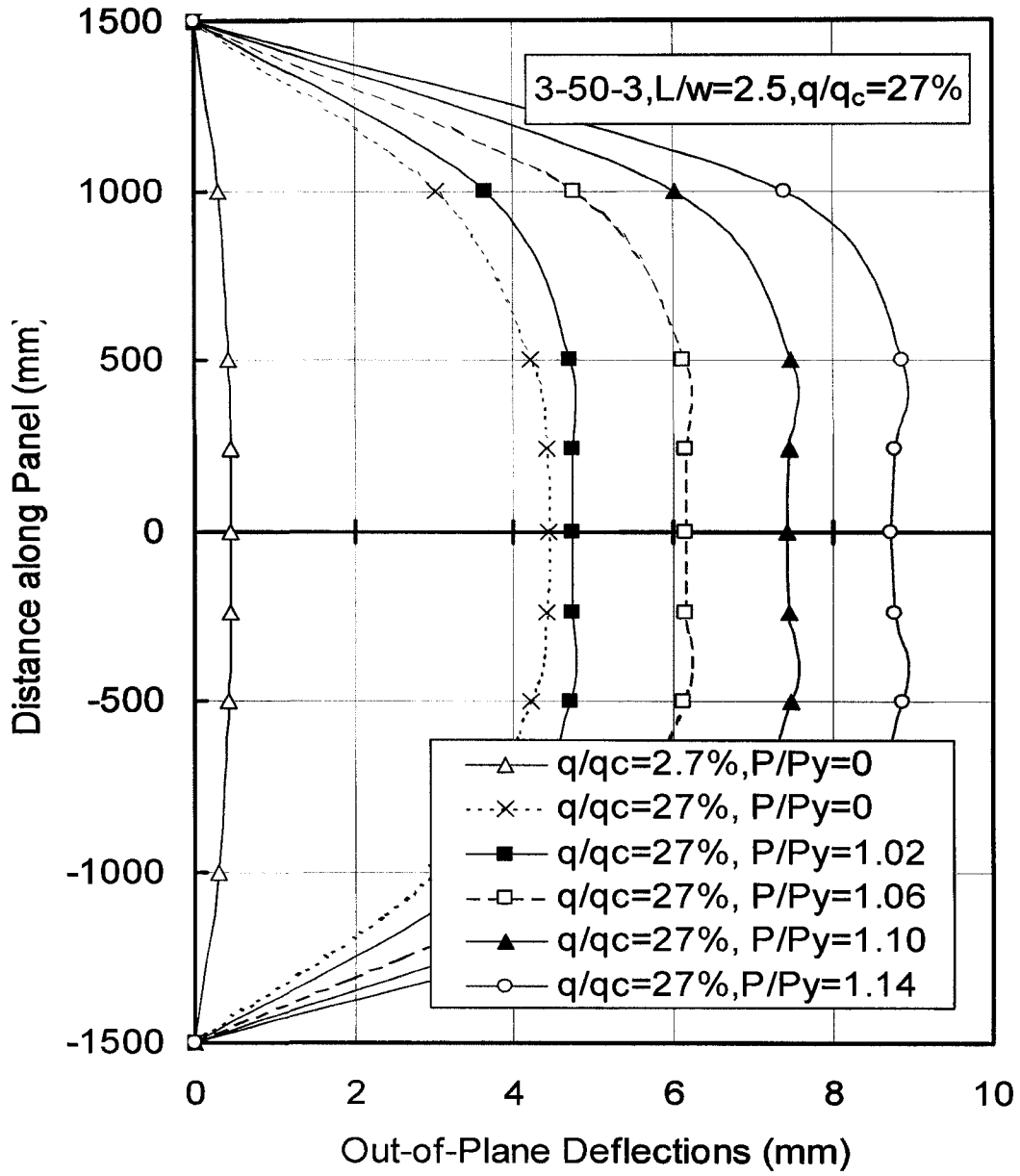

Figure A.6 Out-of-plane deflections along panel length for finite element mode (3-50-3, L/w=2.5, q/q_c =27%)

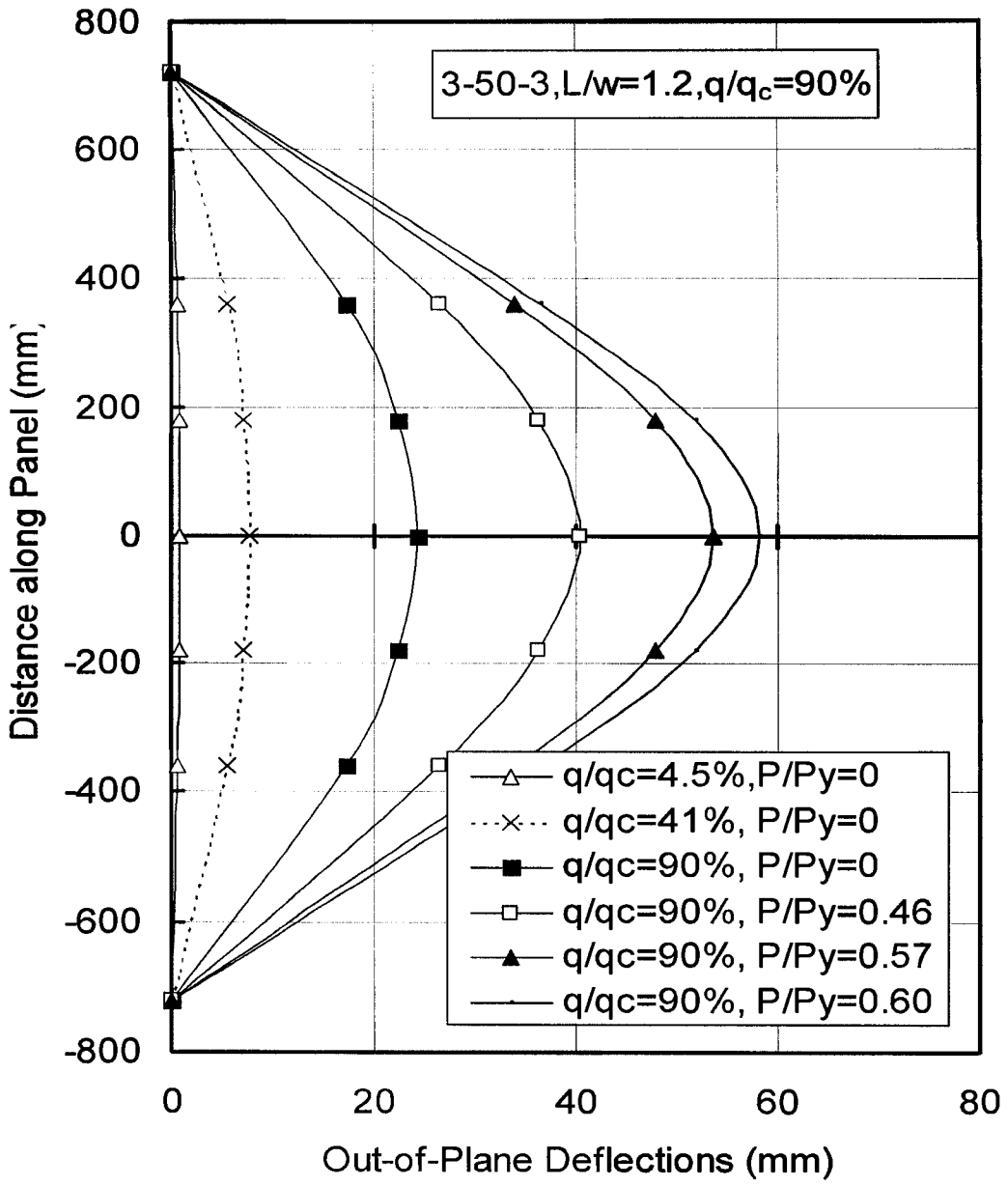

Figure A.7 Out-of-plane deflections along panel length for finite element mode (3-50-3, L/w=1.2, q/q_c =90%)

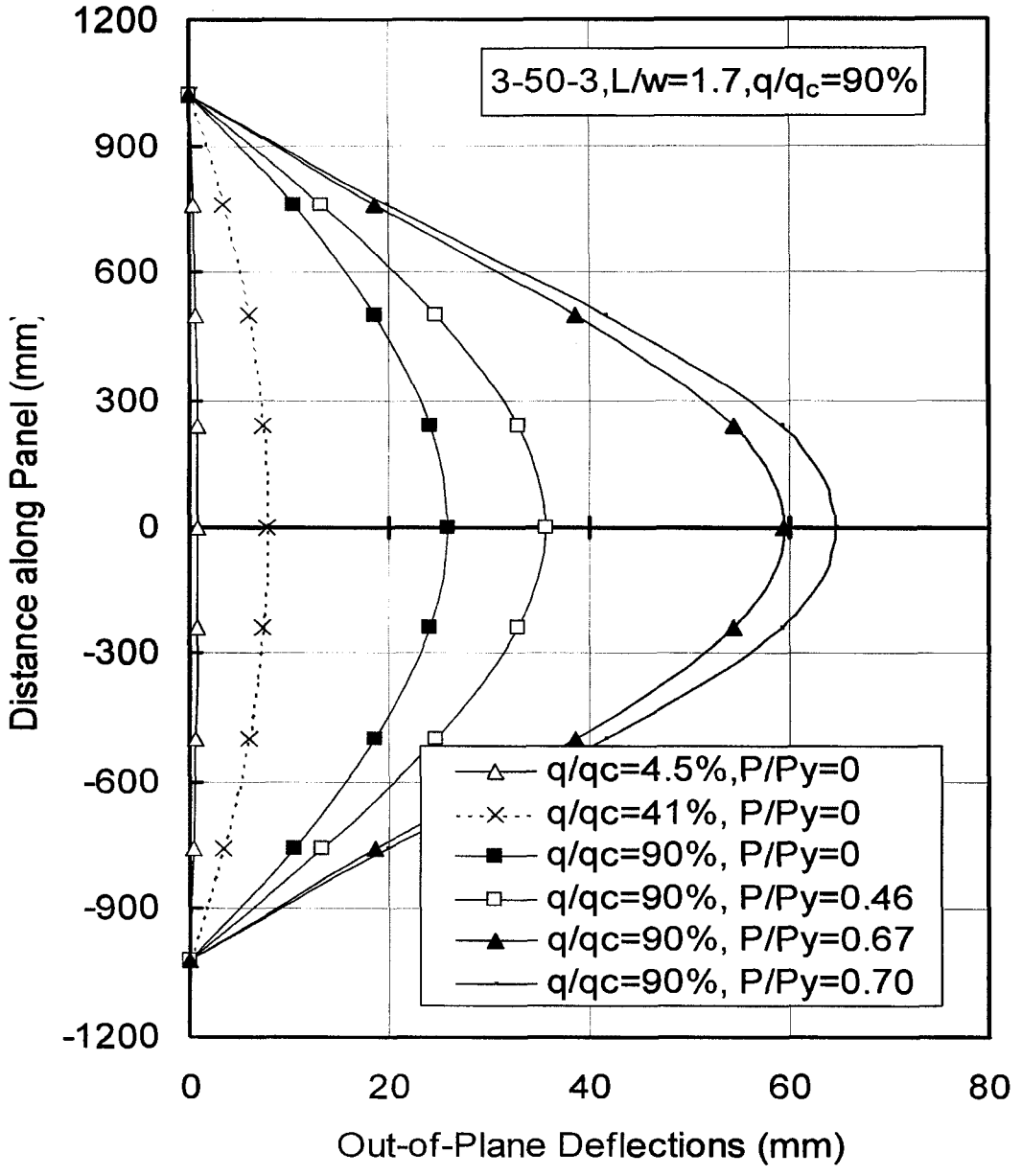

Figure A.8 Out-of-plane deflections along panel length for finite element mode (3-50-3, L/w=1.7, q/q_c =90%)

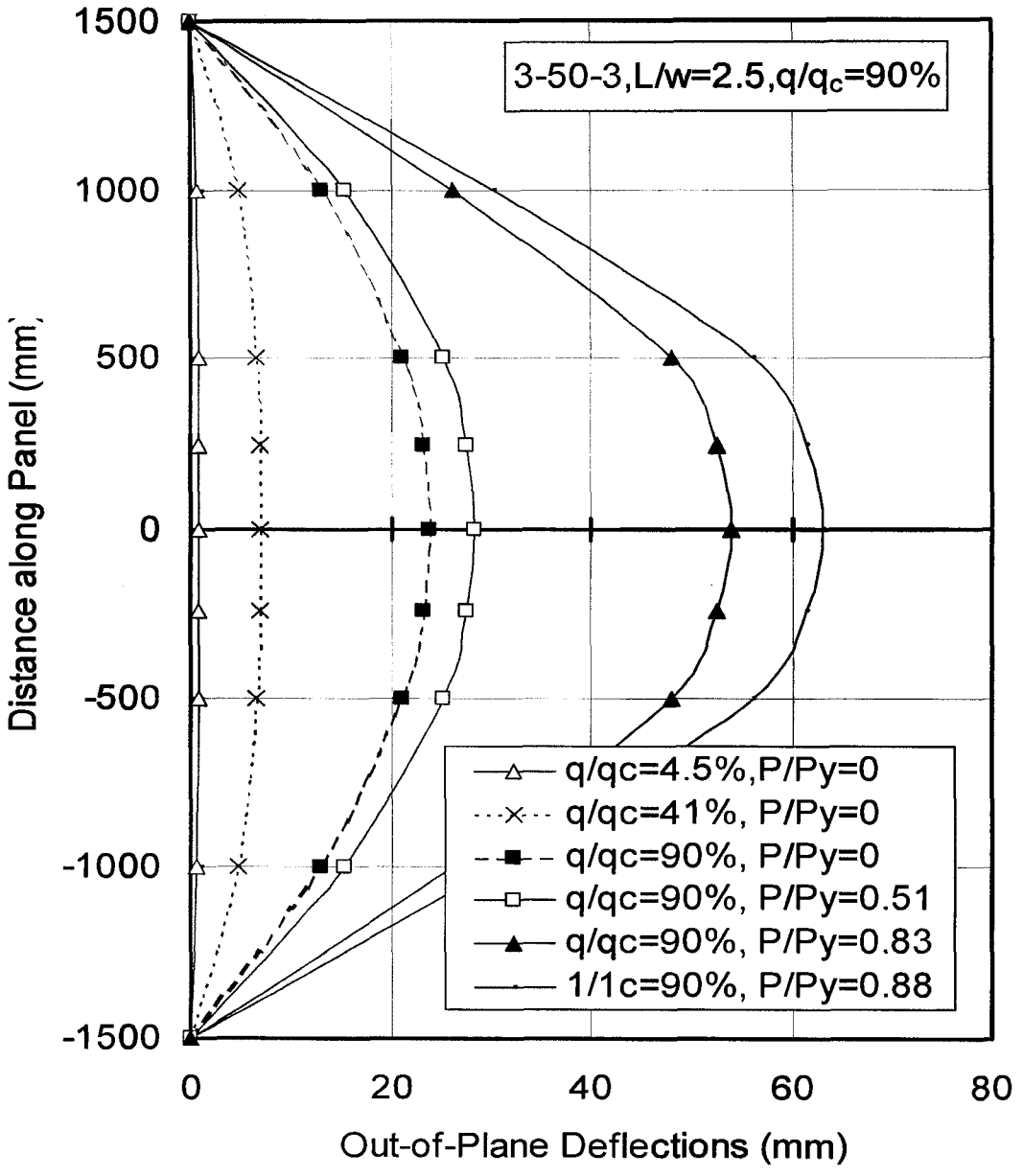

Figure A.9 Out-of-plane deflections along panel length for finite element mode (3-50-3, L/w=2.5, q/q_c =90%)

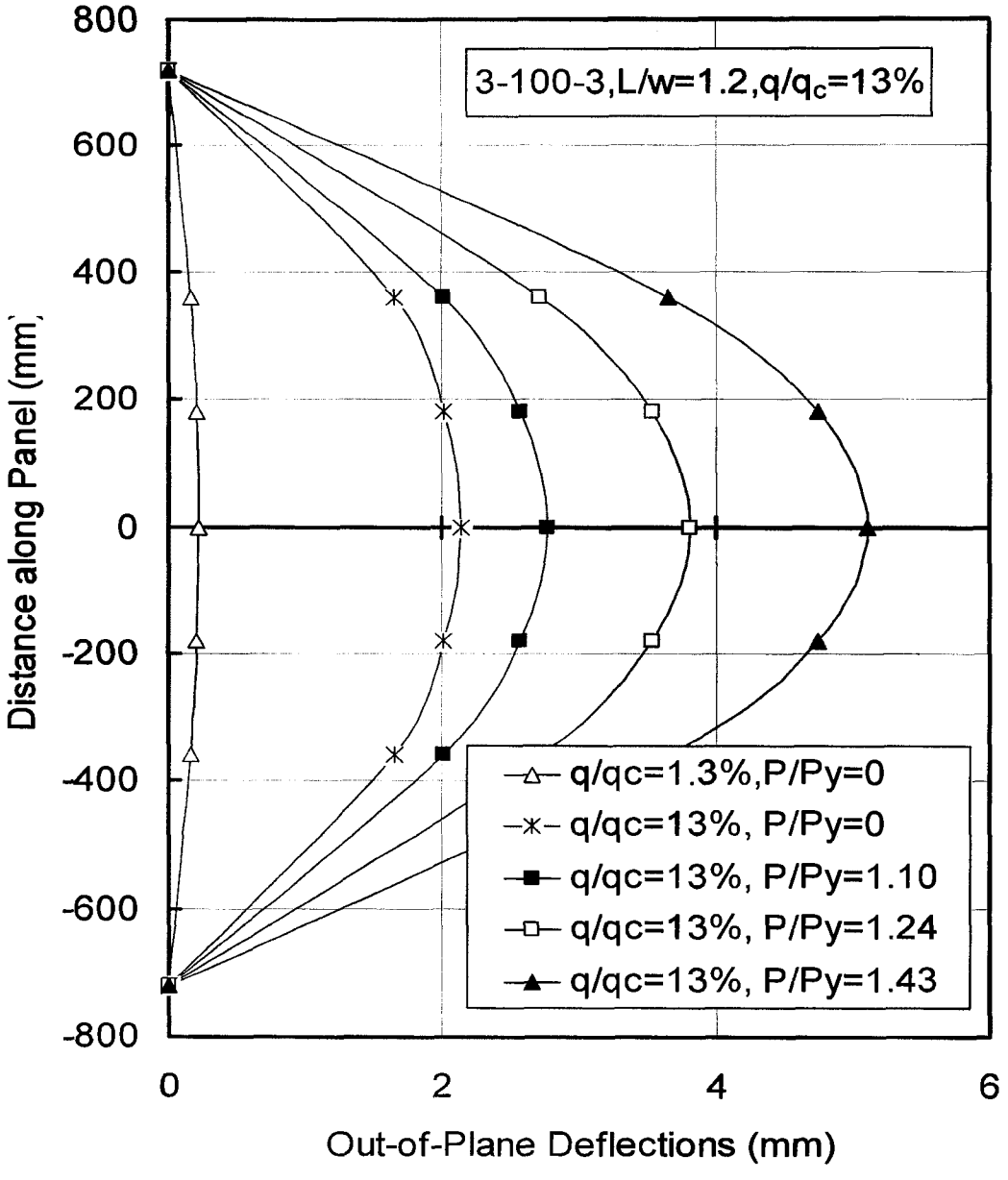

Figure A.10 Out-of-plane deflections along panel length for finite element mode (3-100-3, L/w=1.2, q/q_c =13%)

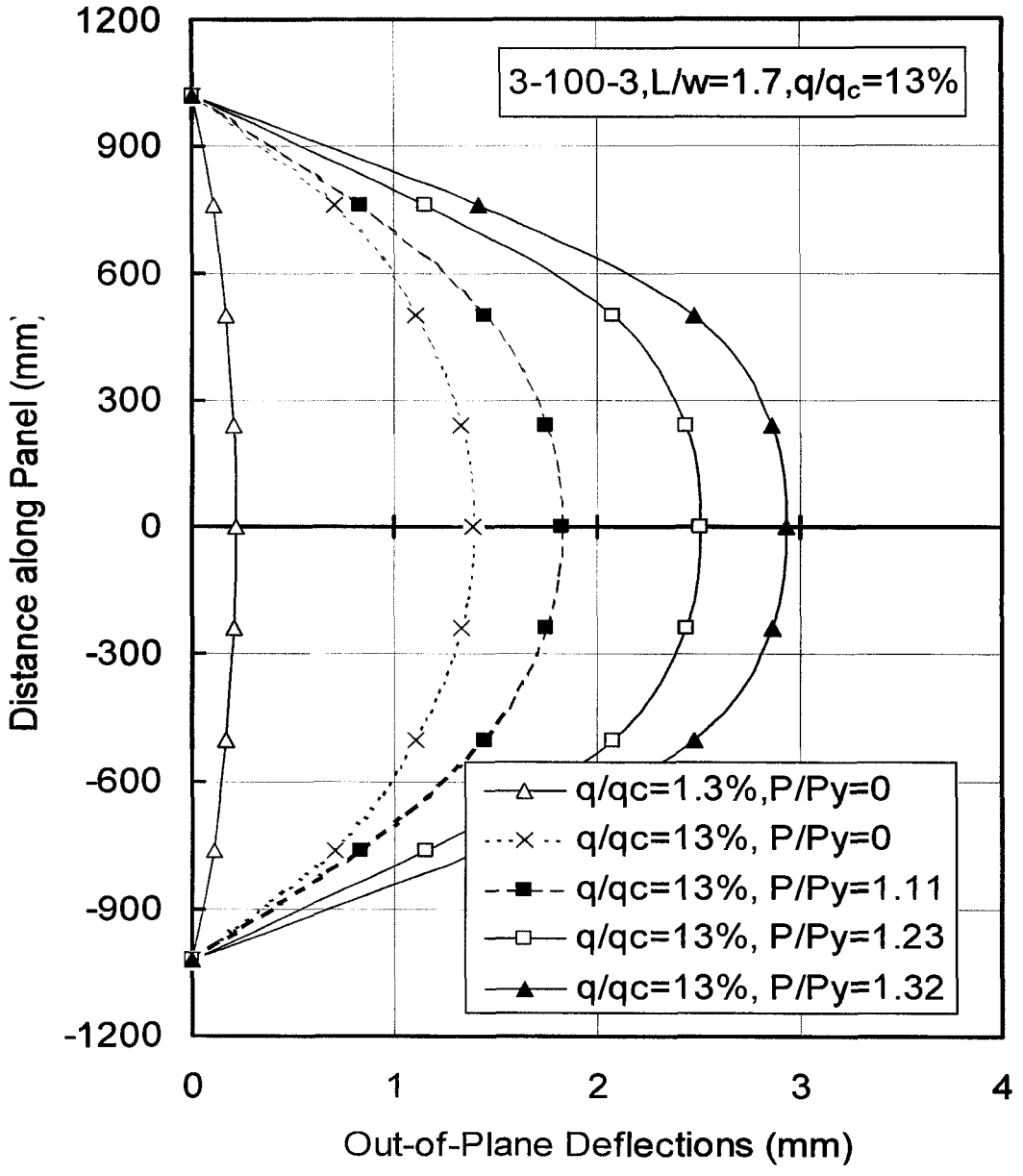

Figure A.11 Out-of-plane deflections along panel length for finite element mode (3-100-3, L/w=1.7, q/q_c =13%)

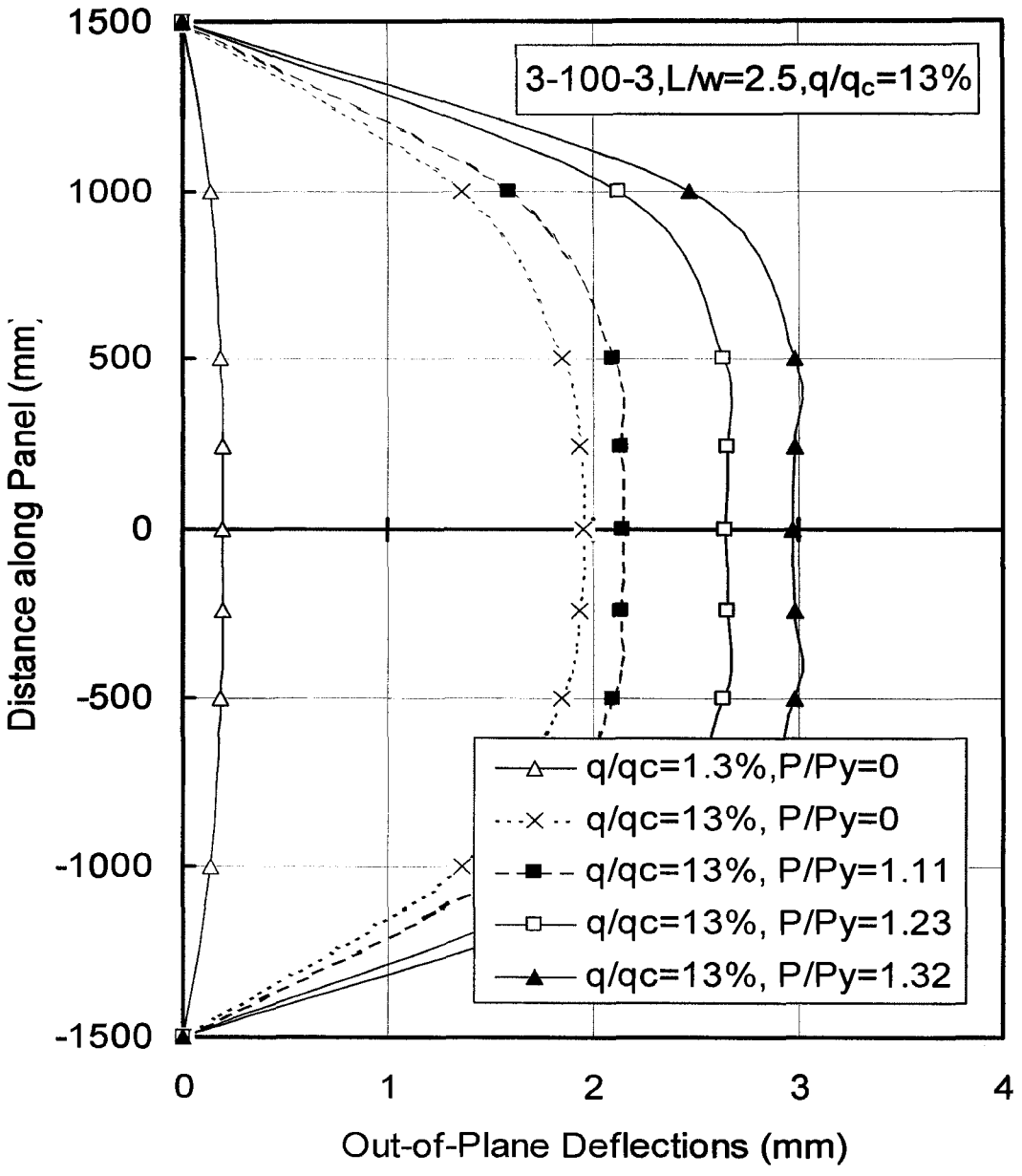

Figure A.12 Out-of-plane deflections along panel length for finite element mode (3-100-3, L/w=2.5, q/q_c =13%)

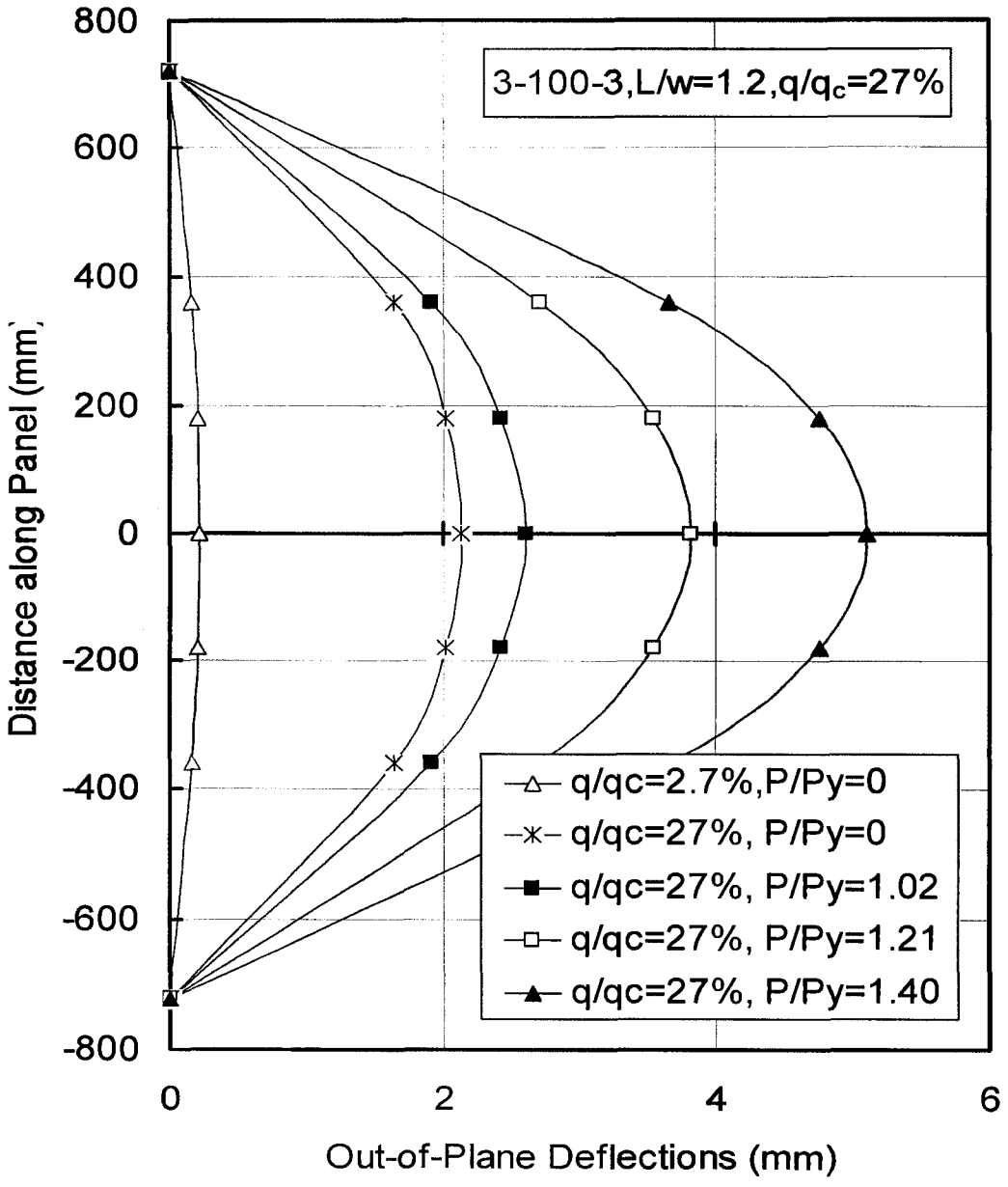

Figure A.13 Out-of-plane deflections along panel length for finite element mode (3-100-3, L/w=1.2, q/q_c =27%)

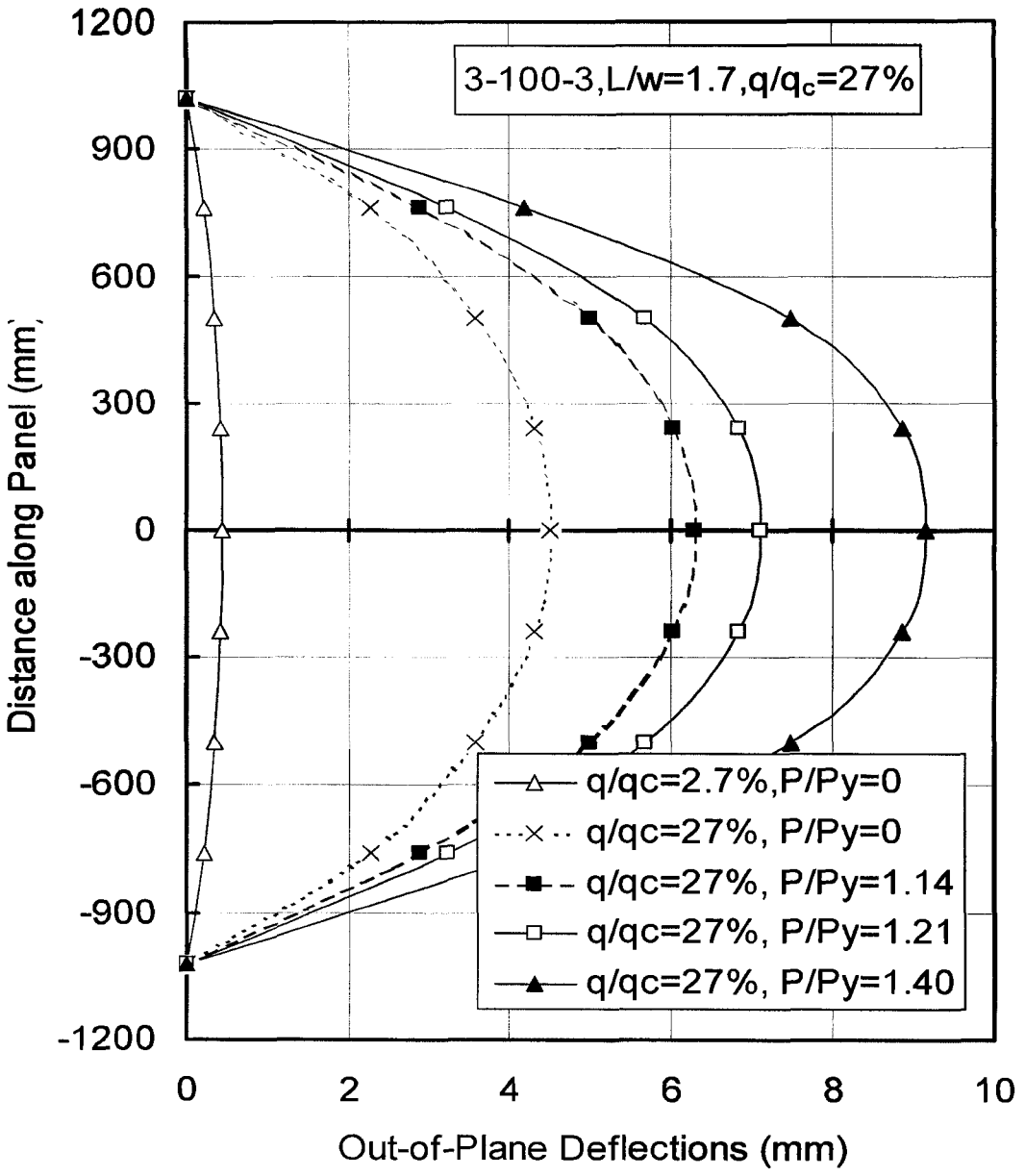

Figure A.14 Out-of-plane deflections along panel length for finite element mode (3-100-3, L/w=1.7, q/q_c =27%)

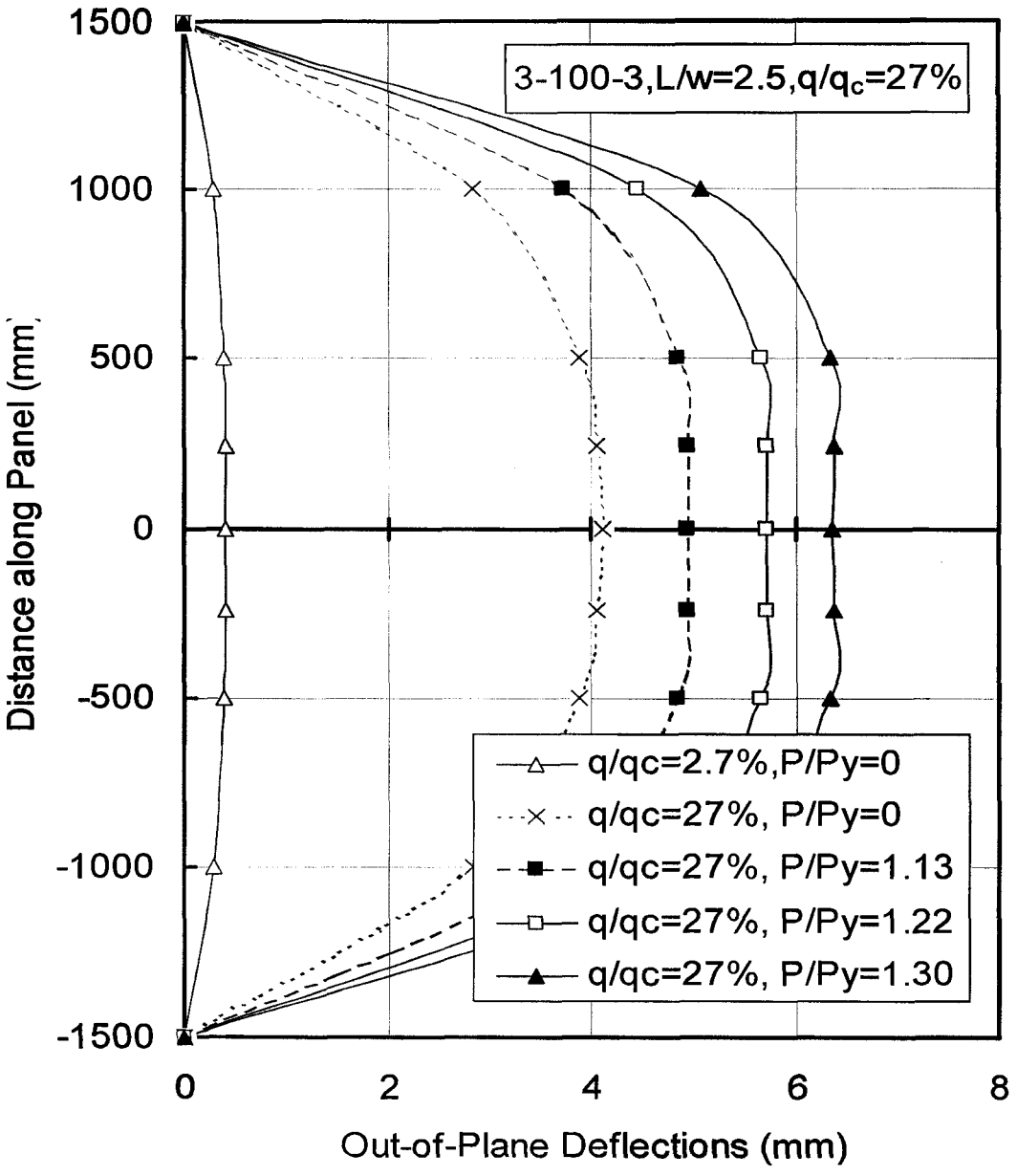

Figure A.15 Out-of-plane deflections along panel length for finite element mode (3-100-3, L/w=2.5, q/q_c =27%)

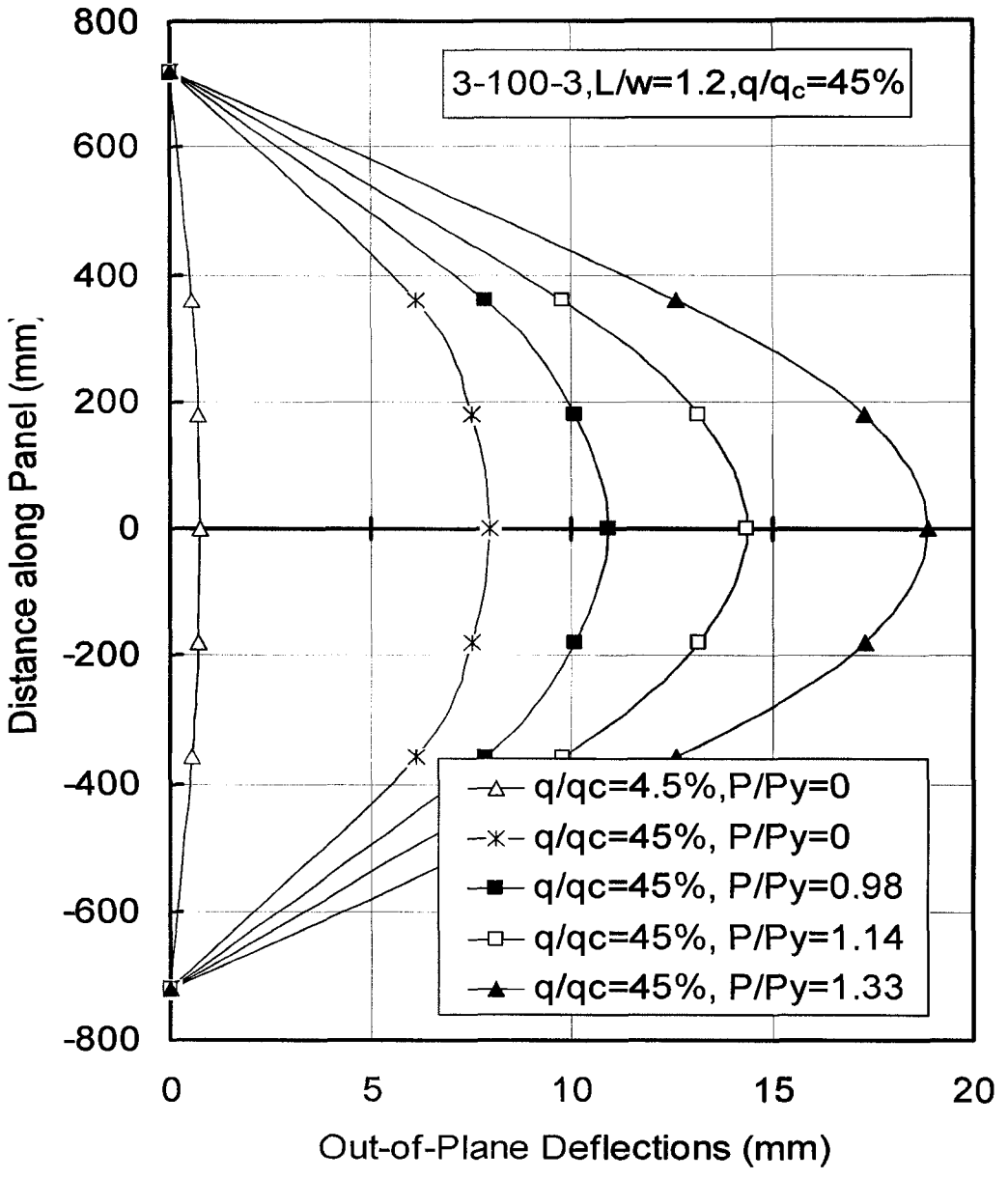

Figure A.16 Out-of-plane deflections along panel length for finite element mode (3-100-3, L/w=1.2, q/q_c =45%)

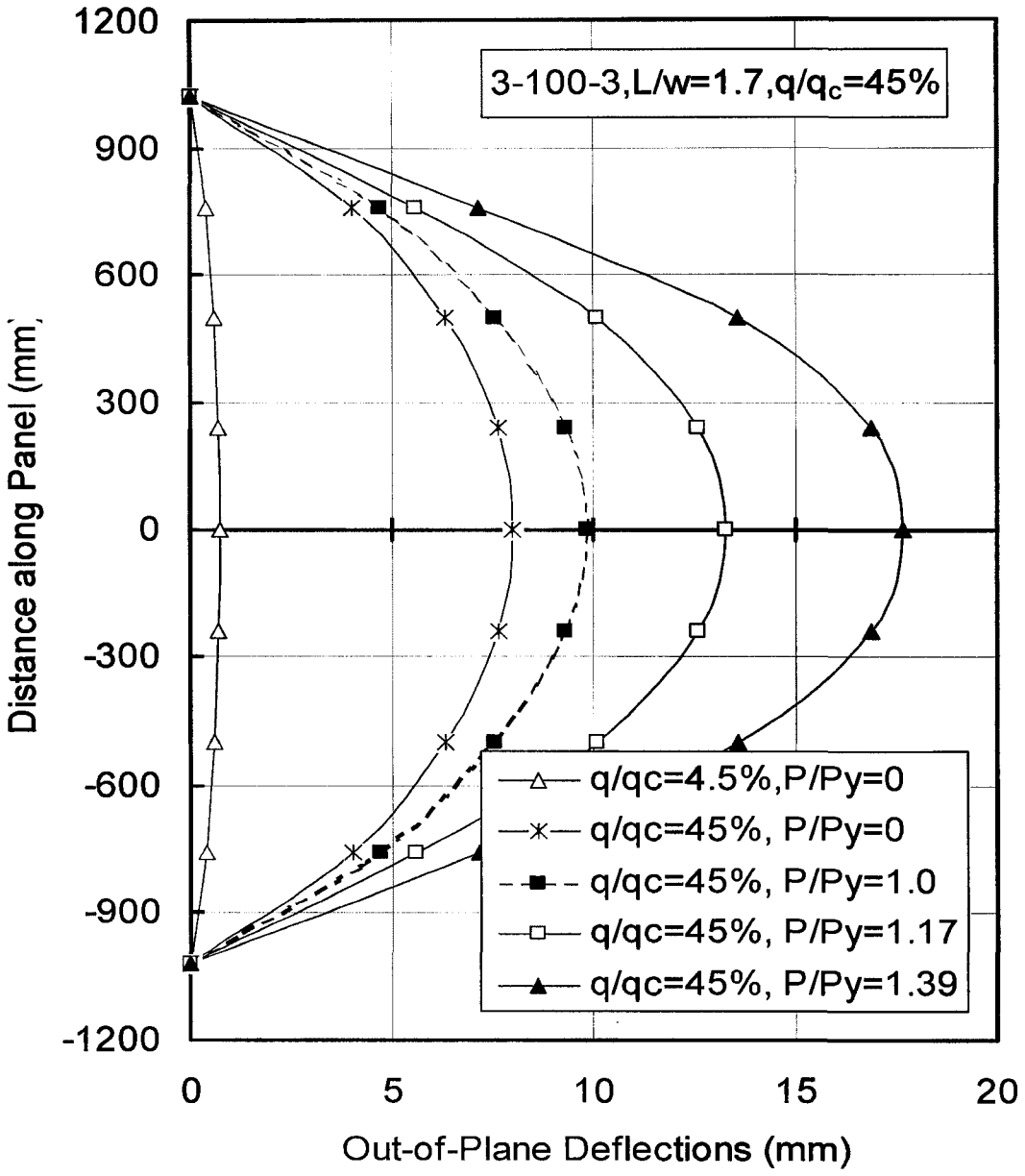

Figure A.17 Out-of-plane deflections along panel length for finite element mode (3-100-3, L/w=1.7, q/q_c =45%)

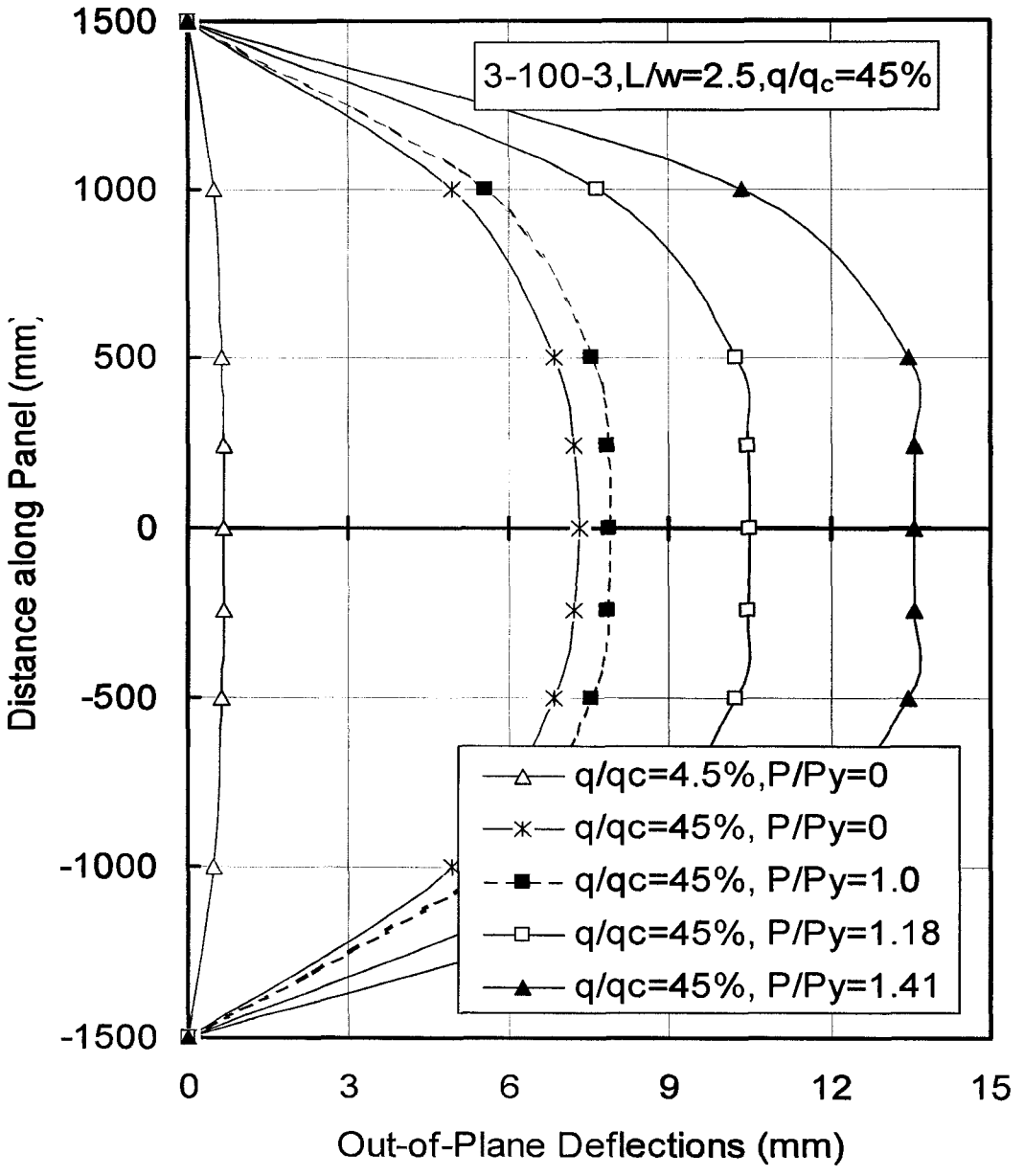

Figure A.18 Out-of-plane deflections along panel length for finite element mode (3-100-3, L/w=2.5, q/q_c =45%)

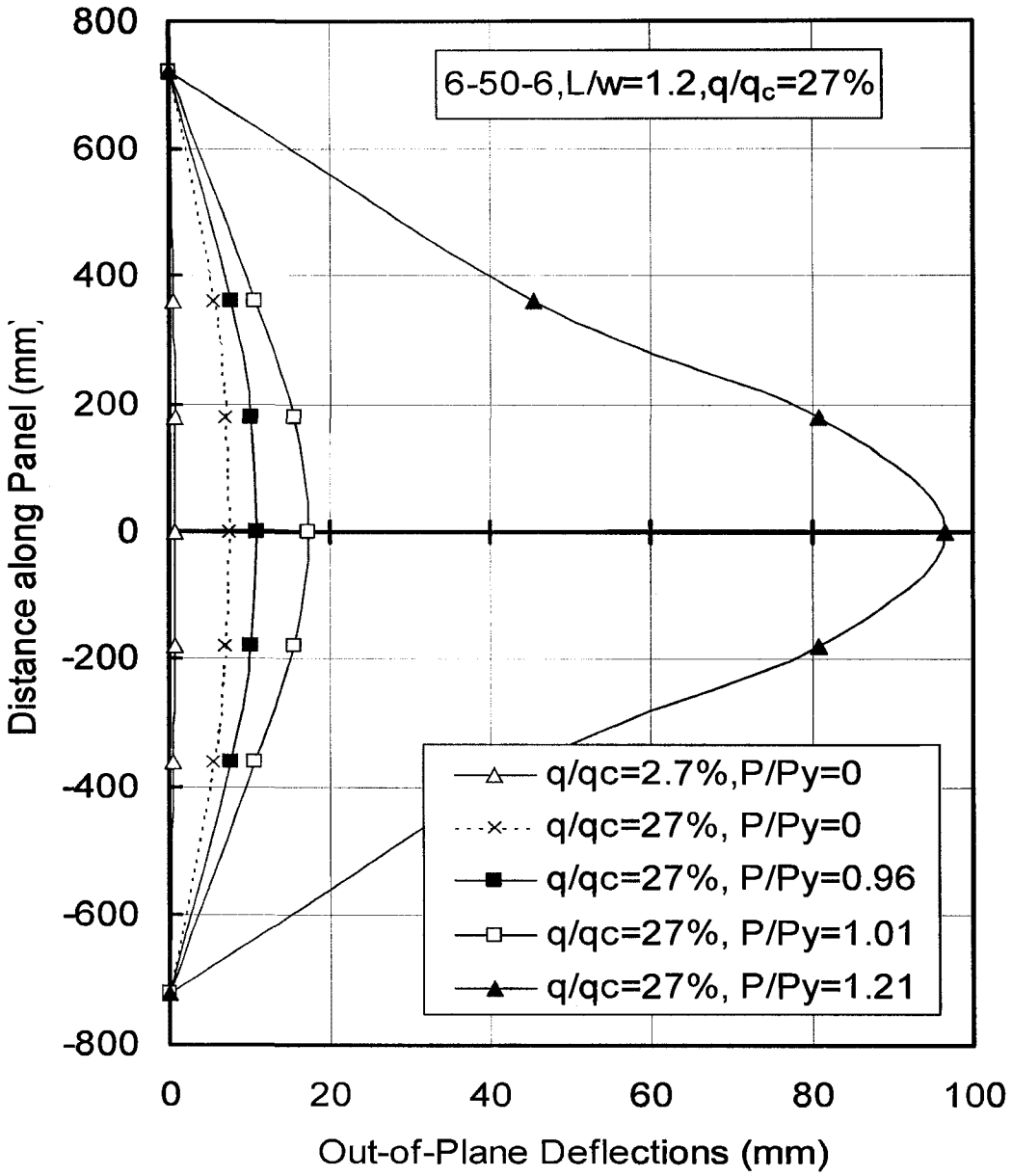

Figure A.19 Out-of-plane deflections along panel length for finite element mode (6-50-6, L/w=1.2, q/q_c =27%)

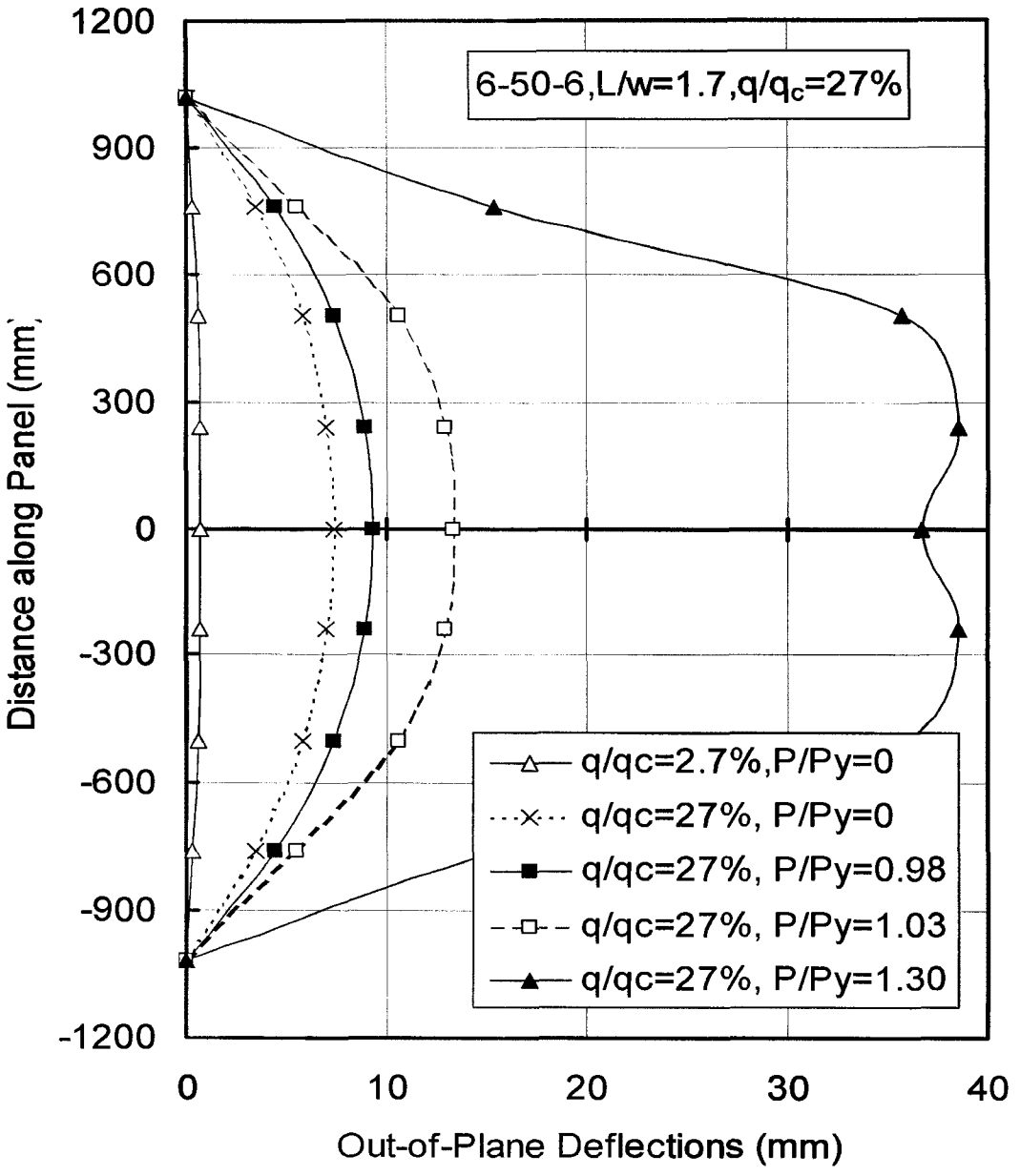

Figure A.20 Out-of-plane deflections along panel length for finite element mode (6-50-6, L/w=1.7, q/q_c =27%)

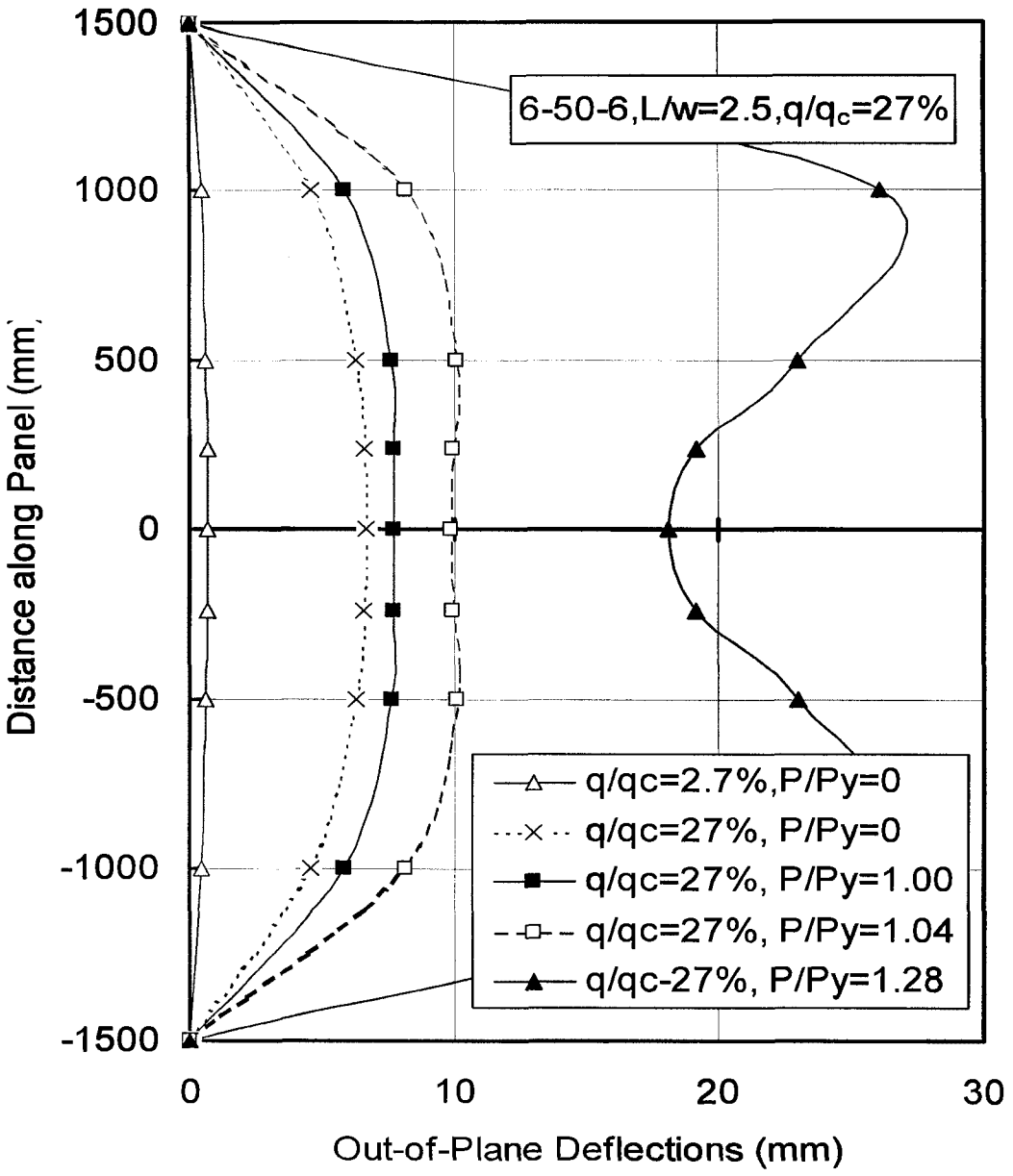

Figure A.21 Out-of-plane deflections along panel length for finite element mode (6-50-6, L/w=2.5, q/q_c =27%)

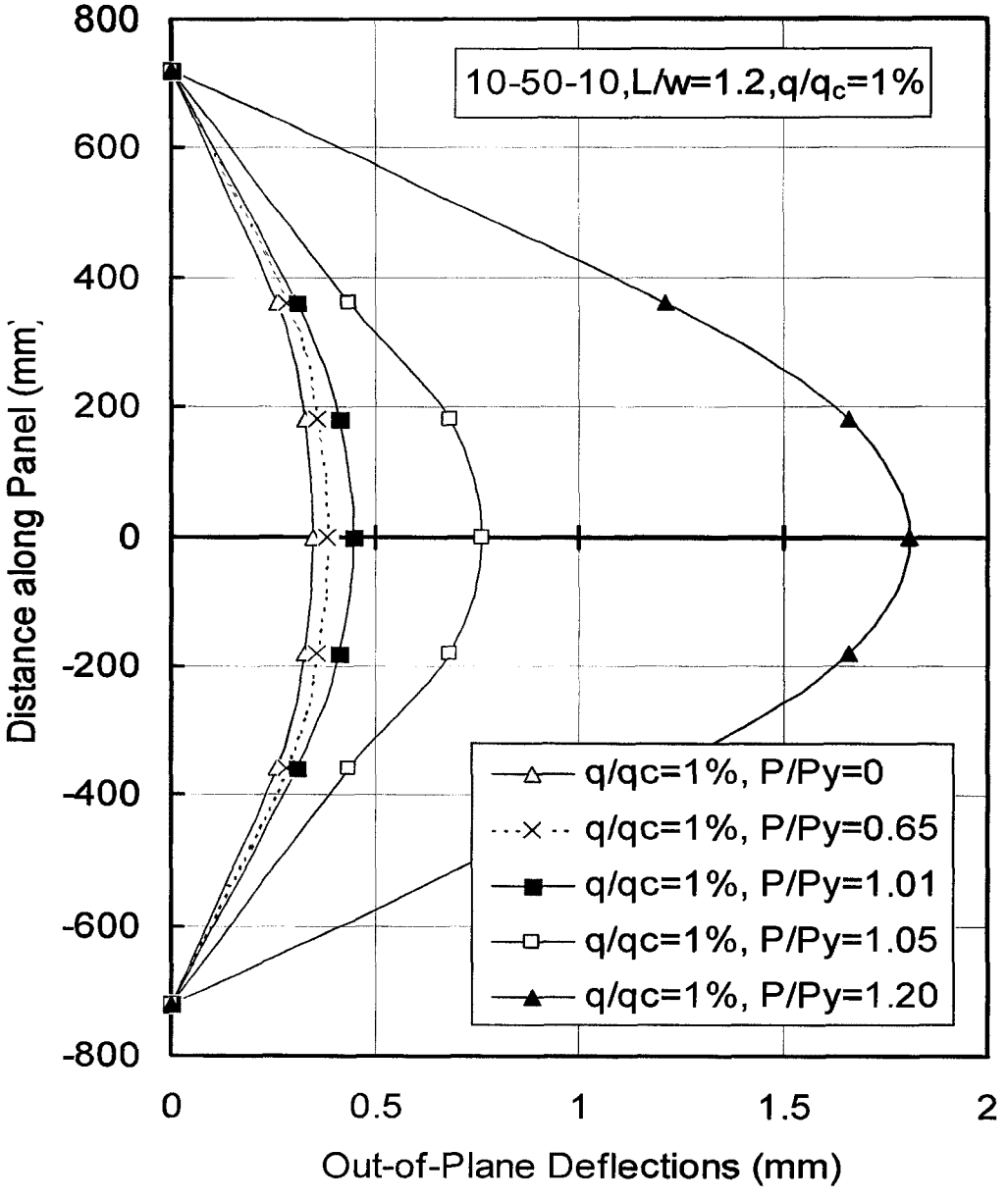

Figure A.22 Out-of-plane deflections along panel length for finite element mode (10-50-10, L/w=1.2, q/q_c =1%)

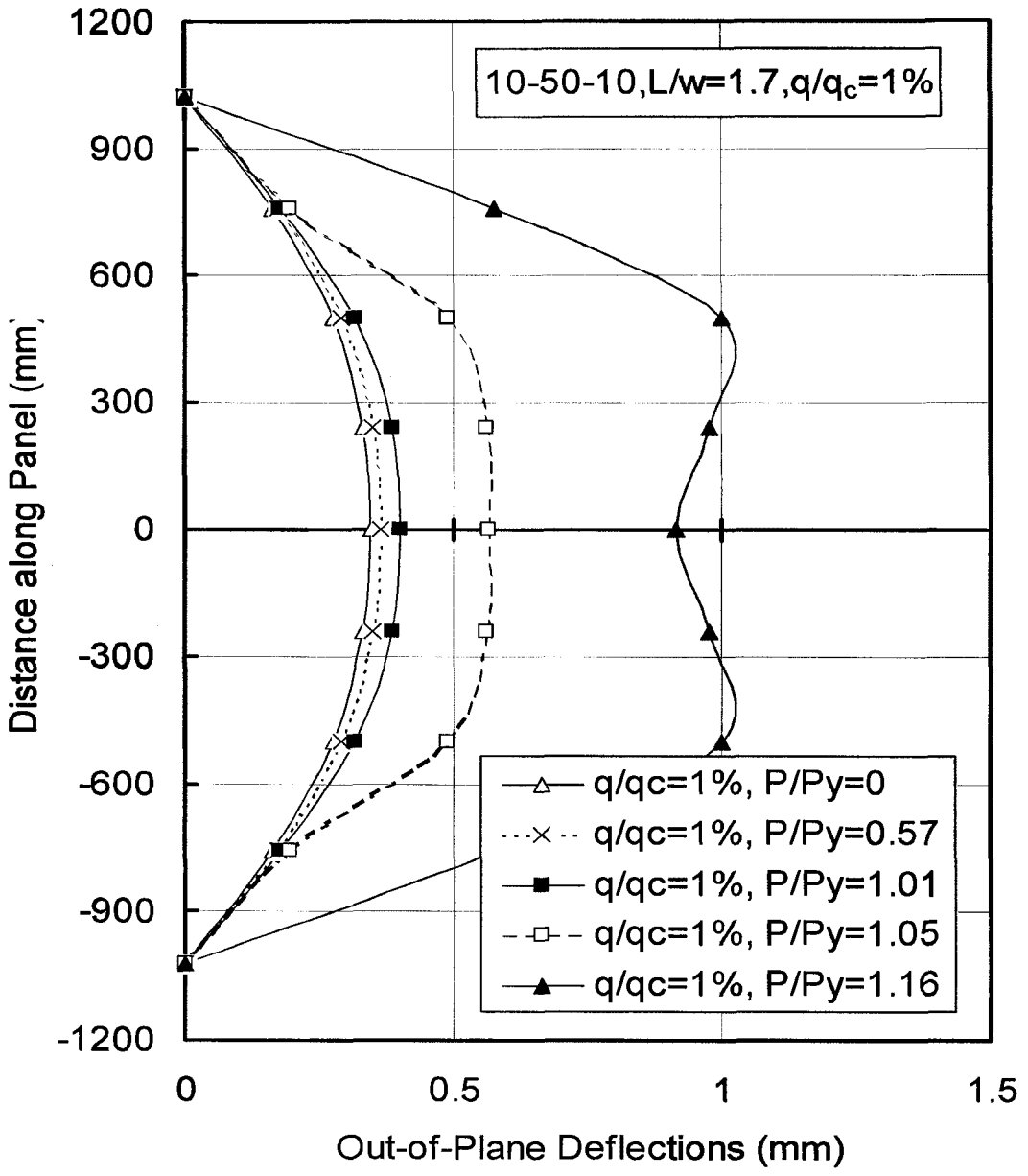

Figure A.23 Out-of-plane deflections along panel length for finite element mode (10-50-10, L/w=1.7, q/q_c =1%)

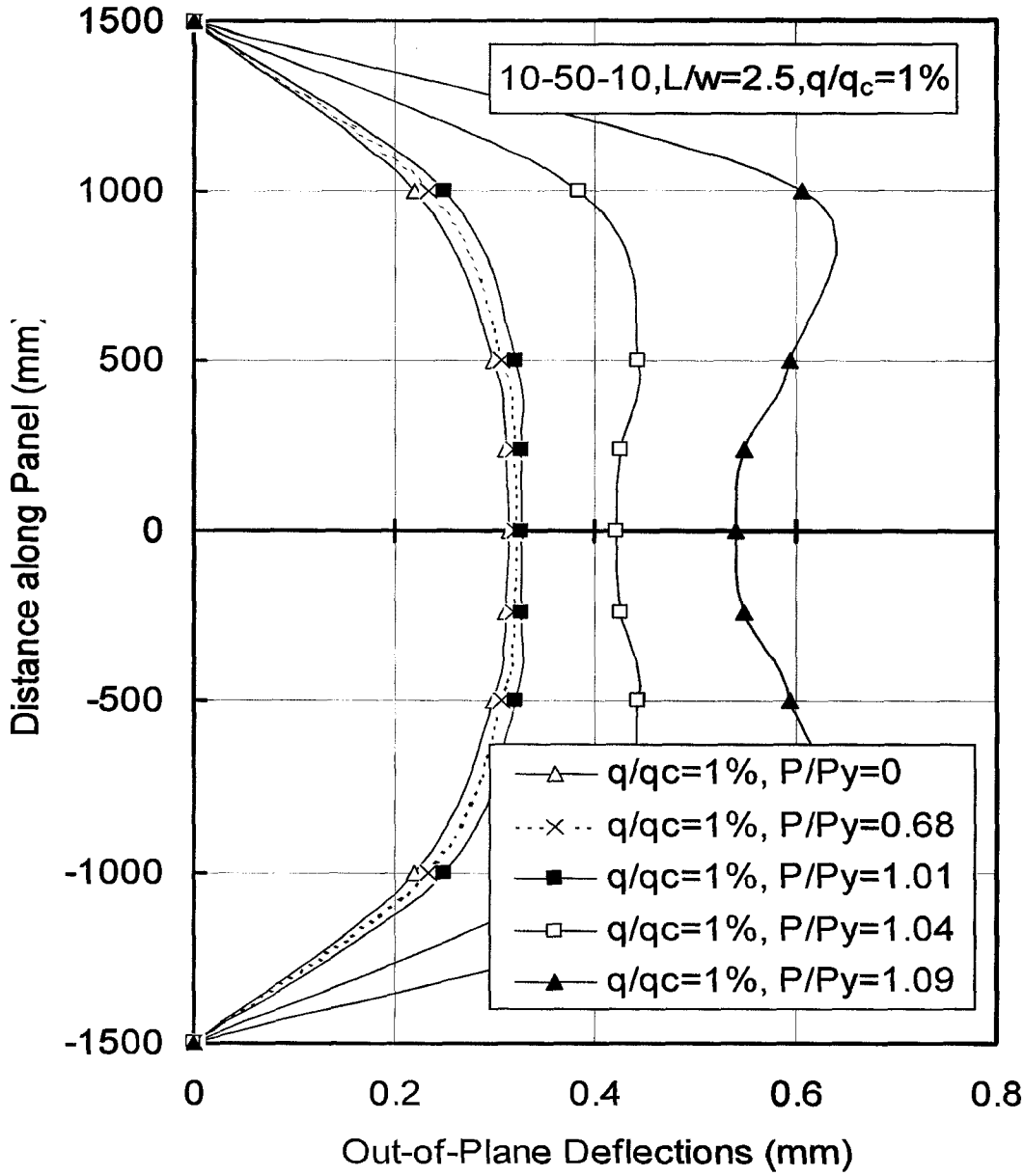

Figure A.24 Out-of-plane deflections along panel length for finite element mode (10-50-10, L/w=2.5, q/q_c =1%)

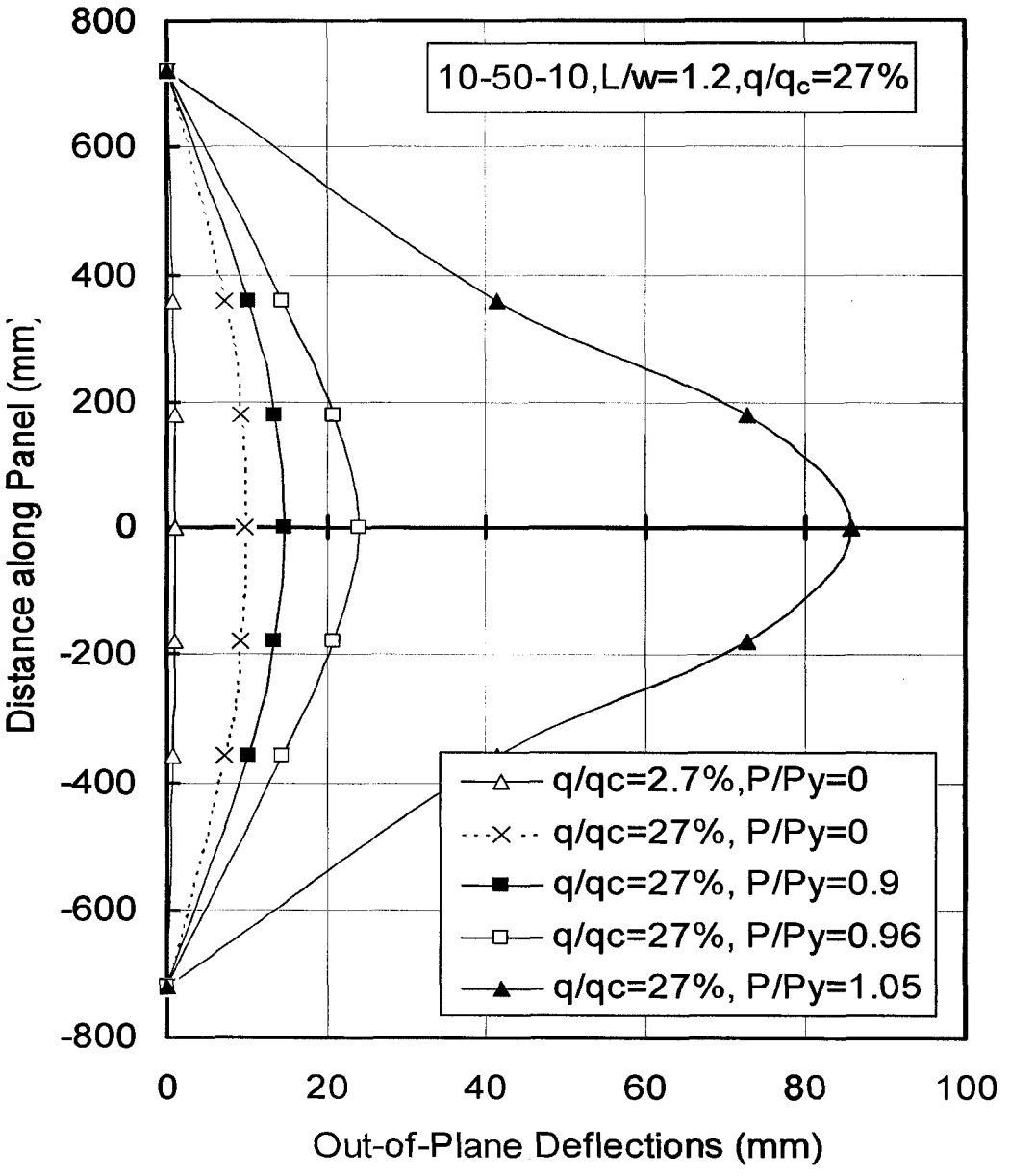

Figure A.25 Out-of-plane deflections along panel length for finite element mode (10-50-10, L/w=1.2, q/q_c =27%)

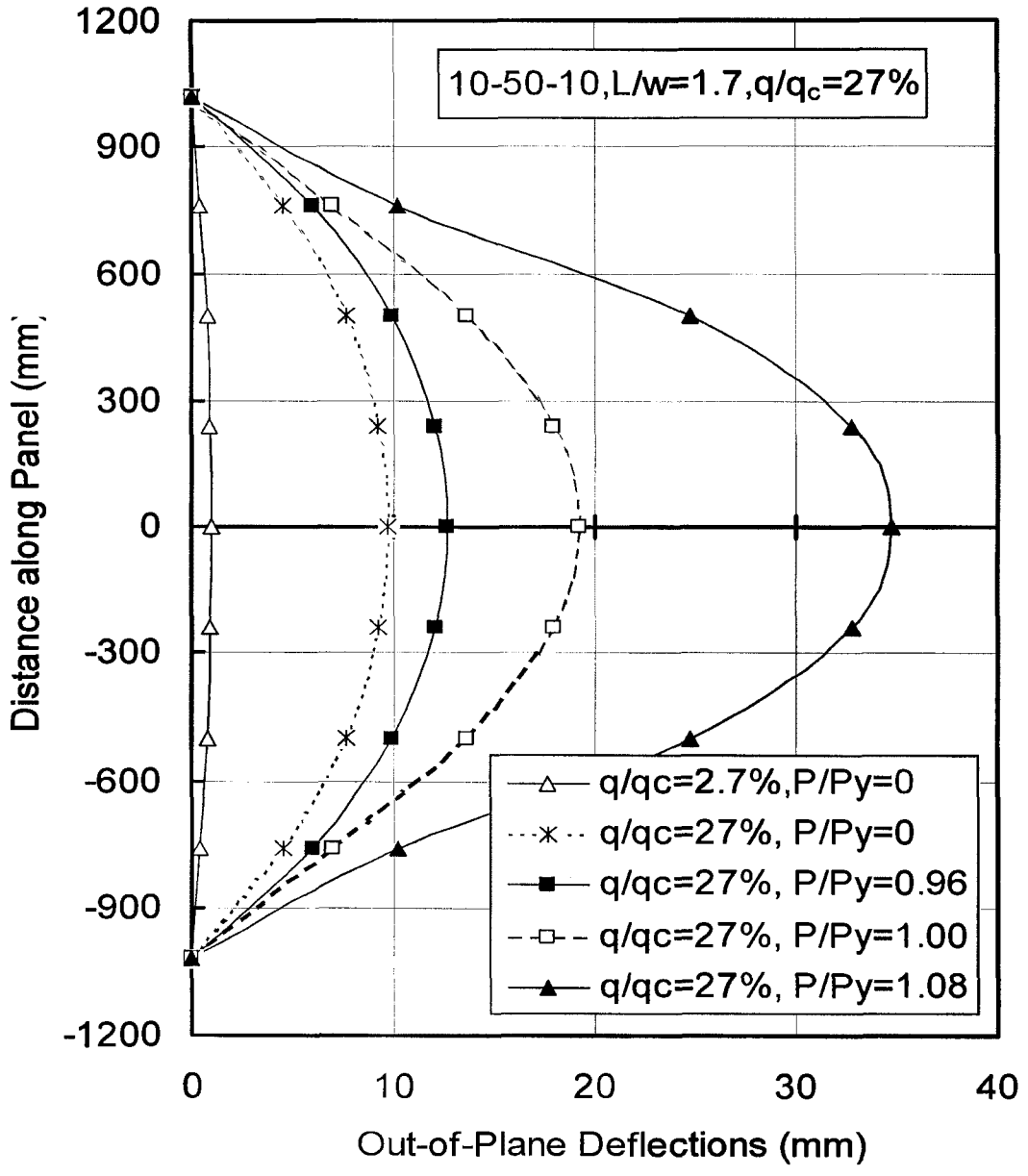

Figure A.26 Out-of-plane deflections along panel length for finite element mode (10-50-10, L/w=1.7, q/q_c =27%)

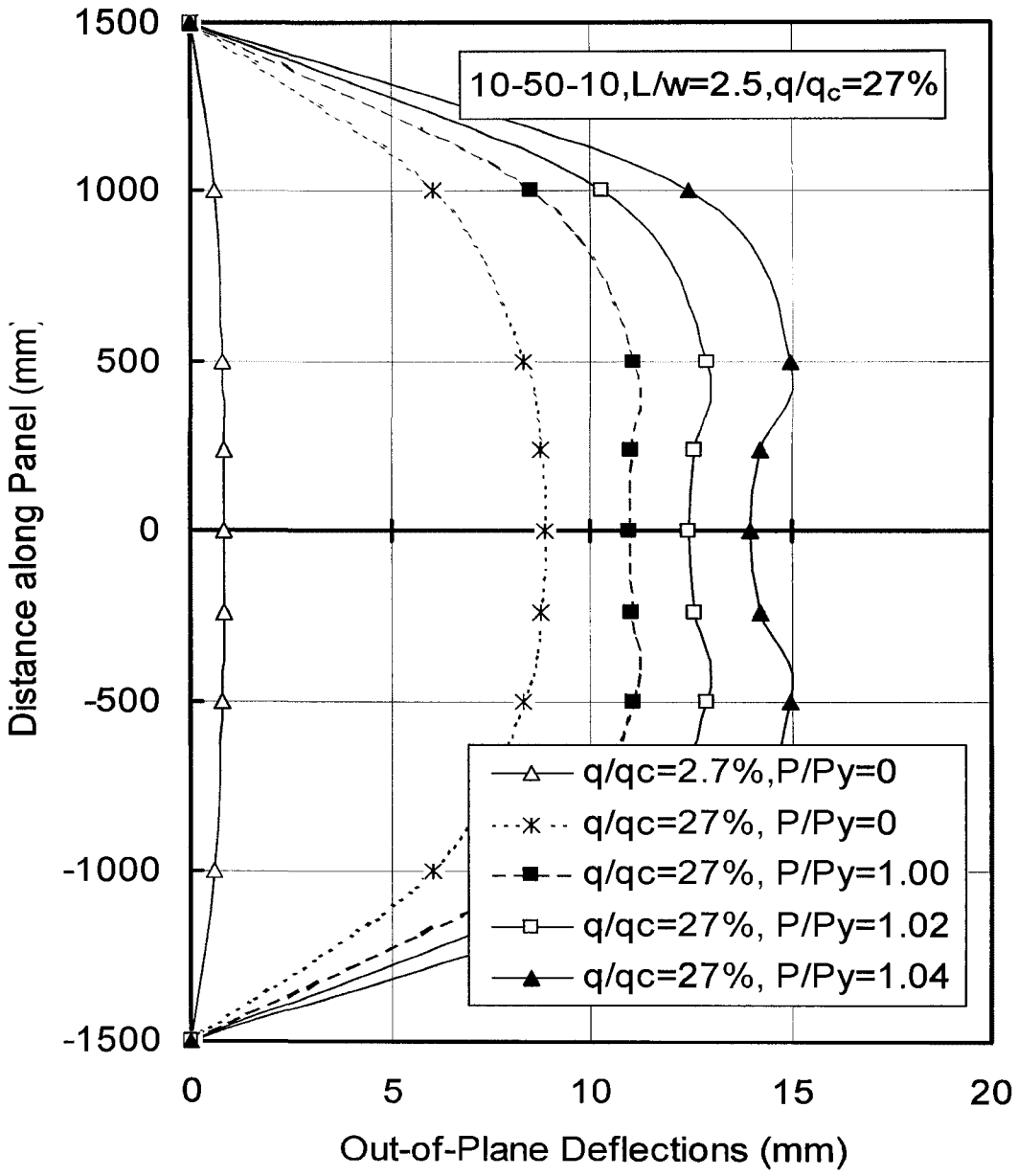

Figure A.27 Out-of-plane deflections along panel length for finite element mode (10-50-10, L/w=2.5, q/q_c =27%)

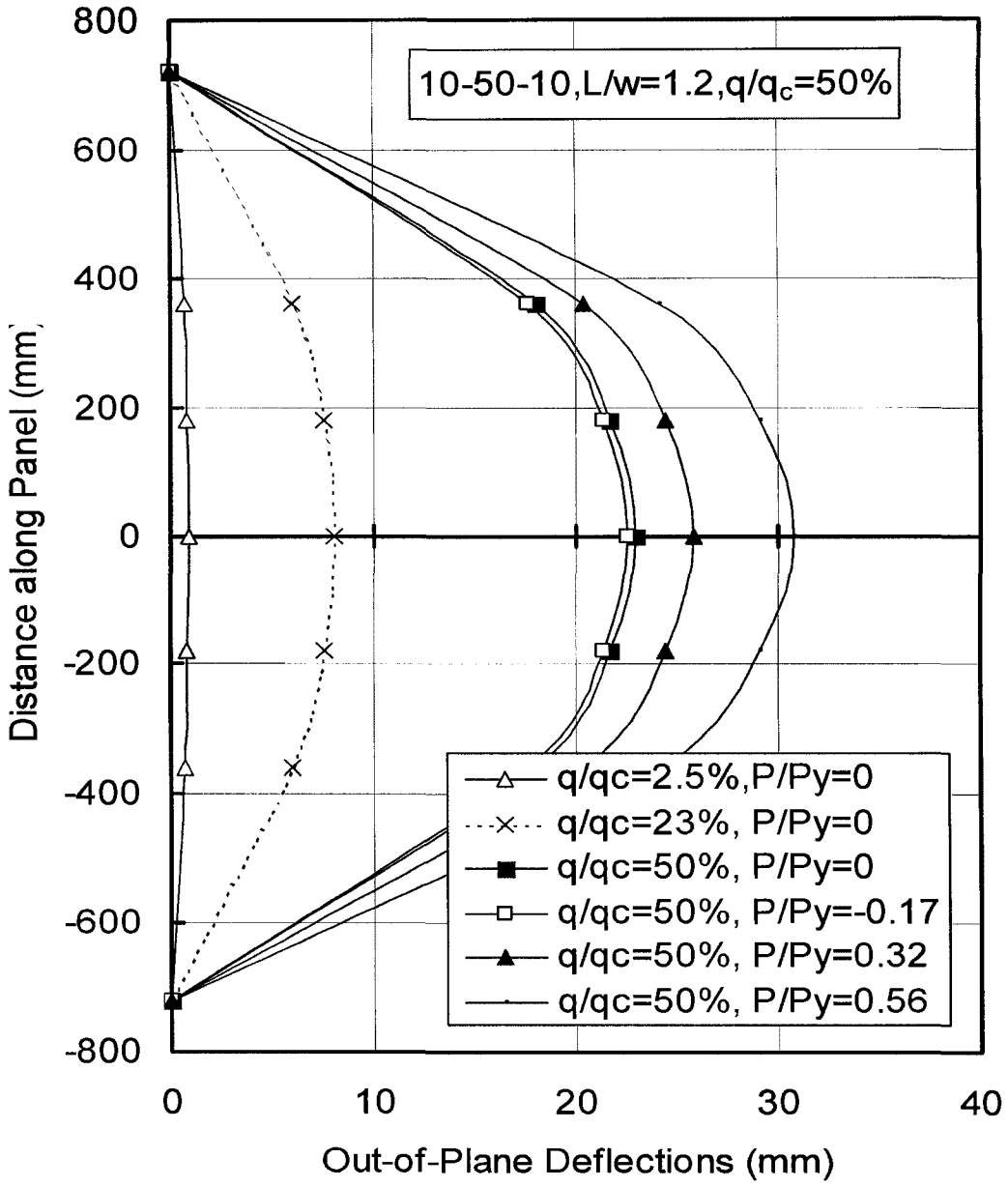

Figure A.28 Out-of-plane deflections along panel length for finite element mode (10-50-10, L/w=1.2, q/q_c =50%)

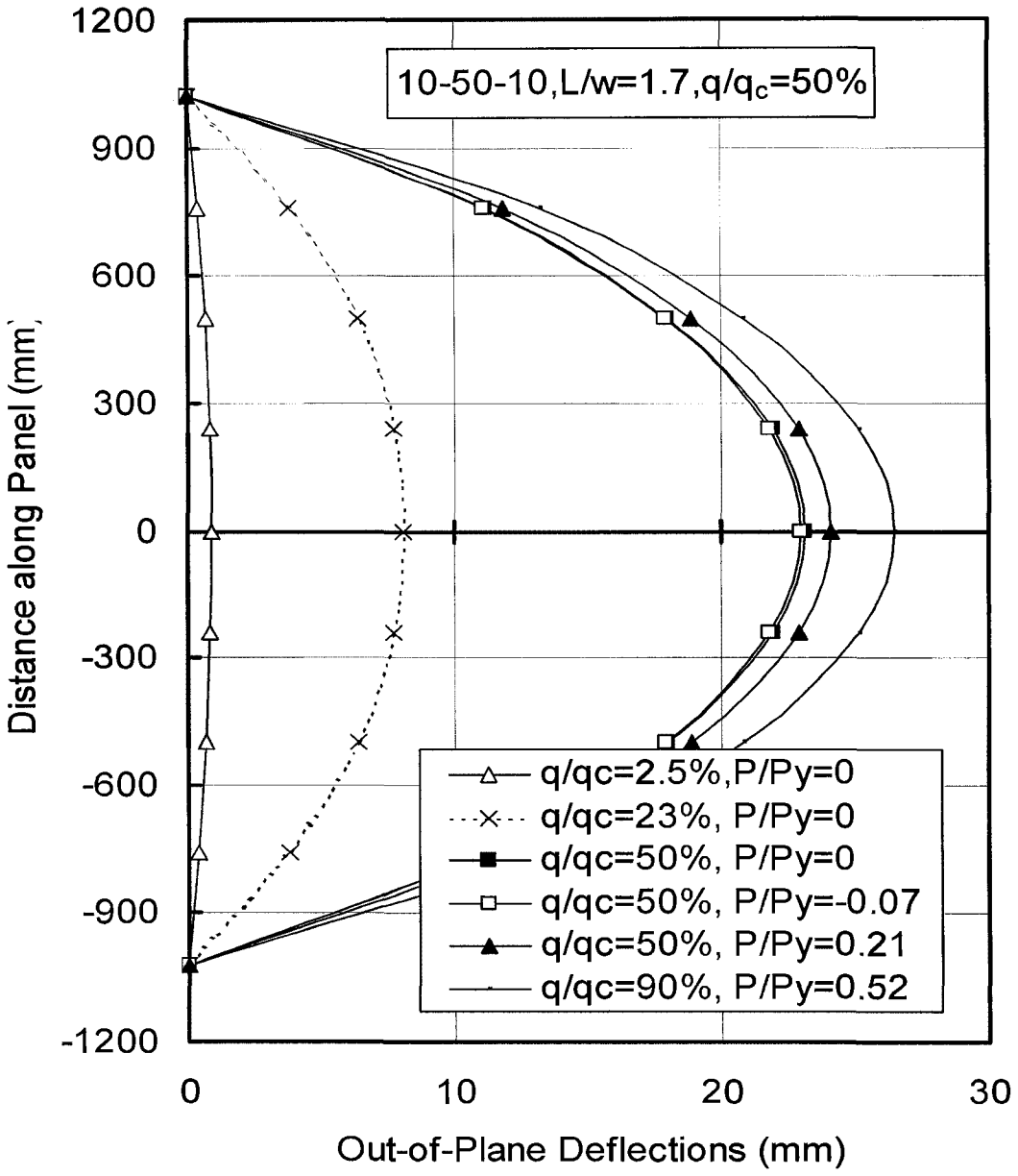

Figure A.29 Out-of-plane deflections along panel length for finite element mode (10-50-10, L/w=1.7, q/q_c =50%)

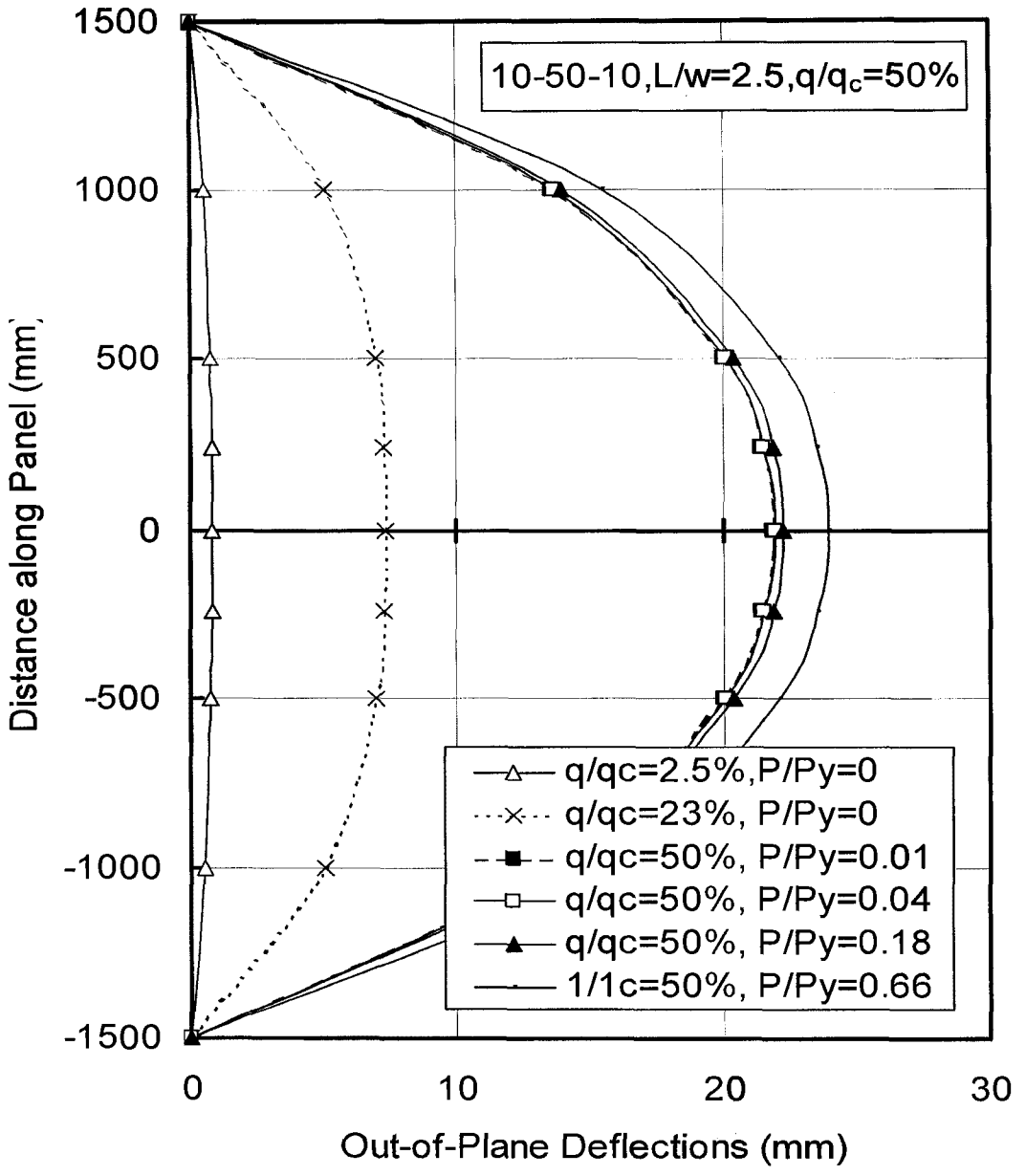

Figure A.30 Out-of-plane deflections along panel length for finite element mode (10-50-10, L/w=2.5, q/q_c =50%)